Gandhinagar Institute of Technology

About Gandhinagar Institute of Technology

Gandhinagar Institute of Technology is established by Platinum Foundation in 2006. It offers under graduate programs in Mechanical Engineering, Information Technology, Computer Engineering, Electronics and Communication Engineering, Electrical Engineering and Civil Engineering and Post graduate program in MBA (Finance, Human Resource Development, and Marketing) and M.E. in Mechanical Engineering with specialization in Thermal Engineering and Computer Aided Design & Computer Aided Manufacturing.

All these programs are approved by AICTE, New Delhi and affiliated to Gujarat Technological University. We have elaborate laboratory facilities and highly motivated and qualified faculty members. We are also arranging technical seminars, conferences, industry-institute interaction programs, workshops and expert lectures of eminent dignitaries from different industries and various reputed educational institutes.

Our students are innovative and have excellent acceptability to latest trends and technologies of present time. Our students have also participated in various technical activities as well as sports activities and have achieved various prices at state level. We have two annual publications, a National level research journal 'GIT-Journal of Engineering and Technology (ISSN 2249–6157)' and 'GIT-a Song of Technocrat' (college magazine).

Gandhinagar Institute of Technology

Gandhinagar Institute of Technology

Editorial Board

Gandhinagar Institute of Technology

Message from Director

It gives me immense pleasure that the seventh issue of our National journal 'GIT-Journal of Engineering and Technology' is being published with ISSN 2249 – 6157 for seventh successive year. The annual journal contains peer reviewed technical papers submitted by the researcher of all domains of engineering and technology. The issue is a result of imaginative and expressive skill and talent of GIT family. Research papers were invited from the researcher of all domains of engineering and technology. More than 61 research papers were received. After peer review about 29 papers are selected and are being published in this issue of the journal.

GIT was established in 2006 and during a short span of eight years; it has accomplished the mission effectively for which it was established. Institute has been constantly achieving the glory of excellence in the field of curricular, co-curricular and extra-curricular activities. For the sixth consecutive year an annual technical symposium TechXtreme-2014 was successfully organized by the institute. More than 3000 students of various technical institutions across the Gujarat participated in the Techfest. The event of Robo roller coaster was first time held in any technical institutions in India. Mr. and Mrs. Gujarat 2014 - A Talent Hunt and a pro-night with Rajdeep Chettarjee were also the main attractions. Prizes worth Rs 2 lacs and trophies were given to the winners of total 33 events. Another annual flagship event Jazba 2013 was organized on 20th September 2013. More than 1000 students of the institute participated in various cultural events of Debate, Quiz, Essay writing, Rangoli, Music, Dance, Drama etc. Famous bollywood actress Ms. Sonal Chauhan was the star attraction of the event.

The institute is two star Resource Center of IIT Bombay for conduction of Spoken Tutorials on various open source software like Linux, Latex, Scilab, Python, Java, Netbeans, C, C++, Liber Office, Php MySQL, etc. During the year institute has organized many workshops on Spoken tutorial and trained more than 1000 students and 300 faculty members. Seminars on Cisco Networking, Robotics, CAD/CAM has also been organized. The institute has also successfully organized Debate Competition, Rangoli Competition, Kite Flying competition, Ratri B4 Navaratri, and Sports activities. Institute has also arranged blood donation drives and more than 150 units were collected from the students and staff members. Students have also participated and won prizes in various sports, technical and cultural events organized by other Institutions including that of GTU. Institute has organized many industrial visits and expert lectures for the students for supplementing the class room teaching. I am extremely happy to mention that throughout the year the faculty members have worked very hard to achieve all kinds of curricular, co-curricular and extra-curricular activities.

The Institute is also emphasis on academic development of its faculty members. During the year, many International and National papers has been published and presented by the faculty members. The faculty members have also been deputed to attend large number of seminars/workshops/training programs/symposiums.

Publication of the journal of national level is not possible without whole hearted support of committed and experienced Trustees of Platinum Foundation Mr. Hareshbhai Rohera, Mr. Ghanshyambhai Thakkar, Mr. Deepakbhai Ravani, Mr. Pravinbhai Shah and Smt. Varshaben M. Pandhi. I take an opportunity to express my deep feelings of gratitude to all the trustees of Platinum Foundation and Mr. Mahendrabhai Pandhi, member of Governing body of the trust for their constant support and motivation.

It's my privileged to compliment the staff members and the students for showing high level of liveliness throughout the year. I also congratulate the team of the 'GIT-Journal of Engineering and Technology' for their untiring effort to bring out this seventh issue of the journal.

Dr N M Bhatt
Director

Gandhinagar Institute of Technology

| Home | Trustee | Editorial Board | Director Message | Papers | Contact Us |

Mechanical Engineering

Sr.No	Paper Title	Author Name	Institute Detail	Author E-Mail Id	Co-Authors Name
1	Design of internal 80 K helium purifier for kW class Helium Refrigerator/Liquefier	Mr.Divyang G Bohra	L D College of Engineering, GTU,Ahmedabad	divyangbohra@gmail.com	Mr.J M Patel Mr.A K Sahu
2	Design considerations for the components of thermoacoustic standing wave engine	Mr.Mrugesh B Khatri	L D College of Engineering, GTU,Ahmedabad	mrugesh.khatri@git.org.in	Dr.S M Mehta
3	Review of Fluid Pairs of Absorption Refrigeration Systems	Mr.Pratik S Parmar	A. D. Patel Institute of Technology,New Vallabh Vidyanagar, Anand	pratik248parmar@gmail.com	Dr.Mitesh I Shah Dr.Vishal N Singh
4	Secondary and Tip Clearance Flows: study and analysis of their behaviour in an axial linear turbine cascade – A review	Prof.Umang J Patdiwala	Kadi Sarva Vishwavidyalaya,Sector - 15, Near KH - 5,Gandhinagar	umangpatdiwala@gmail.com	Dr.P K Shah
5	Replacement of R22 to manage lifetime operation of HCFC based	Prof.Nimesh Gajjar	Gandhinagar Institute of Technology, Gandhinagar	nimesh.gajjar@git.org.in	Dr N M Bhatt
6	Review on Wall Climbing Robot	Mr.Kishan P Panchal	Gandhinagar Institute of Technology, Gandhinagar	kishan_61190@yahoo.com	Prof.Dhaval P Patel
7	A Review on an Active Solar Still	Mr.Nikul L Desai	Gandhinagar Institute of Technology, Gandhinagar	nd007er@gmail.com	Dr N M Bhatt Prof.Nimesh Gajjar
8	Design and static analysis of leaf spring by using different cross section.	Ms.Priyanka Kothari	Gandhinagar Institute of Technology, Gandhinagar	priyanka.kothari87@gmail.com	Prof.Amit Patel
9	To Study The Effects of Forming Parameters in Deep Drawing Process For SS304 Using Experiments & Computer Simulations	Prof.Chandrakant Bhatia	Gandhinagar Institute of Technology, Gandhinagar	chand28bhatia@gmail.com	Prof.B.A Modi
10	Review of Solar Air Heaters with Different Augmentation Techniques	Mr.Nitin H Oza	Gandhinagar Institute of Technology, Gandhinagar	mech_oza@yahoo.com	Dr N M Bhatt
11	Frequency Based Method and Static Deflection Measurement Method For Crack Detection in Mechanical components: A Review	Mr.Jatin M Patel	Gandhinagar Institute of Technology, Gandhinagar	jatin.patel3990@gmail.com	Prof.Amit R.Patel Prof.Mitesh J Mungla

To Study The Effects of Forming Parameters in Deep Drawing Process For SS304 Using Experiments & Computer Simulations

Chandrakant Bhatia[a] , Prof B.A Modi[b]*

[a]*Asst.Prof., Department of Mechanical Engineering,Gandhinagar Institute of Technology,Gujrat,India*
[b]*Professor , Department of Mechanical Engineering, Institute of Technology, Nirma University, Ahmedabad 382481, India*

Abstract

The formability of sheet metals is affected by many parameters, like material parameters, process parameters and strain bounding criteria. Factors such as material properties, process, parameters, and strain criteria affect the formability of sheet metals. There are methods developed for evaluating the formability of sheet metals. Sheet metal formability is measured by simulating tests, mechanical tests, finding the limit dome height and drawing forming limit diagrams. In order to successfully obtain the final desired parts, it is necessary to study the influence of the forming parameters on the hydro formability. In this study FE simulation of conventional deep drawing is carried out to find the effective tool design, (die and punch) and to identify the process parameters for successful deep drawing. A typical industrial component had been chosen as a case study. For experiments validation of it, FE simulations were carried out. The effects of various parameters such as blank holding force, friction, die entry radius, punch nose radius, etc has been done.

Keywords: Computer Simulation, Sheet Metal Forming Parameters, HMDD

DR	Drawing Ratio
LDR	Limit Drawing Ratio
FLD	Forming Limit Diagram
FEA	Finite Element Analysis
HMDD	Hydro Mechanical Deep Drawing

1. Introduction.

In all exiting forming process one of the most advanced is hydro mechanical deep drawing. This technology of hydro mechanical deep drawing combines the features of conventional deep drawing and hydro forming and widely used in many industries, especially automobile and aircraft industry. In conventional sheet metal forming, The process begins with a sheet metal blank held on the upper surface of the die, A sheet metal blank is a at piece of sheet metal used to form the finished product. One force holds the sheet metal blank in position (blank holder force) and another force punches or draws the material into the desired shape. The tooling required to produce the part consists of a male punch and a female die. Clearance between these parts is closely controlled to minimize movement of the part therefore preventing the sidewalls from wrinkling, The die and the punch have sufficient radii or relief to allow for the metal to be formed without tearing the material .Many factors such as mechanical and metallurgical properties, die and punch geometry, lubrication, sheet thickness ,sheet roughness, punch speed, etc. contribute to the success or failure of the forming to varying degrees in an interdependent manner, Therefore, an understanding of the formability of sheet metals is essential for the production of quality components..

In this study the industrial component Canister is taken for analysis .In which Limit Drawing Height and thinning problem are predominant. The component is manufactured in two parts. The lower half and upper half are drawn separately and are joined with welding methods (MIG).during the deep drawing process with the current geometry of the tools the drawing ratio obtained is less than the required also the thinning occurs at the bottom of component. So It is extremely difficult to get the required geometric specifications of the component .So the lower part of component is taken as a case study to investigate and to improve formability using SS304 in deep drawing For same .The detail drawing of required component is shown in Figure 1(a) and the component that can be produced experimentally is shown in Figure 1(b)

---

* Corresponding author. Tel.: +91-9913919302; +91-8128407352.
E-mail address: Chand28bhatia@gmail.com, ba.modi@gmail.com
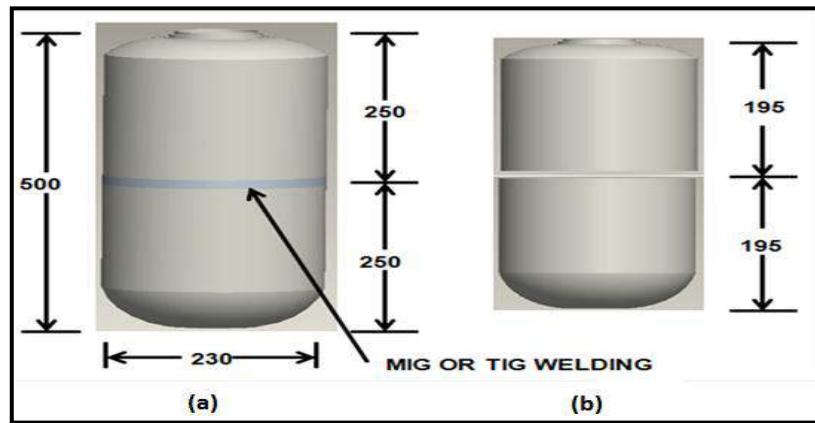
Figure1. (a) Required geometry of canister (b) experimentally produced canister with existing geometry

2. Material Characterization

The samples were prepared according to the ASTM A370 standard for determining the mechanical properties like yield strength, ultimate tensile strength, strain hardening exponent and anisotropy, etc The material SS304 was analyzed for tensile testing using uniaxial tensile testing machine and for chemical compositions spectroscopy technique was used .The detail report and compositions are summarized in the Table 1 & Table 2.

Table.1. Testing reports of Material SS304

Sr no	Degree	Y.S (MPa)	U.T.S (MPa)	K (MPa)	R	n	% elongation
1	90	409.27	677.92	1206.93	1.077	0.200	47.20
2	45	408.26	671.82	1208.92	1.077	0.201	47.70
3	0	402.00	673.60	1202.19	0.909	0.200	37.68
	Average	406.64	674.44	1207.69	1.102	0.200	-

Table.2 Chemical properties of material SS304.

Sr. no	Elements	Percentage (%)
1	Carbon	0.030
2	Silicon	0.392
3	Manganese	1.434
4	Phosphorous	0.026
5	Sulphur	0.008
6	Chromium	18.524
7	Nickel	8.012

3. FE Simulations Results of Canister under Case Study

The component shown in Figure.1 with its geometric dimensions was successfully produced upto 195 mm were as required depth is 250 mm. A FE simulation was also carried out for the same geometry using the blank diameter 460 mm which is less then the required size due to limitations in existing facilities. The blank holding force, die entry radius and punch nose radius is taken as (450 KN , 8 mm, and 70 mm).the Figure 2.shows the thinning prediction of canister with FE simulations
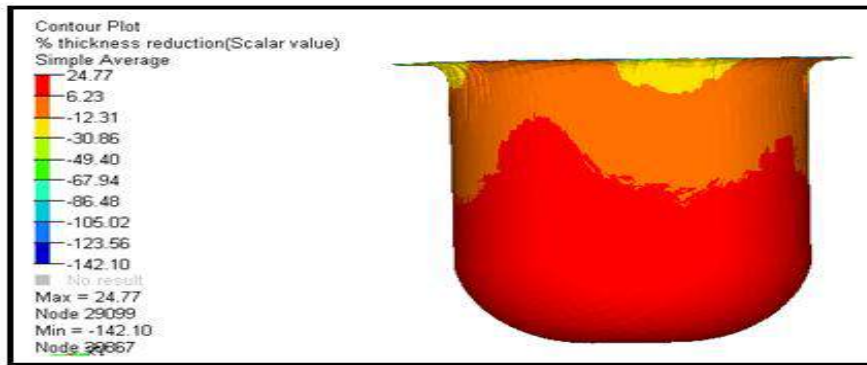
Figure.2. Percentage thinning prediction with FE simulations for canister

The Figure.3 shows simulations results of thickness contour of canister which indicates the maximum and minimum thickness at the top flange and bottom of the component. The thickness found is not in acceptable limit
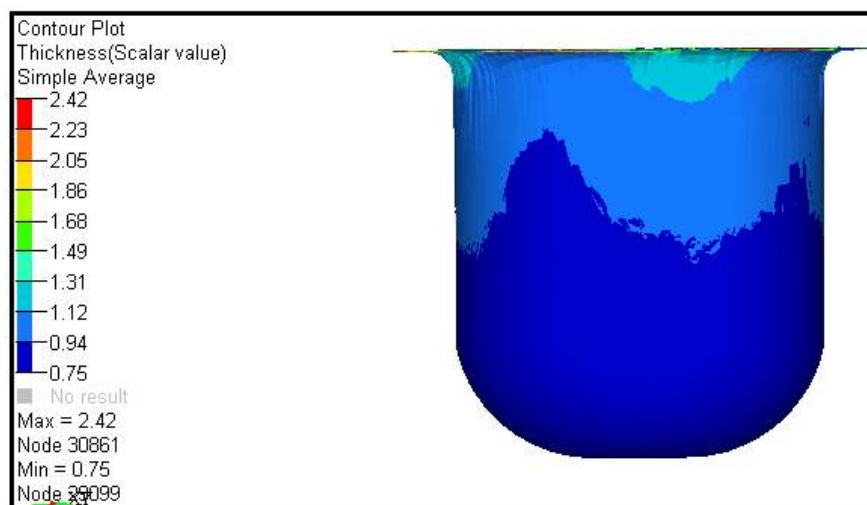
Figure.3.Thickness prediction with FE simulation for canister

Figure.4 shows the Formability diagram indicating thinning and thickening which represents in different regions of component and is not in acceptable limit .
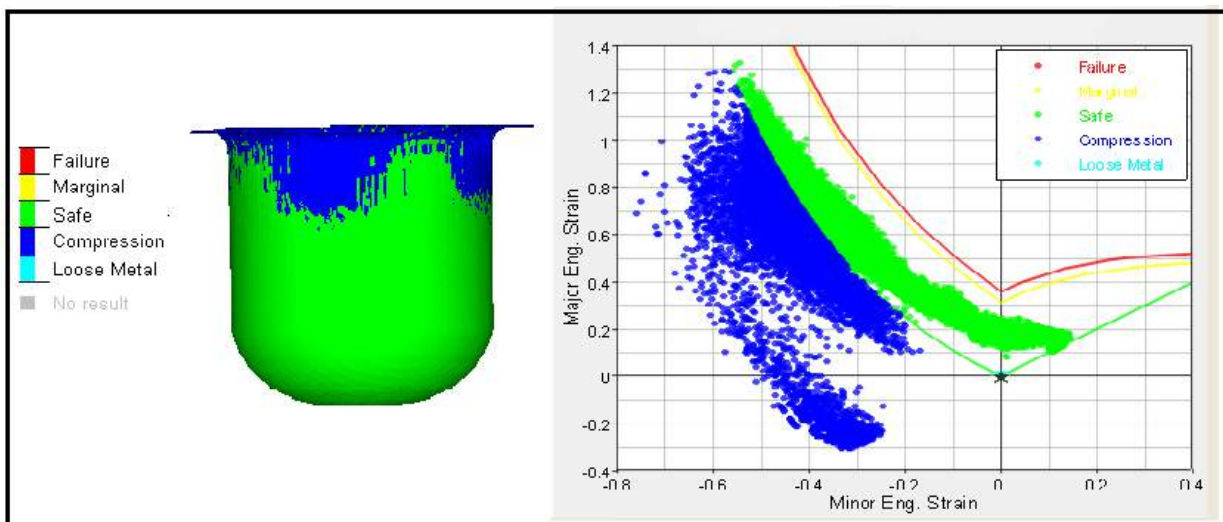
Figure.4. Strain distribution prediction with FE simulation for canister

The above results show the excessive wrinkles and thickening of canister. Hence it is required to determine geometric parameters of die and punch for the successful forming of the canister. So several FE simulations were performed with the geometric and process parameters as tabulated in Table .3

Die entry radius was varied from 15-25 mm. friction was varied from 0.125-0.05 and blank holding force was varied from 450-900 KN .The minimum thickness and maximum thickness were selected as criterion for formability .Min thickness criteria represents max thinning at punch nose radius and Max thickness criteria represents max thickness at flange and wrinkling gives the idea about it significantly.

Table.3. Summary of results with different geometry & process parameters

Sr .no	Die entry radius (mm)	Friction	Blank holding force (kn)	Thickness min (mm)	Thickness max (mm)
1	15	0.1250	900.0	0.84	1.89
2	20	0.0875	675.0	0.86	2.47
3	20	0.0500	675.0	0.86	2.35
4	15	0.0875	675.0	0.83	2.38
5	20	0.0500	450.0	0.85	1.94
6	20	0.0875	900.0	0.87	2.38
7	25	0.0500	900.0	0.82	2.40
8	25	0.1250	900.0	0.82	2.27
9	25	0.0875	675.0	0.83	2.32
10	20	0.0875	675.0	0.86	2.31

It was observed that the thickening (wrinkles) were under control with geometric and process parameters used as shown(dark) in Table 3 for simulation. At the same time thinning was also under This can be attributed to uniform strain distribution and hence successful deep drawing of canister is possible. the results are shown in Figure.5
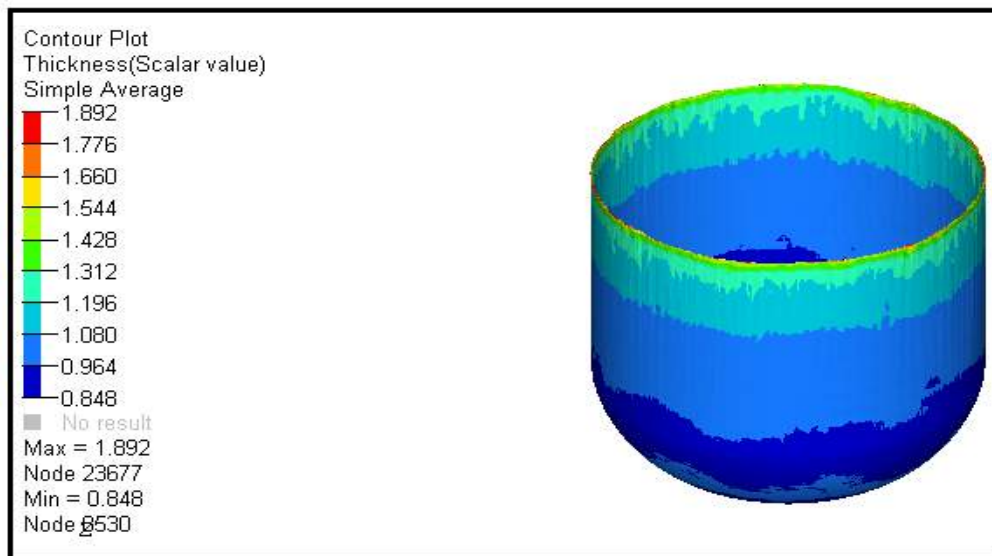
Figure.5. Thickness prediction with FE simulation canister

Fig 6(a)and 6(b) shows the comparison between FE simulation results of canister with existing and modified geometry. so it has been observed that thinning is reduced by 9.6% and thickening is also reduced by 52.29%. The height obtained is 215 mm , Hence we can say that the formability can be enhanced with improved thickness distribution in the drawn component.
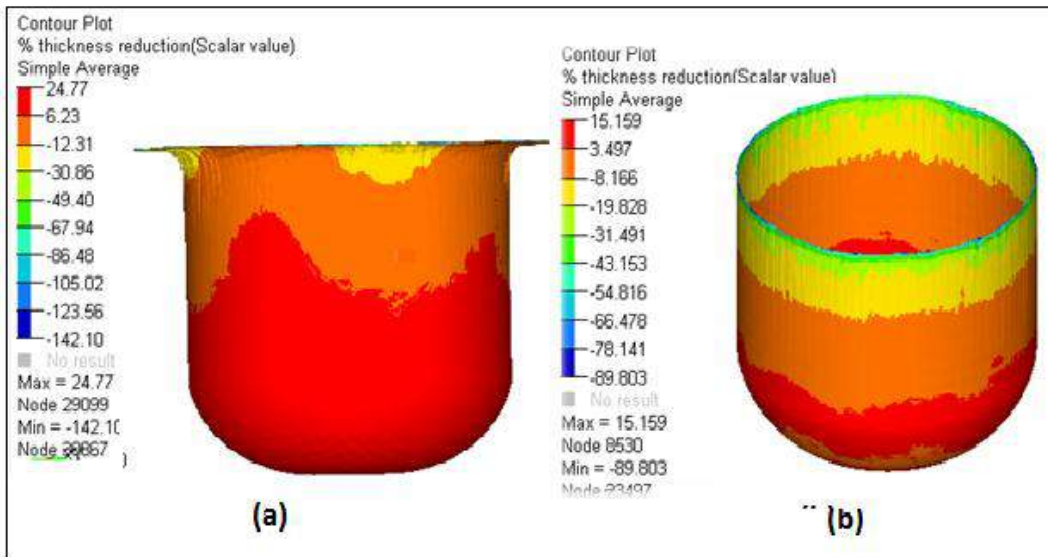
Figure.6. Comparison of existing & modified FE simulations results of canister

4. Experimental Results with Modified Geometry
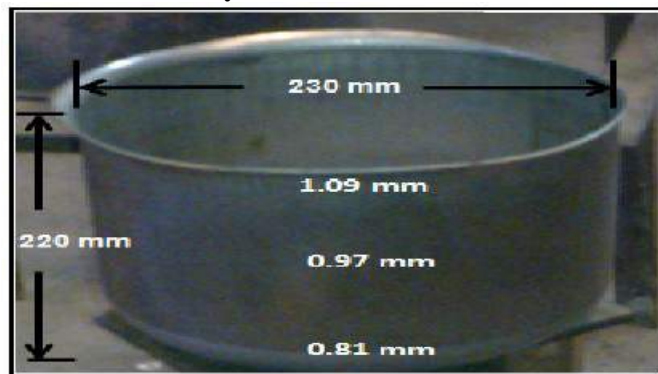
Figure.7.Experimental deep drawing of canister with modified geometry

To validate the simulations results with the practically deep drawing of component the die was fabricated with die entry radius of 15 mm and punch nose radius of 86 mm . The Figure 7 shows the actual drawn component in which 19% percent of thinning occurs also the drawing height obtained is 220 mm. These geometric parameters almost satisfy the actual requirement and match with the simulations results but there are some wrinkles and non uniformity thickness is achieved. To overcome these problems the hydro mechanical deep drawing was used and experiments were carried out to study formability.

5. Conclusions
1. Optimum geometric parameters and blank holding force has been worked out with FE analysis and design of experiment technique.
2. Increase in punch nose radius improves formability and it makes possible to draw the canister for larger depth. The draw depth could be increased from 195 mm to 220 mm.
3. Die entry radius has great influence on formability .An optimum value of 15 mm has been found out to increase draw depth without wrinkle development.

6. References

[1] Swadesh Kumar Singh a, Amit Kumar Gupta. Application of support vector regression in predicting thickness strains in hydro-mechanical deep drawing and comparison with ANN and FEM 2010 Technology-3, pp 66-72

[2] Zhiyuan Zhanga, Shengdun Zhaob, Yong Zhangb. novel response variable for finite element simulation of hydro-mechanical deep drawing. 2008 Technology- 208 pp 85-89

[3] T. Khandeparkar, M. Liewald . Hydro mechanical deep drawing of cups with stepped geometries. 2008 Technology 202 pp 246-254

[4] S. Thiruvarudchelvan , M.J. Tan Fluid-pressure-assisted deep drawing School of Mechanical and Production Engineering, Nanyang Technological University 2007 Technology-192 pp 8-12

[5] Hyunbo Shima, Dong Yol Yang, A simple method to determine pressure curve for sheet hydro-forming and experimental verification School of Mechanical Engineering, Yeungnam University 2005 Technology-169 pp 134-142

[6] ASTM Handbook, Standard test methods and Definitions for Mechanical Testing of Sheet Product", ASTMS

Design of internal 80 K helium purifier for kW class Helium Refrigerator/Liquefier

Divyang Bohra[a], JM Patel[b], AK Sahu[c]

[a] Student, Mechanical Engg Dept. LD College of Engineering,Ahmedabad-380019, India
[b] Professor, Mechanical Engg Dept. LD College of Engineering,Ahmedabad-380019, India
[c] Scientist-Engineer, Institute For Plasma Research, Gandhinagar, India

Abstract

The Helium Refrigerator/Liquefier (HRL) is normally operated with helium gas having purity better than 99.999 % by volume which is equivalent to having 10 PPM (parts per million) impure gas in the helium gas. Although sufficient precautions and impurity removal procedures are used, still, in the process of gas transfer or due to some other processes before reaching to liquefaction, impurity level sometimes can go as high as 100 PPM. These impurities consist of mainly gases present in the air, like N_2, O_2, Ar, H_2O, CO, CO2, NxOy, CxHy, H_2 and traces of Ne. These gases condense at significantly higher temperature compared to the LHe temperature (4.5 K). If such high level of impurity enters the process equipment placed inside the cold box of the HRL, then it can condense and choke the pipe lines and valves leading to large pressure drop and inefficient liquefaction process. Some time, condensed and frozen impurity can destroy the blades of turbines of HRL. Hence, to be on safer side generally, internal purifiers are placed at two temperature levels inside the cold box to take care the operational problem due to impurities. One is at ~80 K to remove nitrogen, oxygen and other gases having normal boiling points above 77 K. Another one is at ~20 K to remove hydrogen and neon gases. This project is about the design and analysis of 80 K purification system. Activated charcoals will be used to adsorb impure gases from cold helium gas at 80 K and ~14bar.

Keywords: Adsorption; Activated charcoal; Nitrogen; Isotherms; Pressure

Nomenclature		
A	Cross-sectional area of bed	m^2
c	Conversion constant	dimensionless
D	Diameter of bed	m
D_p	Equivalent particle diameter	mm
E_o	Characteristic Adsorption Energy	kJ/mol
e_w	Weld efficiency of joint	dimensionless
f_p	Friction factor	dimensionless
K	Length to diameter ratio	dimensionless
L	Length of bed	M
l	Level of impurity	ppm
M_{N2}	Mass of adsorbent for nitrogen	kg
M_{O2}	Mass of adsorbent for oxygen	kg
M_{Ar}	Mass of adsorbent for argon	kg
M_{total}	Total mass of adsorbent	kg
$\dot{m}$	Mass flow rate	kg/s
P	Inlet pressure	bar
P_{sat}	Saturation pressure	bar
P_{par}	Partial pressure	bar
Δp	Pressure drop	mbar
Re	Reynold's number	dimensionless
S_a	Allowable stress of material	MPa
t	Thickness of adsorber vessel	mm
t_h	Thickness of head of adsorber vessel	mm
U	Superficial velocity	m/s
U_i	Interstitial velocity	m/s

V	Volume flow rate	m^3/s
V_e	Volume of effluent	m^3
V_{ad}	Volume of adsorbent	m^3
V_{in}	Volume of impurity at inlet	m^3
V_{N2}	Volume of nitrogen impurity	m^3
V_{O2}	Volume of oxygen impurity	m^3
V_{Ar}	Volume of argon impurity	m^3
W	Volume Adsorbed	cm^3/g
W_o	Micropore volume	cm^3/g
Greek Symbols		
ρ_{char}	Density of charcoal	kg/m^3
ρ_{he}	Density of helium	kg/m^3
ε	Void fraction	dimensionless
μ	Dynamic viscosity of helium	Pa.s
β	Affinity coefficient	
Subscripts		
a	allowable	
ad	adsorbent	
Ar	argon	
char	charcoal	
e	effluent	
h	head	
he	helium	
i	interstitial	
in	inlet	
N_2	nitrogen	
O_2	oxygen	
p	particle	
w	weld	

1. Introduction

Helium is classified as rare gas, and it is one of the important gases now-a-days, which is becoming a most useful gas in many areas like space research, energy programs and defence as well as the medical, computer and fibre optics field. Against this background the worldwide consumption of pure helium has increased by between 5 to 10 percent a year in the past decade, with biggest growth in its use as a coolant for the superconducting magnets in magnetic resonance imaging (MRI) body scanners. Current helium consumption is estimated to be about 100 million cubic meters, and is predicted to continue to rise by 4 to 5 percent annually. In India, helium is an expensive and exported consumable. Therefore, a helium purifier is an integral part of any cryogenic centre to conserve helium gas. As the helium gas with above mentioned impurities after passing through the molsieve bed enters the first heat exchanger where its temperature is reduced to about 90K. Then it passes through second heat exchanger where GN_2 is used to bring helium temperature down to ~80K. Thereafter the helium gas enters the adsorber (carbon) bed where the impurities like N_2, O_2 and Ar are removed / adsorbed. [1]

1.1. Adsorption

Whatever the nature of the forces holding a solid together, it can be regarded as producing a field of force around each ion, atom or molecule. At the surface of the solid, these forces cannot suddenly disappear and thus reach out in space beyond the surface of the solid. Due to these unsaturated and unbalanced forces, the solid has a tendency to attract and retain on its surface molecules and ions of other substances with which it comes in contact. Thus when a gas is brought in contact with solid, generally a part of the gas is taken up by the solid. If the gas molecules penetrate into the solid, the process is usually called absorption. If the gas molecules stick to the surface of the solid in one or more layers, the process is called adsorption. If there is a very strong reaction between the solid and the gas, the adsorption process is called the chemical adsorption. If only weak intermolecular forces, called van der waals forces are brought into play, the process is called

physical adsorption. The substance attached to the surface is called adsorbate, and the substance to which it is attached is known as adsorbent.[2,3]

1.2. Adsorbent

To be technically effective in commercial separation process, whether this be a bulk separation or purification, an adsorbent material must have a high internal volume which is accessible to the components being removed from the fluid. Such a highly porous solid may be carbonaceous or inorganic in nature, synthetic or naturally occurring, and in certain circumstances may have true molecular sieving properties. The adsorbent must also have good mechanical properties such as strength and resistance to attrition and it must have good kinetic properties, that is, it must be capable of transferring adsorbing molecules rapidly to the adsorption sites. In most applications the adsorbent must be regenerated after use and therefore it is desirable that regeneration can be carried out efficiently and without damage to mechanical and adsorptive properties. The raw materials and methods of producing adsorbents must ultimately be inexpensive for adsorption to complete successfully on economic grounds with alternative separation processes.

The high internal surface area of an adsorbent creates the high capacity needed for a successful separation or purification process. Adsorbents can be made with internal surface areas which range from $100m^2/g$ to over $3000m^2/g$. For practical applications, however the range has been restricted to about $300-1200m^2/g$. For most adsorbents the internal surface area is created from pores of various sizes. The structure of an adsorbent is shown in idealized form in fig.1.2. Many adsorbent materials, such as carbons, silica gels and aluminas, are amorphous and contain complex networks of interconnected micropores, mesopores and macropores. In contrast, in zeolitic adsorbents the pores or channels have precise dimensions although a macro porous structure is created when pellets are manufactured from zeolite crystals by the addition of binder. Fluid molecules which are to be adsorbed on the internal surface must first pass through the macroporous structure into the micro pores where the bulk of the molecules are adsorbed. [2-6]
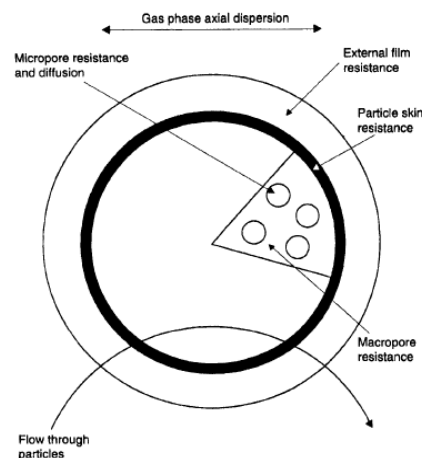
Fig.1 General structure of an adsorbent particle and associated resistances to the uptake of fluid molecules. (Courtesy: Adsorption Technology and Design, Thomson and Crittenden, Butterworth)

1.3. Adsorption Isotherm

If a quantity q of a gas or vapour is adsorbed by a porous solid at constant temperature and the steady state equilibrium partial pressure is p then the function q(p) is the adsorption isotherm. Isotherms can take one of the several forms (known as types I to V) illustrated by figure 2. Each of these types is observed in practice but by far the most common types are types I, II, and IV. An inherent property of type I isotherm is that adsorption is limited to the completion of a single monolayer of adsorbate on the adsorbent surface. Type I isotherms are observed for the adsorption of the gases on microporous solids whose pore sizes are not much larger than the molecular diameter of the adsorbate; complete filling of these narrow pores then corresponds to the completion of a molecular layer. Type II isotherms do not exhibit a saturation limit. Near to first point of inflexion of such isotherms a monolayer is completed following which adsorption occurs in

successive layers. Adsorbents which have a wide distribution of pore sizes from type II isotherms, condensation of the adsorbate vapour occurring within the larger pores. The adsorbents display a higher capacity for adsorption as the adsorbate saturated vapour pressure is approached. Similarly type III isotherms, which are continuously convex with respect to the partial pressure axis, shows a steady increase in adsorption capacity with increasing relative pressure. Type IV isotherms are similar to type II isotherms except that adsorption terminates near to a relative pressure but then a point of inflexion is reached and a saturation limit is approached as the relative pressure is further increased.[4]
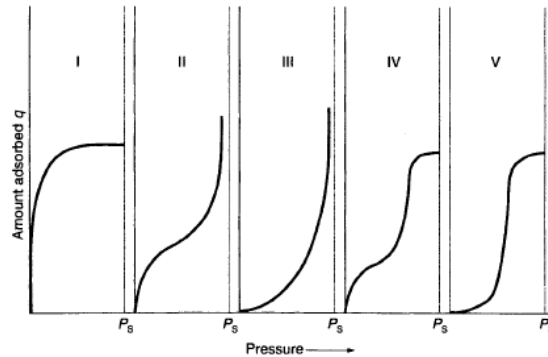
Fig.2.The five types of Isotherms (Courtesy: Adsorption Technology and Design, Thomson and Crittenden, Butterworth)

1.4 Fixed Bed Process

Vessels and columns which hold the adsorbent in a fixed position appear initially to provide distinct advantages over their counterparts in which the adsorbent is allowed to move. First, such equipment is simple and relatively inexpensive to fabricate. Secondly, minimal attrition of adsorbent occurs when it remains in fixed position. However, despite their simplicity, fixed beds have a disadvantage, i.e. As fluid is passed through a fixed bed of adsorbent the transfer of adsorbate molecules from the feed to the solid initially occurs at bed entrance. Once the adsorbent in this region becomes saturated with the adsorbate molecules, the zone in which the mass transfer occurs move progressively through the bed towards the exit, as shown schematically in fig. 3. When the breakthrough of the adsorbate begins to occur it is necessary to take the bed offline so that the adsorbent can be regenerated. At any instant in time in the adsorption step it is clear from fig.3 that the adsorbent particles upstream and downstream of the mass transfer zone (MTZ) do not participate in mass transfer process. Upstream of the MTZ, the adsorbent will be in equilibrium with the feed and unable to adsorb further adsorbate molecules. Downstream of the MTZ, the adsorbent will not have been in contact with any adsorbale molecules and therefore, despite having the capability of doing so, will also be unable to adsorb adsorbate molecules. Thus, if the time selected for progress of MTZ through the bed is long the bed will be large and it will contain a large inventory of expensive adsorbent. In addition the pressure drop will be proportionately large. [4]
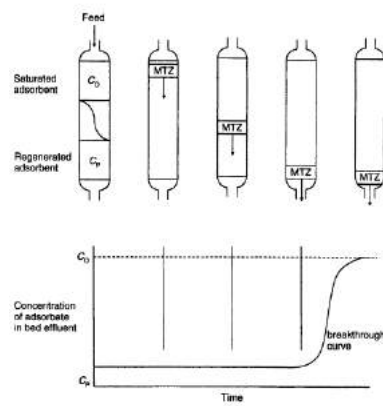
Fig. 3 Sketch showing the concentration profile, mass transfer zone, and break-through curve in packed bed adsorption (Courtesy: Adsorption Technology and Design, p 97).

1.5 Mass Transfer Zone

Progress of the mass transfer zone (MTZ) through a fixed bed for a single adsorbate in a diluents is shown schematically in fig. 3 and 4. In practice, it is difficult to follow the progress of the MTZ inside a column packed with adsorbent because it is difficult to make meaningful measurements of parameters other than temperature. By following the progress of the exotherm which accompanies the adsorption process it is possible to gain an indication of the MTZ.[8]
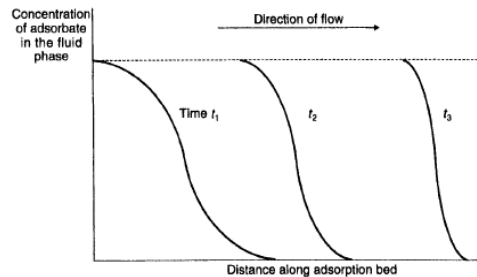
Fig. 4 Development and progression of a mass transfer wave along a fixed adsorption bed (Courtesy: Mass transfer operations, Robert E. Treybal, p 624).

2. Adsorbent Selection

2.1. Classification of Pore size

Activated carbon is the most widely used sorbent. Its usefulness derives mainly from its large micropore and mesopore volumes and the resulting high surface area. The pore size distribution of a typical activated carbon is given in Figure 5, compared with several other sorbents.[2,6]
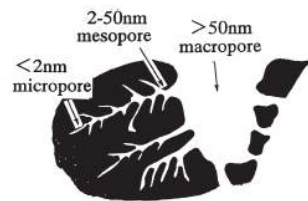
Fig. 5 Pore structure of activated carbon (Courtesy: Porous carbons, Satish M Manocha, Dept. of material science, SP university, VV Nagar)

Table.1

	Micropore	Mesopore	Macropore
Diameter(nm)	<2	2-50	>50

2.2. Comparison between zeolite and activated carbon

The results are for comparison between zeolite and activated carbon are shown in fig. 6 and 7 for the Molecular sieves 13X and granular GI grade activated carbon, expressed in mass of nitrogen gas adsorbed per unit mass of adsorbent, $\Delta m/M$, i.e. the mass fraction, as a function of gas pressure. The series of curves have the shape of Type I adsorption isotherms described in literature.[12]

(a).   (b).
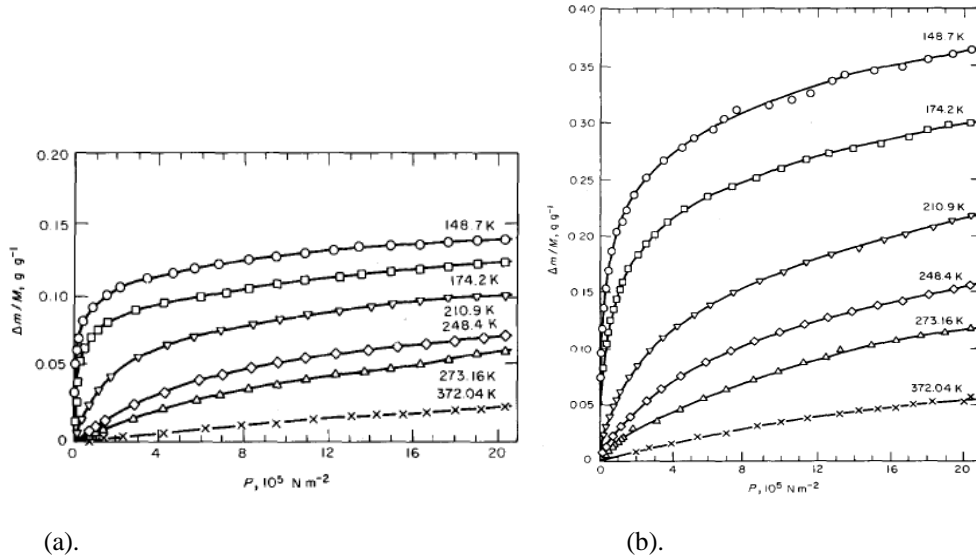
Fig. 6 (a). Nitrogen adsorption isotherms in Molecular sieves 13X. **(b).** Nitrogen adsorption isotherms in granular GI grade activated carbon.

3. Design

3.1 Mass of Adsorbent

Several expressions have been proposed to describe the quantity of gas that may be adsorbed by a unit mass of adsorbent. But since the relative pressure ratio for present case is very low i.e. of the order of 10^{-5} to 10^{-2} the use of Dubinin-Radushkevich (DR) equation is most appropriate.[3,10] The DR equation is given as;

$$W = W_o e^{(-A/E)^2} \tag{1}$$

Where,

$$A = RT \ln(P_s/P) \tag{2}$$

And,

$$E = \beta E_o \tag{3}$$

3.2 Pressure drop

From a fluid mechanical perspective, the most important issue is that of the pressure drop required for the liquid or the gas to flow through the column at a specified flow rate.   R. Shankar Subramanian to calculate this quantity relied on a friction factor correlation attributed to Ergun.[10] The Ergun equation that is commonly employed is given below:

$$f_p = \frac{150}{Re_p} + 1.75 \tag{4}$$

Here, the friction f_p factor for the packed bed, and Reynolds number Re_p, are defined as follows;

Where,

$$f_p = \frac{\Delta p}{L} \frac{D_p}{\rho V_s^2} \left(\frac{\varepsilon^3}{1-\varepsilon}\right) \tag{5}$$

And,

$$Re_p = \frac{D_p V_s \rho}{(1-\varepsilon)\mu} \qquad (6)$$

3.3 Adsorber vessel design

Since the pressurized helium gas has to be passed through the adsorber vessel, it can be designed considering a pressure vessel. [9] According to the ASME Section VIII, the minimum thickness of the cylindrical shell can be given by;

$$t = \frac{pD}{2S_a e_w - 1.2p} \qquad (7)$$

The minimum thickness for spherical shells, hemispherical heads is given by;

$$t_h = \frac{pDK}{2S_a e_w - 0.2p} \qquad (8)$$

Where

$$K = \text{constant} = 1/6\,[2 + (D/D_1)^2]$$

4. Results

The design methodology described above was used to calculate the mass, pressure drop and adsorber vessel dimensions. The adsorber vessel dimensions were set after doing number of iterations of L/D ratio, void fractions and equivalent particle diameter for pressure drop within acceptable range.

(a).   (b).
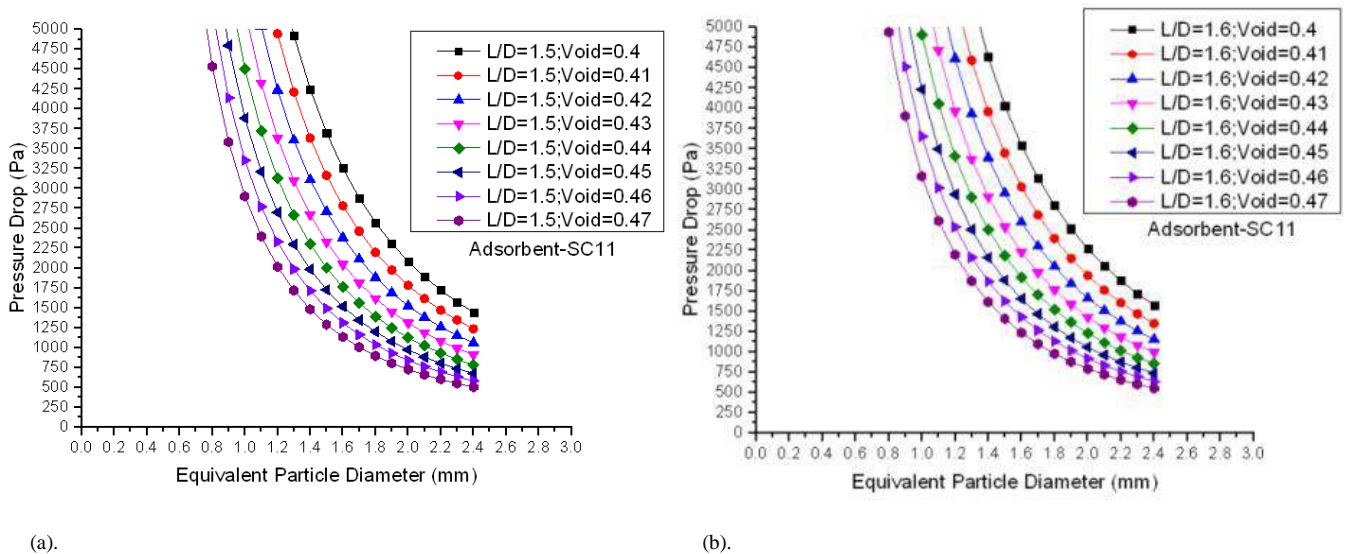
Fig.7 (a-b) Pressure drop variation with respect to equivalent particle diameter for (a). L/D=1.5 and (b). L/D=1.6

The above figure is a result of number of iterations done to fix the optimum L/D ratio, void fraction as well as particle diameter. Let say take void = 0.43, and particle diameter = 1.5 mm then for these two parameters the pressure drop in case of L/D ratio 1.5 is ~2250 Pa and in case of L/D ratio 1.6 pressure drop is ~ 2750 Pa. Thus to choose an optimum L/D ratio, voidage and particle diameter for our operating conditions many such iterations were done and then we selected the one such set which fulfills our pressure drop restrictions.

Conclusion

The present work deals with the design of adsorption based helium purification system. In context to the design requirements it can be concluded from above literature survey that activated carbon especially shell based seems to be more effective as compared to the different adsorbents disused in the literature. In addition to this, the design calculation gives us an overview of the appropriate values of mass of adsorbent, dimensions of the adsorber bed and pressure drop calculated using different equations from respective references. Since the pressure drop is a function of many parameters, the variables taken are optimized after several iterations. Now the available pressure drop comes within the allowable range.

Acknowledgement

References

[1] Jitendra Bhusan, "Helium Purification by Gas Adsorption method", NIT Raurkela.
[2] Douglas M. Ruthven, "Principles Of Adsorption and Adsorption Processes", John Wiley & Sons, 1984.
[3] Roopchand Bansal & Meenakshi Goyal, "Activated Carbon Adsorption", CRC Press, 2005.
[4] Barry Crittenden & W John Thomas, "Adsorption Technology & Design", Elsevier Science & Technology Books, April   1998.
[5] Ralph T. Yang, "Adsorbents: Fundamentals and Applications", John Wiley & Sons Publication, 2003.
[6] M. Douglas Levan, Giorgio Carta, "Perry's Chemical Engineer's Handbook", 8th edition, McGraw-Hill Publication, 2008.
[7] Satish M Manocha, "Porous Carbons", Department of Materials Science, Sadar Patel University, Vallabh Vidhyanagar.
[8] Robert E. Treybal, "Mass-Transfer Operations", third edition, McGraw-Hill publications, 1981.
[9] Randall F. Barron, "Cryogenic Systems", second edition, Clarendon Press, Oxford, 1985.
[10] Ralph. T. Yang, "Gas Separation by Adsorption Process", Imperial college Publication.
[11] D. Martins, I. Catarino, D. Lopes, I. Esteves, J.P. Mota, G. Bonafait, "Low Temperature Adsorption Versus Pore Size In Activated Carbons", Cryocoolers 16, 2011.
[12] L.C. Yang, T.D. Vo, and H.H. Burris, "Nitrogen Adsorption Isotherms For Zeolite and Activated Carbon", cryogenics, 1982.
[13] R. Shankar Subramanian, "Flow Through Packed Beds and Fluidized Beds".

Design considerations for the components of thermoacoustic standing wave engine

Mrugesh Khatri[a], Dr. S. M. Mehta[b]

[a]*Mechanical Engineering Department, L. D. College of Engineering, Ahmedabad-380 015, India.*
[b]*Mechanical Engineering Department, L. D. College of Engineering, Ahmedabad-380 015, India.*

Abstract

The paper includes innovative type of thermoacoustic engine (TAE). In the engine the pressure oscillations are created which provides driving force similar to the compressor. The important components of engine are hot working gas, heat exchanger, stack, ambient heat exchanger, resonator tube etc. This article includes the important aspects of the main component of engine i.e. stack. It covers the heat transport process as well as design aspects of the stack of engine. Also the generalize design considerations of different components of thermoacoustic engine are included in the paper.

Keywords: Thermoacoustic engine, components, working gas, heat exchanger, stack, resonator.

Nomenclature

K	thermal conductivity (W/m^{2}K)
c	heat capacity (J/K)
y_0	optimum plate spacing or plate half thickness (m)
l_c	length of heat exchanger (m)
l	plate half thickness (m)
a	acoustic velocity (m/s)
A	area of stack (m^2)
P_0	antinode pressure amplitude (Pa)
n	no of plates
R	inner radius of resonator pipe (m)
BR	blockage ratio

Greek symbols

δ_k	thermal penetration depth of gas (m)
δ_s	thermal penetration depth of stack (m)
δ_v	thinner viscous boundary layer (m)
ρ	density (kg/m^3)
ω	angular frequency (rad/sec)
η	shear viscosity (Ns/m^2)
ν	kinematic viscosity (m^2/s)
σ	Prandtl number

Subscripts

g	working gas property
s	stack material property

1. Introduction

The thermoacoustic engine involves fluid dynamics, thermodynamics and acoustic. It uses the heat energy to generate power inform of pressure oscillations or acoustic energy. The principle is used for the purpose of power generation as well as for refrigeration. The thermoacoustic system which develops power is engine that has components hot buffer, hot heat exchanger, resonator tube etc. The engine has heat energy as an input to system where as pressure wave is the output of engine. In case of refrigerator the driver is the loudspeaker which provides acoustic energy. The refrigerator has components like acoustic power generator, cold heat exchanger, stack, hot heat exchanger, resonator tube, etc. In case of engine, if the oscillations are within fixed length than it is standing wave type engine and the other one is travelling wave type engine. The standing wave engine has stack where as the travelling wave engine contains regenerator. The standing wave thermoacoustic engine has different components like hot buffer, working gas, hot heat exchanger, stack, ambient heat

exchanger, resonator tube etc. In order to design the engine it is necessary to take few considerations in order to improve the efficiency of the engine.

2. Main text

2.1. Basic principle of thermoacoustic

The prime-mover cycle also consists of two adiabatic (1-2, 3-4) and two isobaric heat transfer steps (2-3, 4-1) as a Brayton cycle. Applying a large temperature gradient along the channel.[1].
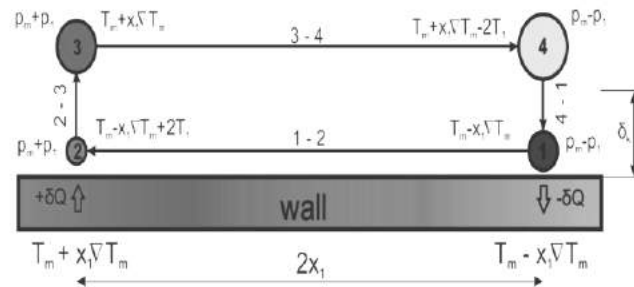
Fig. 1. The parcel of gas which is neither isothermal nor adiabatic has imperfect thermal contact with the wall (a macroscopic Lagrangian view)

When a parcel of gas is compressed (1-2), it warms up but is still colder than the local wall position. The heat then flows from the wall into the parcel which expands (2-3). As a consequence of this expansion a gas (3-4) will be displaced to the other side of the stack. In step (4-1) a parcel of gas is warmer than the wall and the heat flows into the wall which is illustrated in Fig. 1. A gas contracts and work is done by the acoustic work.[1]

The only difference with the refrigerator case is that a small temperature gradient is generated along the stack by the acoustic work, so that the directions of heat transfer in steps 3-2 and 1-4 are reversed. The net-work produced in one cycle is given by the area 1234 in Fig. 2 as a result of standing wave can be sustained by a large temperature gradient along the walls of the channel.[1]
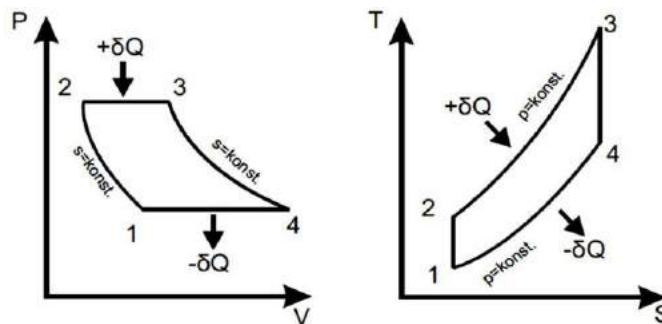
Fig. 2. Schematic p-V and T-s diagram of the ideal thermoacoustic cycle

As a typical parcel of the gas oscillates along the axis of the channel, it experiences changes in temperature, caused by adiabatic compression and expansion of the gas by the Scott Backhaus, sound pressure and by heat exchange with the solid wall of the channel. A thermodynamic cycle, with the time phasing called for by Rayleigh, results from the coupled pressure, temperature, position, and heat oscillations. The time phasing between gas motion and gas pressure is such that the gas moves hot-end while the pressure is rising and cool-end while the pressure is falling. Deliberately imperfect heat exchange between the gas and the solid wall of the channel is required in order to introduce a significant time delay between gas motion and gas thermal expansion/contraction, so that Rayleigh's criterion is met. The imperfect thermal contact results when the characteristic lateral dimension of the channel is one or more thermal penetration depths in the gas at the frequency of the oscillation.[2]
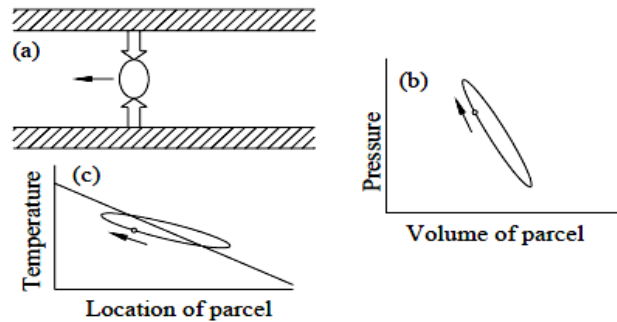
Fig. 3. The standing-wave engine process (a) A parcel of gas oscillating horizontally in a channel. At this instant of time, it moves left (small arrow) and absorbs heat from the channel walls (large arrows). (c) The straight line shows temperature vs position in the channel walls, and the ellipse shows temperature vs position and time of the parcel. (b) Pressure and volume of the parcel trace out a clockwise ellipse as functions of time.

The process shown in Fig. 3 occurs in a single channel, and the temperature gradient is maintained by a heat source outside of one end of the tube and a casual heat sink to atmospheric air along and in the other end of the tube. However, in standing-wave engines, the process occurs in many channels in parallel, all of which contribute to the acoustic power generation.[2]

2.2. Thermoacoustic standing wave engine

The fig. 4 shows the schematic diagram of thermoacoustic standing wave engine.[3]
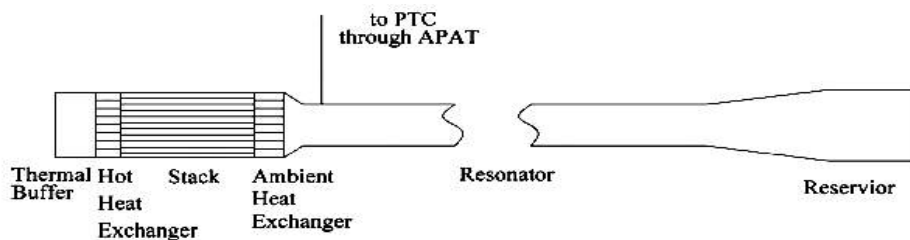
Fig. 4. Schematic representations of the 300 Hz thermoacoustic standing wave engine[3]

The components of thermoacoustic standing wave engine are thermal buffer, hot heat exchanger, stack, ambient heat exchanger, resonator, reservoir etc. The heat input is given at hot heat exchange to the gas inside the engine. This gas parcels takes up heat form hot heat exchanger and moves to stack i.e. towards cold heat exchanger. As gas parcels comes in contact with cold heat exchanger side of stack they rejects heat in the cold heat exchanger and moves back to the hot heat exchanger end of stack. Thus oscillating motion of gas is produced. This results in production of acoustic power in the engine. This power has less pressure magnitude, which results in losses in the pulse tube cryocooler. To overcome the problem acoustic power amplifier tube (APAT) is being introduced. The amplification process takes inside the tube.

2.3. Working gas

The choice of working fluid especially gas for a thermoacoustic engine is an important aspect to be considered as it affects power and efficiency.[4]

The heat that is carried on stack is proportional to expression $p_m a A$, where, p_m = average gas pressure, a = sound velocity in gas, and A = the cross-sectional area of stack. The cooling power is proportional to average gas pressure p_m inside the system.[4]

The thermal penetration depth can be written as:[4]

$$\delta_k = \sqrt{\frac{2 \cdot K_g}{\rho_g c_p \omega}}$$ (1)

Heat carried is also proportional to sound velocity in gas. The higher is the sound velocity, the larger is the heat carried to the stack. The sound velocity in gases like hydrogen and helium is high. Since helium also has a high thermal conductivity, it is an appropriate gas to be used in these systems. As the thermal conductivity of gas gets higher, the heat transfer between the fluid particles and the stack plates gets easier. Therefore the thermal penetration depth increases with thermal conductivity and building the stack gets easier.[4,5]

Light gases are generally preferred for the thermoacoustic engine because they have high thermal conductivity. This leads to high thermal penetration depth because it is directly proportional to the thermal conductivity. Generally light gases like, hydrogen, helium, neon etc are used in order to achieve the maximum speed of sound in the gas. The helium is more preferred compared to hydrogen because hydrogen is flammable which requires extra care to be taken in handling. In order to reduce viscous dissipation the Prandtl number of gas is being reduced. One of the methods of reducing Prandtl number is by adding masses. As an example, the blending of 20% xenon inside helium decreases the Prandtl number from 0.67 to 0.2. As the result, the efficiency of the system increases.[4,5]

2.4. Heat exchanger

Heat exchangers which are placed at both ends of the stack provide heat transfer with the environment. The thermal conductivity of heat exchanger material should be as high as possible.[4]

Copper has a high thermal conductivity, and it is a good heat exchanger material. Heat exchangers are made of parallel plates like stack. It should be noticed not to obstruct gas oscillations when they are placed near stack.[4]
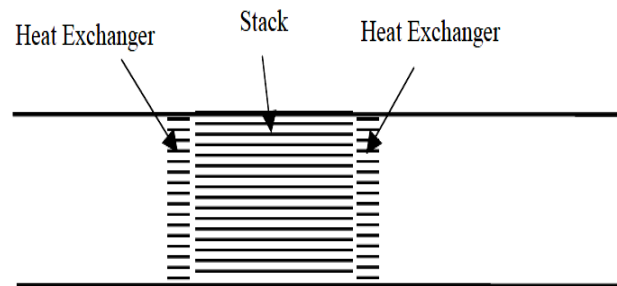
Fig. 5. The positions of stack and heat exchangers

The function of heat exchangers in a thermoacoustic engine is to transfer heat from an external source to the working fluid in the sealed resonator chamber and they are used to maintain the temperature gradient across the stack. The active heat exchange takes place between the working fluid and a series of closely spaced, parallel plates with their surfaces aligned with the direction of the wave propagation and positioned at either end of the stack. The heat exchanger should provide high heat transfer coefficient and low acoustic power dissipation to the thermoacoustic side. The hot heat exchanger supplies heat to hot end of the stack and ambient heat exchanger extracts heat from other end of stack. The blockage ratio is considered as same as that of stack so plate size and spacing used for heat exchanger is identical to that of stack for the present system. This allows the gas parcels to move freely from heat exchanger to stack. With the assumption of same heat transfer coefficient and temperature difference between solid plate and the working fluid, the hot heat exchanger requires more heat transfer area compared to ambient heat exchanger. So the length of hot heat exchanger is chosen as twice the length of ambient heat exchanger. The optimum PS (y_0) and length of heat exchanger (l_c), which is equal to the peak to peak displacement of the working gas is given by the following expression:[4,5]

$$y_0 = 2l\frac{a}{A}$$

(2)

$$l_c = \frac{P_0}{a\omega\rho_m}\sin(kl)$$

(3)

The blockage ratio, plate spacing and plate thickness are identical to the stack, in order to reduce the disturbance to gas oscillations. The heat transfer is more in hot heat exchanger, hence length is double that the length of cold heat exchanger.

2.5. Stack

It provides solid heat capacity and large cross sectional area to maintain a good thermal contact between gas and solid stacks. They are finely divided in small parallel channels with hydraulic radius comparable to thermal penetration depth. The stack is placed at a certain location in the resonator, where the magnitude of local acoustic impedance |Z| is larger than $\rho_g a/A$, because the magnitude of gas velocity amplitude is relatively small to reduce the viscous dissipation of viscous power. Acoustic impedance is defined as the ratio of complex pressure to volumetric flow rate. A good stack should minimize the ordinary heat conduction along temperature gradient and viscous dissipation of acoustic power. The minimum thickness of the stack plate should be $8\delta_s$, where δ_s is solid thermal penetration depth, which is defined as:[5]

$$\delta_s = \sqrt{\frac{2 \cdot K_s}{\rho_s c_s \omega}} \tag{4}$$

The above equation states that the thermoacoustic effects are optimal if the plate thickness is in the range of 6−8δs. The thermal penetration depth is defined as the layer around the stack plate where the thermoacoustic phenomenon occurs. It is measured perpendicular to the direction to the motion of gas and it gives approximately the distance that the heat can diffuse through the gas.[5]

By placing heat exchangers at either side of the stack, heat can be moved so that the temperature difference across the stack is created. As a result sound wave can be induced. In order to maximize the hydrodynamic heat flow, the stack material with large $K_s \rho_s c_s$ in comparison to $K_g \rho_g c_p$ is favorable. Successful operation of a standing wave engine requires an imperfect thermal contact between the gas and the stack which is obtained when the spacing between the plates is roughly two to four times of thermal penetration depth of gas. Viscous penetration depth is defined as the thickness of the layer of fluid around the stack plate that is restrained in its movement under the influence of viscous forces. Within this layer, viscous dissipation is responsible for the loss of kinetic energy, so that the fluid layer of thickness *dv* in the vicinity of each stack plate contributes less to the thermoacoustic effect.[5]

The expressions for the plate number for an array of parallel plates are obtained from the equation:[5]

$$n = \frac{R}{l + y_0} \tag{5}$$

The blockage ratio or porosity is defined as the ratio of area available to gas in the stack to the total area of the stack. It is expressed as:[5]

$$BR = \frac{y_0}{y_0 + l} \tag{6}$$

To reduce the negative effect on the performance a material of the stack must be chosen with a low thermal conductivity. On the other hand, we must take a heat capacity C_s larger than the heat capacity C_p of the working gas, so that the plate temperature can be considered steady.[1]

The thermal boundary layer there is a thinner viscous boundary layer defined as:[1]

$$\delta_v = \sqrt{\frac{2\eta}{\omega \rho_m}} \tag{7}$$

The thermal and viscous penetration depths ratio are related by the Prandtl number, describes the extension of the thermoacoustic effects expected from any chosen working fluid:[1]

$$\sigma = \left(\frac{\delta_v}{\delta_k}\right)^2 = \frac{\rho_m c_p v}{k} \tag{8}$$

A lower value for Prandtl number, characteristic of the inert gases, promotes thermoacoustic effects. For most gases (as air) is $\sigma \approx 2/3$. A mixture of the inert gases has also been used. For a mixture of Helium and Xenon $\sigma = 2$, the Prandtl number can be that small.[1]

Various geometric and material parameters of the thermoacoustic standing wave engine are concluded in table 1.

Table 1. Material and geometric parameters of stack

Material parameter	Geometric parameter
Thermal conductivity (K_s)	Length (L)
Density (ρ_s)	Stack centre position (x_s)
Specific heat (c_s)	Plate thickness (l)
	Plate spacing (y_0)
	Cross sectional area (A)

2.6. Resonator tube

The resonance tube is one of the key components of a thermoacoustic engine. A smooth, linear cylindrical resonator pipe without steps, misalignments and abrupt transitions should be used to avoid unwanted eddying or non-linear pressure variations that would greatly complicate the analysis. Resonance frequencies are mainly determined by the length of the resonator. Prolongation of resonance tube may leads to decrease of working frequency and increase of stacks hot end temperature with the same heating power. The velocity amplitude increases from the heater to the water cooler with a certain length of the resonance tube, because the heater is closer to the velocity node. On the other hand, when the resonance tube is prolonged, the relative location of the thermoacoustic core shifts nearer to the velocity node so the velocity amplitude in the thermoacoustic core decreases. For lowest dissipation, resonator should provide sufficient inertance and compliance, thereby maintaining resonance frequency, while simultaneously minimizing the acoustic power dissipation.[5]

3. Conclusion

The present work refers to few important aspects to be considered while designing the components of thermoacoustic system. Working gas should be selected by taking velocity of sound and density taking into consideration. The importance is given to thermal conductivity of heat exchanger material where as the geometrical shapes are similar to the stack so as to reduce obstacles to the movement of gas particle. The stack is designed by considering thermal and viscous penetration depth of material into account. The material of stack should have low thermal conductivity but high specific heat so as to achieve steady state temperature. The resonator length should be designed for minimum acoustic power dissipation.

Acknowledgements

References

[1]   Petr Novotny, Tomas Vit, Magda Vestfalova, Jose Lopes, standing-wave thermoacoustic engines, EPJ Web of Conferences 25, 01061, 2012.
[2]   Scott Backhaus and Greg Swift, new varieties of thermoacoustic engines, LA-UR-02-2721, 9th International Congress on Sound and Vibration, July 2002.
[3]   S. L. Zhu, G. Y. Yu, W. Dai, E. C. Luo, Z. H. Wu, X. D. Zhang, Characterization of a 300 Hz thermoacoustically driven pulse tube cooler, Cryogenics, 49, 51-54 (2009).
[4]   Ibrahim Girgin, Mehmet Turker, Thermoacoustic systems as an alternative to conventional coolers. Journal of Naval Science and Engineering, Vol.8, No.1, pp.14-32 (2012).
[5]   N.M. Hariharan, P. Sivashanmugam, S. Kasthurirengan, Influence of stack geometry and resonator length on the performance of thermoacoustic engine,Applied Acoustics 73,1052–1058 (2012).

Review of Fluid Pairs of Absorption Refrigeration Systems

Pratik Parmar[a,*] , Mitesh Shah[a], Vishal Singh[a]

[a]A. D. Patel Institute of Technology, New Vallabh Vidyanagar, Anand 388345, India.

Abstract

This paper provides the literature review with reference to refrigeration technologies based on absorption principle. Various configurations of Vapour Absorption Refrigeration (VAR) cycles are highlighted. A review of possible working pairs of refrigerant & absorbent is presented. Comparative analysis of various alternative working fluid pairs with the conventional pairs of refrigerant and absorbent is investigated.

Keywords: Absorption refrigeration, Working fluid pair, Absorbent.

Nomenclature	
COP	coefficient of performance
f	solution circulation ratio
LVHX	liquid vapour heat exchanger
Q	heat duty (kW)
SHX	solution heat exchanger
T,t	temperature
Subscripts	
$_{AB}$	absorber
$_{CO}$	condenser
$_{EV}$	evaporator
$_{G}$	generator
$_{H}$	high
$_{I}$	intermediate
$_{L}$	low
$_{W}$	cooling water

1. Introduction

In the vapour absorption refrigeration system, a physicochemical process replaces the mechanical process of the vapour compression refrigeration (VCR) system by using energy in the form of heat rather than mechanical work. The main advantage of this system lies in the possibility of utilizing waste heat energy from industrial plants or other sources and solar energy as the energy input. Absorption refrigeration has secured its place in commercial and industrial applications using waste heat. Unavailability of conventional fuels and cost of energy has incorporated its application also in residential sector. A small capacity system based on non conventional source of energy is best suited for any such usage.

The aim of this paper is to provide a basic understanding on the performance of a single-effect absorption refrigeration machine and review alternate fluid pairs. It is hoped that, this paper should be useful for any newcomers and researchers in this field of technology. This paper describes and evaluates the performance of an absorption refrigerator using various working fluid pairs.

1.1. Principle of operation of a single-effect absorption refrigeration cycle:

Consider a system containing two vessels connected to each other as shown in Fig 1(a). Inside the left vessel, there is a quantity of liquid refrigerant. The right vessel contains a binary solution of absorbent & refrigerant. The solution in the right

---

* Corresponding author. Tel.: +91-09624683648.
E-mail address: pratik248parmar@gmail.com

vessel will absorb refrigerant vapour from the left vessel. While the refrigerant vapour is being absorbed, the temperature of the remaining liquid refrigerant will reduce as a result of its vaporization. Refrigeration effect occurs inside the left vessel. At the same time the solution inside the right vessel becomes more diluted because of the higher content of absorbed refrigerant. This is called absorption process. On the other hand, when the refrigerant is absorbed until the solution cannot continue the absorption process; it must be separated out from the diluted solution. Heat is the key of the separation process. It is applied to the right vessel (Fig 1(b)) in order to expel the refrigerant from the solution. Transferring heat to the surrounding causes condensation of the refrigerant vapour. With these two processes, the refrigeration effect can be produced using thermal energy [1].
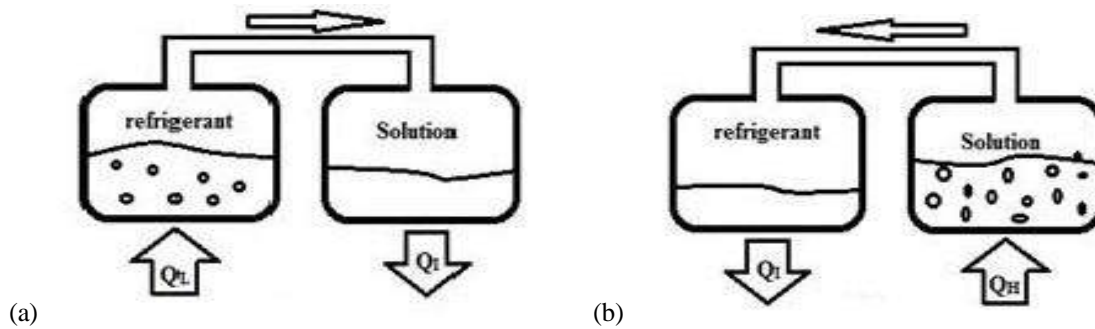
Fig. 1. (a) Absorption process occurs in right vessel causing cooling effect in the other; (b) Refrigerant separation process occurs in the right vessel as a result of additional heat from outside heat source.

A vapour absorption refrigeration system is a heat operated unit which uses refrigerant that is alternately absorbed by and liberated from the absorbent. The vapour absorption system uses heat energy, instead of mechanical energy as in vapour compression system, in order to change the condition of the refrigerant required for the operation of the refrigeration cycle as shown in Fig 2. In this system, the compressor is replaced by an absorber, a pump, a generator, and a pressure reducing valve. These components in the system perform the same function as that of compressor in vapour compression system. The vapour refrigerant from evaporator is drawn into an absorber where it is absorbed by the weak solution of refrigerant forming a strong solution. This strong solution is pumped to the generator where it is heated by utilizing heat energy. During the heating process, the vapour refrigerant is driven off by the solution and enters into the condenser where it is liquefied. The liquid refrigerant then flows into the evaporator through a pressure reducing valve and thus the cycle is completed.
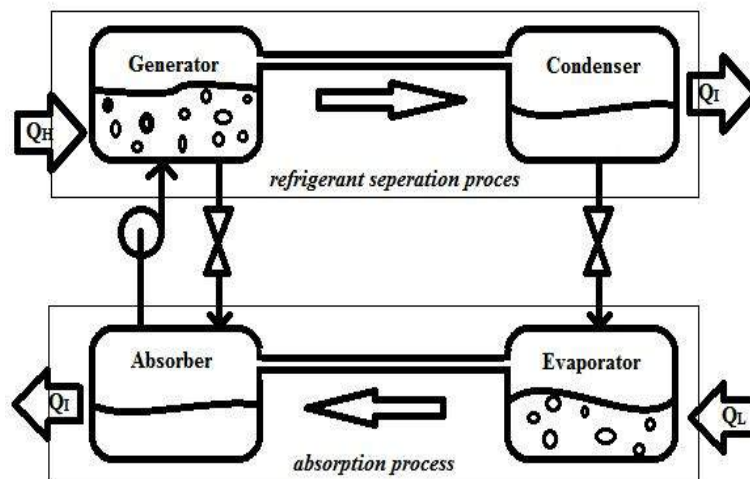
Fig. 2. A continuous absorption refrigeration cycle composes of two processes mentioned in the earlier figure.

As the separation process occurs at a higher pressure than the absorption process, a circulation pump is required to circulate the solution. Coefficient of Performance of an absorption refrigeration system is obtained from the ratio of cooling capacity obtained at evaporator to the total of heat input for the generator and work input for the pump.

The work input for the pump is negligible relative to the heat input at the generator; therefore, the pump work is often neglected for the purposes of analysis [1].

1.2 Various configurations of absorption refrigeration cycles:

Various design configurations available in the literature in context to absorption refrigeration systems are listed below. Srikhirim et al. [2] has provided a detailed review on all these absorption refrigeration cycles.

1. Single-effect absorption system
2. Absorption heat transformer
3. Multi-effect absorption refrigeration cycle
4. Absorption refrigeration cycle with GAX
5. Absorption refrigeration cycle with an absorber-heat-recovery
6. Half-effect absorption refrigeration cycle
7. Combined vapour absorption-compression cycle
8. Sorption-resorption cycle
9. Dual-cycle absorption refrigeration
10. Combined ejector-absorption refrigeration cycle
11. Osmotic-membrane absorption cycle
12. Self-circulation absorption system using LiBr/water
13. Diffusion absorption refrigeration (DAR) system

2. Working fluids for absorption refrigeration system :

2.1 Desirable characteristics of refrigerant-absorbent pair:

Some of the Desirable characteristics of refrigerant-absorbent pair for the absorption system are low viscosity to minimize pump work, low freezing point and good chemical and thermal stability. Irreversible chemical reactions of all kinds such as decomposition, polymerization, corrosion, etc. are to be avoided. A fundamental requirement of absorbent/refrigerant combination is that, in liquid phase, they must have a margin of miscibility within the operating temperature range of the cycle. The mixture should also be non-toxic and non-explosive.

In addition to these requirements, the followings are desirable,
- Solubility requirement: The refrigerant should have good solubility in the absorbent so that a strong solution highly rich in the refrigerant is formed in the absorber by the absorption of refrigerant vapour.
- Boiling points requirement: There should a large difference in the normal boiling points of the two substances, at least 200 ºC. So that, almost absorbent-free refrigerant is boiled off from the generator. If absorbent vapour goes with the refrigerant vapour to refrigerant circuit, the refrigeration produced will not be isothermal [3].

2.2 Available working pairs for absorption refrigeration:

Most common refrigerant-absorbent pairs for absorption refrigeration are NH_3-H_2O (ammonia - water) and H_2O-LiBr(water – lithium bromide). Some other available working fluid pairs are listed below.

1. H_2O – LiBr + Organic salts of sodium and potassium (formate, acetate and lactate)
2. H_2O – $LiNO_3$(Lithium Nitrate)
3. NH_3 – $LiNO_3$
4. NH_3 – NaSCN(Sodium Thiocyanate)
5. Monomethylamine – H_2O
6. R23(Trifluoromethane) – DMF(N, N-Dimethyl Formamide)
7. R134a(1,1,1,2-Tetrafluoroethane) – DMF
8. R134a – DMAC(N, N, Di Methyl Acetamide)
9. R134a – DMEU(Di Methyl Ethylene Urea)
10. R22(Chlorodifluoromethane) – DMEU
11. R32(Difluoromethane) – DMEU
12. R124(2-Chloro-1,1,1,2-Tetrafluoroethane) – DMEU
13. R125(Pentafluoroethane) – DMEU
14. R152a (1,1-Difluoroethane) – DMEU
15. TFE(Trifluoroethanol) – TEGDME (Tetraethylenglycol Dimethylether)
16. Methanol – TEGDME

2.2.1 Ammonia – water ($NH_3 – H_2O$):

Ammonia-water working pair has been in use since the 18th century and is one of the oldest working pairs. This pair of fluids can be used for the refrigeration application in the range from 5 ºC down to -60 ºC. Thus lower temperatures well below 0 ºC can be achieved easily using this pair. The preferred heat source temperature for ammonia-water equipment is from 95 ºC to 180 ºC. There is no risk of crystallization using this working pair as ammonia is completely soluble in water (at all concentrations). Absorption system using this pair operates at moderate pressure and no vacuum is required till -30 ºC. It can also be used for air-conditioning, but sometimes there are restrictions for use in building applications due to risks associated with the use of ammonia as it is both toxic and flammable. Another disadvantage of ammonia is incompatibility with materials such as copper or brass. For that reason, steel is normally used as the construction material for ammonia-water absorption equipment. Also, there is small temperature difference between the boiling points of ammonia and water which requires rectifier to obtain a high purity ammonia vapour which cools the vapour produced in the generator [2-3].

2.2.2 Water – Lithium Bromide ($H_2O – LiBr$):

Water-lithium bromide is one of the two most common working pairs. The advantages of this working pair include high safety, volatility ratio, affinity, stability and latent heat. Water is the refrigerant, which evaporates at very low pressures and produces the cooling effect. These systems operate under high vacuum pressures. Since water freezes at below 0°C, the minimum chilled water temperature in the absorption system with H_2O-LiBr is around 5°C. This is the reason why these systems are used for air-conditioning applications and cannot be used for low temperature refrigeration. H_2O-LiBr mixture is miscible if the LiBr mass fraction is lower than 70%, approximately. The LiBr crystallization occurs at moderate concentrations. The phase boundaries are usually included on the working fluid diagrams to remind on the proximity of the crystallization risk. The lithium bromide solution is corrosive to some metals used for construction of absorption equipment (i.e. steel or copper). Corrosion inhibitors can be used to overcome this problem. These additives protect the metal parts and can improve heat and mass transfer performance [2-3].

2.2.3 H_2O – LiBr + Organic salts of sodium and potassium:

Mixtures of lithium bromide and organic salts of sodium and potassium can be used as alternative absorbents with water as refrigerant for absorption refrigeration machines. The main objective is to overpass the limitations of lithium bromide and improve the characteristics and the efficiency of the refrigeration cycle. The major drawbacks of lithium bromide are the crystallization at high concentrations and the high temperature necessary in the generator to reach the boiling point of the lithium bromide solution, more than 90 ºC. Lithium bromide with organic salt mixtures namely sodium formate (CHO_2Na), potassium formate (CHO_2K), potassium acetate (CH_3CO_2K) and sodium lactate ($CH_3CH(OH)CO_2Na$) as an absorbent could show optimal properties.
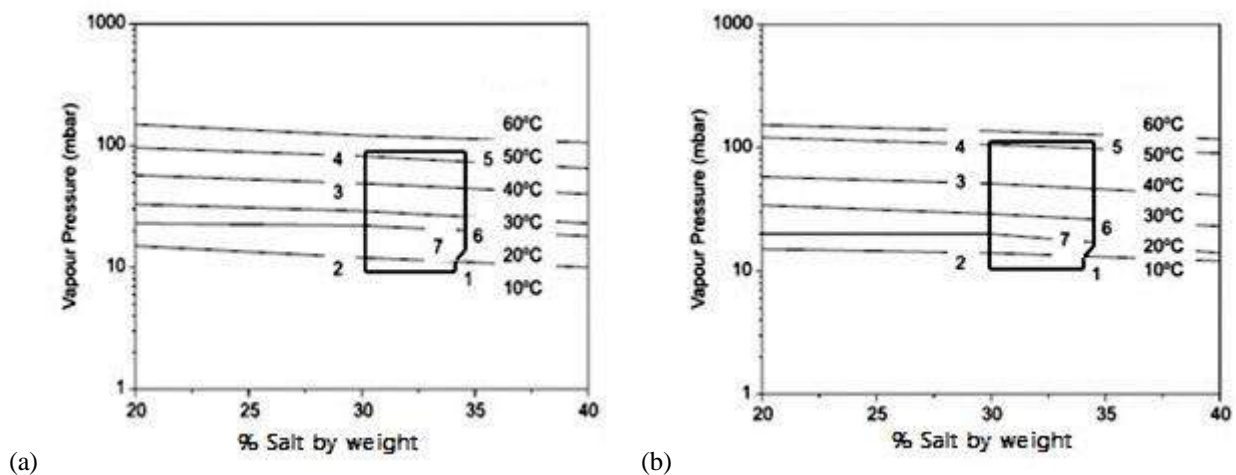
Fig. 3. (a) Absorption refrigeration cycle with LiBr:CHO_2Na=2:1 by mass ratio as absorbent; (b) Absorption refrigeration cycle with LiBr: CH_3CO_2K=2:1 by mass ratio as absorbent [4].

In Fig 3 points 1–7 represent the complete absorption refrigeration cycle. The heating requirements in the generator section can be dramatically decreased using this kind of mixtures, being enough using a waste stream with only a little more than 334.15 K to reach the boiling point of the diluted absorbent mixture. Other advantage of this new working fluid is the low temperature that can be reached without problems of salt crystallization in the absorber [4-5].

De Lucas et. al. [6] has carried out the absorption experiments of water vapour into the LiBr - CHO_2Na (sodium formate) and LiBr - CHO_2K (potassium formate) solutions containing 1000 ppm of n-octanol using an absorption column in order to examine their effect on mass transfer enhancement. The water vapour absorption capacity remarkably increases with the presence of n-octanol in all the studied working fluids. The LiBr + CHO_2Na (sodium formate) + 1000 ppm n-octanol solution at 45% by mass was confirmed to have a better absorption capacity than lithium bromide alone. De Lucas et. al. [7] has measured thermo physical properties (vapour pressure, density, and viscosity) of the (water + lithium bromide + potassium acetate) system $LiBr:CH_3COOK = 2:1$ by mass ratio and the (water + lithium bromide + sodium lactate) system $LiBr:CH_3- CH(OH)COONa = 2:1$ by mass ratio. The vapour pressures were measured in the ranges of temperature 293.15 K to 333.15 K and absorbent concentration from mass fraction 0.20 to 0.50. Densities and viscosities were measured at T = 293.15 to 323.15 K and from mass fraction 0.20 to 0.40.

2.2.4 Water – Lithium Nitrate (H_2O – $LiNO_3$):

Chunhuan et al. [8] has showed the application of H_2O – $LiNO_3$ working fluid in absorption heat pump systems and measured some of the thermo physical properties such as vapour pressure, specific heat capacity and specific enthalpy. Comparison of performances of an absorption heat pump cycle based on $LiNO_3$-H_2O and LiBr-H_2O showed that the cycle based on $LiNO_3$-H_2O has an advantage of 6.3 ℃ in the temperature grade of driving heat source against that based on LiBr-H_2O, while the COP based on $LiNO_3$-H_2O is just slightly higher than that based on LiBr-H_2O under the same operating conditions. The experimental results also show, when the mass concentration of $LiNO_3$ is greater than 36.5%, the molar dissolution heat of $LiNO_3$ is endothermic, which is contrary to that of LiBr.

Also study of the corrosion behavior of materials such as carbon steel and stainless steel 304 in LiBr and $LiNO_3$ solutions at 453.15 K temperature showed large reduction in corrosion thickness using $LiNO_3$ solutions. For these materials pitting corrosion is observed in LiBr solution, while no pitting corrosion is observed in $LiNO_3$ solution. As presented in Fig 4(a), the annual corrosion thickness of carbon steel in LiBr solution is 832.2 µm/a, which is about 150 times larger than that in $LiNO_3$ solution. Also from Fig 4(b) the same for stainless steel AISI 304 in LiBr solution is 14.5 µm/a, which is about 5 times larger than that in $LiNO_3$ solution. So, it can be said that the corrosiveness of $LiNO_3$ solution is less severe than that of LiBr solution [8].

(a)   (b)
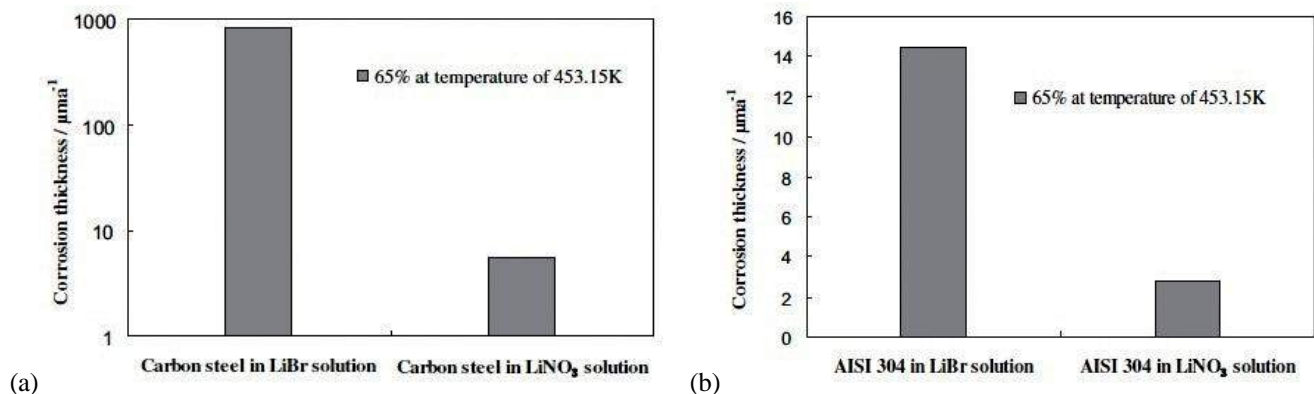
Fig. 4. Comparison of the corrosion behaviour of (a) carbon steel & (b) stainless steel 304 in LiBr and $LiNO_3$ solutions [8].

Jian et. al [9] carried out a cycle simulation for a single effect absorption heat pump with LiBr + $LiNO_3$ + H_2O (mole ratio of LiBr and $LiNO_3 = 4:1$) as a working fluid. Addition of 20 % $LiNO_3$ as an absorbent has enhanced the performance with higher level of COP, lower crystallization temperature, and less corrosiveness, which were basically required for an alternative to the LiBr + H_2O system. Also the experimental solubility of LiBr + $LiNO_3$ and LiBr were compared. Concentration of LiBr + $LiNO_3$ was about 3-8 % higher than LiBr in the temperature range of 0-90 ℃. Higher solubility of absorbent at the same temperature means less risk of crystallization in the absorption heat pump. A great extent of solubility enhancement of absorbent occurred by adding $LiNO_3$.

2.2.5 Ammonia – Lithium Nitrate (NH_3 – $LiNO_3$) and Ammonia – Sodium thiocyanate (NH_3 – NaSCN):

Several authors have studied absorption cycles with Ammonia-lithium nitrate and ammonia- sodium thiocyanate as the alternative working fluid in the past. Compared to conventional working fluids certain benefits have been reported by the authors [10-12].

Abdulateef et al. [10] has developed a computer simulation model to predict the performance of solar absorption refrigeration system using different working fluid. The model is based on detailed mass and energy balance and heat & mass transfer for the each system component. Ammonia-water, ammonia-lithium nitrate and ammonia-sodium thiocyanate systems were compared by plotting diagrams of COP and circulation ratio (f) at varying generator, condenser and evaporator temperatures. This showed that the performance for the NH_3-NaSCN and NH_3-$LiNO_3$ systems is better than that for ammonia-water cycle. However the improvement is not very remarkable but considering the fact that for NH_3-NaSCN and NH_3-$LiNO_3$ systems, no analysers and rectifiers are needed, these two cycles are suitable alternatives to the NH_3-H_2O system. The refrigeration system with ammonia-lithium nitrate can be operated at lower generator temperatures than the other two but, the main disadvantage of this mixture is high viscosity, which penalizes heat and mass transfer processes, especially in the absorber.

Absorption process was analyzed using a mathematical model in a bubble absorber with NH_3-H_2O, NH_3-$LiNO_3$ and NH_3-NaSCN as working fluids using a plate heat exchanger. The results show that NH_3-$LiNO_3$ working fluid obtained lower absorber thermal loads and lower absorbed vapour mass values than NH_3-H_2O and NH_3-NaSCN due to high solution viscosity that decreases the efficiency of the absorption process. While from Fig 5 it can be seen that NH_3-$LiNO_3$ obtained the highest COP value from a single effect absorption refrigeration system simulation at low generator temperature and NH_3-NaSCN obtained a higher COP than NH_3-H_2O [11].
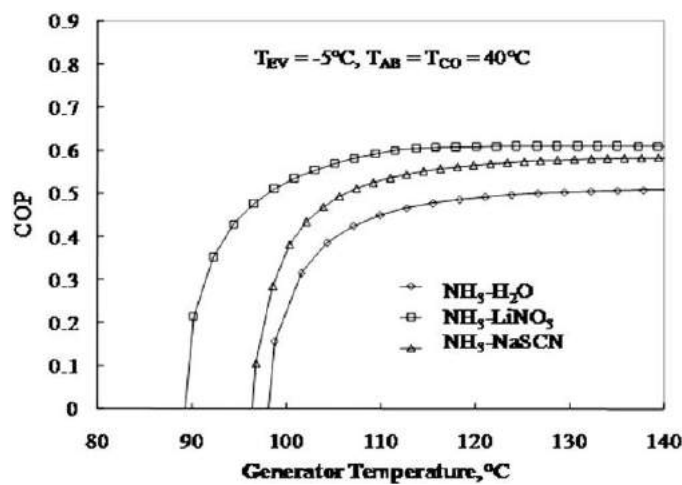
Fig. 5. Coefficient of performance as a function of T_G in a single effect absorption system [11].

Additionally, the effects on the COP of the system from adding the inert gas helium (He) or hydrogen (H_2) to these fluid pairs are studied. These pairs with inert gas were studied at different operating conditions and compared. The results showed that at different operating conditions these fluids presented different characteristics, however these working fluids were highly competitive among them and could be a future substitute for absorption cooling system [12].

2.2.6 Monomethylamine – water:

Romero et al. [13] has analyzed the performance of the monomethylamine – water vapour absorption refrigeration system. Comparative performance of monomethylamine – water working pair with the conventional NH_3-H_2O cycle has been studied as a function of generator temperature at different absorber and condenser temperatures. It showed that the COP values increase sharply until a maximum value is reached and after that the value diminishes smoothly on increasing the generator temperature and it also diminishes on increasing the condensation and absorption temperatures.

From Fig 6 it is observed that the higher values of COP for the monomethylamine-water system is found in the short range of generator temperatures between 63 ℃ and 80 ℃, with COP values from 0.35 to 0.51, these values are bigger than the corresponding ones in the NH_3-H_2O systems. The monomethylamine-water system is a good potential pair for refrigeration cycles for absorption which can be operated at lower generator temperatures that allows the use of heat sources like solar, geothermal, industrial waste or others. An additional advantage of monomethylamine-water system is lower vapour required pressures. This would allow slighter devices to require smaller wall thickness in the components of the system. Also due to normal boiling point of monomethylamine (-6 ℃) vacuum operation problems are avoided [13].

Pilatowsky et. al [14] presented theoretical thermodynamic simulation of a solar driven monomethylamine–water single-stage absorption refrigeration cycle for milk cooling purposes for the rural regions. The results showed that for the evaporator temperatures (-5 to 10 ℃), the monomethylamine–water pair is a good candidate for solar absorption

refrigeration systems. The theoretical coefficients of performance present moderate values at relative low generator and high evaporator temperatures and low absorber and condenser temperature values.
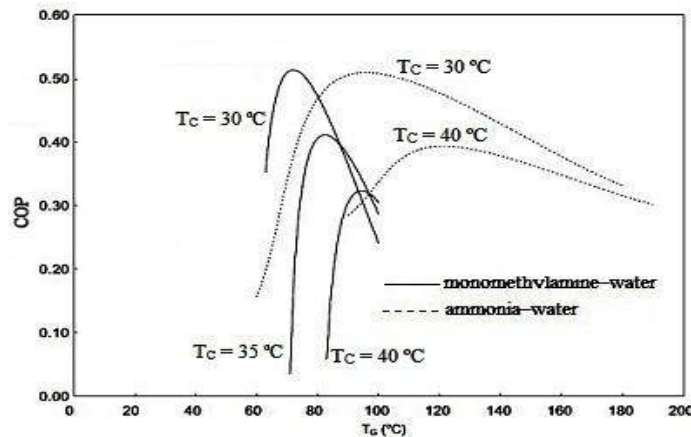
Fig. 6. COP for monomethylamine–water and ammonia–water solutions as a function of generator temperature at three different absorber and condenser temperatures (30, 35 and 40 °C for monomethylamine–water and 30, 40 °C for ammonia–water) [13].

2.2.7 Trifluoroethanol(TFE) – Tetraethylenglycol dimethylether(TEGDME) and Methanol – Tetraethylenglycol dimethylether(TEGDME):

Two organic fluid pairs TFE – TEGDME and Methanol – TEGDME have found applicability for absorption refrigeration system as refrigerant-absorbent mixtures. Cycles working with fluid mixtures TFE - TEGDME & Methanol - TEGDME were analyzed and compared with conventional ammonia – water system to show the effect of the generator temperature on the COP with vapour exchange double lift cycle for refrigerating applications driven by low grade thermal energy (70 – 100 °C). The double lift absorption cycle can operate in this range of heat source temperature with a COP of about 0.45 for TFE-TEGDME and Methanol - TEGDME, which is slightly higher than that for the working pair ammonia-water as presented in Fig 7 [15].
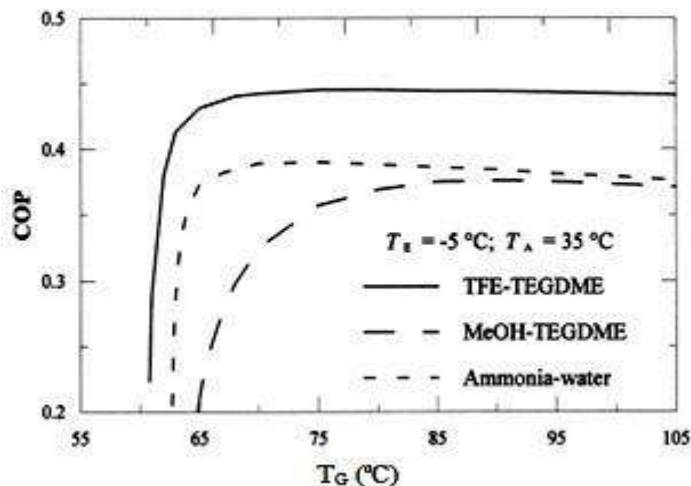
Fig. 7. Effect of T_G on COP for TFE – TEGDME, Methanol – TEGDME and ammonia – water system [15].

The COP of vapour exchange double lift cycle is better for the TFE-TEGDME fluid mixture with a minimum generator temperature of about 65 °C. The COP of Methanol – TEGDME, however, is best in the series-flow double lift cycle, but the circulation ratio per unit of refrigeration load is about twice, and the minimum generator temperature is 10 °C higher, than with TFE-TEGDME. The vapour exchange double lift cycle using TFE-TEGDME seems to be the better combination in terms of COP and the minimum temperature requirement for the operation of the system [15].

Long et al. [16] has numerically investigated the potential of TFE–TEGDME working fluid used in the diffusion absorption refrigeration system with two cooling mediums, viz. water (32 °C) and air (35 °C). Optimum generator temperature and corresponding COP were found for water cooled and air cooled system. Also the system performance was

compared with the same ammonia water system and it has been concluded that the TFE–TEGDME mixture is a good working fluid for the DAR cycle.

2.2.8 Refrigenrants R22, R32, R124, R125, R134a and R152a – Absorbent DMEU:

Jelinek et al. [17] has presented the performance of a single-stage triple pressure level (TPL) absorption cycle with different refrigerant–absorbent pairs. Four HFC refrigerants namely: R32, R125, R134a and R152a which are alternative to HCFC, such as R22 and R124, in combination with the absorbent dimethylethylenurea (DMEU) were considered. The highest COP and the lowest circulation ratio (f), were found as a function of the generator temperature for a given evaporating and cooling water temperatures. The highest maximum of COP was achieved with the solution R22-DMEU followed by R32-DMEU, R124-DMEU, R152a-DMEU and R134a-DMEU. The lowest generator temperature at maximum COP was achieved by R125-DMEU followed by R124-DMEU, R22-DMEU, R134a-DMEU, R32-DMEU and R152a-DMEU as shown in Fig 8(a).
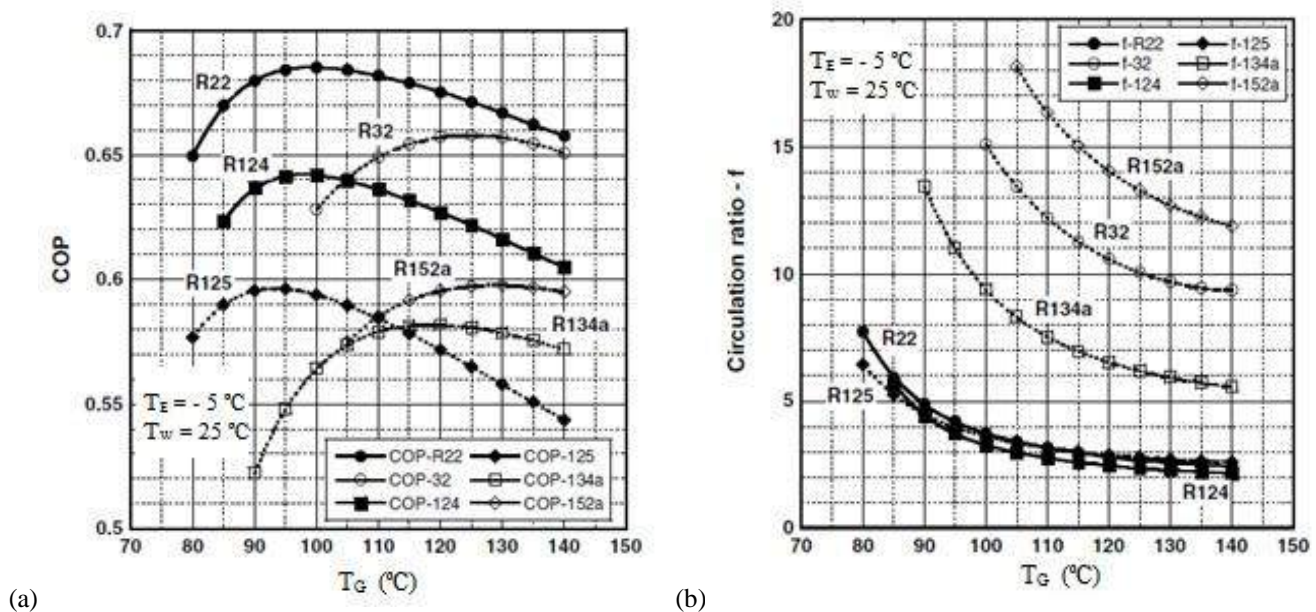
Fig. 8. Variation of (a) COP and (b) circulation ratio with generator temperature, for evaporator temperature of -5ºC and cooling water temperature of 25ºC [17].

Form Fig 8(b), the lowest circulation ratio was achieved by R124-DMEU followed by R22-DMEU, R125-DMEU, R134a-DMEU, R32-DMEU and R152a-DMEU. Based on this analysis, it was said that R124-DMEU is the preferable pair among the compared working fluids while among working fluids based on HFC the preferable pair is the R125-DMEU [17].

2.2.9 R23 – DMF:

Zanjun et. al. [18] has considered the R23 and DMF binary mixture as a promising new working fluid or part of new working fluid for the absorption cycle. The solubility of R23 in DMF was measured experimentally using an apparatus at various temperatures and pressures. The vapour pressures for the mixture R23 + DMF were also measured in the temperature range from (283.15 - 363.15) K and in the concentration range from (9.65 - 79.79) mass %. R23 with a high GWP (14,800) has a high impact in environment, but R23 still seems to be the most available one or one component of mixture refrigerants for the application below -40 ºC at present. This is based on the fact that it is much easier to find a suitable absorbent for R23. This work shows that the mixture (R23-DMF) might be a promising working pair for the absorption refrigeration cycle.

Also He and Chen [19] experimentally presented the application of R23 with R32 & R134a as a refrigerant and DMF as an absorbent. Refrigerating temperature of −47.2 ºC under the generating temperature of 163 ºC has been achieved. Results of experimental analyses have implied that these fluids can be used in the deep-freezing to obtain as low as −50 ºC temperature by utilizing low-potential thermal power.

2.2.10 R134a – DMAC:

Experiments have been carried out with R134a-DMAC as working fluid in the Single Stage Vapour Absorption Refrigeration System. An experimental set up of 1 kW capacity is designed and fabricated using R134a-DMAC as working fluid and hot water as heat input. Experimental studies on the developed system are performed to evaluate the effects of various operating parameters on the system performance. It is observed that sink temperature plays an important role in performance of the system. As the heat source temperature increases, heat quantities at generator, absorber, condenser and evaporator increase, while the circulation ratio decreases. Solution heat exchanger effectiveness, absorber effectiveness and generator effectiveness increase with increase in heat source temperature. At the sink and source temperatures of 20 and 80 ◦C respectively and a typical heat input of 4 kW, the system attained steady state in two hour. A steady evaporator temperature of about −4 ℃ is achieved. For the designed system and tested conditions an actual COP of 0.25 to 0.45 is attained [20].

Performance of R134a-DMAC working fluid is also investigated with half effect vapour absorption refrigeration cycle. Simulation studies on this system for solar energy based cold storage system showed the COP of about 0.35 - 0.46 for an evaporating temperature of -5 ℃ to 5 ℃ with a heat input at 70 ℃, absorber temperature at 25 ℃ and condensing temperature of 20 - 30 ℃. When compared to ammonia-water, R134a-DMAC gives a marginally higher COP in the half effect cycle at low heat source temperatures. From these, it was showed that the R134a-DMAC refrigerant absorbent combination may be considered as one of the most favorable working fluids when a half effect system is to be operated with low temperature heat sources [21].

Also Roy and Maiya [22] theoretically evaluated the performance of R134a–DMAC based VAR system with rectifier, SHX and LVHX. Efficient SHX has been found essential owing to its large heat duty. This liquid causes cooling loss with residual liquid in the evaporator which can be recovered significantly by using LVHX. Rectifier loses its importance if high efficiency LVHX is used.

2.2.11 R134a – DMF:

Experimental investigation has been carried out on the performance of compact generator of R134a/DMF based vapour absorption refrigeration system. The system uses brazed plate heat exchangers as generator, condenser, absorber, evaporator and solution heat exchanger and has a rated cooling capacity of 1 kW. The influence of driving temperature ratio, driving pressure ratio, R134a mass fraction and solution two phase Reynolds number is studied. This kind of system can be operated with low grade thermal energy such as solar energy, waste heat, etc. [23].
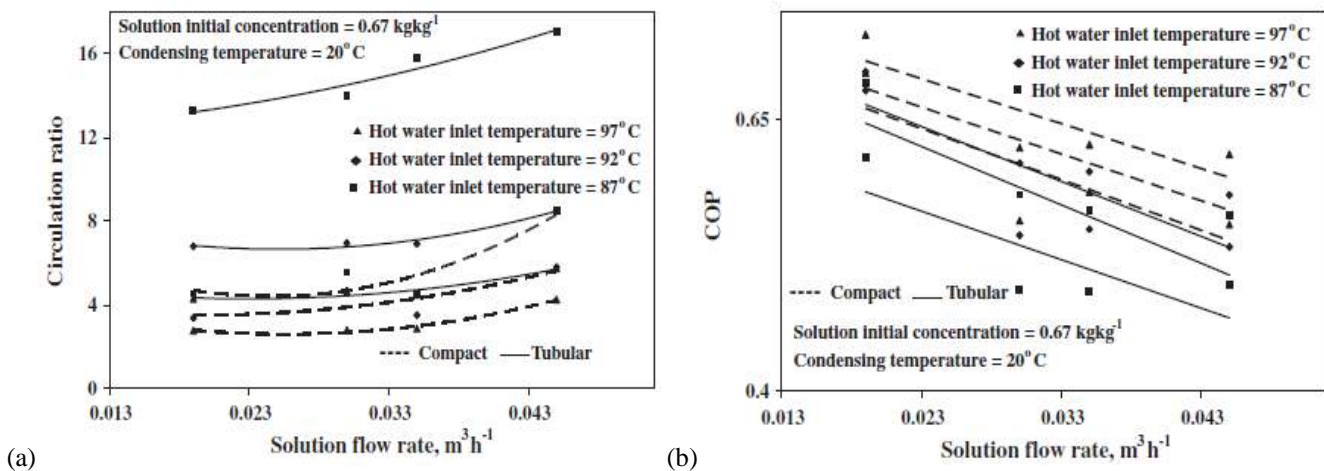
Fig. 9: Effect of solution flow rate on (a) circulation ratio and (b) COP for different hot water inlet temperatures [24].

Also, performance of compact generator and tubular generator using an R134a–DMF has been compared experimentally. Two types of generators, a brazed plate heat exchanger and stainless steel concentric tubes, are investigated. Form the investigated experimental results it has been concluded that the compact generator performed better than the tubular generator for the same operating conditions. It is clear from the Fig 9 that for compact generator higher COP is achieved with lower circulation ratio [24].

Suresh and Mani [25] carried out experimental investigations to study heat and mass transfer characteristics of R134a in DMF solution in a vertical glass absorber. Effect of operational parameters viz., gas flow rate, solution flow rate, solution initial concentration, solution pressure, solution temperature and cooling water flow rate on absorber performance was

analyzed. Absorption rate and heat transfer rate increase as the gas flow rate, solution flow rate, cooling water flow rate and solution pressure increase whereas they decrease as the solution initial concentration and solution temperature increase. Heat and mass transfer rates determined from the experiments were compared with numerical model developed by them and the agreement was fair. Suresh and Mani [26] have carried out experimental investigations to study heat and mass transfer characteristics of R134a in DMF solution in a compact bubble absorber of vapour absorption refrigeration system of 1 TR capacity. Plate heat exchangers have been used as system components. Circulation ratio, generator temperature and absorber temperature influence the absorber performance significantly. Heat and mass transfer effectiveness of absorber are better at lower circulation ratios and higher generator temperatures.

2.3 Newly proposed absorbent properties:

In past various experimental and simulation studies has been performed with new working fluids for the absorption refrigeration. Some of these newly proposed absorbents are needed to be studied for the human hazard possibilities while handling for their application.

Exposure of these absorbents may be harmful to human health. Such certain effects and properties of absorbents DMF, DMAC, DMETEG and DMEU are tabulated in Table 1. This data has been gathered from the various MSDS of these fluids [27-34].

Table 1. Properties of new absorbents [27-34]

Properties	DMF	DMAC	DMETEG	DMEU
Chemical Name	N, N, Di Methyle Formamide	N, N, Di Methyl Acetamide	Di Methyl Ether Tetra Ethylene Glycol	Di Methyl Ethylene Urea
Appearance	Colorless	Colorless to pale yellow	Colorless	Colorless
Boiling Point (ºC)	153	165	276	225.5
Freezing Point (ºC)	-60.4	-20	-30	8
Density (Kg/m^3)	944	940	1009	1040
Eye Iritation	Yes	Yes	Yes	Yes
Skin irritation	Less	Less	May be	Yes
Inhalation	Respiratory tract irritation, Dizziness, Nausea, Abdominal pain, Vomiting, etc.	Respiratory tract irritation	Respiratory tract irritation	Respiratory tract irritation
Ingestion	Irritate the gastrointestinal tract and above mentioned.	Toxic	Digestive tract disturbances	Harmful
Sensitive	Hygroscopic (store under nitrogen)	Mildly Hygroscopic	Hygroscopic	Hygroscopic (store under inert gas)

3. Conclusion

The paper provides the fundamental principles of the absorption refrigeration system with available design configurations. Sixteen different refrigerant absorbent pairs are presented in this paper. Comparative performance evaluation of these newly proposed pairs is explained.

Also these fluid pairs are compared with conventional working fluid NH_3 - H_2O and LiBr - H_2O cycles for the same operating conditions. Most of the alternate fluid pairs have found to be competitive with the conventional ones. Yet all of these pairs lack for systematic availability of the thermo-physical properties at different pressures, temperatures and concentrations such as Specific enthalpy, Specific heat capacity, Dynamic viscosity, Thermal conductivity, etc.

Moreover, Toxicity and human hazards characteristics of many of the suggested alternative pairs cannot be neglected. Effects of such fluids on human health are tabulated in the table. Risk involved in the handling and operation of any such fluid has also prevented its applicability as a working fluid of absorption refrigeration.

Though most of the new working fluids have found to be the alternative to conventional LiBr-H_2O and NH_3-H_2O, it is not suggested for any specific pair to be the most promising working fluid. Any newcomer in this field can study conventional fluid pairs for the design and analysis purpose as their thermo-physical properties are very well available in the literature.

However for an existed single effect system H_2O – Libr + Organic salts of sodium & potassium may be alternate to H_2O – Libr only and NH_3-$LiNO_3$ may be used in place of NH_3-H_2O for lower generator temperature requirements. Also among compared fluid pairs for TPL absorption system R125 – DMEU could be the promising fluid.

References

[1] Aphornratana S, Sriveerakul T, 2007, Experimental studies of a single-effect absorption refrigerator using aqueous lithium–bromide: Effect of operating condition to system performance, Experimental Thermal and Fluid Science 32, p. 658.

[2] Srikhirim P, Aphornratana S, Chungpaibulpatana S, 2001, A review of absorption refrigeration technologies, Renewable and Sustainable Energy Reviews, p. 342.

[3] Arora CP., 2008, Refrigeration and Air conditioning, 2nd Edn, Tata McGraw Hill Publishing Company, India.

[4] Donate M, Rodriguez L, Lucas A.D, Rodriguez J.F, 2006, Thermodynamic evaluation of new absorbent mixtures of lithium bromide and organic salts for absorption refrigeration machines, International Journal of Refrigeration 29, p. 30.

[5] De Lucas A, Donate M, Molero C, Villasenor J, Rodriguez J, 2004, Performance evaluation and simulation of a new absorbent for an absorption refrigeration system, International Journal of Refrigeration 27,p. 324.

[6] De Lucas A, Donate M, Rodriguez J, 2008, Applying surfactants to improve the absorption capacity of mixtures of lithium bromide and formates in absorption refrigeration coolers, International Journal of Refrigeration 31, p.1073.

[7] De Lucas A, Donate M, Rodriguez J, 2006, Vapour pressures, densities, and viscosities of the (water + lithium bromide + potassium acetate) system and (water + lithium bromide + sodium lactate) system, J. Chem. Thermodynamics 38, p.123.

[8] Chunhuan L, Qingquan S, Wanliang M, 2013, Thermophysical properties and application of $LiNO_3$-H_2O working fluid, International journal of refrigeration, p. 1.

[9] Jian S, Lin F, Shigang Z, Qingquan S, Wanliang M, 2010, Performance calculation of single effect absorption heat pump using LiBr + $LiNO_3$ + H_2O as working fluid", Applied Thermal Engineering 30, p. 2680.

[10] Abdulateef J.M, Sopain K, Alghoul M.A, Sulaiman M,Y, Zaharim A, Ahmad I, 2007, Solar absorption refrigeration system using new working fluid pairs, International journal of Energy 3, p. 82.

[11] Cerezo J, Best R, Romero R.J, 2011, A study of a bubble absorber using a plate heat exchanger with NH_3 - H_2O, NH_3 - $LiNO_3$ and NH_3 - NaSCN, Applied Thermal Engineering 31, p. 1869.

[12] Acuna A, Velazquez N, Cerezo J, 2013, Energy analysis of a diffusion absorption cooling system using lithium nitrate, sodium thiocyanate and water as absorbent substances and ammonia as the refrigerant, Applied Thermal Engineering 51, p. 1273.

[13] Romero R, Guillen L, Pilatowsky I, 2005, Monomethylamine–water vapour absorption refrigeration system, Applied Thermal Engineering 25, p. 867.

[14] Pilatowsky I, Rivera W, Romero J.R, 2004, Performance evaluation of a monomethylamine–water solar absorption refrigeration system for milk cooling purposes, Applied Thermal Engineering 24, p. 1103.

[15] Medrano M, Bourouis M, Coronas A, 2001, Double-lift absorption refrigeration cycles driven by low temperature heat sources using organic fluid mixtures as working pairs, Applied Energy 68, p. 173.

[16] Long Z, Luo Y, Li H, Bu X, Ma W, 2013, Performance analysis of a diffusion absorption refrigeration cycle working with TFE–TEGDME mixture, Energy and Buildings 58, p. 86.

[17] Jelinek M, Levy A, Borde I, 2008, The performance of a triple pressure level absorption cycle (TPLAC) with working fluids based on the absorbent DMEU and the refrigerants R22, R32, R124, R125, R134a and R152a, Applied Thermal Engineering 28, p. 1551.

[18] Zanjun G, Yingjie X, Peng L, Xiaolong C, Xiaohong H, Wang Q, Guangming C, 2012, Solubility of refrigerant trifluoromethane in N,N-dimethyl formamide in the temperature range from 283.15 K to 363.15 K, International journal of refrigeration 35, p. 1372.

[19] He Y, Chen G, 2007, Experimental study on an absorption refrigeration system at low temperatures, International Journal of Thermal Sciences 46, p. 294.

[20] Muthu V, Saravanan R, Renganarayanan S, 2008, Experimental studies on R134a-DMAC hot water based vapour absorption refrigeration systems, International Journal of Thermal Sciences 47, p. 175.

[21] Crepinsek Z, Goricanec D, Krope J, 2009, Comparision of the performances of absorption refrigeration cycles, WSEAS Transactions on Heat and Mass Transfer 3, p. 65.

[22] Roy S, Maiya M.P, 2012, Analysis of R134a–DMAC vapour absorption refrigeration system with add-on components, International Journal of Sustainable Built Environment 1, p. 26.

[23] Balamurugan P, Mani A, 2012, Heat and mass transfer studies on compact generator of R134a/DMF vapour absorption refrigeration system, International journal of refrigeration 35, p. 506.

[24] Balamurugan P, Mani A, 2013, Comparison of compact and tubular generators performance for R134a–DMF, Experimental Thermal and Fluid Science 45, p. 54.

[25] Suresh M, Mani A, 2012, Experimental studies on heat and mass transfer characteristics for R134aeDMF bubble absorber, International journal of refrigeration 35, p. 1104 .

[26] Suresh M, Mani A, 2013, Heat and mass transfer studies on a compact bubble absorber in R134a-DMF solution based vapour absorption refrigeration system, International journal of refrigeration 36, p. 1004.

[27] Material safety data sheet of Dimethyl formamide, ScienceLab: Chemicals & Laboratory Equipment, May 2013.

[28] Material safety data sheet of Dimethyl formamide, Fisher scientific India, June 2007.

[29] Material safety data sheet of N, N, Dimethylacetamide, ScienceLab: Chemicals & Laboratory Equipment, May 2013.

[30] Material safety data sheet of N, N, Dimethylacetamide, Fisher scientific India, December 2006.

[31] Material safety data sheet of Dimethyl EtherTetraethylene Glycol, Mathesongas USA, December 2008.

[32] Material safety data sheet of Dimethyl EtherTetraethylene Glycol, Fisher scientific India, July 2009.

[33] Material safety data sheet of Di Methyl Ethylene Urea, Fisher scientific India, December 2011.

[34] Material safety data sheet of Di Methyl Ethylene Urea, Spectrum chemicals and laboratory products, September 2008.

Secondary and Tip Clearance Flows: study and analysis of their behaviour in an axial linear turbine cascade – A review

U J Patdiwala[a]*, P K Shah[b]

[a]Research Scholar, KSV University, Gandhinagar 382015, India
[b]Professor, SAL College of Engineering, Ahmedabad 38006,0 India

Abstract

The problem that arises in the aerodynamic design and the performance of an axial flow turbine is the prediction and analysis of behaviour of secondary flows and tip clearance flows. Most of the studies reviewed and deal with plane or annular cascade flows. Also the effect of tip clearance is not covered. The basic secondary flow and tip clearance phenomena for a linear turbine cascade, as measured and verified by a many of researchers is described in this paper. Sieverding has given a review of secondary flow literature and its analysis around 1985. Recent work that shows refined secondary flow vortex structures is also examined. A flow parameter based on inlet boundary layer properties used to predict horseshoe vortex is presented. Work on secondary flow and tip clearance loss reduction, containing endwall fences and endwall profiling is briefly reviewed. The identification of flow structures and the accurate quantification of the secondary flows are essential for the investigation of the physical mechanisms. This paper presents the review and survey of literature on secondary and tip clearance flow loss investigations and their various methods to improve the turbine performance. It is concluded that accurate routine prediction of these flow losses has not yet been achieved, and must await either a better turbulence model or more experiments to reveal new endwall loss production mechanisms.

Keywords: linear axial turbine; blade cascade; secondary flow; tip clearance flow

Nomenclature

n	normal coordinate
p	pressure
P_0	total pressure
R	streamline curvature radius
v	velocity
Y_{local}	local pressure loss coefficient
ρ	density
$_{1,2}$	suffix

1. Introduction

Flow in turbines is highly complex and three dimensional. The complexity and three-dimensionality is due to three dimensional blading, interaction of boundary layer with blade leading edge, secondary flows formation, tip clearances vortex, corner vortex and boundary layer development on the end walls as well as in blade passages. Most important among these are secondary flows, and tip clearance flow. A good understanding of secondary flow physics and their associated losses help turbine designer to improve efficiency and aerodynamic performance of turbine to a certain level. Hence in axial turbines, the need for understanding of secondary flows and its reduction are significant and ever increasing in the modern era.

The basic structure of secondary flow within a turbine is well understood and consists of four major vortices viz. the passage vortex (PV), two legs of the horseshoe vortex, ahead of blade leading edge and a counter vortex located towards the end of suction surface of blade, also known as endwall corner. The study of phenomenon of secondary flow is found in Sieverding and Langston and reported various developments.

---

* Corresponding author. Tel.: +919925518974
E-mail address: umangpatdiwala@gmail.com

1.1 Secondary Flow

The secondary flows originate from specifically developing endwall boundary layers ahead of turbine blade leading edge and are associated with the presence of longitudinal vortices with a dominant streamwise component of the vorticity. They are driven by transverse static pressure gradients and mass forces acting on fluid elements in curvilinear motion through the blade-to-blade passage. The secondary flows also modify the shape of endwall boundary layers from which they originate. The problem of endwall flows, especially secondary flows, is discussed in this paper. The picture of endwall flows in turbine blade-to-blade passages is extremely complex, dominated by the presence of secondary flows. There are a number of secondary flow models documenting the progress in our understanding of the secondary flows over the years. Some of these models are briefly presented here in Fig 1 (a) to Fig 1 (c). The main type of secondary flow is the induced recirculating flow, which leads to the formation of a passage vortex. The source of the induced recirculating flow is the cross flow in the endwall boundary layer that forms as a result of force equilibrium in curvilinear motion. The momentum equation in the cross-stream direction can be written in the form

$$\rho\, v^{2}/\, \partial p\,/\, \partial n \qquad\qquad\qquad\qquad (1)$$

With a decrease of the velocity in the boundary layer, a reduction of the streamline curvature radius in the boundary layer flow is required in order to balance the pitch-wise pressure gradient formed in the channel. As a consequence, the boundary layer flow is turned more than the main flow in the blade-to-blade channel, leading to a crossflow from the pressure to suction surface in the endwall boundary layer. A compensating return flow must then occur at a certain distance from the endwall, giving rise to the recirculating flow described by Langston (1980), Sharma and Butler (1987) and Goldstein and Spores (1988), which can be seen in Fig. 1. From this recirculating flow, a passage vortex is formed. Downstream in the blade-to-blade passage, due to the pressure-to-suction side pressure difference, the passage vortex locates near the blade suction surface. As a result of the recirculating flow in the neighbouring blade-to-blade passages, a vortex layer is formed at the trailing edge, which is quickly rolled-up downstream into a shed trailing edge vortex.
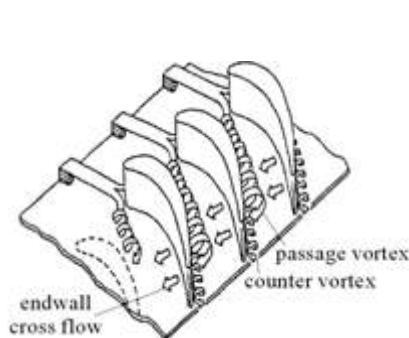
Fig.1(a)–secondary flow model of Langston (1980)   Fig.1 (b) – secondary flow model of Sharma and Butler (1987)
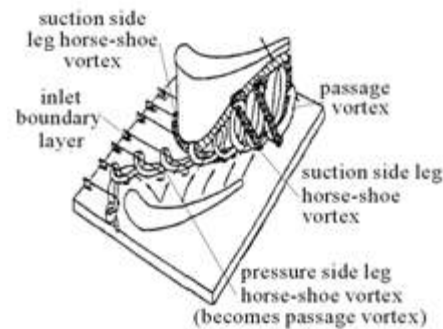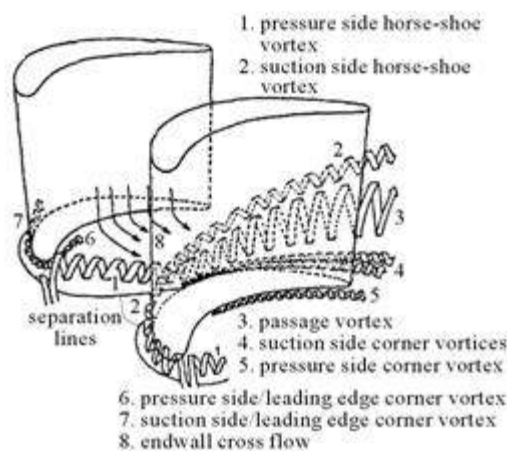
Fig.1. (c) – secondary flow model of Goldstein and Spores (1988),

Another element of secondary flows is a horse-shoe vortex. The process of formation of the horse-shoe vortex upstream of the leading edge and its downstream transport was explained by Langston et al. (1980), Marchal and Sieverding (1977). The model illustrated in Fig. 2 comes from the paper by Marchal and Sieverding (1977). The boundary layer fluid upstream of the leading edge is decelerated by the adverse pressure gradient and separates at a saddle point S1. The boundary layer fluid elements form a reverse recirculating flow just before the leading edge. This reverse flow separates at another saddle point S2. The upstream boundary layer rolled-up in the recirculating zone flows past the leading edge and is transported downstream in two legs – pressure-side and suction-side leg of the horse-shoe vortex. The suction-side leg of the horse-shoe vortex moves near the suction surface of the blade. The pressure-side leg subject to the pressure gradient towards the suction surface moves across the blade-to-blade passage towards this surface. The legs of the horse-shoe vortex move along the lift-off lines that are lines of the saddle points as illustrated in Fig. 2. The location of the horse-shoe vortex lift-off lines, especially that of the pressure-side leg depends on the load of the front part of the blade. All main forms of secondary flows meet at the suction surface of the blade. The model that explains the transport of the horse-shoe vortex, where the pressure-side leg of the horse-shoe vortex together with the endwall cross flow form the main recirculating flow and the resulting passage vortex, whereas the suction-side leg of the horse-shoe vortex stays apart counter-rotating with respect to the passage vortex, comes from the work of Langston (1980).
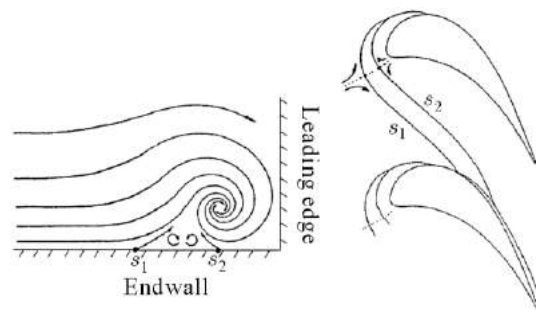
Fig. 2. Separation of the endwall boundary layer upstream of the blade leading edge and formation of the horse-shoe vortex- model given by Marchal and Sieverding (1977)

1.2 Tip clearance flow
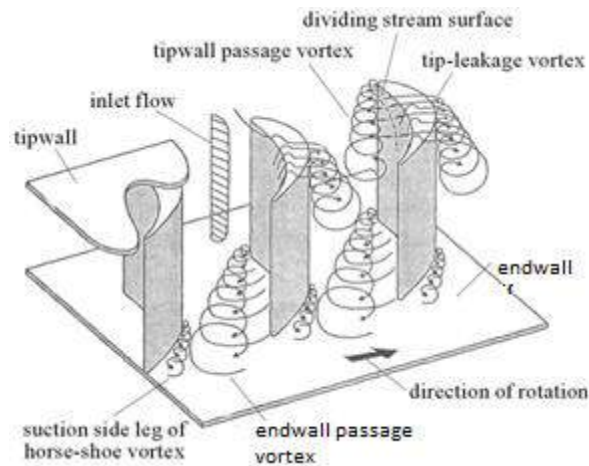
Fig 3. Tip leakage and passage vortices at the tip endwall with a clearance, Sjolander (1997)

The tip region above the leading edge of the blade is divided into two streams aiming towards low pressure regions at the suction surfaces of the neighbouring blades – a main stream of the tip leakage flow going through the tip gap over the blade and a stream of cross-flow going across the blade-to-blade passage. The tip leakage flow leaving the tip gap separates from the endwall under conditions of adverse pressure gradient and forms a tip leakage vortex. The cross-flow blocked by the development of the tip leakage vortex also separates from the endwall and rolls up into a passage vortex. The stream dividing line between the tip leakage and cross-flow lies at the pressure side of the blade tip. The tip leakage and passage vortices are characterised by the opposite sense of rotation. The relations between the circulation and size of the two structures depend on many factors such as the tip gap size and flow turning angle etc.

2. Secondary and Tip clearance loss sources

Secondary flows and tip clearance are an important source of losses in turbines, especially in cascades with short-height blading and high flow turning in the blade passages. Due to the complex nature of endwall boundary layer flows and secondary flows, the evaluation of endwall losses is not an easy task.   The secondary flow and tip clearance loss regions are given by Sieverding, (1985) and Gregory-Smith, (1997) which are as follows:
• Formation of the inlet boundary layer upstream of the blade leading edge
• Formation of the boundary layer downstream of the horse-shoe vortex lift-off lines
• Shear effects along the horse-shoe vortex lift-off lines, separation lines and along dividing surfaces between the passage vortex, other vortices, main flow and blade surfaces, especially at the suction surface of blade trailing edge

The processes of mixing due to secondary and tip clearance flows are usually not accompli- shed in the blade row where they originate and are continued in the downstream blade-to-blade passages. Considerable non-uniformities in the distribution of magnitude and direction of the velocity at the inlet to the subsequent blade row may lead to local separations and upstream relocation of the laminar- turbulent transition at the blade in the secondary flow dominated region. The most decisive for the level of secondary and tip clearance losses are the blade span-to-chord ratio, flow turning in the cascade and inlet boundary layer thickness, which is accounted for in all experiment-based loss correlations for turbine cascades as given by Craig and Cox (1971), Traupel (1977). In the correlation of Traupel, the endwall losses are reversely proportional to the span-to-chord ratio in the blade span range in which there is no interference between secondary flow vortices from the opposite endwalls. For short blades this corelation is more complex. The endwall losses increase with the increased flow turning and increased inlet boundary layer thickness.

The secondary and tip clearance loss coefficient is calculated as the difference between inlet total pressure (P_{01}) and local total pressure (P_{02}) at each location downstream of the cascade, non-dimensionalised with the dynamic pressure based on pitch and spanwise mass averaged velocity.

$$Y_{Local} = 2\left(P_{01} - P_{02}\right)\Big/\left(\rho v_2{}^2\right)$$

$$(2)$$

3. Method of reduction of secondary and tip clearance losses

3.1 Endwall fences

The endwall fences effectively prevent the movement of the flow field in the end wall region. At the leading edge, the flow field splits into two sections and moves either side of the blade. Fences prevent the movement of pressure side leg of horseshoe vortex towards the suction side, and effectively reduce the influence of passage and corner vortex on the flow near the end wall region. Kawai et al. [1989] have done few experiments on measurement of total pressure losses. They have suggested that the fences were most effective when the height of the fence is 1/3 of the inlet boundary layer thickness and located half a pitch away from the blades as shown in fig.4 . The size of loss core is reduced when streamwise fence are attached. The streamwise fence reduced the total pressure losses within the boundary layer. The total pressure loss is reduced by 15%, 25% for fences heights of 12 mm and 16 mm respectively as suggested by Govardhan et al. [2010]

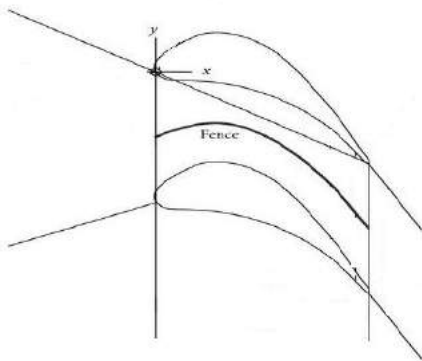
Fig. 4 Arrangement of stremwise fence
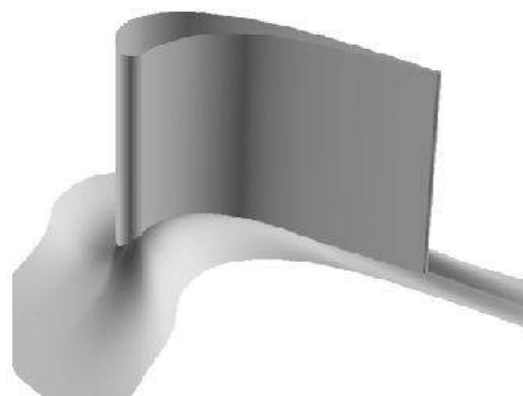
Fig. 5 Endwall profiling

3.2 Endwall profiling

Ingram, G. L. et al. described the design and testing of a profiled end wall geometry for a low-speed linear turbine cascade as shown in fig. 5, they showed a reduction in overall loss of secondary and tip clearance flows. Non-axisymmetric endwall profiling works by reducing the cross passage pressure gradient at the endwall by means of streamline curvature. This reduced pressure gradient then results in less secondary flow and therefore loss. Endwall profiling also has the general effect of keeping the secondary loss and flow much closer to the endwall. Profiled endwalls have been shown to reduce secondary flow loss by 31 percent approximately.

4. Conclusions

The formation of endwall flows and evolution of vorticity from the endwall boundary layers was explained in the paper. Several models of secondary flows in turbine cascades were presented.

End wall losses are reduced by the boundary layer fences due to weakening of the cross flow. Fences effectively reduce the strength of the large loss core and resulting in lesser aerodynamic loss in the turbine passage. In overall, it could be concluded that fences reduce the secondary losses and improve the turbine cascade performance nearly by 15-20%. Also overturning in the flow is reduced by various heights of fences.

Endwall profiling also has the general effect of keeping the secondary loss and tip clearance flow much closer to the endwall. Profiled endwalls have been shown to reduce secondary losses as well as tip clearance losses.

Table 1. Comparison of the various models

Type of Flow	Model-1	Model-2	Model-3
Secondary flow	Langston Model Leading edge horse shoe vortex generation theory	Sharma and Butler Model Horse shoe vortex becomes passage vortex	Goldstein and Spores Model Pressure side and suction side horse shoe vortex formation
Tip Clearance flow	Sjolander Model Recalculating flow issues like a jet of vortex in tip gap	Siverding Model Difference of pressure between pressure surface and suction surface develops counter vortex towards suction surface	Kawai et al Model 1/3 height of the fence are effective to reduce tip clearance losses in turbine blade passage
Reduction in the Secondary and Tip Clearance flow losses	Govardhan Model Streamwise fences are capable to reduce the flow losses	Ingram, G. L Model The effect of end-wall profiling of blade reduce the pressure losses	Jiaqi Luo et al. Model Secondary Flow Reduction by Blade Redesign and Endwall Contouring

5. References

[1] Sieverding, C. H. Recent progress in the understanding of basic aspects of secondary flows in turbine blade passages. ASME J. Engng Gas Turbines Power, 1985, 107, 248 – 252.

[2] Moore, H. and Gregory-Smith, D. G. Transition effects on secondary flows in a turbine cascade. ASME paper 96-GT-100, 1996. 28. Sjolander S.A., 1997, Secondary and tip-clearance flows in axial turbines,VKI LS 1997-01

[3] Eckerle W.A., Langston L.S., 1987, Horseshoe vortex formation around a cylinder, Trans. ASME, J. Turbomachinery, 109, 278-2868. Goldstein R.J., Spores R.A., 1988, Turbulent transport on the endwall in the region between adjacent turbine blades, Trans. ASME, J. Heat Transfer,

[4] Traupel W., 1977, Thermische Turbomaschinen, Band I, Springer-Verlag, Berlin 1. Craig H.R.M., Cox H.J.A., 1971, Performance estimation of axial flow turbines, Proc. Inst. Mech. Eng., 185, 32/71, 407-424

[5] Gregory-Smith, D. G., Ingram, G., Jayaraman, P., Harvey, N. W., and Rose, M. G. Non-axisymmetric turbine end wall profiling. In Proceedings of the 4th European Conference on Turbomachinery, Florence, March 20 – 23, 2001, pp. 653 – 664.

[6] Ingram, G. L., Gregory-Smith, D. G., Rose, M. G., Harvey, N. W., and Brennan, G. The effect of end-wall profiling on secondary flow and loss develop-ment in a turbine cascade. ASME paper GT-2002-30339, 2002.

[7] Ingram, G. L. Endwall profiling for the reduction of secondary flow in turbines, PhD Thesis, University of Durham, 2003.

[8] Govardhan, M., Rajender, A., and Umang, J. P., (2006), " Effect of streamwise fences on secondary flows and losses in a two-dimensional turbine rotor cascade" Journal of Thermal Science 15, 296-305.

[9]Gregory-Smith D.G., 1993-2002, Durham low-speed turbine cascade, Turbo-machinery workshop test case No. 3, Proc. ERCOFTAC Seminar and Workshop on Turbomachinery Flow Prediction, I-VIII

[10] Sharma O.P., Butler T.L., 1987, Prediction of endwall losses and secondary flows in axial flow turbine cascades, Trans. ASME J. Turbomachinery, 109, 229-236

[11] T. Suthakar, Akash Dhurandhar, 2012, "Numerical Investigation of Secondary Flow In An Axial Flow Compressor Cascade" International Journal of Computational Engineering Research IJCER, Vol. 2, Issue No.3, 647-656

[12] Govardhan, M., Promodkumar Maharia, 2010, "Secondary Loss Reduction by Streamwise Fences in a Reaction Turbine Cascade" The 7th Jordanian International Mechaincal Engineering Conference (JIMEC'7) Amman, Jordan

[13] Jiaqi Luo, Juntao Xiong, Feng Liu and Ivan McBean, 2010 "Secondary Flow Reduction by Blade Redesign and Endwall Contouring using an Adjoint Optimization Method", Proceedings of ASME Turbo Expo 2010: Power for Land, Sea and Air GT2010, Glasgow, UK

Replacement of R22 to manage lifetime operation of HCFC based equipments

Nimesh Gajjar[a], Dr N M Bhatt[a]

[a]Gandhinagr Institute of Technology, Moti Bhoyan-382721, India

Abstract

R22 is a Hydrochlorofluorocarbon (HCFC) commonly used in air conditioning, process chiller and industrial refrigeration plant applications. Because of worldwide discussion and reaction on global warming and ozone depletion, it is necessary to replace refrigerants having lower or zero ozone depletion and global warming potential. R22 will soon be phased out due to ozone depletion potential. It is an opportunity for improved environmental performance include the wider acceptance of refrigerants other than R22 which is used as alongside the highly ozone depleting (ODP) CFC's, but has a relatively low ozone depletion potential. However, even this lower ODP is no longer considered acceptable. Users of refrigeration are facing new choices with regard to selection of refrigerants because CFC and HCFC refrigerants are being phased out to protect the ozone layer. There is considerable confusion and controversy regarding the best choices, particularly when the environmental issue of global warming is taken into account. This paper considers the choice and availability of different refrigerants as substitute of R22, to avoid losing lifetime operation of designed and manufactured equipments for R22 like bottle cooler, chillers, vapour source heat pump, air conditioner etc.

Keywords: R22, GWP, ODP, refrigerant, Phase-out, CFC, HCFC, HFC, R22, R407C, R410A, R134a, Ozone depletion, Zeotropic refrigerant mixture

1. Introduction

In the 1980s, the depletion of stratospheric ozone, a compound which absorbs harmful UV-B radiation was discovered; the root cause of the problem was determined to be atmospheric halogen gases. Atmospheric ozone (O_3) is created when oxygen molecules (O_2) collide with free oxygen atoms (O); however, upon exposure to solar radiation, halogen gases create compounds that are highly reactive with ozone molecules, breaking them apart, and leaving oxygen (O_2). One of the halogen atoms principally responsible for depleting ozone in this manner is chlorine (Cl), commonly used in so called Chlorofluorocarbon (CFC) and Hydrochlorofluorocarbon (HCFC) refrigerants.

The Montreal Protocol, modified by the EU enforces the end of supply of (HCFCs) from 2015, including the ozone-depleting refrigerant gas R22, in refrigeration, heat pump and air conditioning (AC) systems [6]. R22 is commonly used in AC systems pre-dating 2004 and so its ban will have a major effect on air-conditioning costs. There are a range of possibilities when considering changing from R22 to an alternative refrigerant with low GWP & ODP. Delaying equipment replacement may buy time to allow alternative technology to become more readily available and established. The choice between competing refrigerants has always been complex. Nevertheless, there used to be fairly clear divisions between different types of refrigerant. CFCs and HCFCs were the refrigerant of choice for the vast majority of small, medium and many large sized refrigeration systems. This was because of their excellent safety characteristics (non-toxic and non-flammable) and good materials compatibility (allowing use of copper components).

R22 has been commonly used in residential heat pump, air conditioning and refrigeration systems since the 1990s following the phase out of chlorofluorocarbons (CFCs) in developed countries in 2000. The demand for R22 equipment has been increasing, especially in developing country markets. Of particularly high demand are refrigerated appliances for small and mid size shops and restaurants at affordable costs. The appliances are mostly factory made plug-in units with hermetic refrigerant circuits—such as bottle coolers, ice cream freezers, commercial freezers / refrigerators, beer coolers. The companies manufacturing these appliances are often small compared to household appliance manufacturers, so existing equipment and personnel knowledge about refrigeration and safety standards are not always adequate. R22 is a well performing refrigerant in use in small refrigerated appliances, with the exception of applications with high discharge temperatures at low evaporation temperatures in freezers.

Table 1. Applications of refrigerant R22 [7]

Residential Uses	Commercial and Industrial uses
Window and split air-conditioning units	Packaged air conditioners and heat pumps
Dehumidifiers	Chillers
Central air conditioners	Retail food refrigeration
Air-to-air heat pumps	Cold storage warehouses
Ground-source heat pumps	Industrial process refrigeration
Ductless air conditioners	Transport refrigeration

2. Replacement of R22 in different applications

The necessity for non-chlorinated refrigerants pursuant to the new regulations resulted in the investigation of HCFC-22 replacements. in the 1990s. Several refrigerant alternatives emerged from these studies, with none being a perfect replacement in the sense that it mimics the performance of R22 in all applications. Those refrigerants that have shown the greatest potential as R22 replacements are known as hydrofluorocarbons (HFCs), compounds that contain no chlorine atoms and so have very little or no ozone depletion potential. Of these alternatives, the most commonly considered to be candidates to replace R22 are HFC refrigerants R410A, R134a, and R407C. R410A and R407C are blends, while R134a is composed of a single constituent. R410A is composed of a 50/50 mixture of R-32 and R-125, while R407C is composed of 23% R-32, 25% R-125, and 52% R134a by weight. When considering alternative refrigerants, the advantages and disadvantages of each (including R22) must be carefully considered.

Table 2. Properties of refrigerant R22and its replacement [5]

Refrigerant	Atmospheric lifetime (Years)	ODP	GWP (100 Years)
R22	12	0.034	1780
R134a	14	~ 0.0	1320
R407C	a	~ 0.0	1700
R410 A	a	~ 0.0	2000
R290	b	0.0	~ 20
a. Atmospheric lifetimes are not given for blends			
b. Unknown			

2.1. Replacement of R22 in Scroll Chillers [6]

For scroll chillers, the most popular R22 replacement options include:
- R410A a zeotropic mixture of 50% HFC-32 and 50% HFC-125
- R407C a zeotropic mixture of 23% HFC-32, 25% HFC-125, and 52% HFC-134a.

R407C requires the least changes for component and system manufacturers, as well as installation and service contractors. The safety classification and handling characteristics are similar to R22 (non-flammable, low toxicity). R410A requires significant changes for component and system manufacturers but has offsetting benefits. The safety classification is the same as R22.

2.1.1. Transition from R22 to R407C

R407C has capacity and pressure close to R22. In fact, its operating characteristics are so similar to HCFC22 that it can be used in either existing R22 systems (requires some changes such as the oil) or in new systems that were originally designed for R22. Unlike R410A, the system efficiency of R407C is somewhat lower than R22 (~5% lower), especially in systems that were originally designed for R22. R407C is a zeotropic blend, meaning the resulting mixture does not act as a single compound. At a given pressure, it evaporates over a range of temperatures, rather than at a single temperature.

R407C has been used considerably in Europe, where the phase out of ozone depleting refrigerants (including R22) was accelerated, and manufacturers did not have time to re-design systems for higher pressure R410A refrigerant. In systems in which glide is acceptable, R407C has become a popular option for manufacturers who want to move quickly to an HFC

alternative. In the long run, however, the lower-efficiency performance of this refrigerant may make it a less attractive alternative compared to R410A for medium and high-temperature applications. R407C has an ODP of zero and no scheduled phase out date. It has been designated an A1 refrigerant in ASHRAE Standard 34 – Designation and Safety Classification of Refrigerants.

2.1.2. Transition from R22 to R410A

Operating pressures in a R410A refrigerant system are about 50% higher than a comparable R22 system. As a result, R410A cannot be used as a direct, functional replacement in R22 systems. R410A equipment has been specifically designed to operate at higher pressure, with a thicker compressor shell, heavier wall tubing and superior control and protections. The more robust materials, in turn, enable manufacturers to create heavier, better welds at joints, helping to improve their resistance to abuse. In addition, consistent field experience indicates that R410A offers greater compressor sound reduction than those units using R22. Another property that reduces the required amount of refrigerant is the lower liquid density of the refrigerant. This leads to a 12% reduction in the mass of the refrigerant required. The total of these effects is an overall reduction of 25% to 30% charge reduction in fully optimized R410A systems. Field-testing and the product history to date for R410A equipment suggest that these units are more reliable than R22 units. For residential and light-commercial to commercial AC, the overwhelming choice is R410A. But this refrigerant, a blend of R32 and R125 with very low glide (less than -17.22 ℃), has very different characteristics from R22; in particular, its operating pressure and volumetric capacity are significantly higher. This implies a major equipment redesign instead of simple component changes. For larger equipment, R410A will play a role.

2.2. Replacement of R22 in Commercial Appliances like Freezer and Bottle Cooler [4]

Propane (R290) can be introduced in many of today's R22 applications. No other single component refrigerant has such similar thermodynamic behaviour to R22. In climates characterized by high ambient temperatures, R290 provides improved performance in terms of discharge temperature and pressure. The experience built up over several years of production, mainly with commercial refrigerated appliances (ice cream freezers, commercial freezers/ refrigerators, ...), demonstrates that R290 is a promising alternative for R22, as components (e.g. compressors) are available in the market and R290 is compatible to the most commonly used heat exchangers and materials. However, application possibilities have been limited due to safety concerns. Safety standards for appliances are available, covering refrigerant charges up to 150 grams (g) per system. Appliance producers manufacturing R290 systems must be equipped accordingly, and service technicians must be trained in safe handling procedures.

Table 2. Thermodynamic Comparison of R290 to Other Refrigerants [4]

Parameters	R22	R290	R134a
Pressure	**	**	↑↑
Pressure ratio low back pressure (LBP)	**	↑↑	↓↓
Discharge temperature	↓↓	↑↑	↑↑
Volumetric capacity	↑↑	↑↑	↓↓
Capacity loss	**	**	**
COP	**	**	**

Legend: ** = acceptable; ↑↑ = good; ↓↓ = problematic

Refrigerants taken into the comparison are R22, R290, R134a, R404A and R600a. For the comparison two conditions were chosen, which represent operation of a commercial freezer display case and a bottle cooler at high ambient temperature.

- Low Back Pressure - Freezer evaporating/condensing/return (suction) gas at -35/50/20 ℃
- Medium Back Pressure - Bottle cooler evaporating/condensing/return (suction) gas at -10/55/20 ℃

R290 has a long history in refrigeration. It has been in use since before CFCs were developed and was re-introduced for use in heat pumps after the CFC phase out. Its thermodynamic data, efficiency, and material compatibility are well known. In some countries, appliance manufacturers and food producers began using R290 as a replacement for R404A or R134a in appliances shortly after 2000, due to environmental concerns. The energy efficiency and reliability of the appliance using R290 is expected to be equivalent to or better than that of equipment using R22. Because R290 has no ODP and a very low

GWP, assuming that R290 has the same energy efficiency as R22, the environmental impact is reduced. Based on estimated charge sizes and leak rates, emission savings are estimated to be 25 tonnes of R22 per 100,000 appliances.

2.3. Replacement of R22 in Domestic Air Conditioner

2.3.1. R290 as a replacement of R22 in Domestic Air Conditioner[3]

Performance of a domestic split type air conditioner was evaluated by using two different refrigerants, i.e., R22 and R290. The experimental investigation was conducted by using a 1 hp air conditioning unit. Power consumptions by the complete system including the evaporator as well the by the compressor alone were measured by clamp meter. Temperature was also measured at different locations by digital fluke thermometer whereas digital multi meter was used to measure the current supplied to the system. The air conditioner was run for six hours each time by setting three different set point temperatures, i.e., the cold air temperature coming out from the evaporator. From the measured information, coefficient of performance (COP), and energy efficiency ratio (ERR) were calculated for each refrigerant. The results revealed that R290 refrigerant has better COP and EER compared to R22 refrigerant. The usage of R290 refrigerant can reduce energy consumption up to 11 %. In addition to that, at the same air conditioning unit, the amount of R290 refrigerant required is relatively half of that required by R22 refrigerant. Due to R290 chemical properties, this refrigerant can easily be compressed and expanded compared to R22 refrigerant. As a result of these properties, the compressor requires less energy to compress the refrigerant which in turn increases the life span of the compressor. The only limitation of R290 is flammability. R290 refrigerant need to be handle with extra care due to its flammability properties.

2.3.2. R410A as a replacement of R22 in Domestic Air Conditioner [1]

R410A is a long-term alternative refrigerant with zero ODP (ozone-depleting-potential) for replacing R22. The performance comparison of AC included the cooling capacity, EER (energy efficiency ratio), annual power consumption of AC and the global warming impact of refrigerants adopted by the AC. It was concluded that the adoption of R410A could be helpful for AC to decrease their heat exchanger size or improve their operation efficiency for power saving. Moreover, compared to R22, R410A could in fact help alleviate its overall impact on global warming through significantly reducing the indirect global warming impact caused by operating R410A AC.

2.4. Replacement of R22 in Air Source Heat Pump [2]

The dynamic performance characteristics of the air source heat pump (ASHP) with refrigerants R22 and R407C during frosting and defrosting were studied. The results show that both refrigerant systems have similar performance characteristics, except that the performance of the R407C system deteriorated faster than that of the R22 system under frosting, and the performance of the R407C system attains its steady state faster than that of the R22 system after defrosting. R407C refrigerant can be used in either existing systems or in new systems that were originally designed for R22.

2.5. Replacement of R22 in Vapour Compression Heat Pump [6]

The performance of an air to water vapor compression heat pump has been investigated experimentally. The main purpose of study was to investigate the possibilities of using R134a as a working fluid to replace R22 for vapor compression heat pumps. Pure R22, pure R134a and some binary mixtures of R22/R134a were considered as working fluids. The performance of the system was characterized by mixture ratio, COP and evaporator air inlet temperature. Comparisons are made between the pure refrigerants and refrigerant mixtures on the basis of the COP. Experimental results show that the mixture ratio affects the COP significantly, and the COP could be improved by using pure R134a or an appropriate mixture of R134a/R22 instead of pure R22. The maximum COP occurred at a mixture ratio of around 50/50% R134a/R22. For a mass percentage of 50% of R134a, the COP was enhanced by about average 25%.

3. Conclusion

There are a range of possibilities when considering changing from R22 to an alternative refrigerant with higher performance and low global warming potential alternatives becoming more available. Delaying equipment replacement may buy time to allow alternative (zero ODP and lower GWP) technology to become more readily available and established. For scroll chillers R22 can be replaced by R407C and R410A (with 1.5% higher GWP). R410A can be used in medium and high temperature applications with higher performance in place of R22 and R407C. R290 is more efficient option for (ice cream freezers, commercial freezers/ refrigerators and domestic air conditioning unit. Since R290 is highly flammable it should be

used careful consideration to safety. By R134a and mixture of R22/134a, the performance of vapour compression heat pump is improved and COP is increased about 25%.

References

- Journal articles

[1] W. Chen, 2008, A comparative study on the performance and environmental characteristics of R410A and R22 residential air   conditioners, Applied Thermal Engineering, Volume 28, Issue 1, January 2008, Pages 1–7

[2] Zhiqiang Liu, Xiaolin Li, Hanqing Wang, Wangming Peng, 2008, Performance comparison of air source heat pump with R407C and R22 under frosting and defrosting, Energy Conversion and Management, Volume 49, Issue 2, February 2008, Pages 232–239

[3] M. M. Rahman and H. Y. Rahman, 2012, Hydrocarbon as refrigerant for domestic air conditioner: a comparative study between R22 and R290, Elixir Thermal Engg.. 53 (2012) 11976-11979

[4] Heinz Jürgensen, Propane as R22-Replacement in Commercial Appliances, Danfoss Compressors GmbH

[5] James M Calm, Piotr Domanski, R22 replacement status, ASHRAE Member

- Technical reports

[6] Refrigeration, Air Conditioning and Heat Pumps Technical Options Committee (RTOC), UNEP, 2010 Assessment

[7] An Independent Review of the Role of HFC Refrigerants by March Consulting Group, Refrigeration and Global Warming.1997

[8] Refrigerants for Residential and Commercial Air Conditioning Applications, Emerson Climate Technologies, October 2008

Review on Wall Climbing Robot

Kishan P Panchal[a], Prof. Dhaval P Patel[b]

[a]*Student of M.E. CAD/CAM, Mechanical Engineering Departement, Gandhainagar Institute of Technology,Gabdhainagar,Gujarat,India*
[b]*Assistant Professor,Mechanical Engineering Departement, Gandhainagar Institute of Technology,Gabdhainagar,Gujarat,India*

Abstract

Mobile Robot is the automatic machine which can move in the environment. Here different wall climbing robot system are reviewed and analyze the best wall climbing robot for the particular applications like surveillance & rescue operation, inspection of oil & chemical tanks, window cleaning of high rise buildings, inspection of storage tank in nuclear power plants . Different locomotion systems, climbing mechanisms are researched for the best wall climbing robot system. Different wall climbing robot systems have different climbing mechanism for different wall surface and environmental conditions. Mobility of wall climbing robot is also depend on the wall surface. Here some wall climbing robot with different climbing mechanism is reviewed and choose the proper climbing robot with high efficiency, greater mobility and low cost. Robot's weight is one of the major affect during the development of the wall climbing robot system.

Keywords: Climbing robot, Robot motion, Adhesion system, Locomotion mechanism, Robot weight

1. Introduction

Wall climbing robots are the useful devices which can adopt many applications in this fast growing technology. Wall climbing robots are capable to take the place of difficult human tasks which are very difficult, risky and time consuming work. There is always the problem with the safety for the difficult human tasks for the climbing robot can do that task easily and fast with minimum time requirement. Climbing robot can be excess where the direct access by human operator is difficult. Wall climbing robot should be as light as possible because weight is the major cause for it so for that wall climbing robot should make as light as possible at low cost. It should capable to carry its own weight as well additional weight with its full efficiency of work. Many researchers have done many work on the climbing robot and developed robot model experimentally and tested for different work and environment. In wall climbing robot main two major mechanisms are there one is locomotion system and another is adhesion system. Different locomotion systems are design and developed by different researchers. Mainly wheeled and tracked type locomotion systems are used in different wall climbing robot and in the latest technology magnetic wheeled type and legged type locomotion system is used to move the robot in different directions. In the latest technology now-a-days researchers have design the wall climbing robot which can transits between wall surface and ceiling surface[2]. Second is the adhesion system by which robot can climb on the wall surface. Different adhesion systems are developed by the researchers categories by suction mechanisms[3], gripping mechanism[4] and low pressure vacuum mechanisms[5]. All these adhesion systems has its own advantages & disadvantages depending upon the applications. Here different locomotion systems and adhesion systems are reviewed from the different research works and analyze the efficient wall climbing robot system.

1.1. Applications of wall climbing robot

Wall climbing robots are capable to do the difficult task which human operator cannot do very easily so for that case we can use this kind of robots. Wall climbing robot is used in the inspection of oil tank[6] and storage tank of nuclear power plants[7]. Climbing robots are also used in the ship inspection and surveillance of the high rise buildings where human operators are difficult to do it. These kind of robots are used in the anti-terrorist actions, in the cleaning of sky-scrapers, and window cleaning of high rise buildings[8]. They are also used in the non-destructive testing and also capable to transport the loads in the high rise buildings[17]. Different wall climbing robots has different climbing capability on the different surfaces like climbing robot with claws can only climb on the rough surfaces of the wall[4] and centrifugal impeller based wall climbing robot can only climb on the flat surface of the wall[9]. Specially design rotor package with centrifugal impeller is designed for the proper adhesion system[2].

2. Technologies for locomotion systems in climbing robots

Different locomotion systems are design and developed by the different researchers for different kind of purposes. Locomotion systems used in the climbing robots are wheeled type[2], tracked type[3], legged type[4] and electro-adhesive caterpillars[10] which have different climbing capability for different kind of tasks. Wheeled type locomotion systems are the most efficient locomotion system for the climbing robots because its controllability is easy as compare to other systems and it has less complexity for that four wheeled and three wheeled locomotion systems are used for the climbing on the flat wall surface, glass surfaces and wooden surfaces[11]. In the inspection of the high rise building and its window cleaning wheeled type locomotion system is preferred because it is easy to control[8]. In the inspection of the oil tank[6] and in-pipe robot, magnetic wheels are used which are capable to stick on the metallic surfaces of the oil tanks and pipes in less time[6][12]. Climbing robots are move by the linear actuators by which suction cups are engaged and disengaged to move over vertical surfaces[13]. Tracked type locomotion systems are capable to move without slipping over the vertical surfaces and it has more torque than wheeled type locomotion systems. Tracked type locomotion systems are used in the inspection of the oil tank in which small magnet blocks are attached in the tracked and it is capable to move on the vertical surfaces[6]. Tracked type locomotion systems are capable to carry more weight than wheeled type locomotion systems. In tracked type locomotion systems, small suction pads are attached on the tracked and it is capable to move over the vertical surfaces[3]. In the legged type locomotion systems, specially designed claws are attached on the legs of the robot which can climb only on the vertical rough surfaces[4]. Legged type locomotion systems has more complexity than wheeled and tracked type locomotion systems.

3. Technologies for adhesion systems in climbing robots

This section is reviewed the different adhesion systems of the wall climbing robots. Different adhesion systems adopted in climbing robot are suction cups, centrifugal impeller based, magnetic, electro-adhesion and gripping to the surfaces. The most common adhesion system used in the climbing robots are suction cup, centrifugal impeller and gripping based systems.

3.1. Suction cup based adhesion systems

In this type of adhesion systems, suction pads are attached to the micro pumps and as the micro pump activates the suction is created in the suction cup simultaneously and the robot is adhere properly on the vertical surfaces with high payload capacity.
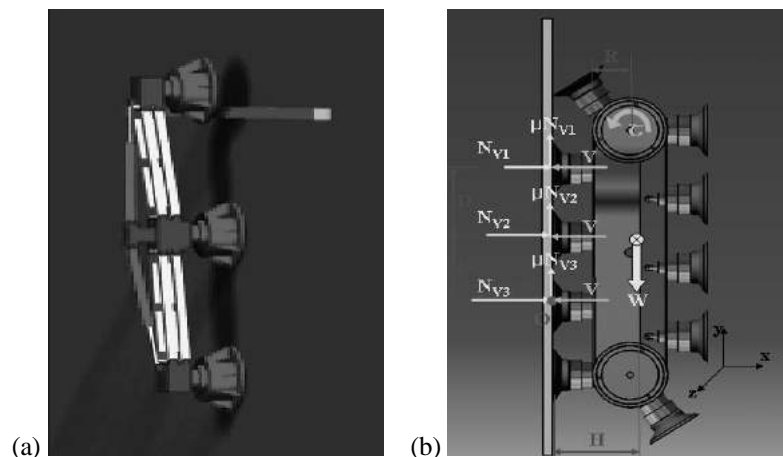
Figure. 1. Suction based climbing robots (a) Alicia 3 Robot[17] and (b) Robot with passive suction cups[3]

As shown in figure. 1(a) in alicia3 robot three suction cups are there which are activated simultaneously and climb over the vertical surfaces. This type of climbing robot is used in the automatic wall inspection. It has three suction pads linked in series by two rods and this climbing robot can pass over the obstacle in a few steps by detaching the three modules one by one at lower speed[17]. In another climbing robot as shown in figure. 1(b), number of suction pads are installed over the two tracks of the climbing robot and it is capable to move over the vertical surfaces. The suction pads which attached to the

vertical plane are activated in sequence by specially designed mechanical valves with the climbing speed of 15 m/min[3]. The design of these adhesion systems are very complex and cost of the robot is also very high.

3.2. Centrifugal impeller based adhesion systems

In this type of adhesion systems, negative pressure is created by the high speed rotation of the closed type centrifugal impeller with backward curves vanes and air will entered from the inlet of the impeller eye and exits radially and adequate adhesion pressure is produced by it to stick the robot properly on the vertical surfaces[1]. As shown in figure. 2(a) city climber has the centrifugal impeller based adhesion system with wheeled type locomotion. It has the capability to climb the vertical surfaces and transits between the different surfaces with strong adhesion force and high mobility. It is capable to move on virtually any kind of smooth or rough surfaces with payload capacity of 4.2 kg[2]. The overall weight of this robot is very low.

(a)   (b)
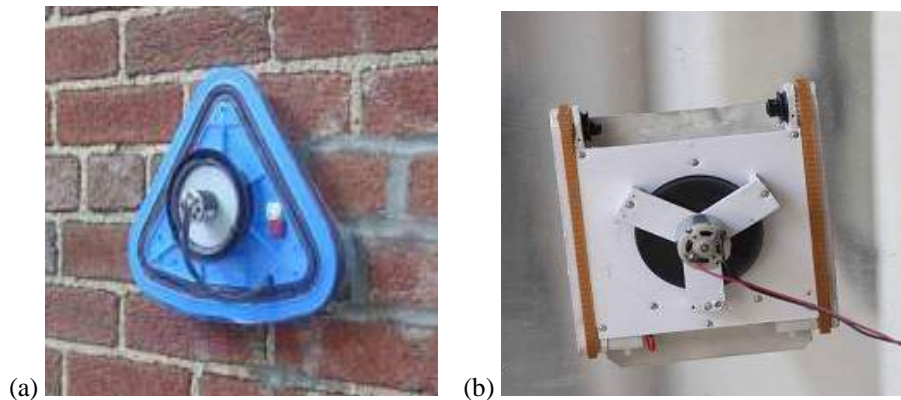
Figure. 2 Centrifugal impeller based adhesion system (a) City Climber[2] and (b) Novel low cost climbing robot with tracked locomotion system[1]

Here another centrifugal based climbing robot as shown in figure. 2 (b) has tracked type locomotion system and it is capable to move over the wall surface and also transits between the ground surface and vertical surface. It is the lightest climbing robot with the weight of 120 grams with the payload capacity of 500 grams. Here centrifugal impeller with backward curve vanes are used which hold the robot on the vertical surface at low cost without any complexity. This type of climbing robot is made from the foam board material whose weight is very less so overall weight of the robot will decreases[1].

3.3. Gripping based adhesion system

Previous all the adhesion systems are the most efficient for the climbing robots for the flat surfaces. If number of obstacles increases on the vertical wall surfaces than previous kind of adhesion systems are not work properly.

(a)   (b)
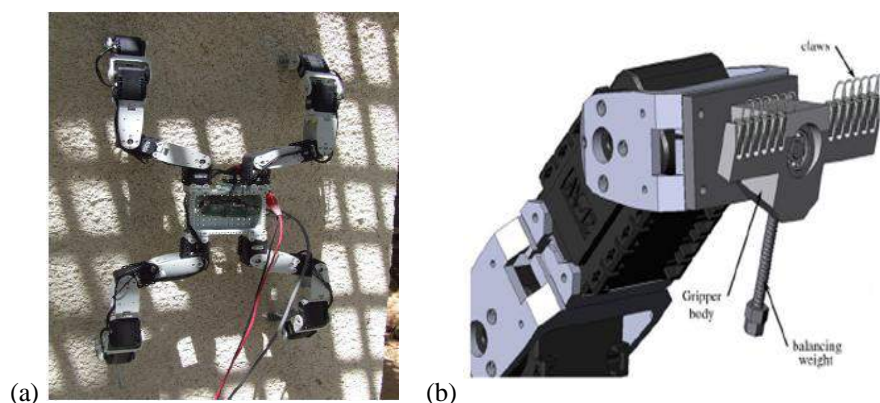
Figure. 3. Gripping based adhesion system (a) CLIBO prototype climbing robot[4] and (b) Gripping device of CLIBO Prototype robot[4]

Gripping based adhesion system is used in the climbing robot which can capable to climb the vertical surfaces with the obstacles easily. Gripping based adhesion system in wall climbing robot can be use only for the rough surfaces due to its design and complexity. This type of wall climbing robot has legged type locomotion system and gripping attachment is attached on the each leg of the robot to move the robot in the vertical direction. Gripping based adhesion system in wall climbing robot is shown in the figure. 3(a) in which specially designed claws are attached on the legs of the climbing robot. As shown in figure. 3(b), on the tip of the each leg 12 fishing hooks are attached to climb on the rough surfaces and it is capable to hold the 3 kg. weight. The balancing weight is attached in the opposite direction of the claws which are helpful to balance the robot during the climbing. This type of robot is use for the surveillance and inspection purposes which is capable to move on the construction buildings for the inspection purpose and also use for the inspection of the bridges and dams where human workers are difficult to reach. It has four legged locomotion system which is move by the electric actuators and cross the obstacles on the wall surface. This robot is only use for the vertical climb on rough surface due to its specially designed claws[4].

3.4. Magnetic based adhesion system

In magnetic based adhesion system, Permanent magnets are used as shown in figure. 4(a). Here robot is made of a box shape aluminium frame. It has the tracked type locomotion system in which permanent magnets are placed in evenly spaced steel channels as shown in figure. 4(a). As the climbing robot is shown in figure. 4(b) has two DC motors with the planetary gearbox of ratio 15:1 used to drive the robot on the vertical surfaces of the oil tank at the speed of 10 m/sec with the on board battery setup[6].

(a)   (b)
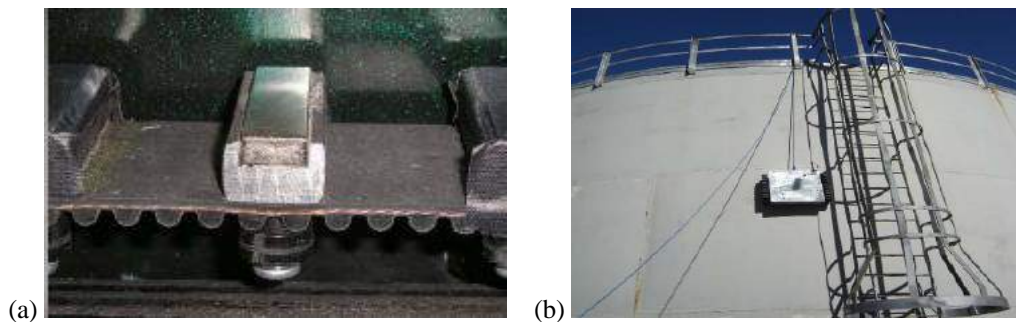
Figure. 4. Magnetic based adhesion system (a) Magnetic track wheel[6] and (b) Inspection on Oil tank[6]

This type of adhesion system can be use only on the metal surfaces so this type of climbing robot can be use for the inspection of the oil tanks, vessels and chemical tanks. One of the main disadvantage is life of the magnets because magnetic based wall climbing robot can only used on the metal surfaces so continuous use of this type of climbing robot weakens the magnets after the long use ands new magnets have to replace at the fix interval time.

4. Conclusion

Different wall climbing robot's locomotion mechanisms and adhesion mechanisms are analyzed. Their main applications are for inspection, surveillances purposes as well they are use for the window cleaning of the high rise buildings. This paper is presented the reviewed different wall climbing robotics systems of different locomotion systems with different technologies in adhesion system to the different wall surfaces.

References

- Journal articles:

[1] Aravind Sekhar R, Amritha Mary, Sanju N Raju, Akhil G Ravi, Vijitha Sharma, Gauri Bala, 2013. "A novel design technique to develop a low cost and highly stable wall climbing robot", 4th International Conference on Intelligent Systems.
[2] Jizhong Xiao and Ali Sadegh, 2007. " City-climber: a new generation wall-climbing robots", ISBN 978-3-902613-16-5, pp. 546.
[3] Hwang Kim, Dongmok Kim, Hojoon Yang, Kyouhee Lee, Kunchan Seo, Doyoung Chang and Jongwon Kim, 2008. " Development of a wall-climbing robot using a tracked wheel mechanism", Journal of Mechanical Science and Technology 22, pp. 1490-1498.
[4] Avishai Sintov, Tomer Avramovich, Amir Shapiro, 2011." Design and motion planning of an autonomous climbing robot with claws", Robotics and Autonomous System 59, pp. 1008–1019.

[5] Jizhong Xiao, Ali Sadegh, Matthew Elliott, Angel Calle, Avinash Persad, Ho Ming Chiu, July 2005. " Design of mobile robots with wall climbing capability", IEEE/ASME International Conference on Advanced Intelligent Mechatronics.

[6] Love P. Kalra, Jason Gu, Max Meng, December 2006. " A wall climbing robot for oil tank inspection", Proceedings of IEEE International Conference on Robotics & Biomimetics.

[7] Leoncio Briones, Paul Bustamante, Miguel A. Serna, 1994. " Wall-climbing robot for inspection in nuclear power plants", IEEE.

[8] Tohru Miyake, Hidenori Ishihara, Ryu Shoji and Shunichi Yoshida, June 2006. " Development of small-size window cleaning robot", IEEE International Conference on Mechatronics and Automation.

[9] Shanqiang Wu, Mantian Li, Shu Xiao and Yang Li, June 2006. " A wireless distribution wall climbing robotic system for reconnaissance purpose", Proceedings of IEEE International Conference on Mechatronics and Automation.

[10] Guangzhao Cui, Keke Liang, Jinchao Guo, Huiping Li and Dongdong Gu, 2012. " Design of a climbing robot based on electrically controllable adhesion technology", international conference on solid state and materials.

[11] Young Kouk Song, Chang Min Lee, Ig Mo koo, Duc Trong Tran, Hyungpil Moon and Hyouk Ryeol Choi, Sept. 2008. "Development of Wall Climbing Robotic System for Inspection Purpose", IEEE/RSJ International Conference on Intelligent Robots and Systems.

[12] Md Raziq Asyraf Md Zin, Khairul Salleh Mohamed Sahari, Juniza Md Saad, Adzly Anuar, Abd Talip Zulkarnain, 2012. " Development of a low cost small sized in-pipe robot", Procedia Engineering 41,pp. 1469-1475.

[13] Wang Yan, Liu Shuliang, Xu Dianguo, Zhao Yanzheng, Shao Hao & Gao Xueshan, May 1999. " Development & application of wall-climbing robots", IEEE International Conference on Robotics and Automation.

[14] Yu Yoshida and Shugen Ma, December 2010. " Design of a wall-climbing robot with passive suction cups", ieee international conference on robotics and biomimetics,

[15] Manuel F. Silva, J. A. Tenreiro Machado, J´ozsef K. Tar, 2008. " A survey of technologies for climbing robots adhesion to surfaces" IEEE.

[16] R. Lal Tummala, Ranjan Mukherjee, Ning Xi, Dean Aslam, Hans Dulimarta, Jizhong Xiao, Mark Minor And Girish Dangi, December 2002. " Climbing the walls", IEEE Robotics & Automation Magazine.

- Edited Books:

[17] Domenico Longo, Giovanni Muscato, March 2006. " The alicia3 climbing robot", IEEE Robotics & automation magazine.

[18] Dong Sun, Jian Zhu and Shiu Kit Tso, October 2007, " A climbing robot for cleaning glass surface with motion planning & visual planning", Climbing & walking Robots.

A Review on an Active Solar Still

Desai Nikul[a], N M Bhatt[a] *, Nimesh Gajjar[a],

[a]Gandhinagar Institute of Technology, Moti Bhoyan 382721, gandhinagar, Gujarat, , India.

Abstract

Water is a basic need of human life on earth for survival and good health. The drinking water availability is reducing day by day. There will be no water left on earth which is safe for drinking without purification after 20-25 years from today. Only 1% fresh water is in liquid state, and nearly all of this is polluted by both diseases and toxic chemicals, there is often enough water available but it is salty and brackish. To overcome this problem there is a need for sustainable source and eco-friendly technique for water distillation. Among the conventional distillation process, Solar still is a useful device that can convert the saline water into potable water. Solar still can effectively remove impurities such as salt, heavy metals as well as eliminates microbiological organisms. Passive solar still is used for solar distillation system due to its simplicity, reliability and cost effectiveness, however the yield is low. Different active solar distillation methods have been developed to overcome this issue. This article provides review on different studies on active solar distillation system.

Keywords: Active Solar Still, Flat Plate Collector, Hybrid (PV/T) System, Evacuated Tube Collector.

1. Introduction

Water is said to be a basic need of human life without it life is impossible. The need of fresh water is becoming an important issue in many area of the world. The world population which is increasing rapidly together with industrial and agriculture development all over the world contributes to the pollution and depletion of fresh water resources. So importance of potable water supply can't be ignored. Water which covers ¾ of total earth surface, however only a little amount about 3% sources of water are portable. Less than 1% water is fresh within human reach and rest of water in the form of ice. Even this small fraction of water which is stored as ground water and water in lakes and rivers etc is believed to be adequate for survival of life and vegetation on earth. From that fresh water, 30% is underground, most of it in deep, hard-to-reach aquifers. Lakes and rivers both contain just a little more than 0.25% of all fresh water. People in remote and rural areas depend on underground water for drinking. In rural areas potable water is very scarce and the establishment of a human survival in these areas depends on how such water can be made available. In some of these areas water is too saline to be used as a drinking water. The salinity of brackish water varies with different locations. In this situation fresh water has to be supplied to the longer distance or by establishing the expensive water distribution networks which are much costly for a small population. Nowadays increasing water pollution in rivers and lakes by industrial and sewage disposal has resulted in lack of fresh water in many big towns and cities around the world. Salinity in water should be given the most importance for such analysis. It is expressed in parts per million (ppm). The excessive saline water can causes problems of stomach, laxative effects, and problem of taste [1]. According to World Health Organization, the permissible limit of salinity in water is 500 ppm. World Health Organization (WHO) reports estimate, 3900 children die daily due to water-borne diseases (2010). One child dies or goes blind per minute due to consumption of contaminated water. Approximately 13% of the world's population lack access to potable water. Annually, 1.8 million people die from de-hydration due to diarrhea [2]. Increasing demands of energy and environmental issue has focused much attention on resources which are providing a renewable energy. The solar energy is one of the most economical in rural areas having less population and low rainfall. Solar still is capable of producing clean and potable water which can be used for cooking, drinking and can be used in industries as a distilled cleaner. It is the maintenance free technology which can be operated by any non skilled person with less number of problems. The different parameters which can increase the efficiency and productivity of solar still are variation in design, depth of water, variation in salt concentration, location, use of different absorber materials and use of evaporating techniques. Solar still can effectively purify seawater and even raw sewage water. Solar stills can effectively remove salts/minerals (Na, Ca, As, Fe, Mn), bacteria (E.coli, Cholera, Botulinus), parasites, heavy metals and TDS. Basic principal of working of solar still is "Solar energy heats water, evaporates it (salts and microbes left behind), and condenses as clouds to return to earth as rainwater" [3]. In conventional basin type solar still, it consists of airtight basin with black-lined which contains saline water. A sloping transparent cover is provided at the top. Solar radiation is absorbed effectively

by the black surface and heat is transferred to the water in the basin. Temperature of the water increases and it increases the rate of evaporation. Due to evaporation water vapour is produced, rises upward and condenses on the inner side of the glass cover which is relatively cold. Condensed water particles trickle down and collected in the storage container as distilled water. In active solar still, the temperature of water in basin could be raised by additional thermal energy supplied by collector into the solar still.

2. Active Solar Still

The solar water distillation system is classified into two types, passive and active solar still. In passive solar still direct solar energy is the only source of energy which increase the water temperature hence it works at lower temperature and daily productivity is comparatively low. To increase the temperature and productivity of the solar still, active methods have been developed. In active solar still, direct solar energy as well as extra thermal energy is fed into the basin with the help of solar collector. To increase the productivity of solar still many variants of active solar stills have been developed by many researchers. This article provides a review on development of different types of active solar still.

2.1. Solar still coupled with flat plate collector

Solar still integrated with flat plate collector in which additional thermal energy is supplied to the basin by circulating the water into the system, is either by force circulation mode or natural circulation mode.

2.1.1. Force circulation mode

In this system the flat plate collector supplies an additional thermal energy via circulating water by the help of a pump. The effect of temperature and internal heat transfer coefficients on the performance of solar still integrated with a panel of collector through a heat exchanger was studied by Tiwari and Dhiman [4]. It was observed that during the operation of solar still the internal convective and radiative heat transfer coefficients can be considered as a constants and evaporative heat transfer coefficient was very important parameter which was totally depends on temperature of the water and glass. They also found that with the varied heat exchanger length from 6 to 12 m, the yield was raised by 12% and efficiency of system varied from 15 to 19%. With increase in basin area and water depth, the mass of water also increased due to which the temperature of water and productivity decreased as reported by the Sanjeevkumar and Tiwari [5]. They also suggested that, with increase in number of collector, yield also increased. Sanjeevkumar et al. [6] carried out the annual performance of an active solar still for Delhi climatic conditions and conclude that, for optimum yield the glass cover and collector inclination should be 15° and 20° respectively. The internal heat transfer coefficients depends on temperature difference between water and inner glass cover and they also depend on material of condensing cover as presented by Tiwari et al. [7]. They developed a computer model to predict the performance of solar still based on inner and outer temperature of glass cover. Singh and Tiwari [8] carried out performance of passive and active solar still for different Indian climatic condition. They inferred that on the basis of numerical computations, the annual yield depends on inclination of condensing glass cover, inclination of collector and water depth. They also found that, for maximum yield, optimum collector inclination was 28.58° and glass cover inclination was 18.58° for New Delhi climatic conditions. It was inferred that the convective heat transfer coefficient significantly depends on water depth as reported by Tripathi and Tiwari [9]. They performed experiments for 24 hours during winter month for different water depth and the study showed that for higher water depth more yield was obtained during the off shine hours as compared to day time due to storage effect. Tiwari et al. [10] have made an attempt to evaluate inner and outer glass temperature and its effects on yield. They found that higher yield is obtained for an active solar still as compared to the passive solar still due to higher temperature difference. They have also carried out study on effect of condensing cover material on yield of an active solar still. It is observed that copper gives higher yield as compared to glass and plastic due to higher thermal conductivity. Tiwari et al. [11] developed the thermal model of active solar still on two assumptions (i) temperature of inner and outer glass is equal and (ii) temperature of inner and outer glass is not equal. They observed that the daily yield values were 3.08 kg and 2.85 kg for the two above condition respectively. Sethi et al. [12] designed, fabricated and tested a basin type double slope solar still coupled with flat plate collector. The experiments were conducted to investigate the effect of water depth on productivity and instantaneous thermal efficiency. From their study they found that maximum yield is 4.82 kg at 3 cm depth of water and minimum yield is 4.36 kg at 5 cm water depth. They also found that maximum instantaneous thermal efficiency is 46.96 % at 4 cm water depth and daily yield was decreased with increase in water depth.
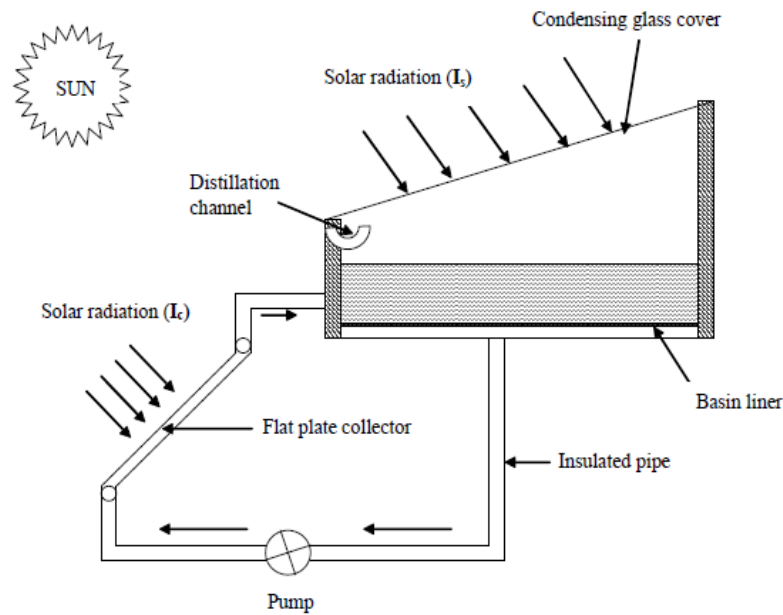
Fig. 1. Schematic diagram of an active solar still integrated with a flat plate collector [11].

2.1.2. Natural circulation mode

The solar still coupled with flat plate collector under natural circulation mode has various advantages over forced circulation mode as it does not need electricity to run the pump for circulating the water into the system and cost effectiveness as reported by Lowrence and Tiwari [13]. They developed a theoretical model of a single basin solar still coupled with a panel of collector under natural circulation mode. From their study they observed that, efficiency of simple solar still was less than active solar still and daily yield of solar still decreased with increase in water depth. Yadav [14] presented a transient analysis of a single basin solar still coupled with flat plate collector under natural circulation mode. Numerical calculations were carried out and compared with the system operation using force and thermosyphon mode. They have observed that force circulation mode was slightly better than thermosyphon mode but it could be preferred over the force circulation mode because of simplicity in design and reliability in operation.

Yadav [15] studied the transient performance of a solar still coupled with flat plate collector under thermosyphon mode. The study revealed that the evaporative heat transfer coefficient depended on temperature when evaluating performance of solar still. Single slope solar still coupled with flat plate collector in which mirrors are fixed inside the solar still was investigated by Badran and Al-tahaineh [16]. They found 36% more yield with coupling of flat plate collector. Their result showed that at 2 cm water depth output is higher and observed that solar still productivity proportional to the solar radiation intensity. Bodran et al. [17] experimentally studied a single stage basin type solar still connected with flat plate collector. They performed experiment with tap water and saline water as a feed. From their study they found that with tap water, the productivity was higher compared saline water. The double slope active solar still under thermosyphon mode gave 51% higher productivity compared to double slope passive solar still as reported by Tiwari et al. [18]. They observed that, thermal efficiency and exergy efficiency of double slope active solar still were decreased and increased respectively as compared to double slope passive solar still.
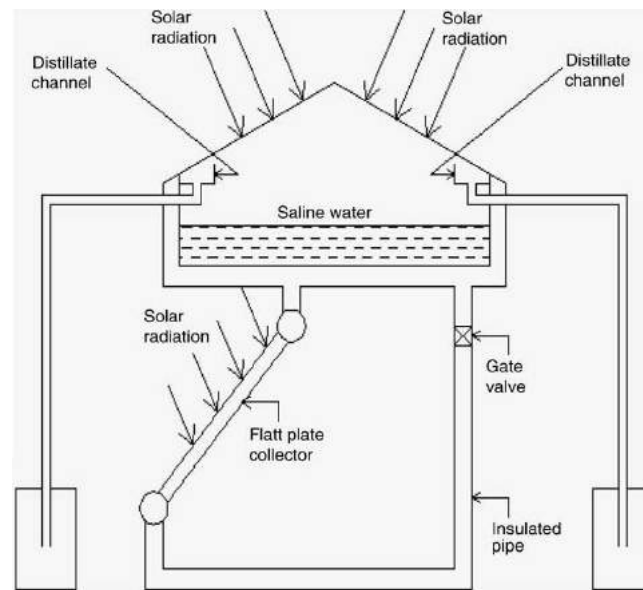
Fig. 2. Schematic diagram of a double slope active solar still integrated with a flat plate collector [18].

2.2 Solar still coupled with hybrid PV/T system

In normal photovoltaic (PV) module, total solar radiation absorbed by PV cell is not fully converted into the electricity and excess energy which not converted into the electricity increases the temperature of PV cell which decreases the efficiency of PV module. Due to this reason, cooling medium is very necessary to carry heat and reduce the temperature of PV cell. So it is necessary to introduce a system which produces electricity and which is in turn used to circulate the water which also carry away the heat of PV cell. Such PV module is termed as a Photovoltaic-Thermal (PV/T) module which convert sunlight into electricity, collect the residual thermal energy and supplied both electricity and heat in usable form.

Shiv kumar et al. [19] carried out experimental study to estimate the internal heat transfer coefficient of a deep basin hybrid PV/T active solar still for New Delhi climatic conditions. Their study showed that, the heat transfer coefficient for the active and passive solar still were 2.41 and 0.78 W/ m^2 K respectively for 5 cm water depth. On the basis of 5 cm water depth life cycle cost analysis of a single slop passive and hybrid PV/T active solar still was carried out by the Shiv kumar and Tiwari [20]. They concluded that, the cost of distillate water of passive solar still is Rs. 0.70/kg and for hybrid PV/T active solar still is Rs. 1.93/kg for 3 years life time of the system. They also found that, the payback period of the passive and hybrid PV/T active solar still on the selling price of distilled water in the range of Rs. 10/kg to 2/kg is 1.1 to 6.2 years and 3.3 to 23.9 years respectively. Shiv kumar et al. [21] developed empirical relation to estimate the glass cover temperature of known value of water and ambient temperature in basin type hybrid PV/T active solar still. The empirical relation developed was based on experiment results of water and ambient temperature in the range of 14℃ and 92℃ and 14℃ to 36℃ respectively. From their study they found maximum relative error of 1.12 % compared to value obtained from a numerical solution for proposed glass cover temperature.

The daily yield and exergy efficiency decreased linearly and nonlinearly with increase in water mass as reported by Tiwari et al. [22]. They observed that on the basis of exergy efficiency, with 50 kg water mass and four collector series higher yield was obtained. Singh et al. [23] designed, fabricated and tested a modified photovoltaic thermal PV/T double slop active solar still. System operated with natural and forced circulation mode. From their experimental study, they concluded that parallel forced circulation mode configuration of solar still produced higher yield than the other configurations and obtained 7.54 kg/day with 17.4 % energy efficiency. The electric efficiency of integrated PV module was in the range of 9.5 to 12.4 % as analyzed by Shiv kumar et al. [24]. They experimentally studied on comparative evaluation of the annual performance of single slop passive and hybrid PV/T active solar still for New Delhi climatic conditions. They found efficiency of active and passive solar still in the range of 9.1 to 19.1 % and 9.8 to 28.4 % respectively.
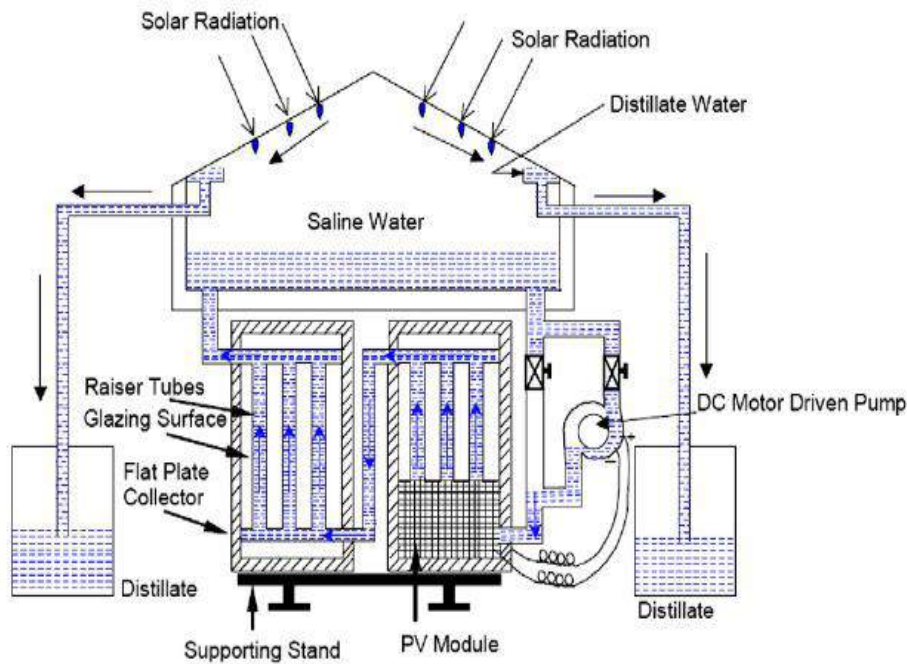
Fig. 3. Schematic diagram of a double slope active solar still integrated with a hybrid PV/T system [23]

2.3 Solar still coupled with evacuated tube solar collector

Compared to the flat plate collector, evacuated tube solar collector has more advantages in terms of higher efficiency and its design to collect the solar radiation from the all angles. Evacuated solar collector consists of two strong borosilicate concentric glass tubes with high chemical and thermal shock resistance. The outer side of inner tube has layer of selective coating that absorbed maximum solar radiation and minimizes the reflection. The outer tube of evacuated tube collector has higher transmisivity and lower reflectivity so that maximum radiation can pass through. The annular space between the inner side of outer tube and outer side of inner tube is provided with vacuum which acts as insulator and to virtually eliminate heat loss by convection and conduction. This traps much more solar radiation effectively and hence higher temperature can be achieved. Evacuated solar collector with efficiency of about 68% was reported by Mahkamov et al. [25]. They carried out study on experimental investigation of the performance of a multistage water desalination still connected to evacuated solar collector with aperture area of 1.7 m^2. The multistage solar still was designed to recover latent heat from evaporation and condensation in four stages. Using test rig with an array of 110 halogens to cover the area of the collector they obtained daily yield of 5 kg. Due to simplicity, low cost, less energy losses and high performance, the evacuated tube were proved to be another option for high temperature distillation system compared to flat plate collector as reported by Firozuddian et al. [26]. From their study it was found that the daily productivity increased by 50.2% by coupling the evacuated tube solar collector with solar still. They also conclude that, the annual yield will be more than other active methods like coupling of flat plate collector, parabolic collector etc. Tiwari et al. [27] inferred that the integration of evacuated tube solar collector with solar still increased the water temperature as well as yield. They found that, yield was decreased with increase in water depth and obtained 3.8 kg/m^2 for 3 cm basin water depth. They also concluded that, to make system efficient the combination between the size of evacuated tube collector and basin water depth needs adjustment. They suggested that, small size of evacuated tube collector with 10 numbers of tubes is preferable.

Double basin active solar still coupled with evacuated glass tube solar collector and use of glass stray inside the solar still, to reduce heat loss of upper portion and to get more output was reported by Meena et al. [28]. Their experimental study showed that, maximum productivity was increased by 14.7% with double basin as compared to single basin solar still. Sampathkumar [29] experimentally investigated performance of a single slope solar still directly coupled with evacuated tubes with black gravel in basin to increase the productivity. From their study they found that, after coupling of the evacuated tubes, production rate increased by 59.48% with black gravel. They also found payback period of setup as 235 days. Productivity of solar still increased from 39 to 59 % with hybrid unit in which evacuated tube collector was coupled to a solar still as concluded by Shobha et al. [30]. They also concluded that efficiency of the solar still was decreased with increase in water depth.

Mitesh et al. [31] studied a single slope active solar still coupled with evacuated glass tube solar collector and performed experiments with different heat storage materials like black, blue and red dye used inside the brackish water. They observed that with black dye the output is higher compared to other dyes and the productivity was increased by 30.38 % with black dye. Panchal [32] experimentally studied double basin solar still with vacuum tubes in which black granite gravel used to increase the output by reducing the quantity of water in basin. From study he found that, the productivity was increased by 65% and 56% with and without black granite gravel respectively due to vacuum tubes. The payback period of setup was also found to be 195 days.
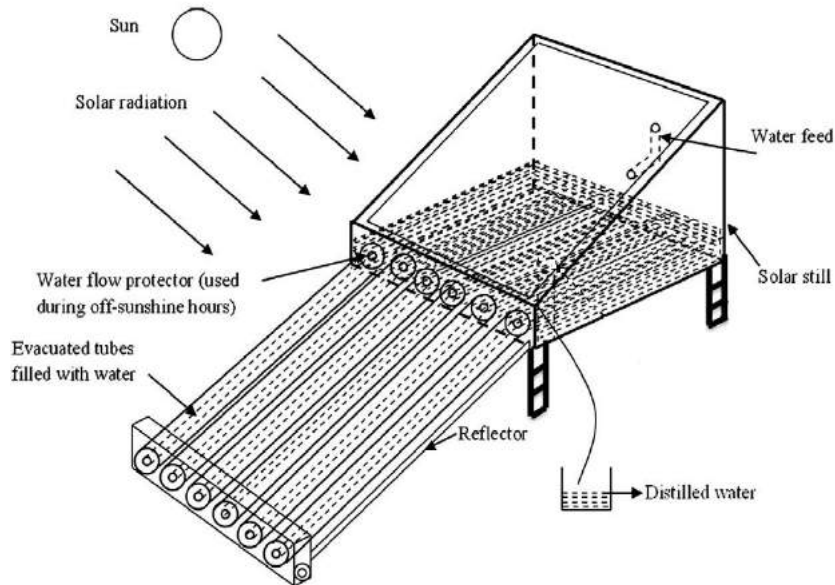
Fig. 4. Schematic diagram of an active solar still integrated with an evacuated tube collector [27].

Conclusion

Based on the review the following conclusions have been drawn.

- Higher water temperature can be achieved by the active solar still compared to the passive solar still due to the additional thermal energy supplied by collector; increase in water temperature is more than $20^{o}C$.
- The length of solar still, depth of water in basin, inlet water temperature and solar radiation are the major parameters which affects the performance of the still.
- Solar still coupled with flat plate collector with forced circulation mode gives higher yield than that of the thermosyphon mode.
- The yield is directly related to thermal conductivity of condensing cover materials. Yield increases with conductivity of condensing cover material.
- The evaporative heat transfer coefficient between water and inner glass cover depends significantly on the water temperature. The coefficient increases with increase in water temperature.
- The distilled output varies with the water depth and it decreases with increase of water depth in basin. However optimum value of water depth depends on type of solar collector used and its thermal efficiency.
- The solar still feed with water at constant rate gives higher yield in comparison to a still with water filled only once in a day.
- Double basin system is more appropriate for increasing the productivity of the solar still because of lower heat loss from the upper portion of the solar still and recovering latent heat of condensation from lower still. The multistage solar desalination system with heat recovery system produces higher yield than the simple solar still.
- The yield is higher in hybrid photovoltaic/thermal (PV/T) active solar still compared to the passive solar still.
- Due to simplicity, low cost, less energy losses and high performance the evacuated tube collector is proved to be better option for higher temperature distillation when compared to other collector. To make the system efficient, the combination between water depth and size of evacuated tube collector needs adjustments. Evacuated tube

collector with 10 numbers of tubes is preferable. With increase in number of evacuated tube, temperature of water inside the active solar still increases and hence the productivity also increases.

- The higher productivity is achieved, when energy storage materials are used.
- The exergy efficiency of double slope active solar still is higher than the exergy efficiency of double slope passive solar still.

References

[1] Moses Koilraj Gnanadason, Palanisamy Senthil Kumar, Gopal Sivaraman, Joseph Ebenezer Samuel Daniel, 2011, "Design and Performance Analysis of a Modified Vacuum Single Basin Solar Still", Smart Grid and Renewable Energy 2, 388-395.

[2] World Health Organization, 2013, Report on "Ending Preventable Child Deaths from Pneumonia and Diarrhoea by 2025", The integrated Global Action Plan for Pneumonia and Diarrhoea (GAPPD), 5.

[3] Alpesh Mehta, Arjun Vyas, Nitin Bodar, Dharmesh Lathiya, 2011, "Design of Solar Distillation System", International Journal of Advanced Science and Technology 29, 67-74.

[4] G.N. Tiwari, N.K. Dhiman, 1991, "Performance study of a high temperature distillation system", Energy Conversion and Management 32(3), 283–291.

[5] Sanjeev Kumar, G.N. Tiwari, 1998, "Optimization of collector and basin areas for a higher yield for active solar stills", Desalination 116, 1–9.

[6] Sanjeev Kumar, G.N. Tiwari, H.N. Singh, 2000, "Annual performance of an active solar distillation system", Desalination 127, 79–88.

[7] G.N. Tiwari, S.K. Shukla, I.P. Singh, 2003, "Computer modelling of passive/active solar stills by using inner glass temperature", Desalination 154, 171–185.

[8] H.N. Singh, G.N. Tiwari, 2004, "Monthly performance of passive and active solar stills for different Indian climatic condition", Desalination 168, 145–150.

[9] Rajesh Tripathi, G.N. Tiwari, 2005, "Effect of water depth on internal heat and mass transfer for active solar distillation", Desalination 173, 187–200.

[10] Vimal Dimri, Bikash Sarkar, Usha Singh, G.N. Tiwari, 2008, "Effect of condensing cover material on yield of an active solar still: an experimental validation", Desalination 227, 178–89.

[11] G.N. Tiwari, Dimri Vimal, Arvind Chel, 2009, "Parametric study of an active and passive solar distillation system: energy and exergy analysis" Desalination 242, 1–18.

[12] Sethi A.K., Dwivedi V.K., 2013, "Design, Fabrication and Performance Evaluation of Active Solar Still under Forced Circulation Mode", Research Journal of Engineering Sciences 2(6), 6-12.

[13] S.A. Lawrence, G.N. Tiwari, 1990, "Theoretical evaluation of solar distillation under natural circulation with heat exchanger", Energy Conversion and Management 30(3), 205–213.

[14] Y.P. Yadav, 1991, "Analytical performance of a solar still integrated with a flat plate solar collector Thermosyphon mode", Energy Conversion and Management 31(3), 255–263.

[15] Y.P.Yadav, 1993, "Transient performance of a high temperature solar distillation system", Desalination 91, 145–153.

[16] Badran O.O., Al-Tahaineh H.A., 2005, "The effect of coupling a flat plate collector on the solar still productivity", Desalination 183, 137–142.

[17] Ali A. Badran, Ahmad A. Al-Hallaq, Imad A., Eyal Salman, Mohammad Z. Odat, 2005, "A solar still augmented with a flat plate collector", Desalination 172, 227–234.

[18] Dwivedi V.K., G.N.Tiwari, 2010, "Experimental validation of thermal model of double slope active solar still under natural circulation mode", Desalination 250(1), 49–55.

[19] Shiv Kumar, G.N. Tiwari, 2009, "Estimation of internal heat transfer coefficients of a hybrid (PV/T) active solar still", Solar Energy 83, 1656–1667.

[20] Shiv Kumar, G.N. Tiwari, 2009, "Life cycle cost analysis of single slope hybrid (PV/T) active solar still", Applied Energy 86, 1995–2004.

[21] Shiv Kumar, G.N. Tiwari, M.K. Gaur, 2010, "Development of empirical relation to evaluate the heat transfer coefficients and fractional energy in basin type hybrid (PV/T) active solar still", Desalination 250, 214–221.

[22] M.K. Gaur, G.N. Tiwari, 2010, "Optimization of number of collectors for integrated PV/T hybrid active solar still", Applied Energy 87 (5), 1763-1772.

[23] Gajendra Singh, Shiv Kumar, G.N. Tiwari, 2011, "Design, fabrication and performance evaluation of a hybrid photovoltaic thermal (PVT) double slope active solar still", Desalination 277, 99–406.

[24] Shiv Kumar, 2012, "Annual Performance of Passive and Hybrid (PVT) Active Solar Stills", VSRD International Journal of Mechanical, Auto. & Prod. Engg. 2 (6), 223-231.

[25] Mahmoud. I.M. Shatat, K. Mahkamov, 2010, "Determination of rational design parameters of a multi-stage solar water desalination still using transient mathematical modelling", Renewable Energy 35,52–61.

[26] Syed Firozuddin, Mohd. Aasim Nazeer Ahmad, 2014, "Single Basin Solar Still Performance with Evacuated Tubes Solar Collector", International Conference on Advances in Engineering & Technology, 64-70.

[27] Ragh Vendra Singh, Shiv Kumar, M.M. Hasan , M. Emran Khan , G.N. Tiwari, 2013, "Performance of a solar still integrated with evacuated tube collector in natural mode", Desalination 318, 25–33.

[28] Mitesh I. Patel, P.M. Meena,Sunil Inkia, 2011, "Experimental Investigation on Single Slope double Basin Active Solar Still Coupled With Evacuated Glass Tubes" , International Journal of Advanced Engineering Research and Studies 1(1), 4-9.

[29] Sampathkumar K., 2012, "An Experimental Study on Single Basin Solar Still Augmented With Evacuated Tubes", Thermal Science 16 (2), 573-581.

[30] Shobha.B.S, Vilas Watwe, Rajesh .A.M, 2012, "Performance Evaluation of a Solar Still Coupled to an Evacuated Tube Collector type Solar Water Heater", International Journal of Innovations in Engineering and Technology, 1(1), 72-84.

[31] Mitesh I. Patel, P.M. Meena, Sunil Inkia, 2011, "Effect of dye on distillation of a single slope active solar still coupled with evacuated glass tube solar collector", International Journal of Engineering Research and Applications, 1 (3), 456-460.

[32] H.N.Panchal, 2013, "Enhancement of distillate output of double basin solar still with vacuum tubes", Journal of King Saud University – Engineering Sciences.

Review of Solar Air Heaters with Different Augmentation Techniques

Nitin H. Oza[a],N M Bhatt[a*]

[a] *Gandhinagar Institute of Technogy, Moti Bhoyan, Gandhinagar, 382721, India*

Abstract

The conventional solar air collectors have poor thermal efficiency due to high heat loss and low convective heat transfer coefficient between the absorber plate and flowing air stream. Some attempts have been made to improve the performance of conventional solar air collector by applying various designs and flow arrangements. The use of various turbulators and different augmentation techniques in different forms like fins as longitudinal fins and staggered fins, porous material, packed bed, baffles, wire mesh, ribs, delta winglets, vortex generator, rings, perforated blocks etc, in solar air heater is an effective way to improve the performance of solar air heater by increasing heat transfer coefficient between absorber and the air stream. In this paper an attempt has been made to carry out an extensive review of solar air heaters with different augmentation technique. Based on this review it is found that the due to provision of different augmentation, the heat transfer rate is increased and therefore thermal efficiency or performance of solar air heater increases significantly.

Keywords: Solar air heater, Evacuated tube solar air collector, turbulator, augmentation techniques.

1. Introduction

1.1. Need of solar energy

Rapid increase in energy prices and the continuous reduction of the earth's conventional fuels resources as well as the increased world-wide global warming have been the motivation for the recent growing interest in alternative sources of energy, such as solar energy. The development of renewable energy technologies is important with regarding to energy economy in future. The non-conventional sources of energy are capable of solving all above problems of energy. The renewable energy fulfills the gap between increasing energy demand and diminishing supply of conventional sources of energy. Need of clean environment and the increase in demand of more healthy and hygienic food-products encourages the use of renewable energy in industrial production and domestic processes. Solar energy is the best aspect to avoid energy crisis, to save conventional energy sources and to protect the environment.

1.2. Concept of different augmentation technique or turbulators for solar air heater.

Turbulators in flow field of air create turbulence in flow and improve the heat transfer exchange by convection. The presence of the turbulator in fluid flow results in enhancement of heat transfer from the absorber plate with more pressure drop. The turbulators can create one or more combinations of the following conditions favourable to heat transfer rate with minimum pressure penalty such as breaking the sub-laminar boundary, increasing the turbulent intensity, increase in heat transfer area and generation of vortex and secondary flows. The turbulators of larger height are responsible for high heat transfers but are also responsible for high pressure drop. Attempts have been made in order to solve this problem by providing perforations in the ribs, block and baffles. The perforations enhance the heat transfer and reduce the pressure drop across the channel. The perforations in elements allow a part of the flow to pass thorough these perforations and mix with the main flow to create a higher level mixing and turbulence.

2. Solar air heater

2.1. Single pass solar air heater

The heat transfer and friction factor correlations for packed bed solar air heater for a low porosity system were obtained by Thakur et al [1]. A wide range of geometrical parameters of wire screen matrix like wire diameter of 0.795 to 1.40 mm, pitch of 2.50 to 3.19 mm and number of layers from 5 to 12 were covered**.** The correlations were developed for the Colburn

---

[*]Corresponding author. Mo:+919904406000
E-mail address: nmbhatt19@gmail.com

factor and friction factor for a low range of porosities from 0.6678 to 0.880 and packing Reynolds number ranges from 182 to 1168. It was seen that both the heat transfer coefficient and the friction factor were strong functions of geometrical parameters of the porous packed bed. Volumetric heat transfer coefficient was increased with decrease in porosity. The investigation of heat transfer and friction characteristics of packed bed solar air heater with wire mesh as packing material was also studied by Prasad et al [2]. They concluded that the enhancement of efficiency was a strong function of mass flow rate of air and the porosity of the bed. The bed with lower value of porosity of 0.599 had the best thermal performance with efficiency between 53.3% and 68.5%. The efficiency enhancement was found from 89.5% at minimum mass flow rate of air to 76.9% at the maximum mass flow rate of air in this range of porosity. They found that the heat transfer coefficient was increased with decrease in porosity and with increase of mass flow rate of air. Colburn factor was decreased with an increase of Reynolds number and was increased with an increase of porosity whereas the friction factor was decreased with an increase of Reynolds number and porosity. Colburn factor and friction factor were the strong function of the geometrical parameters like pitch to diameter ratio of wire mesh, number of layers and porosity. As per the comparison between experimental and theoretical value, Colburn factor lied within the maximum deviation of 4.43% where as the maximum deviation of friction factor was 10.53%. An analytical model to predict the thermal performance of a novel parallel flow packed bed solar air heater was developed by Dhiman et al [3]. This model described that a parallel flow solar air heater with feeding packed material in its upper passage enabled to provide a higher heat flux compared to the conventional non-porous bed double flow systems. The effect of different air outlet temperatures, mass flow rate of air and different porosities of the packed material on heat transfer characteristics and thermal performance of parallel flow packed bed solar air heater was examined. The parallel flow packed bed solar air heater was found to be more efficient than the conventional non-porous double flow solar air heaters with 10–20% increase in its thermal efficiency. The effect of the fraction of mass flow rate of air in the upper or lower flow passage of parallel flow packed bed solar air heater performance was also investigated theoretically. The fraction of the mass flow rate of air in the respective passage of the parallel flow packed bed solar air heater was shown to be important parameter in finding the effective thermal efficiency of the heater.
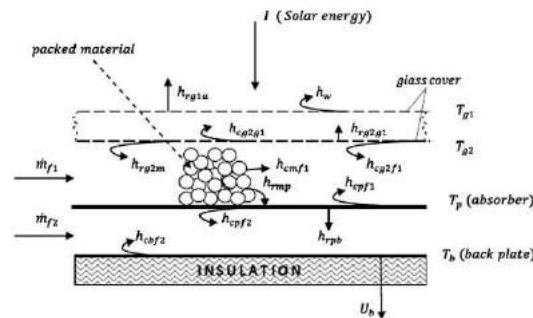
Fig.1. Schematic diagram of parallel flow packed bed solar air heater [3]

The performance of a solar air heater with packed bed latent storage energy for nocturnal use was described by Bouadila et al [4]. They found that the solar air heater gave a uniform useful heat during discharging process. The value of heat flux was 200W/m^2 during 11.00 pm at night. In closed or opened mode the gross daily energy efficiency of the solar air heater as latent storage collector varied between 32% and 45% where as the daily energy efficiency varied between 13% and 25%. In open cycles, the solar air heater latent storage collector gives a daily efficiency of 35%. The solar collector with storage energy had a daily efficiency close to the commercial collector was 45%. The energy and exergy analyses of porous baffles inserted in solar air heaters were analyzed by Bayrak et al [5]. It included the porous baffles with different thicknesses used as passive component inside heaters. Closed-cell aluminum was chosen as porous medium with thicknesses of 6 mm and 10 mm and a total surface area of 50cm^2. They were placed in sequentially and staggered form on the solar air heater. The parameters of inlet and outlet temperatures, absorbing plate temperatures, ambient temperature and solar radiation were measured. The measurements were performed at two various mass flow rates of air of 0.016 kg/s and 0.025 kg/s. By using the first and second laws of thermodynamics, the results of energy and exergy efficiencies of the solar air heater were obtained. Five different types of solar air heaters were tested and compared with each other for their efficiencies. The higher collector efficiency and air temperature rise were achieved by solar air heater with a thickness of 6 mm and air mass flow rate of 0.025 kg/s while the lowest value of efficiency was obtained for the solar air heater with non-baffle collector and air mass flow rate of 0.016 kg/s.

Fig.2. Porous baffles [5]

The numerical analysis of mechanical ventilation solar air collector with internal baffles was analyzed by Jianjun et al [6]. The research included a simple structure of mechanical ventilation solar air collector with internal baffles. A numerical model was developed to predict the internal flow and heat transfer characteristics. The results showed that the inertness of baffles increases the convective heat transfer process and reduces the radiation heat loss, which contributed to improve the efficiency. But the presence of baffles causes flow separation which resulted in flow loss to some limit. The convective heat loss of the top cover plate was important in the total heat loss. The effect of baffle number, thickness of air gap, number of top glass cover and the operating conditions on the collector performance was also analyzed, and the results showed that as for a specific scale collector, the optimum baffle number was three. The operating parameters such as the surrounding temperature, solar radiation intensity had significant effect on the temperature rise but had little effect on collector efficiency, which showed that this kind of solar air collector could be applied in a wide range of geographical latitude.

The thermal performance of a single pass solar air heater with longitudinal fins used with the absorber plate to increases the heat exchange and render the flow of air in the channel was described by Chabane et al [7]. The maximum efficiency of air heater by using five longitudinal fins and without using fins at mass flow rate of air 0.012kg/s was 40.02% and 34.92% respectively. The efficiency of the collector depends on the solar radiation and surface geometry of the collector and also on fins on the back of absorber plate. The thermo-hydraulic performance of concentrated solar air-heater with internal multiple-fin array was investigated by Kasperski and Nems [8]. A Thermo hydraulic efficiency test was used to find the best fin arrangement of the receiver. The tests were carried out to find the thermo hydraulic efficiency of the collector against the volumetric air flux. If there was no limit of the air speed, half-pipe finned technology gave 14% efficiency improvement in relation to the smooth pipe arrangement of the solar collector with black paint and double glass envelope, and 3.3% for the solar collector with selective layer and single glass envelope. If there was a limit of air velocity of 5m/s in piping system, the half-pipe finned technology gives a 13% efficiency improvement compared to the smooth pipe arrangement of the solar collector with black paint and double glass envelope, and 11% for the solar collector with selective layer and single glass envelope. Multiple fin array technology enabled to decrease the demandable air flux of 7-10 times in comparison to the smooth pipe arrangement of the absorber. The efficiency of internal multiple fin array arrangement was higher than the smooth pipe arrangement if the flux was decreased. The collector efficiency of single pass solar air heater with and without using fins was studied by Chabane et al [9]. The collector efficiency of a single pass solar air heater without and with use of fins attached below the absorbing plate was investigated experimentally. Due to attachment of the fins into the interior surface of an absorber plate, the effect of increasing the heat transfer coefficient was compensated with the effect of decreasing the temperature difference of heat transfer, while fins provide an enlarged heat transfer area. The improvements of collector efficiencies in the single pass solar air heaters with, and without fins attached were increased with increasing the mass flow rate of air especially for operating at lower mass flow rate. Experiments were performed for two mass flow rates of air 0.012 and 0.016 kg/s. The maximum efficiency obtained for the 0.012 and 0.016 kg/s with, and without fins were 40.02, 51.50% and 34.92, 43.94% respectively.

2.2. Double pass solar air heater

Ahmed et al. [10] performed the experiments to examine the efficiency of double-pass solar air heater with fin by changing the intensity of solar radiation and the mass flow rate of air. The solar collector with finned absorber had efficiency of more than 75% at a mass flow rate of 0.072 kg/s and solar radiation intensity at 788 W/m^2. The collector with finned absorber was 8% more efficient than flat plate absorber. The efficiency of collector was depended on mass flow rate of air and solar radiation intensity. The efficiency was increased with increase in mass flow rate of air and solar radiation intensity. If the solar radiation intensity varied from 423W/m^2 to 788W/m^2, increase in efficiency was about 20-30%. If the mass flow rate of air varied from 0.04 kg/s to 0.083 kg/s, the efficiency increase was about 35%-50%. The thermal performance of a force convective double-pass solar air collector with staggered fins was studied by Ahmed et al. [11]. The double-pass solar collector with staggered fins had efficiency of more than 75% at a mass flow rate of air 0.083 kg/s and solar radiation intensity at 788 W/m^2. The efficiency of collector was depended on mass flow rate of air and solar radiation intensity. The

efficiency was increased with increase in mass flow rate of air and solar radiation intensity. If the solar radiation intensity varied from 423W/m^2 to 788W/m^2, increase in efficiency was about 25%. If a mass flow rate of air varied from 0.04 kg/s to 0.083 kg/s, the efficiency increase was about 40%.
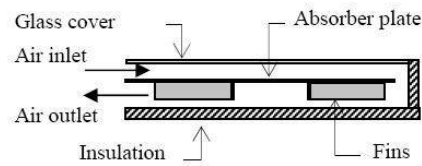

Fig.3. Schematic diagram of a staggered fin double pass solar collector [11]

The performance of double-pass solar air collector with longitudinal fins was described by Ahmed et al. [12]. The effects of mass flow rate of air, number and height of fins on efficiency of the solar collector was evaluated. The collector efficiency increased with increase in number and height of fins. The efficiency of the collector was depended on the mass flow rate of air and it increased with increasing mass flow rate of air. For a mass flow rate of 0.02-0.12kg/s, efficiency of the double pass solar collector with longitudinal fins was about 42-73%**.** Ahmed et al. [13] evaluated the performance of a finned double pass solar air collector. They evaluated the effects of mass flow rate of air and solar radiation on efficiency of the solar air collector. The efficiency of the collector depended on the mass flow rate of air. The efficiency of solar air heater increased with increase in mass flow rate of air. The optimum efficiency was about 70% for the mass flow rates between 0.07-0.08 kg/s. Increase in efficiency was also proportional to solar radiation. The heat-removal factor and overall heat loss coefficient was proportional to the increase in solar radiation. The performance and entropy generation of the double-pass solar air heater with longitudinal fins was analyzed by Paisarn [14]. The effect of the height and number of fins on the performance and entropy generation of solar air heater was evaluated. It was found that the thermal efficiency increased with increasing the height and number of fins. The entropy generation was inversely proportional to the height and number of fins. The performance of double pass solar collector with longitudinal fins provided on both sides of absorber was investigated by Ahmed et al [15]. They showed that the collector efficiency increased as the number and height of fins increases. For a mass flow rate of 0.02-0.1kg/s, the double-pass solar collector efficiency was about 36-73% in upper fins, 37-75% in lower fins, and 46-74% in upper and lower fins. The efficiency of the collector was strongly dependent on the mass flow rate of air.
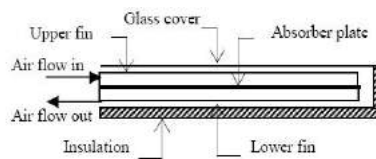
Fig.4. Schematic of the double pass solar collector with longitudinal fin [15]

Energy analysis and improvement potential of finned double-pass solar collector was analysed by Ahmed et al [16]. The analysis showed that the energy efficiency of the finned double pass solar collector was strongly depended on mass flow rate of air. Energy efficiency was increases with increase in mass flow rate of air. The optimum energy efficiency was approximately 77% at mass flow rate of 0.09kg/s. Efficiency was also increased with increase in solar radiation intensity. The optical efficiency of the finned double pass solar collector was approximately 70-80%. The exergy efficiency was between 15% and 28% with improvement potential of approximately 740-1070W for solar radiation of 425-790W/m^2. The improvement potential increased with increasing mass flow rate of air. The performance and cost benefits analysis of double-pass solar collector with and without fins was analysed by Ahmed et al [17]. The effect of mass flow rate of air and solar radiation intensity on thermal efficiency of the collector was evaluated. The thermal efficiency was proportional to the solar radiation intensity at a specific mass flow rate. The thermal efficiency was increased by 9% at a solar radiation intensity of 425-790W/m^2 and mass flow rate of air was 0.09 kg/s. The double pass solar air collector with fins was more cost effective than without fins for mass flow rate of 0.01-0.07kg/s. Also the simulation was obtained for double pass solar collector with fins at Nusselt number of 5.42-36.21. The energy efficiency increased with increase of Nusselt number. If Nusselt number was increased, the outlet temperature of air was decreased at any solar radiation intensity.

Sopian et al [18] evaluated the performance of the double-pass solar air heater with and without porous media in the lower channel. This evaluation included the effect of mass flow rate, solar radiation, and temperature rise on thermal efficiency of the solar collector. Several combinations of upper and lower channel depths were used. It was found that introducing porous media in the second channel also increased the heat transfer area. Such type of collector has a higher thermal performance compared to the conventional single-pass solar collector. The thermal efficiency of the double-pass solar collector with porous media was about 60-70% and it was 20-70% higher than that of without porous media collector.
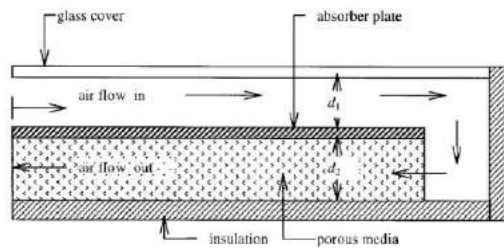
Fig.5. Schematic of a double pass solar collector with porous media in the second channel [18]

The thermal performance of double pass solar air collector with and without porous material was analysed by Ramani et al [19]. They showed that the thermal performance of collector with porous material was 25% higher than without porous material and 35% higher than that of single pass collector. For higher effective thermal efficiency solar collector should be operated at lower mass flux and higher porosity. Thermal performance of a double pass solar air heater with a packed bed above the heater absorber plate to achieve higher outlet temperature of the flowing air was studied by Ramadan et al [20]. It was advised to use the system with higher masses or low porosities of the packed bed. It was observed that the thermo hydraulic efficiency increased with increasing mass flow rate of flowing air until a value of 0.05 kg/s. Beyond the limit of this value, thermo hydraulic efficiency became insignificant and therefore it was advised to operate double pass solar air collector with packed bed with the mass flow rate of air equal to 0.05 kg/s or lower which had a lower pressure drop across the system. It was also observed that, gravel gives slightly better performance than limestone as packed bed.
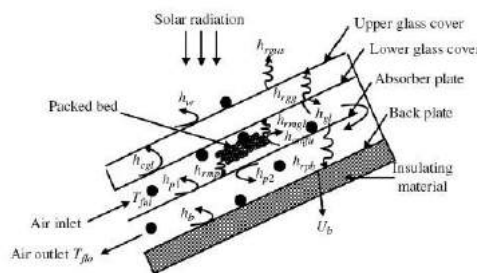
Fig.6. Double pass solar air heater with packed bed [20]

The thermal performance of single and double pass solar air heaters with wire mesh layers instead of a flat absorber plate was evaluated by Aldabbagh et al [21]. This evaluation included the effect of mass flow rate of air on outlet temperature and thermal efficiency. They found that the efficiency increases with increasing the mass flow rate of air. The mass flow rate of air used was between 0.012 and 0.038kg/s. For the same mass flow rate of air, the efficiency of double pass solar air heater was found to be higher than single pass solar air heater by 35-45%. Maximum efficiencies obtained for single and double pass solar air collectors were 45.93 and 83.65% respectively for mass flow rate of air was 0.038kg/s.
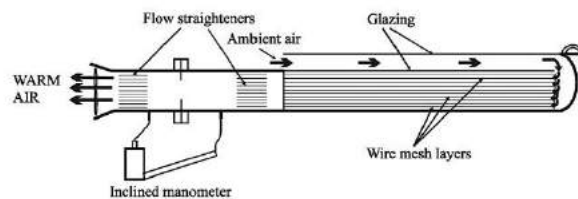
Fig.7. Double pass solar air heater with wire mesh as packing bed [21]

The thermal and thermo hydraulic performance of counter and parallel flow packed bed solar air heaters was determined by Dhiman et al [22]. The efficiency of the counter and parallel flow packed bed solar air heaters was compared theoretically and experimentally. The average absolute deviations for efficiency values were found to be 9.6% and 10.2% for counter flow and parallel flow packed bed solar air heater respectively. Thermo hydraulic efficiency of counter flow packed bed solar air heater was higher than parallel flow until the total mass flow rate of 0.03kg/s. For mass flow rate beyond 0.03kg/s, the thermo hydraulic efficiency of counter flow packed bed solar air heater was decreased, whereas it continuously increased in parallel flow packed bed solar air heater until the total mass flow rate of 0.06kg/s. Parallel flow packed bed solar air heater had 10% higher thermo hydraulic efficiency when air passed steady at different mass flow rate in its upper and lower ducts

compared to the counter flow packed bed solar air heater. Counter flow packed bed solar air heater should be operated at lower total mass flux and higher porosity for higher thermo hydraulic efficiency while parallel flow packed bed solar air heater can be operated at higher total mass flux and lower porosity. El-Sebaii et al [23] evaluated the thermal performance of double pass finned plate solar air heater. They found that the outlet temperature of double pass V-corrugated plate solar air heater as shown in Fig. 8(a) was 2.1 - 9.7% higher than that of double pass finned plate solar air heater as shown in Fig.8(b). The double pass V-corrugated plate solar air heater was 9.3-11.9% more efficient than double pass finned plate solar air heater. The thermal efficiency of double pass finned plate and double pass V-corrugated solar air heater was increased with increasing mass flow rate of air until the 0.04kg/s. Beyond which the increase in thermal efficiency of both type of collector was insignificant. The maximum thermo hydraulic efficiency of the double pass V-corrugated solar air heater was 17.4% higher than that of double pass finned plate solar air heater. The optimum thermo hydraulic efficiency of double pass finned plate and V-corrugated plate were obtained at mass flow rate of air of 0.0125 and 0.0225 kg/s respectively.
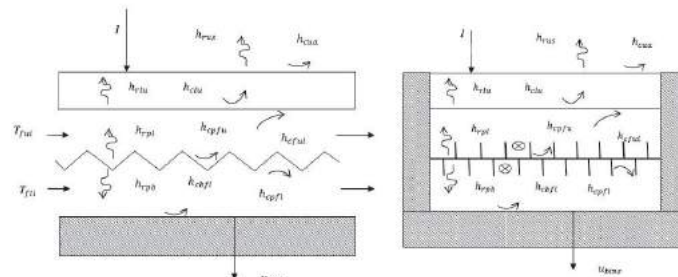
Fig. 8. Double pass (a) V-corrugated plate SAH (b) finned plate solar air heater [23]

The performance of single and double pass solar air heater with fins and steel wire mesh as absorber was studied by Omojaro and Aldabbagh [24]. The study included the effect of mass flow rate of air between 0.012kg/s and 0.038kg/s on outlet temperature of air and efficiency of solar air heater. Efficiency was found to be increased with increase in mass flow rate of air. For same mass flow rate of air, the efficiency of double pass solar air heater was higher than single pass solar air heater by 7-19.4%. Maximum efficiencies for single and double pass air heater were 59.62% and 63.74% at mass flow rate of 0.038kg/s.

2.3. Evacuated tube solar air heater

The thermal performance of one ended evacuated tube solar air collector at different flow rates was evaluated by Yadav and Bajpai [25]. They achieved higher temperature difference at a low flow rate so efficiency was also low. At a high flow rate the efficiency was high but the temperature difference was decreased. With counter flow the efficiency and temperature difference obtained was higher than parallel flow. Attachment of reflectors beneath the evacuated tubes achieved the higher solar radiation incident on them almost twice hence the efficiency increased. Insertion of a copper coil in the circular pipe increased the heat transfer coefficient and worked as fin which resulted in to higher efficiency. The highest temperature difference achieved on a summer day was 36.8^{o}C.
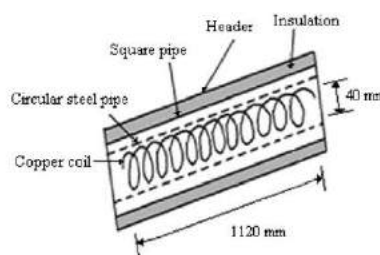
Fig.9. Schematic diagram of a copper coil in a header [25]

The performance of evacuated tube solar collector for heating of air in India was studied by Yadav and Bajpai [26]. The study included the effect of insolation of solar radiation and mass flow rate of air on the outlet temperature of the air with time and type of flow i.e. upward flow and downward flow. It was observed that downward flow condition was more effective and efficient than upward flow condition at all mass flow rate of air due to minimum losses in downward flow with temperature attained of 60°C and more.

3. Conclusion

From the literature review the following conclusion has been obtained

- For solar collector with porous media, the enhancement of efficiency is a strong function of mass flow rate of air and the porosity of bed. The parallel flow packed bed solar air heater is found to be more efficient than the conventional non-porous double flow solar air heaters with 10–20% increase in its thermal efficiency.
- The higher collector efficiency and air temperature rise are achieved by solar air heater with baffle. The inertness of baffles increases the convective heat transfer process, which contributes to improve the efficiency.
- For all types of solar air heater described above the efficiency of collector depends on mass flow rate of air and solar radiation intensity. If mass flow rate of air is increased up to certain limit and solar radiation intensity increases, the efficiency increases.
- The collector efficiency increases as the number and height of fins increases in case of solar air heater with longitudinal fins. The entropy generation is inversely proportional to the height and number of fins.
- The porous media in the second channel of double pass solar air heater also increases the heat transfer area. Such a collector has a higher thermal performance compared to the conventional single-pass solar collector.
- Counter flow packed bed solar air heater should be operated at lower total mass flux and higher porosity for higher thermo hydraulic efficiency while parallel flow packed bed solar air heater can be operated at higher total mass flux and lower porosity.
- Thermal and thermo hydraulic efficiency of double pass V-corrugated plate solar air heater are higher than double pass finned plate solar air heater.
- The provision of a copper coil as fin in the evacuated tube solar collector increases the efficiency by increasing the heat transfer coefficient.

References

[1] N.S. Thakur, J.S. Saini and S.C Solanki Heat transfer and friction factor correlations for packed bed solar air heater for a low porosity system solar Energy 74 (2003) 319-329

[2] S.B. Prasad , J.S. Saini and Krishna M. Singh Investigation of heat transfer and friction characteristics of packed bed solar air heater using wire mesh as packing material Solar Energy 83 (2009) 773-783

[3] Prashant Dhiman, N.S. Thakur, Anoop Kumar and Satyender Singh An analytical model to predict the thermal performance of a novel parallel flow packed bed solar air heater Applied Energy 88 (2011) 2157-2167

[4] Salwa Bouadila, Sami Kooli, Mariem Lazaar, Safa Skouri and Abdelhamid Farhat Performance of a new solar air heater with packed bed latent storage energy for nocturnal use Applied Energy 110 (2013) 267-275

[5] Fatih Bayrak, Hakan F. Oztop and Arif Hepbasli Energy and exergy analyses of porous baffles inserted solar air heaters for building applications Energy and Buildings 57 (2013) 338-345

[6] Jianjun Hu, Xishan Sun, Jinliang Xu and Zhixian Li Numerical analysis of mechanical ventilation solar air collector with internal baffles Energy and Buildings 62 (2013) 230-238

[7] Foued Chabane, Noureddine Moummia and Said Benramache Experimental analysis on thermal performance of a solar air collector with longitudinal fins in a region of Biskra, Algeria Journal of Power Technologies 93 (1) (2013) 52-58

[8] Jacek Kasperski, Magdalena Nems Investigation of thermo-hydraulic performance of concentrated solar air-heater with internal multiple-fin array Applied Thermal Enginnering 58 (2013) 411-419

[9] Foued Chabane, Noureddine Moummi, Said Benramache, Djamel Bensahal and Okba Belahssen Collector Efficiency of Single Pass Solar Air Heaters with and without Using Fins Engineering Journal Volume17 Issue3

[10] Ahmad Fudholi, M.H. Ruslan, M.Y. Othman, M.Yahya, Supranto, A.Zaharim and K. Sopian Collector Efficiency of the Double-Pass Solar Air Collectors with Fins SYSTEM SCIENCE and SIMULATION in ENGINNERING ISBN: 978-960-474-230-1

[11] Ahmad Fudholi, M.H. Ruslan, M.Y. Othman, M.Yahya, Supranto, A.Zaharim and K. Sopian Experimental Study of the Double-Pass Solar Air Collector with staggered Fins SYSTEM SCIENCE and SIMULATION in ENGINNERING ISBN: 978-960-474-230-1

[12] Ahmad Fudholi, M.H. Ruslan, M.Y. Othman, M.Yahya, Supranto, A.Zaharim and K. Sopian Mathematical Model of Double-flow Solar Air Collector with Longitudinal Fins Recent Advances in Fluid Mechanics, Heat and Mass Transfer and Biology ISBN: 978-1-61804-065-7

[13] Ahmad Fudholi, Mohd Hafidz Ruslan, Lim Chin Haw, Sohif Mat, M.Y. Othman, Azami Zaharim, and Kamaruzzaman Sopian Performance of Finned Double-flow Solar Air Collector Recent Advances in Fluid Mechanics, Heat and Mass Transfer and Biology ISBN: 978-1-61804-065-7

[14] Paisarn Naphon On the performance and entropy generation of the double-pass solar air heater with longitudinal fins Renewable Energy 30 (2005) 1345- 1357

[15] Ahmad Fudholi, Kamaruzzaman Sopian, Mohd Hafidz Ruslan,Mohd. Yusof Othman and Muhammad Yahya Thermal Efficiency of Double Pass Solar air Collector with Longitudinal Fins as Absorbers American Journal of Applied Sciences 8 (3): 254-260,2011

[16] Ahmad Fudholi, Kamaruzzaman Sopian, Mohd Yusof Othman, Mohd Hafidz Ruslan and B. Bakhtyar Energy analysis and improvement potential of finned double-pass solar collector Energy Conversion and Management 75 (2013) 234-240

[17] Ahmad Fudholi, Kamaruzzaman Sopian, Mohd Hafidz Ruslan and Mohd Yusof Othman Performance and cost benefits analysis of double-pass solar collector with and without fins Energy Conversion and Management 76 (2013) 8-19

[18] K. Sopian, Supranto, W.R.W. Daud, M.Y. Othman and B. Yatim Thermal performance of the double-pass solar collector with and without porous media Renewable Energy 18 (1999) 557-564

[19] B.M. Ramani, Akhilesh Gupta and Ravi Kumar Performance of a double pass solar air collector Solar Energy 84 (2010) 1929-1937

[20] M.R.I. Ramadan, A.A. El-Sebaii,S. Aboul-Enein and E. El-Bialy Thermal performance of a packed bed double-pass solar air heater Energy 32 (2007) 1524-1535

[21] L.B.Y. Aldabbagh, F. Egelioglu and M. Ilkan single and double pass solar air heaters with wire mesh as packing bed Energy 35 (2010) 3783-3787

[22] Prashant Dhiman, N.S. Thakur and S.R. Chauhan   Thermal and thermo hydraulic performance of counter and parallel flow packed bed solar air heaters Renewable Energy 46 (2012) 259-268

[23] A.A. El-Sebaii, S. Aboul-Enein, M.R.I. Ramadan, S.M. Shalaby and B.M. Moharram Thermal performance investigation of double pass-finned plate solar air heater Applied Energy 88 (2011) 1727-1739

[24] A.P. Omojaro and L.B.Y. Aldabbagh The performance of single and double flow solar air heater with fins and steel wire mesh as absorber Applied Energy 87 (2010) 3759-3765

[25] Avadhesh Yadav and V.K. Bajpai Thermal performance of one ended evacuated tube solar air collector at different flow rates experimental investigation. International Journal of Ambient Energy

[26] Avadhesh Yadav and V.K. Bajpai An Experimental Study on Evacuated Tube Solar Collector for Heating of Air in India World Academy of Science, Engineering and Technology 55 2011

Design and static analysis of leaf spring by using different cross section.

*Priyanka Kothari, **Amit Patel

*PG Student of M.E.Cad/Cam , Gandhinagar Institute Of Technology Kalol, Gujarat
**Assistant Professor, Department Of Mechanical , Gandhinagar Institute Of Technology Kalol, Gujarat

Abstract

Leaf springs are one of the oldest suspension components they are still frequently used, especially in commercial vehicles. This work is carried out on a leaf spring of a TATA ACE EX. The automobile industry has shown increased interest in the replacement of steel spring with composite leaf spring due to high strength to weight ratio. The main function of leaf spring assembly as suspension element is not only to support vertical load, but also to isolate road-induced vibrations. This work deals with replacement of cross section of rectangular steel leaf spring of a light commercial vehicle with cross section of trapezoidal leaf spring using 65si7. Numerical calculations are completed with the help of design equations of spring. Dimension of trapezoidal cross section are to be taken as same dimension of rectangular cross section. The modeling of the leaf spring has been done in Pro-E. Finite element analysis of the leaf spring has been carried out in ANSYS 14.5. Max Von Misses stress and Max Displacement are the output parameters of this analysis.

Keywords: Steel leaf spring, Static analysis, Different cross section

Nomenclature

n_f	Number of extra full-length leaves
n_g	Number of graduated-length leaves including master leaf
n	Total number of leaves b Width of each leaf (mm)
t	Thickness of each leaf (mm)
L	Length of the cantilever or half the length of semi- elliptic spring (mm)
P	Force applied at the end of the spring (N)
P_f	Portion of P taken by the extra full-length leaves (N)
P_g	Portion of P taken by the graduated-length leaves (N)
δ	Deflection of the spring (mm)
σ	Stress of the spring (Mpa)
E	Young's modulus (Mpa)
ρ	Density
h	Height of each leaf (mm)

1. Introduction

Today automotive manufacturers are faced with several complex challenges. In a highly competitive market, customers are demanding more for their money. Motorists wish cars that propose high performance, comfort, refinement, safety as well as increased vehicle customization [9].The automotive industry is also faced with Governments who are consistently introducing legislation that demand improvements in fuel efficiency, reduced emissions, increased recycling and greater safety for both pedestrians and occupants. The circumstances facing the auto industry is most excellently summarized by quoting an article in the Polymotive magazine "Far-reaching efforts to achieve components that are rigid, strong, safe and at the same time, as light as possible are needed in order to survive in automotive manufacturing"[9].

In order to conserve natural resources and economize energy, weight reduction has been the main focus of automobile manufacturer. Weight reduction can be achieved primarily by the introduction of better material, design optimization and better manufacturing processes [5]. Parabolic Leaf sprigs are essential suspension elements used on mini loader trucks necessary to minimize the vertical vibrations, impacts and bumps due to road irregularities and to ensure safety of the loaded cargo. Parabolic Leaf springs are widely used for automobiles. The Parabolic leaf spring absorbs the vertical vibrations and impacts due to road irregularities by means of variations in the spring deflection so that the potential energy is stored in spring as strain energy and then gradually released to maintain comfort[4]. The introduction of composite materials was made it possible to reduce the weight of leaf spring without any reduction on load carrying capacity and stiffness. Since, the composite materials have more elastic strain energy storage capacity and high strength-to-weight ratio as compared to those of steel [5].

1.1 Principle of leaf spring[3]

The suspension leaf spring is one of the potential items for weight reduction in automobile as it accounts for ten to twenty percent of the unsprung weight. The introduction of composites helps in designing a better suspension system with better ride quality if it can be achieved without much increase in cost and decrease in quality and reliability. In the design of springs, strain energy becomes the major factor. The relationship of the specific strain energy can be expressed as [7]

$$U = \frac{\sigma^2}{\rho E} \tag{1.1.1}$$

Where σ the strength is ρ is the density and E is the Young's Modulus.

It can be easily observed that material having lower modulus and density will have a greater specific strain energy capacity. The introduction of composite materials made it possible to reduce the weight of the leaf spring without reduction of load carrying capacity and stiffness due to the following factors of composite materials as compared to steel.

1.2 Semi- elliptic leaf spring

The figure shows a semi- elliptic spring. These springs are usually formed by stacking leafs of steel, in progressively longer lengths on top of each other, so that the spring is thick in the middle to resist bending and thin at the ends where it attaches to the body. A leaf spring should support various kinds of external forces. The top leaf is known as the master leaf. The eye is provided for attaching the spring with another machine member. The amount of bend that is given to the spring from the central line, passing through the eyes, is known as camber [1]. The camber is provided so that even at the maximum load the deflected spring should not touch the machine member to which it is attached. The central clamp is required to hold the leaves of the spring. The central clamp is required to hold the leaves of the spring. However, the bolt holes required to engage the bolts to clamp the leaves weaken the spring to some extent. Rebound clips help to share the load from the master leaf to the graduated leaf.
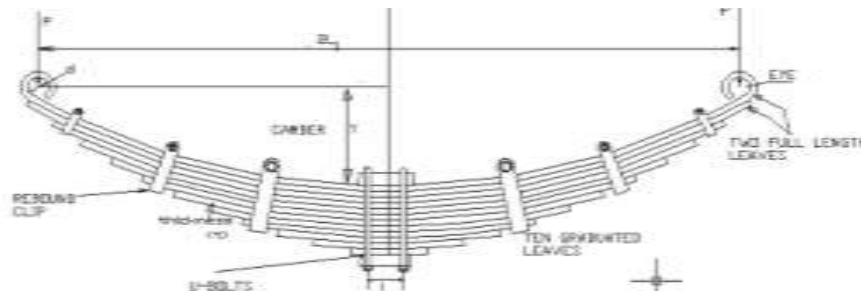
Figure 1.1 semi elliptical leaf spring [3]

2. Problems identification

After reviewing the literatures, we identify some of the problem which generally occurs in case of leaf spring. The usual steel leaf spring has various problems identified which are listed as follow:

- Low strength: It is observed that the leaf springs be likely to break and deteriorate at the eye end segment which is extremely near to the shackle and at the middle.
- More weight: The usual steel leaf spring having more weight, which additionally influences the fuel efficiency.

3. Objective

The objective of the present work is to design & static analysis of leaf spring. Reducing weight while increasing or maintaining strength of products is getting to be highly important research issue in this modern world. This is done to achieve the following.

- To the replace conventional steel leaf spring rectangular cross section with steel leaf spring trapezoidal cross section by using same dimensions for both cross sections.
- Compare the load carrying capacity, stresses, deflection and weight savings of trapezoidal cross section with rectangular cross section of leaf spring.

4. Design calculation of leaf spring for cross section:

4.1 Cross section used for leaf spring

Figure 4.1 rectangular cross section of leaf spring   Figure 4.2 trapezoidal cross section of leaf spring
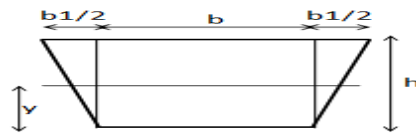
4.1 Input parameters of leaf spring

Table 4.1 geometric property of leaf spring

Design parameter of leaf spring	Value
Number of extra full-length leaves(n_f)	3
Number of graduated leaves(n_g)	0
Total number of leaves	3
Width of each leaf	60mm
Thickness of each leaf	8mm
Span length	860mm
Force applied at the end of the spring	4941N
Half length	405mm
Height of each leaf	8mm

4.2 Design equation for rectangular cross section

The equation of bending stress of spring is given by [11],

$$\sigma = \frac{(18*P*L)}{(b*t^3(2*ng+3*nf))} \tag{4.1.1}$$

$$= \frac{(18*2470*405)}{(60*8^3(2*0+3*3))}$$

$$= 521.015 Mpa$$

The equation of Deflection of spring is given by [11],

$$\delta = \frac{(12*P*L^3)}{(E*b*t^3*(2*ng+3*nf))} \tag{4.2.2}$$

$$= \frac{(12*2470*405^3)}{(2.1*10^5*60*8^3*(2*0+3*3))}$$

$$= 35.60 \text{ mm}$$

4.3 Modification in cross section of leaf spring design.

Table 4.2 theoretical calculation of trapezoidal cross section

Cross section	Stress (Mpa)	Deflection(mm)
60/40	723.39	47.36
60/50	605.35	40.72
60/55	559.00	37.24

From above results it is found that, by using cross-section 60/40 & 60/50 the value of stress is more than rectangular cross section .But by using 60/55 it's found that value of stress & displacement is nearer to rectangular cross section .It's also found that if value of width is increased then its result in decreasing value of stress .So proper trapezoidal cross section for leaf spring is selected 60/55.

4.4 Design equation for trapezoidal leaf spring.

The bending stress in the plate, which is uniform throughout, is given by [10]

$$\sigma = \frac{(M_b*Y)}{I} \tag{4.4.1}$$

Where, moment of inertia I is given by [11],

$$I = \frac{(6*b^2+6*b*b_1+6*b_1^2)}{36*(2*b_1+b_1)} h^3 \tag{4.4.2}$$

Where, neutral axis Y is given by [11],

$$Y = \frac{h*(3*b+2*b_1)}{(2*b_1+b_1)} \tag{4.4.3}$$

By putting the value of equation (4.4.2) & (4.4.3) in (4.4.1), we can get formula for Bending Stress.

$$\sigma = \frac{(36*P*L*(3*b+2*b_1))}{\left(h^2*(6*b^2+6*b*b_1+6*b_1^2)*(2*ng+3*nf)\right)} \tag{4.4.4}$$

$$= \frac{(36*2470*405*(3*55+2*2.5))}{(8^2*(6*55^2+6*55*2.5+6*2.5^2)*(2*0+3*3))}$$

$$= 559.00 Mpa$$

The equation of deflection of spring is

$$\delta = \frac{\left(36*P*L^3*(2*b_1+b_1)\right)}{\left(E*h^3*(6*b^2+6*b*b_1+6*b_1^2)*(2*ng+3*nf)\right)} \tag{4.4.5}$$

$$= \frac{\left(36*2470*405^3*(2*2.5+2.5)\right)}{\left(2.1*10^5*8^3*(6*55^2+6*55*2.5+6*2.5^2)*(2*0+3*3)\right)}$$

$$= 37.24 mm$$

5. Static analysis of leaf spring

5.1 Assumptions for analysis

- Automobile is assumed to be stationary.
- There are 3 parabolic leaf spring two at rear axle and two at front.
- Static study is performed for rear single parabolic leaf spring.
- The conventional leaf spring Material is 65si7.
- Taking factor of safety 2

Table 5.1 mechanical property of material [9]

Parameters	Value
Material of Spring	65Si7
Young's Modulus, E	2.1×10^5 MPa
Poisson's Ratio, ρ	0.266
Tensile Strength Ultimate	1272 MPa
Yield Strength	1158 MPa
Density	7.86×10^6 Kg/mm^3

Table 5.2 Chemical composition of existing Leaf spring [2]

C%	Si%	Mn%	P%	S%
0.50/0.60	0.15/0.35	0.65/0.95	0.035	0.65/0.95

5.2 Boundary condition for analysis
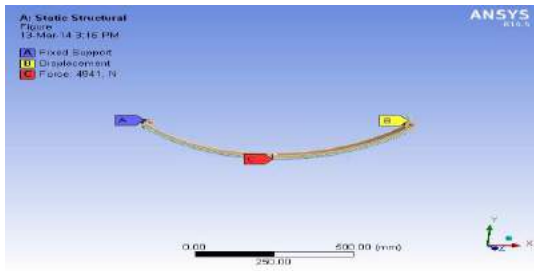
Figure 5.1 boundary condition for rectangular cross section   Figure 5.2 boundary condition for trapezoidal cross section
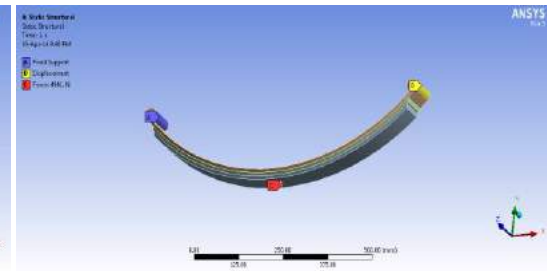
5.3 Output for rectangular cross section for leaf spring
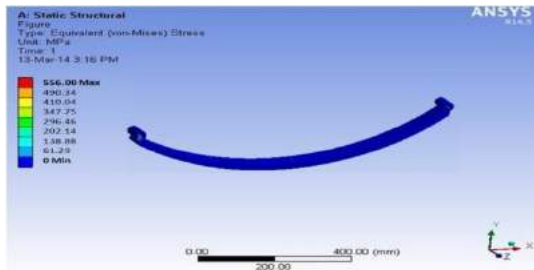
Figure 5.3 Stress generated on leaf spring   Figure 5.4 Deflection of leaf spring
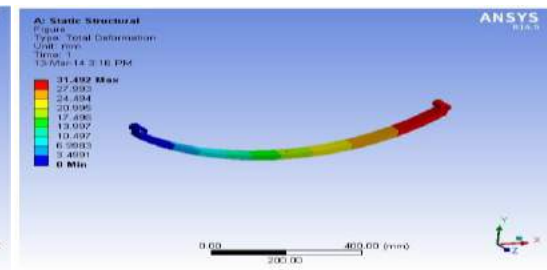
5.4 Output for trapezoidal cross section for leaf spring
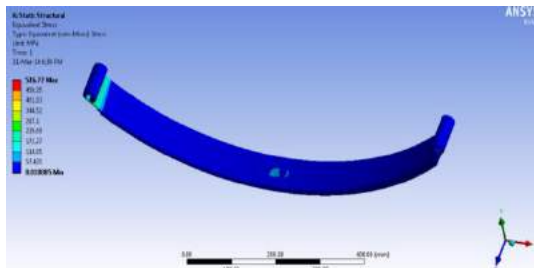
Figure 5.5 Stress generated on leaf spring   Figure 5.6 Deflection of leaf spring
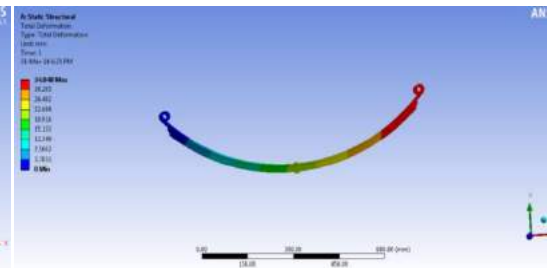
5.5 Results

Cross section	Stress(Mpa)		Deflection(mm)		Variations		Weight of leaf(Kg)
	Analytical	ANSYS Software	Analytical	ANSYS Software	Stress	Deflection	
Rectangular	521.015	556.00	35.60	31.492	6.79%	11.00%	11.700
Trapezoidal	559.00	516.77	37.24	34.492	7.6%	7.24%	10.200

6. Conclusion

- From analysis it is observed that by using trapezoidal cross- section the material is reduced rather than using rectangular cross section .Weight of rectangular cross section of leaf spring is 11.200 kg & weight of trapezoidal cross section of leaf is 10.700 kg .So from result it's proved that weight is reduced by using trapezoidal cross section. So Best cross section for leaf spring is trapezoidal due to weight reductions & stresses also reduced or nearer to rectangular cross section.

- From the static analysis results it is found that there is a maximum von misses stress of 556.00 Mpa in the steel leaf spring for rectangular cross section of leaf and the corresponding von misses stress in Trapezoidal cross section 516.77 Mpa for a given load of 4941N.

- All the FEA results are compared with the theoretical results and it is found that they are within the allowable limits and nearly equal to the theoretical results.

- For trapezoidal cross section of leaf spring, it's also found that as value of width is increased its result in decreasing value of stress.

6.1 Future scope

- We can use graduated leaf for same analysis of cross sections.

- We can use inverted trapezoidal cross sections for leaf & compare difference with cross section in output parameters.

References.

[1] Mahmud M. Shokrieh, Davood Rezaei "Analysis and optimization of a composite leaf spring" Composite Structures, 60 (2003) 317–325

[2]Dakshraj Kothari, Rajendra Prasad Sahu and Rajesh Satanka "Comparison of Performance of Two Leaf Spring Steels Used For Light Passenger Vehicle VSRD International Journal of Mechanical, Auto. & Prod. Engg. VSRD MAP, Vol. 2 (1), 2012, 9-16

[3] Y. N. V. Santhosh Kumar, M. Vimal Teja "Design and Analysis of Composite Leaf Spring" Dept. of Mechanical Engineering, Nimra College of Engineering & Technology, Ibrahimpatnam, Vijayawada.

[4] Manas Patnaik, Narendra Yadav, Ritesh Dewangan "Study of a Parabolic Leaf Spring by Finite Element Method & Design of Experiments"International Journal of Modern Engineering Research Vol.2, Issue 4, July-Aug 2012 pp-1920-1922.

[5] Malaga. Anil Kumar, T.N.Charyulu, Ch.Ramesh "Design Optimization Of Leaf Spring " International Journal of Engineering Research and Applications Vol. 2, Issue 6, November- December 2012, pp.759-765.

[6] Prahalad Sawant Badkar, Prahalad Sawant Badkar "Design Improvements of Leaf Spring of BEML Tatra 815 VVNC 8 X 8 Truck" International Journal of Emerging Technology and Advanced Engineering, Volume 3, Issue 1, January 2013.

[7] H.A.AI-Qureshi " Automobile leaf spring from composite materials " Journal of materials processing technology, 118(2001)58-61

[8] Ashish V. Amrute, Edward Nikhil karlus   "Design and assessment of multi leaf spring" international journal of research in aeronautical and mechanical engineering.Vol.1, Issue.7, November 2013.

[9] Edward Nikhil Karlus, Rakesh L. Himte, Ram Krishna rathore   "Optimization of mono parabolic leaf spring" International Journal of Advances in Engineering & Technology, Mar. 2014.

[10] V.B.Bhandari, Design of machine elements third edition TMG.

[11] Design Data book, Pg-6.1 Faculty of mechanical engineering .Psg College of technology, Coimbatore.

Frequency Based Method and Static Deflection Measurement Method For Crack Detection in Mechanical components: A Review

Jatin M.Patel[a] , Prof. Amit R.Patel[b], Prof. Mitesh J.Mungla[c] *

[a]ME CAD/CAM Student, Ghandhinagar Institue of Technology,Ghandhinagar,India
[b]Assit.Prof.,Ghandhinagar Institue of Technology,Ghandhinagar,India
[c]Assit.Prof.,Ghandhinagar Institue of Technology,Ghandhinagar,India

Abstract

This paper presents review of crack detection method in mechanical components. Various conventional and non-conventional methods are available for crack detection in mechanical components like cantilever beam, simply supported beam, rotating shaft, pipe, rotor etc. At present, multiple techniques, for instance, leakage magnet detection technology, ultrasonic detection technology, eddy detection technology and acoustic emission detection technique, have been widely used in identifying the crack. These traditional non destructive testing technologies are of low efficiency, and require complex instruments. At the same time, they need to detect the tested objects point by point. They are efficient but time consuming, expensive and laborious, particularly for slender beam like components. Therefore, researcher proposed a new detection technique based on vibration, based on natural frequency, based on deflection measurement etc, which can improve detection efficiency so as to determine crack location and size. It is found form the critical literature survey that, the non-conventional is to be developed for the crack detection which is acceptable and experimentally validate.

Keywords: Frequency, Static Deflection, Rotational Spring Model

Nomenclature	
E	Modulus of Elasticity
I	Moment of Inertia
a	Crack Depth
h	Beam Height
K_t	Rotational Spring Stiffness
f(a/h)	Dimensionless local compliance function
M	Bending Moment
P	Load
L	Length of Beam/Pipe
Greek symbols	
θ	Crack angle position
δ	Deflection
Subscripts	
c	Crack Position
nc	Uncracked Position

1. INTRODUCTION

In several areas of civil and mechanical engineering, at present, real challenges arising for the control, maintenance and retrofitting of existing structures and machinery concern the diagnostic identification of damages. Pipe is one of the five leading transportation tools and plays an important role in petrochemical industry, power plants, chemical plants, gas and oil transportation, etc. Crack is present in the component may grow during service and may result in the component failure once they grow beyond a critical limit. It is desirable to investigate the damage occurred in the structure at the early stage to protect the structure from possible catastrophic failures. Developing pipe testing technique can be avoid or decrease accidents and is an important guarantee for the safety service of pipe. Many reasons, such as corrosion damage, fatigue, creep damage and erosion, lead to pipe damage. However, fracture is always the final failure form. Therefore, crack diagnosis in the pipe is the most significant problem in non-destructive testing.

* Corresponding author. Mobile No.095 86 62 02 56
E-mail address: jatin.patel3990@gmail.com

There are various Non-destructive techniques (NDTs) available for the detection of the crack in the structural and mechanical components. To this purpose, non-destructive testing is of great interest under several respects, because it can be provided to direct assessment of integrity of structures during service or can be employed to assess the residual resistance of a structure after the occurrence of a strong seismic event. At present, multiple techniques, for instance, leakage magnet detection technology, ultrasonic detection technology, eddy detection technology and acoustic emission detection technique, have been widely used and available for identifying the crack. These traditional non destructive testing technologies are of low efficiency, and require complex instruments. At the same time, they need to detect the tested objects point by point. They are efficient but time consuming, expensive and laborious, particularly for slender beam like components. Therefore, researcher proposed a new detection technique based on vibration, based on natural frequency, based on deflection measurement etc, which can improve detection efficiency so as to determine crack location and size. It also can be utilized in detecting pipe damage in service.

2. CRACK DETECTION METHODS

Basically Two types of methods are available for detection of crack in mechanical components. one is conventional method and second is non conventional method,

1. Conventional (Non-Destructive Testing -NDT) methods
    I. Leakage magnet detection technology
    II. Ultrasonic detection technology
    III. Eddy detection technology
    IV. Ultrasound acoustics based assessment techniques etc.
2. Non conventional Methods
    I. Natural frequency method
    II. Wavelet analysis
    III. Modal (Vibration) Analysis
    IV. Finite element method of second generation wavelets
    V. Static Deflection Measurement Method
    VI. Wave Propagation Approach
    VII. Combine Wavelet Based Element and Genetic Algorithm
    VIII. Energy Method
    IX. Time-Domain Method
    X. Couple Response Measurement Method
    XI. Residual Error Method

Low detection efficiency, require complex instruments, time consuming, laborious and expensive. Due to this listed limitations, there is scope of alternative of conventional method for crack detection. Therefore, people proposed a new detection technique based on vibration, which can improve detection efficiency so as to determine crack location and size. It can be also utilized in detecting pipe damage in service.

3. REVIEW

3.1. Frequency-Based Method

Kaushar H. Barad et al. (2012) have been investigated detection of the crack presence on the surface of **beam-type structural element** using natural frequency is presented. To use first two natural frequencies of the cracked beam have been obtained experimentally and also used for detection of crack location and size. The crack is present in the component imparts local flexibility to the component and reduces the natural frequency of free vibration of the component. So that local damage also affects the mode shapes of the vibration of the component. Thus, Vibration Based (VBI) method can be a potential method for crack detection. Though, there has been an intense study on crack detection through vibration based inspection, they developed an effective and economically appropriate approach. The crack is modelled and represented by a rotational spring whose stiffness can be determined by using the linear elastic fracture mechanics approach using this approach; damage detection can be done using natural frequency. They have concluded the present method to detect crack location and size is fast and efficient. If Crack with larger crack depth ratio (a/h) imparts greater reductions in natural frequency than that of the smaller crack depth ratio. Hence, the accuracy of results are improves as crack depth increases. Crack present near to fixed end of beam imparts greater reductions in natural frequency than that to present at away from the fixed end [1].

* Corresponding author. Mobile No.095 86 62 02 56
E-mail address: jatin.patel3990@gmail.com

S.M. Murigendrappa et al.(2004) have been investigated Experimental and theoretical study on crack detection in **pipes filled with fluid**. The possibility of representing and modelling crack with straight front, normal to the axis, and part through the thickness in a straight pipe containing fluid under pressure, the fluid considered is water. Use two different materials; aluminium and mild steel have been examined. Crack size of pipe thickness ratio ranging from 0.19 to 0.64 is considered. Within the fluid pressure range of 0- 0.981MPa examined, the stiffnesses obtained by deflection method and natural frequency-based methods show good agreement. The representation and modelling of a crack by the rotational spring is reasonably accurate. The natural frequency-based method can be used to detect the location of an unknown crack in the pipeline. The maximum error in prediction of crack location is 2.6% for all the cases considered ,The error in the crack size prediction using these plots lies in the range -16.44% to 10.30% for aluminium and -5.83% to 12.04% for mild steel [2].

S.M. Murigendrappa et al.(2004) have been investigated the Frequency-based experimental and theoretical identification of multiple cracks in **straight pipes filled with fluid**. This technique work based on measurement of change of natural frequencies has been employed to detect multiple cracks in long pipes containing fluid with different pressures. The fluid considered as water; Three pressures in the range 0– 981 kPa, and crack size to thickness ratio of pipe in the range 0.19– 0.64 are studied. Two simultaneous cracks are considered in the experiments and the crack locations are predicted with an error less than 4.3%. Results on crack-equivalent rotational spring stiffness, which can be useful for the calculation of natural frequencies and crack size predictions of straight pipe [3].

M.R. Naniwadekar et al.(2008) have been investigated On prediction of crack in different orientations in **pipe** using frequency based approach, This technique work based on measurement of change in natural frequencies and modelling and of crack by rotational spring is employed to detect a crack with straight front in different orientations in a section of straight horizontal steel hollow pipe (pipe dimensions: outer diameter 0.0378m and inner diameter 0.0278 m). Crack orientations in pipe of the range is 0–60^0 with the vertical have been examined and also sizes/depths in the range 1– 4mm through the wall of thickness 5mm have been studied. Variation of rotational spring stiffness with crack size and orientation has been obtained experimentally by static deflection and vibration based methods. They have been concluded the spring stiffness reduces as expected, with an increase in crack size and it increases with an increase in the crack orientation angle. The crack location of pipe has been predicted with a maximum error of 7.29%. The sensitivity of the method for prediction of crack location in pipe for variations in experimental data has been examined by changing the difference between the frequencies of pipes with and without crack by ±10% [4].

Michele Dilena et al.(2011) have been investigated the Detecting cracks in **pipes** filled with fluid from changes in natural frequencies, The identification of a single open crack in a straight pipe containing fluid under with pressure by use of frequency measurements. The crack is assumed to be a transverse partial cut of the pipe wall thickness with straight front and it is represented by an equivalent elastic spring, It is shown that the change in the first two frequencies in a simply supported uniform pipe is sufficient to localize a small crack, except for a symmetrical position of pipe and to determine the damage severity. Closed-form expressions are provided for damage location and severity of pipe. Also turns out that the error in prediction of damage location is about 5% in pipe, whereas the error in crack severity of pipe for prediction ranges from 18% to 28% as conclusion[5].

S. Chinchalkar (2001) have been investigated on Determination of Crack Location in **Beams** using Natural Frequencies method. This is numerical method for determining the crack location in a beam with varying depth when the lowest three natural frequencies of the cracked beam are known. The crack is modelled and represented by rotational spring and graphs for spring stiffness versus crack location are plotted for each natural frequency. The point of intersection of the three curves of frequency gives the location of the crack. In earlier work in this area involved the use of the Frobenius technique for solving the governing differential equation analytically and then using a semi-numerical approach for obtain the crack location in beam. In this work, we use the finite element approach to solve the same problem. The beam is modelled by using beam elements and the inverse problem of finding the spring stiffness given the natural frequency is also shown to be related to the problem of a rank- one modification of an Eigen value problem. Examples carried for outlining the accuracy and ease of using this method are shown. The results are compared with those from semi-analytical approaches. The biggest advantage of this method is the generality in the approach, for different boundary conditions and also variations in the depth of the beam can be easily modelled.[6]

D.P. Patil et al.(2003) have been investigated on detection of multiple cracks using frequency measurements. A method for detection of multiple open cracks in a **slender Euler–Bernoulli beams** is presented based on frequency measurements. This method is based on the approach given by Hu and Liang [J. Franklin Inst. 330 (5) (1993) 841], transverse vibration modelling through transfer matrix method and crack is modelled and representation of a crack by rotational spring. The beam is divided into a number of segments, which can be decided by the analyst, and They have been associated with a

* Corresponding author. Mobile No.095 86 62 02 56
E-mail address: jatin.patel3990@gmail.com

damage parameter as consideration. The procedure gives a linear relationship explicitly between the changes in natural frequencies of the beam and the damage parameters for consider in cases. These parameters are determined from the knowledge of changes in the natural frequencies. After obtaining them, each of treated in turn to exactly pinpoint the crack location in the segment and determine its size of beam. The forward or natural frequency determination, problems are examined. This method is approximate, but it can handle segmented beams and any boundary conditions, intermediate spring or rigid supports, etc. The proposed method gives a clear insight into the whole analysis and for case studies (numerical) are presented to demonstrate of the method effectiveness for two simultaneous cracks of size 10% and more of section depth of beam. The differences between the actual and predicted crack locations and sizes are less than 10% and 15% respectively. The numbers of segments of beam is virtually divided limits the maximum number of cracks that can be handled. The difference in the forward problem is less than 5%.[7]

3.2. Static Deflection Measurement Method

S.S.Naik (2012) have been investigated on Crack detection in **pipes** using static deflection measurement, Crack is to be considered as cross-sectional with straight front parallel to its diameter and perpendicular to the plane of deflection. The crack is modelled and represented by a rotational spring stiffness and stiffness can be determined by using the linear elastic fracture mechanics approach. Pipes arrangement like cantilever and simply supported beams have been examined. Experiments have been carried out using steel and aluminium pipes materials to demonstrate the effectiveness of the method. Cracks were introduced by wire-cut machining. They have been concluded max. errors in prediction of crack location of pipe is about 9% for both Al & M.S pipe and Rotational spring stiffness for steel it is higher than Al. and Stiffness is decreases with increases crack depth [8].

Salvatore Caddemi et al.(2007) have been investigated on the identification of a single crack in a beam based on the knowledge of the damage-induced variations in the static deflection of the **beam**. The crack is simulated and represented by an equivalent linear spring connecting the two adjacent segments of the beam they find results for Clamped–clamped beam and other arrangement of beam. Percentage error on the damage location with g_1, g_2 varying along the beam span, for error levels 1% and 5% on the measurement data, and for different values of equivalent stiffness rotational spring: K = 10 GNm/rad (small damage), K = 4.6 GNm/rad (moderate damage), K = 1.5 GNm/rad (severe damage) was concluded[9].

4. CRACK MODEL

Rizos et al. [10] have represented and modelled the crack as rotational spring in modal analysis for a cantilever beam having a rectangular cross section as shown in Fig.1.
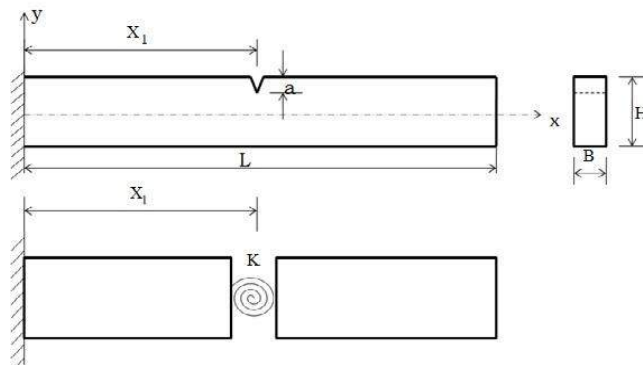
Fig.1 Crack Model by rotational spring

Dimarogonas and Paipetis [11] defined the torsional spring constant K_t in the vicinity of the cracked section of a beam when a lateral crack of uniform depth exists, from crack energy function,

$$c = \frac{5.346 * h * f(a/h)}{EI} \qquad (1)$$

$$K_t = 1/c \qquad (2)$$

* Corresponding author. Mobile No.095 86 62 02 56
E-mail address: jatin.patel3990@gmail.com

where, E is the modulus of elasticity, I is the moment of inertia, a is the crack depth, h is the beam height, c is compliance and K_t is the rotational spring stiffness, $f(a/h)$ is dimension-less local compliance function.

The crack is modelled by rotational spring stiffness for detection of crack in slender pipes is based on the assumption that crack introduces only local discontinuity in the slope at the crack location in pipe and a very small difference is exists between the mode shapes of the pipes with and without a crack. [12] Therefore, a pipe containing a crack, for example in $\theta = 0^0$ orientation, can be conveniently represented by two pipe segments connected by a rotational spring of stiffness K_t at the crack position shown in Fig.2
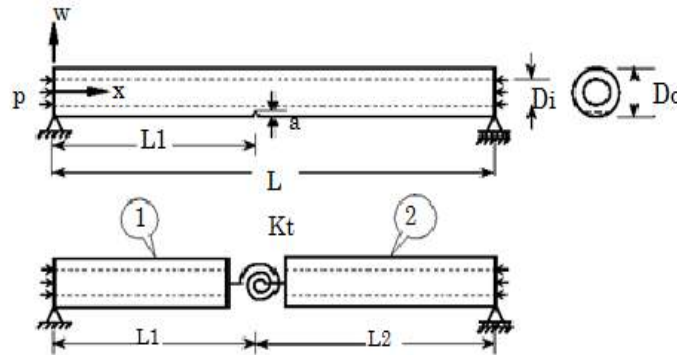
Fig.2 Crack in vertical orientation and its representation by rotational spring

When the rotational spring is used to represent by crack, The spring is acts as sink for the energy released due to the crack. This energy is equal to the difference in energies of pipes with and without crack. The spring stiffness Kt can be determined experimentally using static deflection method or vibration based method. For a cantilever beam with load acting at the free end,

$$K_t = \frac{M_{empty\,pipe}^2}{P(\delta_c - \delta_{nc})} \tag{3}$$

where P is load acting at the free end, $M_{empty\,pipe}$ is the bending moment due to P at the crack section at a distance L_2 from the support and, δ_c and δ_{nc} are the deflections along the load line for pipes with and without crack respectively. This relation provides the basis for determination of variation of K_t with crack size by the deflection method. Thus, if K_t is known, crack size a/t can be obtained using these plots.[12]

5.CONCLUSION

From critical literature review it is found that various methods are developed for detection of crack in mechanical components. And find the gap between different alternative methods against the conventional (NDTs) Method for same objective. In case of Frequency Based method for crack detection, the main reason for the popularity of natural frequencies method as damage indicators is that natural frequencies are rather easy to determine with a high degree of accuracy. A sensor placed on a structure and it is connected to a frequency analyser gives estimates of several natural frequencies. Problems exist, when the size of the damage is small. The presence of measurement errors of results in a degradation of the ability to predict the size of the crack accurately. The existing methods give a proper estimation of moderate cracks (about 20% of the height of the beam) .To overcome limitations related to natural frequencies, many research studies have been focused on utilizing changes in mode shapes (Stubbs and Kim, 1966; Kim and Stubbs, 2002). The idea of using mode shapes as crack identification tool is the fact that the presence of a crack causes changes in the modal characteristics. Rizos et al. (1990) suggested a method for using measured amplitudes of two points of a cantilever beam vibrating at one of its natural modes to identify crack location and depth [10]. Recently, an interesting comparison between a frequency-based and mode shape-based method for damage identification in beam like structures has been published by Kim et al. (2003) [13] The advantage of using mode shapes is that changes in mode shapes are much more sensitive compared to changes in natural frequencies. Using mode shapes, some of drawbacks. The presence of damage may not significantly influence mode shapes of the lower modes usually measured. Furthermore, environmental noise and choice of sensors used can considerably affect the accuracy of the damage detection procedure. To overcome these difficulties, modal testing using scanning laser

* Corresponding author. Mobile No.095 86 62 02 56
E-mail address: jatin.patel3990@gmail.com

vibrometers have been developed .The laser vibrometer was used as a vibration transducer, has the advantage of being non-contacting and measures at a controlled position with high accuracy. In case of static deflection measurement method for crack detection is experimentally validate easily compare to other methods also deflection is easy to measure by dial gauges compare to natural frequency & wavelet methods and not require complex instruments like FFT analyser, accelerometers etc,[8].

Hence the gap is to be identifying among the various literature representing different method for crack detection that's why the static deflection measurement method is experimentally validate easily compare to Frequency Based crack detection methods.

ACKNOWLEDGMENT

REFERENCES

[1] Kaushar H. Barad , D.S.Sharma, Vishal Vyas, "Crack detection in cantilever beam by frequency method" .NUiCONE, Procedia engineering 51(2013) 770-775

[2] S.M. Murigendrappa, S.K. Maiti , H.R. Srirangarajan, "Experimental and theoretical study on crack detection in pipes filled with fluid", Journal of Sound and Vibration 270 (2004) 1013–1032

[3] S.M. Murigendrappa, S.K. Maiti , H.R. Srirangarajan, "Frequency-based experimental and theoretical identification of multiple cracks in straight pipes filled with fluid", NDT&E International 37 (2004) 431–438

[4] M.R. Naniwadekar, S.S. Naik, S.K. Maiti, "On prediction of crack in different orientations in pipe using frequency based approach", Mechanical Systems and Signal Processing 22 (2008) 693–708

[5] Michele Dilena, Marta Fedele Dell'Oste, Antonino Morassi, "Detecting cracks in pipes filled with fluid from changes in natural frequencies", Mechanical Systems and Signal Processing 25 (2011) 3186–3197

[6] S. Chinchalkar, "Determination of Crack Location in Beams using Natural Frequencies", Journal Of Sound And Vibration (2001) 247(3), 417-429

[7] D.P. Patil, S.K. Maiti, "Detection of multiple cracks using frequency measurements", Engineering Fracture Mechanics 70 (2003) 1553–1572

[8] S.S.Naik, "Crack detection in pipe using static deflection measurement", J.Inst.Eng.India Ser,93(3)(2012) 209-215

[9] Salvatore Caddemi, Antonino Morassi, "Crack detection in elastic beams by static measurements", International Journal of Solids and Structures 44 (2007) 5301–5315

[10] Rizos, P, Aspragathos, N., Dimarogonas, "Identification of crack location and magnitude in a cantilever beam from the vibration modes". Journal of Sound and Vibration 138, 381–388

[11] Dimarogonas A. D., and Paipetis, S. A., 1983. "Analytical Methods in Rotor Dynamics". Elsevier Applied Science, London.

[12] Sachin S. Naik and Surjya K. Maiti, "Special issues related to detection of circumferential crack at different orientation in pipe by vibration method", ICSV14(2007)

[13] Jeong-Tae Kim , Yeon-Sun Ryu , Hyun-Man Cho , Norris Stubbs , "Damage identification in beam-type structures: frequency-based method vs mode-shape-based method", Engineering Structures 25 (2003) 57–67

* Corresponding author. Mobile No.095 86 62 02 56
E-mail address: jatin.patel3990@gmail.com

Gandhinagar Institute of Technology

| Home | Trustee | Editorial Board | Director Message | Papers | Contact Us |

Compuer Science Engineering

.

Sr.No	Paper Title	Author Name	Institute Detail	Author E-Mail Id	Co-Authors Name
1	Image Mining: Procedure and Categorization Methods	Ms.Janki Naik	Gujarat Technological University,Ahmedabad	janki.naik@git.org.in	Mr.Anirudhdha Nayak Mr.Akash Mehta
2	Optimize the Performance of Raptor Code for Long Term Evolution	Mr.Kumpal J Patel	G.H Patel College of Engineering and Technology, Vallabh Vidyanagar	kumpal.patel7@gmail.com	Prof.Mayank A Ardeshanab
3	Comparative Study on Multiprotocol Label Switching	Mr.Sarthak R Patel	Gandhinagar Institute of Technology, Gandhinagar	sarthak.patel@git.org.in	Mr.Gaurav Patel
4	An Enhancement In Automatic Web Personalization Based On Web Usage Mining	Prof.Brinda Y Pandit	Gandhinagar Institute of Technology, Gandhinagar	brinda.pandit@git.org.in	

Image Mining: Procedure and Categorization Methods

Ms. Janki Naik[a], Mr. Anirudhdha Nayak[b], Mr. Akash Mehta[c]

[a]Gujarat Technological University,Ahmedabad-380061,India
[b]Assistant Professor,Gandhinager Institute of Technology, Gandhinagar-382721, India
[c]Lecturer, Gandhinagar Institute of Technology, Gandhinagar-382721, India

Abstract

Image Classification is an important task in the field of computer vision. Image classification refers to the labelling of images into one of predefined categories. Classification includes image pre-processing, image segmentation, feature extraction and image classification. Some classification techniques have been developed for image classification. In this survey various methods for categorization of images are considered such as Artificial Neural Network, Support Vector Machine and Decision Tree.

Keywords: Image classification, Artificial Neural Network, Support Vector Machine and Decision Tree.

1. Introduction

Image mining deals with the extraction of implicit knowledge, image data relationship, or other patterns not explicitly stored in the image databases. It utilizes methods from computer vision, image processing, image retrieval, data mining, machine learning, database, and artificial intelligence. Rule mining has been implemented to huge image databases [1]. It is an interdisciplinary endeavour that essentially draws upon expertise in computer vision, image processing, image retrieval, data mining, machine learning, database, and artificial intelligence [2]. Advances in image acquisition and storage technology have led to tremendous growth in significantly large and detailed image databases [3]. A large number of image data such as satellite images, medical images are generated every day. These images, if analyzed, can reveal useful information to the human users. Image mining systems that can automatically extract semantically meaningful information (knowledge) from image data are increasingly in demand. The main obstacle to rapid progress in image mining research is the lack of understanding of the research issues involved in image mining. In this paper, fig. 1 shows basic steps for image classification. In next section we define different image Classification techniques with its advantages and disadvantages.
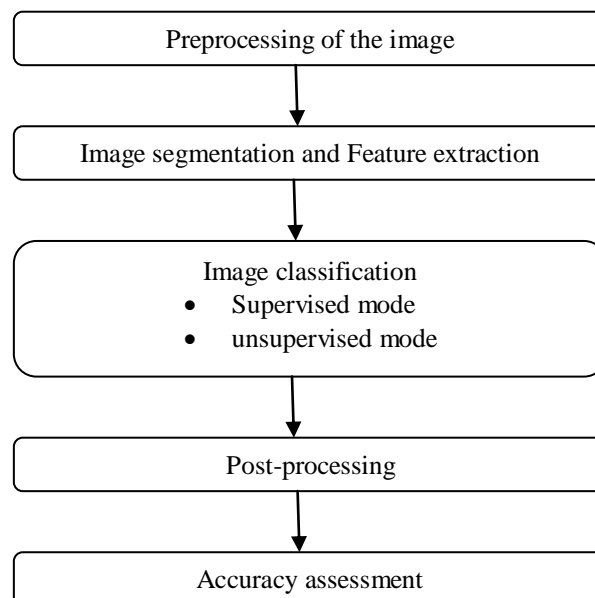
Fig. 1. Steps for Image Classification

1.1. Image Preprocessing

[6]The task of image preprocessing is to enhance the image and to reduce speckle without destroying the important features of ultrasound images for diagnosis. It also includes atmospheric correction, image transformation, main component analysis etc.

1.2. Image segmentation and Feature extraction

[6]Image segmentation divides the image into non-overlapping regions, and it separates the objects from the background. The boundaries of the lesions are delineated for feature extraction. Some image segmentation techniques such as texture analysis, edge detection and thresholding methods can be used on image.

Here is the list of features which are generally extracted from images [4]:

- DCT coefficients of average colour in rectangular grid
- CIE L*a*b* colour of two dominant colour clusters
- Histogram of local edge statistics
- Haar transform of quantised HSV colour histogram
- Average CIE L*a*b* colour
- Three central moments of CIE L*a*b* colour distribution
- Co-occurrence matrix of four Sobel edge directions
- Magnitude of the 16 x 16 FFT of Sobel edge image
- Histogram of four Sobel edge directions
- Histogram of relative brightness of neighbouring pixels

1.3. Image Classification

Selected features which are extracted using feature extraction method can be used to classify the suspicious regions into different categories. Many machine learning techniques such as support vector machine (SVM), Decision Tree (DT) and artificial neural network (ANN) have been used for classification.

2. Image Classification Techniques

Here are some methods for Image classification [5].

2.1. Artificial Neural network

Artificial Neural Network is a type of artificial intelligence that imitates some functions of the person mind. It has a normal tendency for storing experiential knowledge. An ANN consists of a sequence of layers, each layer consists of a set of neurones. All neurones of every layer are linked by weighted connections to all neurones on the preceding and succeeding layers. It uses Stochastic approach. Performance and accuracy depends upon the threshold selection and fuzzy integral.

Advantages:

- It is a non-parametric classifier.
- It is an universal functional approximator with arbitrary accuracy.
- It is a data driven self adaptive technique.
- It efficiently handles noisy inputs.

Disadvantages:

- It is semantically poor.
- The training of ANN is time taking.
- Difficult in choosing the type network architecture.

2.2. Decision tree

DT calculates class membership by repeatedly partitioning a dataset into uniform subsets Hierarchical classifier permits the acceptations and rejection of class labels at each intermediary stage. This method consists of 3 parts: Partitioning the nodes, find the terminal nodes and allocation of class label to terminal nodes.

Advantages:

- Does not require an extensive design and training.
- Provides hierarchical associations between input variables to forecast class membership and provides a set of rules n are easy to interpret.
- Simple and computational efficiency is good.

Disadvantages:

- The usage of hyperplane decision boundaries parallel to the feature axes may restrict their use in which classes are clearly distinguishable.
- Becomes complex calculation when various values are undecided and/or when various outcomes are correlated.

2.3. Support Vector Machine

Good separation is achieved by the hyper plane that has the largest distance to the nearest training data point of any class (functional margin), generally larger the margin lower the generalization error of the classifier. SVM can handle more input data very efficiently. Performance and accuracy depends upon the hyperplane selection and kernel parameter.

Advantages:

- It gains flexibility in the choice of the form of the threshold.
- It provides a good generalization capability.
- The problem of over fitting is eliminated.
- Reduction in computational complexity.
- Simple to manage decision rule complexity and Error frequency

Disadvantages:

- Result transparency is low.
- Training is time consuming.
- Structure of algorithm is difficult to understand
- Determination of optimal parameters is not easy when there is nonlinearly separable training data.

3. Conclusion

This paper provides a brief knowledge about the basic steps for image classification and different classification methods. Approaches for image classification can be categories as supervised and unsupervised. This survey provides basic knowledge about the advantages and disadvantages of various classification methods.

References

[1] C. Ordonez and E. Omiecinski (1999), "Discovering association rules based on image content," Proceedings of the IEEE Advances in Digital Libraries Conference (ADL'99).

[2] M. C. Burl et al. Mining for image content. In Systemics, Cybernetics, and Informatics / Information systems: Analysis and Synthesis, (Orlando, FL), July 1999.

[3] O. Zaiane and J. Han (1998), "Mining MultiMedia Data," CASCON'98: Meeting of Minds, Toronto, Canada, pp 83-96, November.

[4] Ville Viitaniemi ,Jorma Laaksonen "Techniques For Image Classification,Object Detection And Object Segmentation", TKK Reports in Information and Computer Science

[5] Pooja Kamavisdar, Sonam Saluja, Sonu Agrawal" A Survey on Image Classification Approaches and Techniques", International Journal of Advanced Research in Computer and Communication Engineering Vol. 2, Issue 1, January 2013

[6]https://www.researchgate.net/post/Can_anyone_think_of_challenges_associated_with_liver_cancer_ultrasound_image_enhancement_segmentation_classification_and_progression

Optimize the Performance of Raptor Code for Long Term Evolution

Kumpal J. Patel[a], Mayank A. Ardeshana[b]

[a]Student, G.H Patel College of Engineering and Technology, Vallabh Vidyanagar-388120, India
[b]Assistant Proffessor ,G.H Patel College of Engineering and Technology, Vallabh Vidyanagar-388120, India

Abstract

In this paper we studied the performance of Raptor Code over Additive White Gaussian Noise (AWGN) Channel. Long Term Evolution (LTE) is a recent standard for mobile data network, which includes multimedia broadcast and multicast services where the same data is transmitted to multiple users in specific manner. In LTE most important point of demanding is to improve the robustness against packet loss. To improve packet loss and to support effective point to multipoint delivery of data LTE has included Forward Error Correction scheme. The standard FEC scheme is based on Raptor Codes. Raptor Coding is very useful in case of packet loss while transmission as it recover all data back from insufficient data at receiver. Raptor Codes are serially concatenated code with Low Density Parity Check (LDPC) code and Luby Transform (LT) code. In our work we have implemented Raptor code, Studied it's Performance and simulation results are obtained for Bit Error Rate Vs Overhead, also LDPC code is implemented for Log Domain and Min-Sum algorithms and results are obtained in terms of Bit Error Rate Vs SNR.

Keywords: Long Term Evolution (LTE), Multimedia broadcast and multicast services (MBMS), Low Density Parity Check code (LDPC), Luby Transform code (LT).

1. Introduction

The long term evolution represents a major advance in cellular technology. LTE is the current standard for wireless mobile communication. LTE is designed to meet carrier needs for high-speed data and media support as well as high capacity voice support well into the next decade. LTE includes a key feature, enhancement of multimedia broadcast and multicast services. Multimedia broadcast and multicast services is a point to multipoint standard. Long Term Evolution (LTE) has been designed to support only packet switched services, which provides both the transmission mode single cell and multi cell broadcast and multicast services [4]. In LTE most important point of demanding is to improve the robustness against packet loss. To improve packet loss and to support effective point to multipoint delivery of data LTE has included Forward Error Correction scheme. Nowadays packet-level forward error correction codifications are applied to many systems from standard design for mobile terrestrial TV to satellite communication. Forward Error Correction helps to ensure the correct reception of data by reducing or avoiding the loss of packets caused by blockages and signal fading.

Specifically, fading and shadowing phenomena may cause partial or total loss of the data being transferred. These phenomena can last for a period of time comprising several packets and therefore we need a way to ensure correct reception of sent packets. Generally in point to point communications, ARQ (Automatic Repeat reQuest) is used [6]. When a packet is not received, a resend is asked. But in our scenario ARQ is not suitable as we face very high return times and limited return channel capacity. Also ARQ is not suitable at all in broadcasting, because normally we don't have a return channel or when it is available, ARQ would imply frequent repetition of data for one or other of the terminals. Other technique suitable for broadcast system is Forward Error Correction.

Forward Error Correction (FEC) Codes exist as Reed-Solomon codes, which can recover the K source symbols from the coded symbol of all K and N the number of symbol transmitted. However the rate R=K/N should be determined in accordance with the erasure probability p, before transmission. If p changes or p is less than or greater than expected, it will cause problem at the decoder side or will result in a lower transmission rate achievable [4]. Another disadvantage of this coding scheme is high cost of encoding and decoding.

Low-density parity-check (LDPC) codes are a class of linear block codes [6]. The name comes from the characteristic of their parity-check matrix which contains only a few 1's in comparison to the amount of 0's. Their main advantage is that they provide a performance which is very close to the capacity for a lot of different channels and linear time complex algorithms for decoding. There is variety of decoding method for LDPC code such as Min sum algorithm, Sum product algorithm, log domain algorithm etc. Sum product algorithm can achieve good decoding performance but requires a large hardware complexity so alternative solution is to use Min sum algorithm, which reduces hardware complexity of sum product algorithm.

Tornado code has been developed for this purpose as an extension of LDPC codes with reduced complexity of encoding [4]. They can manage the rate adjustment, but not yet effective especially when the channel is subject to frequent changes.

Luby transform codes (LT codes) are the first class of practical fountain codes that are near-optimal erasure correcting codes. They were invented by Michael Luby in 1998 [6]. Like some other fountain codes, LT codes depend on sparse bipartite graphs to trade reception overhead for encoding and decoding speed. The distinguishing characteristic of LT codes is in employing a particularly simple algorithm based on the exclusive or operation to encode and decode the message. LT codes are rate less because the encoding algorithm can produce an infinite number of message packets. They are erasure correcting codes because they can be used to transmit digital data reliably on an erasure channel. In order to decrease the complexity even more, we can decrease the reliability of the decoder. Thus we would have a reduced degree distribution for the same overhead constraint. Therefore, utilizing an erasure correcting pre-code would then correct the erasure arising from the weakened decoder. If the pre-code is a linear time block code, like an LDPC code, Raptor code provide marvellous encoding and decoding speeds while providing near optimal performance for the BEC.

Raptor codes are an extension of the other part of LT codes combined with a system of pre coding [7]. The design and degree distribution pre coding is the heart of raptor codes. In order to systematically increase the reliability of the transmission FEC code is used.

The rest of the paper is organized as follows. In section 2, we briefly introduce the FEC concept and some FEC schemes. Section 3 presents simulation result of Raptor code and LDPC code for min sum and log-domain algorithm. Finally, in section 4 we draw our conclusion.

2. Forward Error Correction Technique

Forward Error Correction codification consists in obtaining n codified elements from the k original elements that need to be sent. We define the coding rate as

$$r = k/n \qquad (1)$$
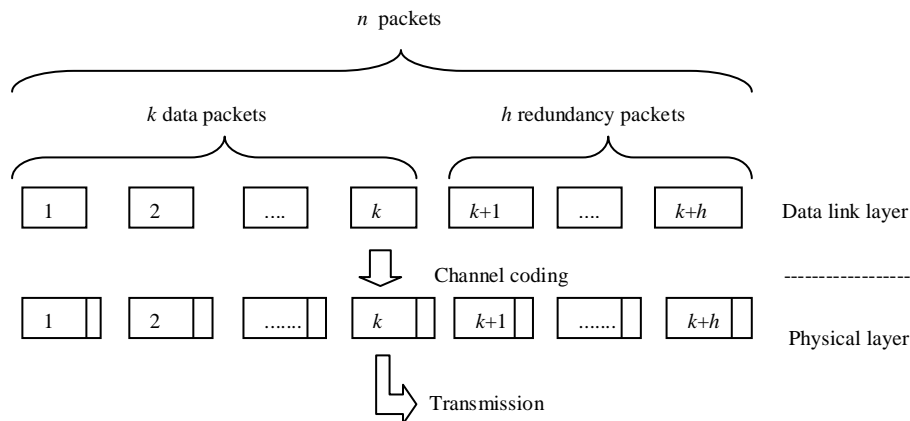
Fig.2.1 Packet level FEC applied to group of packets [6]

In order to recover the original elements in the receiver, at least k' elements must be received, where k' is equal or greater than k. If we need more than k elements in order to recover the original ones, we will face a coding inefficiency. This inefficiency is defined as

$$\eta = k'/k \qquad (2)$$

Inefficiency is always a number greater or equal to 1. For optimal case $\eta = 1$.

2.1 Raptor Codes

Raptor codes are fountain codes, meaning that as many encoding symbols as desired can be generated by the encoder on-the-fly from the source symbols of a source block of data [7]. Raptor codes are one of the first known classes of fountain codes with linear encoding and decoding time. The systematic Raptor Encoder is used to generate repair symbols from a source block that consists of K source symbols. In preparation of the encoding; a certain amount of data is collected within a FEC source block. The data of a source block are further divided into k source symbols of a fixed symbol size. The decoder is able to recover the whole source block from any set of encoding symbols only slightly more in number than the source

symbols. The Raptor code specified for MBMS is a systematic code producing n encoding symbols E from k < n source symbols C, so as the original source symbols are within the stream of the transmitted symbols [4]. This code can be viewed as the concatenation of several codes. The most inner code is a non-systematic Luby-Transform (LT) code with l input symbols F, which provides the fountain property of the Raptor codes. This non-systematic Raptor code is not constructed by encoding the source symbols with the LT code, but by encoding the intermediate symbols generated by some outer high-rate block code. This means that the outer high rate block code generates the F intermediate symbols using k input symbols D. Finally, a systematic realization of the code is obtained by applying some pre-processing to the k source symbols C such that the input symbols D to the non-systematic Raptor code are obtained. Considering the performance of Raptor codes the most typical comparison is that to an ideal fountain code [7]. An ideal fountain code can produce from any number k of source symbols any number m of repair symbols with the property that any combination of k of the k+m encoding symbols is sufficient for the recovery of the k source symbols. That is the point of the most important differentiation between an ideal fountain code and the standardized Raptor code. While an ideal code has zero reception overhead i.e., the number of received symbols needed to decode the source symbols is exactly the number of source symbols, the Raptor code has a performance close to that property.

2.1.1 Raptor Encoding Process

Raptor codes are serially concatenated codes with a pre-code as the outer code and the LT code [9] as the inner code. Pre-code is also a serially concatenated code, which uses an LDPC code and a code with dense parity (Gray code) check matrix as the outer code and the inner code, respectively. For Raptor Encoder source object is divided into Z>=1 number of source blocks. Each source block has K source symbols of size T bytes each. Each source block is encoded independently from the next Block. The systematic Raptor codes generate encoding symbols which contain K source symbols plus repair symbols. In this systematic Raptor code, K original input symbols are first encoded to L=K+S+H intermediate symbols by precode. Here, S and H are the amount of redundancy added by the outer and the inner codes of the pre-code, respectively. And then, we can generate any number of encoding symbols as needed with those intermediate symbols. The intermediate symbols are related to the source symbols by a set of source symbol triples. The encoding process is to produce repair symbols by bit-wise XORing specific source symbols. The whole process is divided in following steps [4].

Step 1:- The first step in encoding can be performed by generating an LxL encoding matrix, A to calculate L intermediate symbols as

$$C = A^{-1} D \qquad\qquad (3)$$
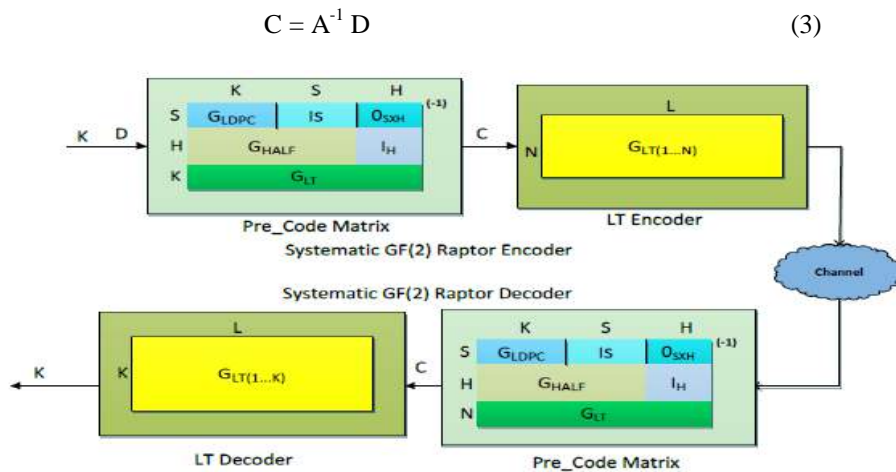
Fig. 2.2 Block diagram of raptor encoder and decoder [4]

Where, C represents column vector of the L intermediate symbols, D represents column vector of S+H zero symbols followed by the K source symbols. The precode matrix A consists of several submatrices as shown in figure 2.2. In this matrix A, the top S+H rows represent the constraints of the pre-code on C, and the bottom K rows, each corresponding to a source symbol of D, represent the generator matrix of the LT code. (GLDPC)S x K and (HHa1f) H x (S + K) correspond to a LDPC check matrix and a high dense parity check matrix, respectively. I_S be the S x S identity matrix I_H be the H x H identity matrix 0_SxH be the S x H zero matrix and (GLT) KxL is a LT encoding matrix. (GLDPC)S X K and (HHa1f) H X (S+ K) are known on the both encoder and decoder side.

Step 2:-The second encoding step is to generate the repair symbols from L intermediate symbols using LT encoding process. At the end of step 2 final transmitted streams are generated.

2.1.2 Raptor Decoding Process [4]:

The N received symbols are input to the decoder where

$$N = K + R - Ls \qquad (4)$$

Where K defines the no. of source symbols, R defines the repair symbols and Ls represent loss symbols. Matrix A of (M x L) can be formed similar to the encoding process using received N symbols where

$$M = S+H+N \qquad (5)$$

Where S is LDPC symbols, H Half Symbols and N received symbols respectively. The matrix, A is a bit matrix that satisfies A x C = E using matrix multiplication in GF (2). Intermediate symbols C can then be decoded if the bit matrix A is square (L x L) and invertible. Since the number of received encoding symbols, N > K in most cases, so following steps should be taken for decoding.

Step 1:- The first step in decoding is to convert (M x L) matrix A to an (L x L) matrix using Gaussian Elimination method [4]. Improved Gaussian elimination, consisting of row/column exchange and row Ex-OR, is used in the 3GPP Raptor decoding algorithm. In the decoding process, the original matrix A will be converted into an identity matrix. Besides, vector C and D change concurrently. Let （N ≥ K） be the number of received encoding symbols and M=S+H+N. The vector D=(D[0],… ,D[M-1]) is the column vector of M symbols with values known to the receiver, where D[0]，… ,D[S+H-1] are zero-valued symbols that correspond to LDPC and Half symbols, D[S+H]，… ,D[M-1] are the received encoding symbols for the source symbols. When the original matrix A is converted into identity matrix successfully, we can get the intermediate symbols from D. Before Gaussian elimination, we assume C[0]=0,C[1]=1，…,C[L-1]=L-1 and D[0]=0, D[1]=1，… ，D[M-1]=M-1 initially. In the process of Gaussian elimination, the vectors C and D change concurrently with the changes of matrix A. The process abides by the rules as follows:

- If the row i of **A** is exclusive-ORed into row i', then symbol D[d[i]] is exclusive-ORed into symbols D[d[i']];
- If the row i of **A** is exchanged with row i', then the value d[i] is exchanged with the value d[i'];
- If the column j of **A** is exchanged with column j', then the value c[j] is exchanged with the value c [j'].

It is clear that C[c[0]]，C[c[1]],.., C[c[L-1]] =D[d[0]]，D[d[1]]，… ，D[d[L-1]] at the end of successful decoding.

2.2 LDPC decoding methods

LDPC decoding is based on the parity check matrix which can also be represented using bipartite graph [12]. Columns in the parity check matrix represent variable nodes and rows in the matrix represent check nodes. Each variable node corresponds to one bit of the codeword and each check node corresponds to one parity check equation. Let C be a regular LDPC code of length N and dimension K whose parity-check matrix A with M=N-K rows and N columns contains exactly d_v 1's in each column (column weight) and exactly d_c 1's in each row (row weight) A_{mn} is the value of the m_{th} row and n_{th} column in A. The set of bits that participate in check is denoted: $\{N_m\}$. The set of checks that participate in bits M_n. Assume code word C= $[c_1, c_2, c_3…c_N]^T$. Before transmission it is mapped into signal constellation as vector t= $[t_1, t_2,...,t_N]^T$. Where t_N = 2* C_n-1 which is transmitted over AWGN channel. Received vector is r= $[r_1,r_2…r_n]^T$. Here r_n= $t_N + v_N$, where v_N is AWGN noise.

Assume L_n = A priori information of bit node, n

$\overline{L_n}$ =A posteriori information of bit node, n

$E_{m,n}$ =The check to bit message from m to n

$F_{n,m}$ =The bit to check message from n to m

2.2.1 Min sum algorithm

Min sum algorithm starts with initialization step [12]. Take received vector r_n as a priory information L_n and initialize bit to check message as $F_{n,m} = L_n$. Next is horizontal step which is check node processing by sending check to bit message $E_{m,n}$ as

$$E_{m,n} = 2 \tanh^{-1} \prod_{\underset{n}{n' \epsilon N(m)}} \tanh\left(F_{n'}, \frac{m}{2}\right) \tag{6}$$

After this we will retrieve posteriori information of bit node $\overline{L_n}$ is given by following equation.

$$\overline{L_n} = L_n + \sum_{m \in M(n)} E_{m,n} \tag{7}$$

Now, in bit node processing we will send bit to check message $F_{n,m}$ which is given by following equation

$$F_{n,m} = \overline{L_n} + \sum_{m' \in \frac{M(n)}{m}} E_{m,n} \tag{8}$$

Final step is decoding attempt where If $\overline{Ln} > 0$ then $\overline{c_n} = 0$ else $\overline{c_n} = 1$, If A $\overline{c_n} = 0$ then the algorithm stops and $\overline{c_n}$ is considered as a valid decoding result. Otherwise, it goes to next iteration until the number of iteration reaches its maximum limit.

2.2.2 Log domain algorithm [12]

Initialization process of log domain algorithm starts with setting $n_{m,n}^{[0]} = 0$ for all (m,n) with A(m,n)=1 and set $\lambda_{m,n} = L_c r_n$ also set the loop counter =1. Now for each (m, n) with A (m, n) =1 compute

$$n_{m,n} = 2 \tanh^{-1}\left(\prod_{j \in m,n} \tanh(\lambda_{mj})/2\right) \tag{9}$$

Now for n=1.2.....N compute log pseudo posterior probabilities as

$$\lambda_n = L_c r_n + \sum_{m \in M_n} n_{m,n} \tag{10}$$

Last step is decoding attempt in which we set $\overline{c_n} = 1$ if $\lambda_n > 0$, else set $\overline{c_n} = 0$. If A $\overline{c_n} = o$ then stop, otherwise if the number of iteration < maximum number of iteration loop to check node update otherwise decoding failure and stop. After working on both this algorithm we come to know that log domain algorithm is better than min sum algorithm.

3. Simulation Results

Encoded symbol which are combination of source symbol and redundant symbol are transmitted over AWGN channel and decoded using Belief Propagation algorithm. We have implemented raptor code for different information length (n) and code length (k) and results are obtained in terms of Reception Overhead versus Bit Error Rate. For code length of 230 symbols, information length of 250 symbols and fixed code rate of 0.90, Overhead versus bit error rate graph is obtained as shown in figure 3.1.
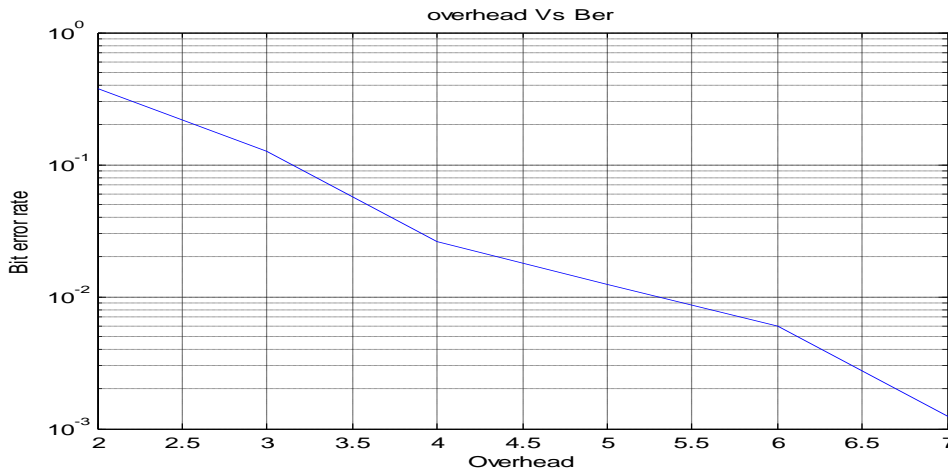
Fig. 3.1 Overhead Vs Bit Error Rate

Figure 3.2 shows that with increase in number of additional symbol i.e. Reception Overhead bit error rate decrease up to 10^{-3}.Similarly for information length (n) of 165, code length (k) of 149 and code rate of 0.9.Result are obtained for Overhead versus Bit Error Rate. Code rate is a ratio of code length (k) to information length (n).with increase in overhead here also bit error rate is decreases up to 10^{-3}
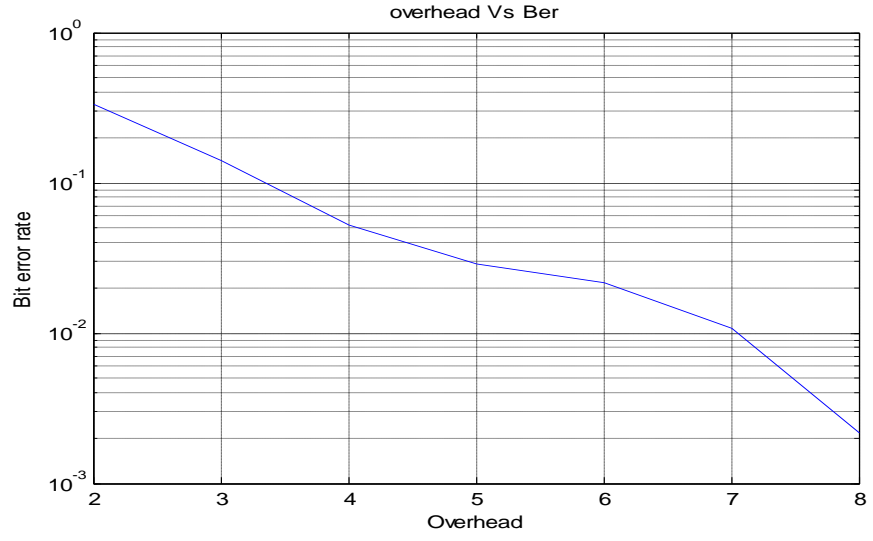
Fig. 3.2 Overhead Vs Bit Error Rate

By comparing above to figure it is observed that for larger value of code length and for more number of redundant symbols bit error rate is decreased up to 0.001, for comparatively smaller value of overhead.

We have implemented Low density parity check code by designing a parity check matrix of size nxk, where k and n are the code length and information length of generated parity check matrix. Code rate R=k/n is 0.5, encoded symbol is transmitted over Additive White Gaussian Noise Channel and decoding technique used is log domain algorithm.
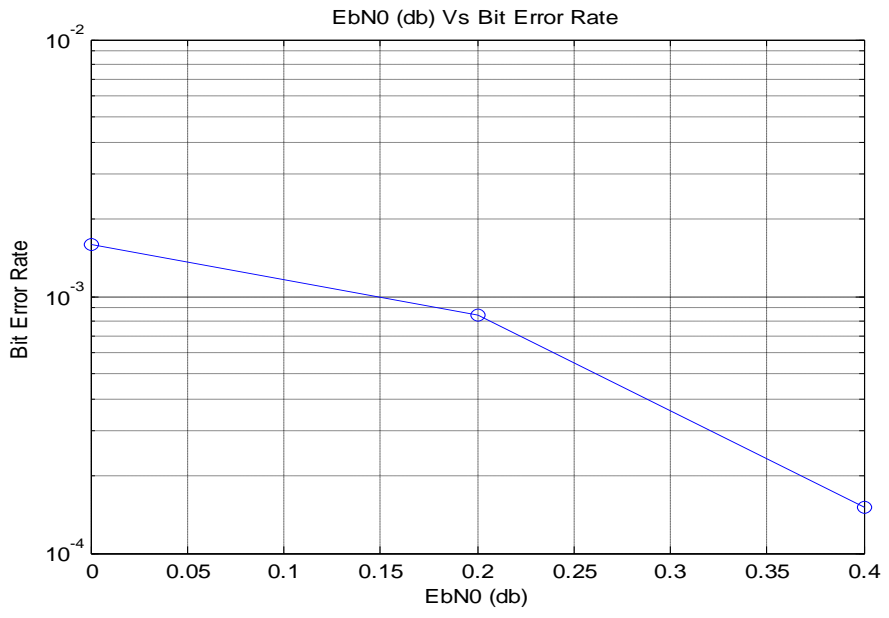
Fig. 3.3 Eb/N0 (db) Vs Bit Error Rate (Log Domain)

For above parameter graph is obtained between Signals to Noise Ratio Vs Bit Error Rate. With increase in SNR bit error rate is reduced up to 10^{-4}. For smaller value of SNR, BER is reduced at great level using log domain algorithm.

Similarly results are obtained for parity check matrix of 1000x2000, AWGN channel, code rate of 0.5 and min sum algorithm as a decoding algorithm. Also graph is plotted for Signal to Noise ratio Vs Bit Error Rate. It shows that with increase in SNR, BER is reduced up to 10^{-3}.
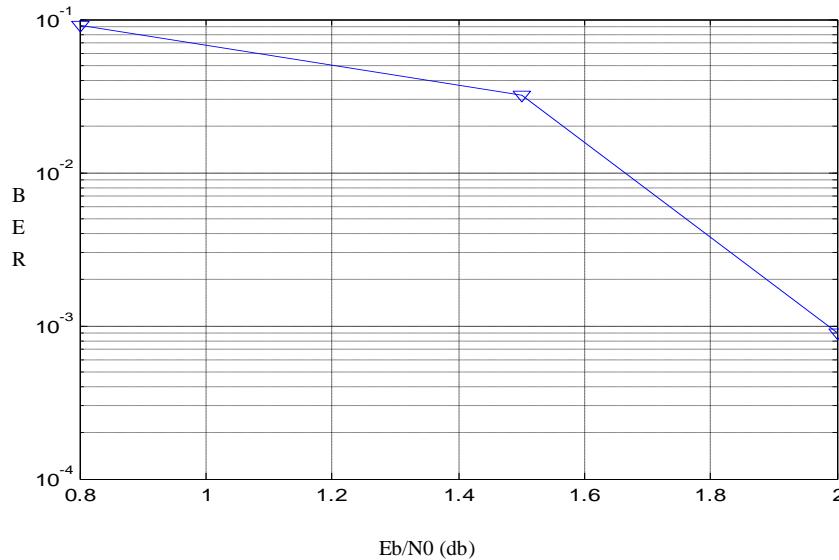
Eb/N0 (db)

Fig. 3.4 Eb/N0 (db) Vs Bit Error Rate (Min Sum)

By comparing both figures for two different algorithms, we can conclude that for log domain algorithm BER is reduced up to 10^{-4} for smaller value of SNR compared to Min Sum algorithm in which SNR values are higher and Bit Error Rate is reduced to 10^{-3}. So it is concluded that Log Domain algorithm is better compared to min sum algorithm. Comparison table between log domain and min sum algorithm is shown below.

Table 3.1 Comparison of log domain and min sum algorithm

Decoding algorithm	SNR value (db)	Bit Error Rate
Min Sum algorithm	2.0	0.001
Log Domain algorithm	0.2	0.001

4. Conclusion

We have provided an implementation of raptor code which is most recent member of systematic fountain code. To verify superiority of raptor code we implemented mat lab code for raptor encoder and decoder, and results are obtained for different information symbol length. From obtained results graph is plotted between overhead and bit error rate. from the result we can conclude that for small value of reception overhead ,there are more number of bits in error but as the value of reception overhead increases bit error rate is reduced. In our work we have reduced bit error rate up to 10^{-3} for small value of overhead. Also we have implemented Low Density Parity Check Decoder for two different algorithm, Log Domain and Min-sum algorithm. By comparing output of this two different algorithm we come to know that in Log domain algorithm Bit Error rate is low for small value of Signal to Noise ratio. However in min sum algorithm bit error rate is high for small value of Signal to noise ratio comparatively, so we conclude that log domain algorithm   is better compared to Min Sum algorithm. In our work we have taken parity check matrix of size 1000x2000 and decoding algorithm is log domain than BER is 10^{-3} for SNR value of 0.2 db. For min sum algorithm BER is 10^{-3} for SNR value of 2.0 db.

References

[1] Philipp M. Eittenberger, Todor Mladenov, Udo R. Krieger "Raptor Codes for P2P Streaming" 20th Euromicro International Conference on Parallel, Distributed and Network-Based Processing (PDP), 2012.

[2] Pasquale Cataldi, Miquel Pedros Shatarski, Marco Grangetto, Enrico Magli "Implementation and performance evaluation of LT and Raptor codes for multimedia applications" C.so Duca degli Abruzzi, 24 - 10129 Torino,2004

[3] Auguste Venkiah, Charly Poulliat, and David Declercq " Jointly Decoded Raptor Codes: Analysis and Design for the BIAWGN Channel" Hindawi Publishing Corporation EURASIP Journal on Wireless Communications and Networking, Article ID 657970, 11 pages , 2009

[4] Avani U Pandya, Sameer D Trapasiya, Santhi s Chinnam "Performance Analysis of AL-FEC Raptor Code over 3GPP EMBMS Network" IJRET Volume: 2 Issue: 4 ISSN: 2319-1163 601-608, APR 2013.

[5] Sohaib A Qazi, Muhammad Shoaib, Usman Javaid, Shahjad Asif "A comparative Analysis of LDPC Decodes for Image Transmission over AWGN Channel" FIT'09, CIIT, Abbottabad ACM 978-1-60558-642-7/09/12, December 16-18-2009.

[6] Rafael Montalb´an Guti´errez, Gonzalo Seco-Granados "Efficiency Comparison of LDPC-LDGM and Raptor Codes for PL-FEC with Very Large Block Sizes" Wireless Telecommunications Symposium, Prague, page 1-6, 2009.

[7] A. Shokrollahi, "Raptor codes" Information Theory, IEEE Transactions on, vol. 52, no. 6, pp. 2551–2567, June 2006.

[8] 3GPP TS 36.300, "Evolved Universal Terrestrial Radio Access Network (E-UTRA and E-UTRAN): Overall Description", V10.8.0, Release 10, 2012.

[9] M. Luby, "LT codes", Proc. 43rd Ann. IEEE Symp. On Foundations of Computer Science, pp. 271–282, Nov. 2002.

[10] M. A. Shokrollahi and M. Luby, "Raptor codes", Foundation and Trends in Communication and Information Theory, Vol.6, n. 3-4, pp. 1-4,2001.

[11] Gauri Joshi, Joong Bum Rhim, John Sun, Da Wang, "Fountain Codes," Study material of Digital Communication, MIT, December 7,2010.

[12] Mohammad Rakibul Islam, Dewan Siam Shafiullah, Muhammad Mostafa Amir Faisal, Imran Rahman, " Optimized Min-Sum Decoding Algorithm for Low Density Parity Check Codes" (IJACSA) International Journal of Advanced Computer Science and Applications, Vol. 2, No. 12, 2011

Comparative Study on Multiprotocol Label Switching

Sarthak R Patel[1], Gaurav R Patel[2]

[1,2]*PG Scholar, LJIET, Ahmedabad*

Abstract— **This paper is part of a series about IP Networking and the Alcatel 7770 Routing Core Platform. This paper discusses MPLS as a key technology that will enable IP networks to become more robust, reliable and ready for the demands of next generation services that can support business applications in addition to customer-based Internet services. This paper describes the vision of the role of MPLS in next generation networks, the key to doing MPLS well: traffic management and traffic engineering, Alcatel MPLS-enabled next generation solution.**

Index Terms— **MPS, label switched router (LSR), label switched paths (LSP), ATM**

I. INTRODUCTION

Wether you're an established service provider trying to keep your network operating at peak performance, or a newcomer hoping to garner a piece of the potentially lucrative networking pie, you know that maintaining or growing market share is challenging. The continual increase in users, connection speeds, traffic, ISP networks and new applications places a huge demand on the Internet infrastructure and the service providers whose networks constitute the Internet. Multiprotocol label switching (MPLS) is a key technology for enabling service providers to respond to the challenges in next generation internetworking [1].

This paper describes:
- The role of MPLS in next generation networks
- The key to doing MPLS well: traffic management and traffic engineering
- MPLS-enabled next generation solution

II. THE CHALLENGES FACING NEXT GENERATION NETWORKS

Businesses are now using the Internet and are demanding value-added services, as well as intranet and extranet services and applications from their service providers. The new business focus for Internet service providers has introduced a requirement for a whole new level of service quality that includes reliability, performance and the ability to deliver differentiated service levels (for example, Gold, Silver, Bronze). And, thanks to technological developments, we now have an opportunity to go beyond simply adding more bandwidth to handle the load; it's time to focus on increasing efficiency and removing uncertainty in network performance. Providers need to reduce the time and complexity in control and management across multiple layers of protocols. MPLS technology was developed in direct response to the requirement to improve the controllability, efficiency, and reliability — and thereby profitability — of IP networks.

The basis of the next generation network is an IP optimized infrastructure, suitable for the full range of legacy, as well as new services. Next generation networks must integrate many of the qualities and attributes of switched networks: predictability, reliability and manageability. These qualities have been delivered in today's switching networks by focusing on such attributes as traffic, path and fault management. MPLS is key to enabling service providers to simplify traffic engineering in IP networks.

III. FOLLOWING THE MPLS PATH TOWARD CONVERGENCE

The convergence of networks is an evolutionary process bringing together aspects of the switching and routing worlds from both the product and standards development perspectives. Both switching and routing have strengths that they bring to a converged network, as illustrated in Table 1. Router and switch vendors each have years of development experience in their respective product spaces.

TABLE 1
Router and switch vendors each have years of development experience in their respective product spaces.

---

* Corresponding author. Tel.: +91 9409055685; *E-mail address:* patelsarthakr@gmail.com

Technology	Strengths	Weaknesses
ATM Switching	Traffic management	Large number of paths
	Fault management	Transparent overlay
	Network management	
	Ability to engineer Quos	
Native IP Routing	Dynamic route selection	Traffic engineering difficult
	Any-to-any reach ability	Variable performance
	Feature richness	

A. *IP Networks Today*

As Internet service demands increase, the real challenge becomes how to scale the network while improving overall performance and containing operational expenses. For starters, there is the incremental cost and effort of managing network changes at both the routing and switching layers. In a fully meshed router network over ATM, many virtual circuits have to be added for each router, and since each router appears to be adjacent to all the other routers, the number of adjacencies rises quickly with each additional router, stressing the scaling and stability of the routing protocols.

The bandwidth requirements of a data network can be met in several ways, including high capacity ATM switches, and gigabit and terabit IP routers. Large routers facilitate scaling in that higher capacity and higher performance IP routers are able to consolidate one large mesh into a number of smaller meshes. However, native IP routers that have evolved from corporate enterprise networking, no matter how big, cannot directly address the cross-layer management issues, nor can they satisfy the need for traffic engineering with basic IP routing protocols — something switches were designed to do in the first place. MPLS provides the answer for the next generation of carrier grade routers by bringing routing and switching protocols together in a shim layer between IP and Layer 2.

B. *How MPLS Works*

Briefly, MPLS defines labels associated with IP forwarding properties and the signaling mechanisms used to assign them. The protocol results in IP switched paths, which are called label switched paths (LSPs). Using IP routing protocols, a label switched router (LSR) can set up paths across the network following specific topological routes and / or other constraints, such as resource availability and explicit routes. The granularity of control in the form of a path lends itself to traffic engineering, combining path-oriented values of switching with IP routing protocols.

Once traffic is mapped onto LSPs, MPLS forwards data along these predefined paths by means of label swapping: MPLS looks up input port and incoming label and swaps it for outgoing port and outgoing label, independent of the encapsulated IP header fields (such as the IP destination address to which native IP routers perform a longest match lookup, which is bypassed in LSRs).
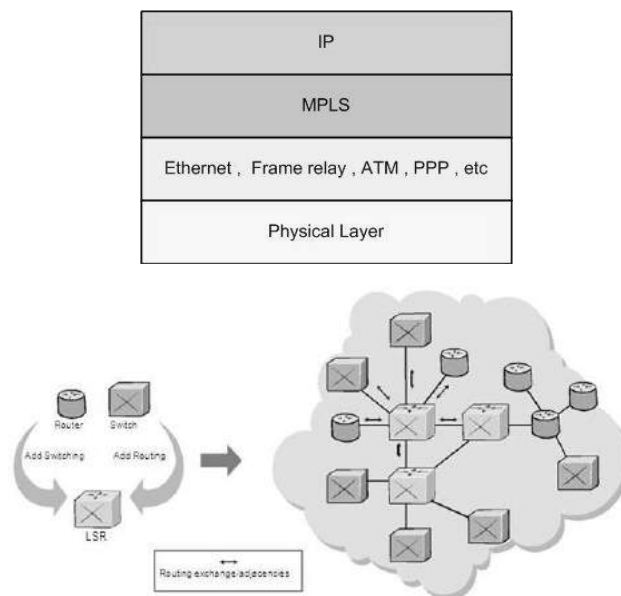
Figure 1: The role of LSRs in the network

Another important aspect of MPLS is that label switched paths are defined to operate over many link layer types including Ethernet, frame relay, ATM and packet over SONET/SDH (POS). This effect of unifying path control across different media yields significant gain in overall traffic control and management of bandwidth utilization and is one of the cornerstones of Alcatel's technology convergence vision. LSRs in the core of the network participate in IP routing control plane and become true IP routing peers (Figure 1), transforming the IP network from a transparent overlay into a converged Layer 2 and 3 networks[2].

However, not all LSRs are equal: capabilities relating to managing services, paths, traffic congestion and failures are specific to an LSR and subject to how MPLS has been implemented. Some LSRs are still focusing on the traditional best-effort Internet level of service. These LSRs will not be up to the task of handling business class IP, voice, or video services. To take full advantage of the capabilities of an MPLS-enabled IP network, LSRs must first of all be reliable and predictable in performance behavior and must, secondly, support the full range of advanced traffic management and traffic engineering functions.

C. *Applying MPLS Technology*

Currently there are two major applications of MPLS in IP networks: traffic engineering (TE) and virtual private networks (VPNs).

Traffic engineering is an overused term that often carries different meanings. To some, it represents the ability to administratively control routes more flexibly than least cost hop-by-hop routing, with a view to improving efficiency in the use of bandwidth in the core. To others, it may imply quality of service.

MPLS enables network-based IP-VPNs, a service offered by the network service provider that appears to the customer as a private network [3]. VPNs benefit from MPLS because of the notion of tunnels. The complexity of VPNs with sophisticated classification rules, overlapping addresses and many distinct forwarding tables are hidden from core (transit) nodes. MPLS provides a mechanism called label stacking, which facilitates a transparent method of tunneling VPN traffic across a shared backbone. This level of trans-patency enhances the scalability of VPNs, even for full meshed topologies, in the provider network.

IV.   CAPITALIZING ON THE POWER OF MPLS

All LSRs must speak IP routing and MPLS signaling protocols, and provide standards-based interfaces. These are the basic criteria for interoperability. However, to deliver new value-added IP services, the network must be able to deliver differentiated service levels in a cost-effective way. The efficiency of the network — its ability to squeeze every bit of performance out of the available bandwidth — is one of the key values of traffic and path management.

A. *Traffic Management*

Traffic management is a set of functions to control and prioritize how traffic is queued, serviced and, under severe congestion, discarded. It is undertaken to:

- establish distinct quality of service (QoS) levels
- efficiently use the available bandwidth

Providing QoS support extends the range of services that can be offered and differentiated across the network, increasing the revenue potential of the network with diverse capabilities spanning from real time streaming video to storing and forwarding electronic mail. Bandwidth efficiency improves the use of existing infrastructure and essentially reduces the operational and infrastructure costs of planning and growing the network. Figure 2 shows an example of how bandwidth may be allocated for different classes of services.

Sophisticated traffic management capabilities have been available in switched networks for some time. With IP QoS protocols and MPLS, similar management capabilities can now be delivered in an IP network environment. Although MPLS is not strictly necessary for IP QoS to be implemented in the network, e.g. in a pure IP hop-by-hop routing network, traffic management of LSP-based traffic is necessary if the combined benefits of IP QoS and MPLS are to be realized in the network[4].

The benefits of traffic management can be viewed from the subscriber and provider perspectives. QoS capabilities closely relate to the subscriber-visible behavior of the network: the subscriber who has paid for a premium service knows what to expect. Most importantly, traffic manage-ment enables the service provider to implement a "pay for performance" level of service where preferential treatment can be provided to those willing to pay for it. Bandwidth efficiency is key to the service provider in that it has a direct bearing on the costs of offering any service, and the timing for additional equipment acquisitions and facility upgrades. In legacy router-based networks, it is neither technically nor operationally feasible to perform traffic management. For this reason, service providers are forced to overprovision their networks in order to satisfy their service level agree-mends (SLAs) with customers. Over provisioning seems like a simple solution, especially with the declining cost of underlying transport due to the increasing availability of fiber optic networks. Still, the impact on capital and operational expenditures in the network is significant, since over provisioning affects every element in the data path, not just transport.

Increasingly, IP networks are becoming prone to congestion hotspots in the backbone caused by surges in demand of popular content web sites this is a phenomenon that cannot be addressed simply by over provisioning. Traffic management and engineering is the answer and the next generation of label switch routers will give service providers the freedom and flexibility to engineer their networks for performance, reliability and profitability.

V. AN OVERVIEW OF TRAFFIC MANAGEMENT

In order to achieve interoperability and compatibility, traffic management standards are being created for IP QoS. MPLS traffic management standards efforts (in the IETF) currently revolve around standards defined for IP. As MPLS networks mature, it is anticipated that MPLS will also carry payloads other than IP and, therefore, MPLS traffic management standards will expand in scope accordingly.

Standards for IP QoS have only recently become firm enough to be considered implementable. Two sets of standards exist, known as differentiated services (DiffServ) and integrated services (IntServ), each addressing a different level of granularity for QoS. IntServ is trying to ensure that an application can request a specific level of service end-to-end across the network, while DiffServ is concerned with a scalable aggregate approach in which QoS can be supported in the high speed core. The IETF is bringing the two efforts into an interworking framework for IP QoS, to ensure they complement each other and interoperate in a seamless way. Work on MPLS traffic management has also started with support for DiffServ, with the initial goal of ensuring that QoS mechanisms are compatible with label switching.

The IntServ model provides end-to-end quality of service for applications, ranging from throughput guarantees to limits on the end-to-end delay and packet loss. It makes use of a protocol known as the resource reservation protocol (RSVP) to ensure that required forwarding resources are available and reserved on all hops along the routed path. IntServ
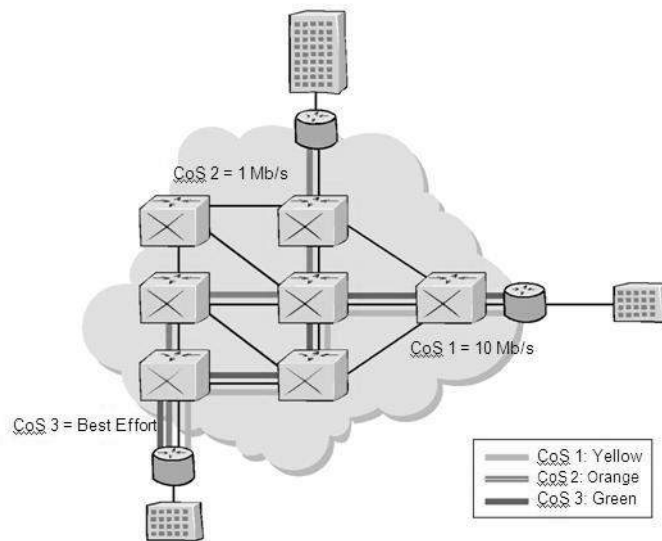
Figure 2: Different classes of service can support different throughput speeds

requires all nodes in the path to keep IntServ protocol states for each traffic stream. Clearly, this is not scalable in a busy carrier scale IP backbone, however, it can be useful for smaller feeder networks and corporate enterprise networks. The way to carry IntServ traffic across a carrier backbone is to aggregate IntServ traffic streams at the edge of the network for DiffServ style traffic management in the core.

The Integrated Services Working Group has standardized two types of services: the guaranteed service (GS) and the controlled-load (CL) service.

Guaranteed service (GS) provides guaranteed bandwidth with an upper bound on the end-to-end delay and no packet loss. GS is aimed at applications with stringent real time delivery requirements such as delay sensitive multimedia applications (audio and video).

Controlled-load (CL) service, on the other hand, is intended to provide roughly the same QoS under heavy as well as light network loads, but without any firm guarantees, such as a delay upperbound. Unlike IntServ, traffic management in DiffServ is performed on traffic aggregates instead of individual application level flows. At the ingress edge node, customer traffic streams are classified into behavior aggregates (BA) and packets are labeled with a DiffServ codepoint (DSCP) to indicate the traffic management policy to be effected by routers in the core of the network. A well-defined set of traffic manage-ment policies are defined by DiffServ. As these policies are applied uniformly at each hop in the traffic path, they are appropriately called per hop behaviors (PHB).

It is important to emphasize here that traffic management is performed on behavior aggregates at each hop in a DiffServ network. This is the key scaling property of DiffServ. Since each packet belonging to a BA carries a label with the appropriate DSCP, a DiffServ node in the network knows exactly how to treat it, since it is configured to know about all the PHBs associated with the DSCPs. No state information on the traffic is necessary in the core of the network.

Three PHB types have been defined as part of the DiffServ standard. They are the assured forwarding (AF) PHB type, the expedited forwarding (EF) PHB type, and the best-effort (BE) PHB type.

Diffuser behavior aggregates can be mapped to MPLS by multiplying the number of DiffServ BAs into the number of MPLS forwarding equivalence classes (FEC) (routing entries that can be mapped to the same LSP) to create a table of BA-FEC

tupples. The mapping of BA-FEC tupples to LSPs can be done in three ways, as described in a recent IEFT draft

- E-LSP – EXP-inferred PHB scheduling class LSP. Map each FEC to an LSP; map DSCPs for all the BAs (a maximum of eight) in this FEC to equivalent MPLS EXP values (the mapping could be signaled when the LSP is set up or be configured statically); mark EXP

- field in MPLS headers accordingly when encapsulating IP packets. Since the EXP field can only support eight values, this method cannot accommodate more than eight DSCPs (currently 14 DSCPs have been defined for DiffServ). Further optimization can be done by moving the drop precedence consideration out of the EXP field and mapping them to equivalent Layer 2 functions

- (in Layer 2 header); this would reduce the number of DSCPs to be mapped to only six.

- L-LSP – Label only-inferred PHB scheduling class LSP. Create an LSP for each BA-FEC tupple. Each LSP would have an equivalent traffic management profile to the DiffServ BA it is carrying. This approach causes the number of LSPs for a given FEC to multiply by the number of BAs. Optimization can be done by using the EXP field (or L2 functions as above) to carry the drop precedence value of the DSCP, thus potentially reducing the number of LSPs to one third. For example, only four LSPs would be required to support the AF group type (per FEC), instead of twelve.

A hybrid of E-LSP and L-LSP can be used. For example, it may be useful to implement L-LSP for EF and E-LSP for AF and BE.

Since DiffServ packets must be processed as aggregates on a per hop basis, MPLS packets arriving at a core node cannot be simply forwarded by label swapping. Packets from all LSPs must go through DiffServ PHB processing at each hop, where some packets may be demoted to a lower PHB and must be relabeled accordingly. An important constraint to be aware of is that packets from the same microflow must be forwarded on the same LSP to preserve packet ordering.
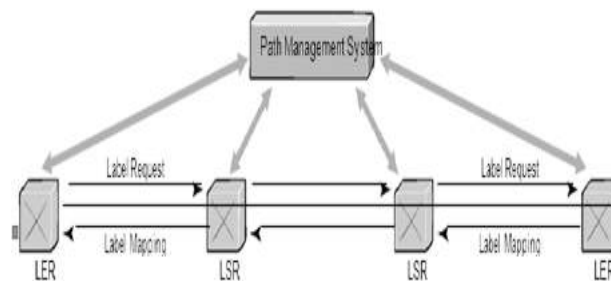
Figure3.Path management system

While extra processing is required for MPLS to support DiffServ, the model is still deemed scalable, as there is no state information to be kept at each node about the traffic, and the PHB processing can basically be scaled with processor and memory technology.

There are also supervisory functions related to traffic management. For example, some form of LSP connection admission control (CAC) may be required to monitor and control how much bandwidth is allocated to each LSP. Congestion monitoring and event notification is useful to identify hotspots in the network and trigger traffic engineering action as necessary. QoS policies need to be managed and fine-tuned to reflect traffic patterns and network resources. In short, QoS needs to be an integral part of service and network management systems.

Alcatel has an integrated solution for IP and MPLS traffic management. From our high density multiservice edge to our terabit core architecture, traffic management is seam-lessly integrated and centrally managed. Our implementation of IP QoS and MPLS is strictly standards-based and highly interoperable. We have the industry leading network management platform that takes the complexity of the protocols out of network operations while ensuring that service level agreements are implemented correctly in the network. Our tools ensure that traffic management can be engineered, deployed, monitored, and controlled in the most efficient and yet flexible manner.

A. *Path Management*

For network operators, MPLS paths become entities that must be managed, driving requirements for network management, fault management, planning, maintenance, restoration, admission control, routing control, signaling, policy control, and so on. The capabilities that apply to managing MPLS paths are analogous to those used in support of ATM paths. Point-and-click GUI interfaces, which have been a part of Alcatel's award-winning network management system for over a decade, provide simple yet powerful provisioning, monitoring, and traffic engineering capabilities.

In the event of degraded performance or outright failure of a path, resiliency becomes a key part of managing paths. Because MPLS paths extend the capabilities of the network, it may not be possible or safe to simply revert to routing traffic packet by packet (based on the IP header) in the event of a network fault. In applications such as VPN, the relevant information or equipment capabilities may not be present to enable the correct recovery decisions to be made at core LSRs. Therefore, the path

must be quickly re-established over a working route in order to restore the service in the event of a failure[5].

Recent efforts in the IETF MPLS working group have started to address MPLS-based recovery[5], looking at path rerouting and protecting switching. While standards are being devel-oped, Alcatel is leveraging our experience to implement fast restoration at the LSP level, using state-of-the-art parallel processing for LSP reroutes and advanced traffic engineering techniques for configuring protection switching LSPs.

Alcatel actively participates in standards activities to ensure interoperability and compatibility in our implementation.

VI. AN OVERVIEW OF PATH MANAGEMENT IN MPLS

An LSP is a simplex Layer 2 tunnel consisting of a concatena-tion of one or more label switched hops, analogous to an ATM or frame relay PVC (Figure 4)[6]. There are several ways to set up paths in an MPLS network; the three most common ones are:

Generic LSP (G-LSP) – a network defined path, computed along normal (IGP) routing topology, signaled by means of the label distribution protocol (LDP). This type of LSP is expected to grow in practice with the advent of services such as MPLS-BGP VPN, which relies on the MPLS technique known as label stacking in combination with G-LSP path management. The generic switching label at the top of the label stack is used to route packets from the ingress LSR to the egress LSR while the next level label is used to identify the VPN context for the packet.

A.Explicit route LSP (ER-LSP) – a user defined path, signaled by means of the constraint-routed label distribution protocol (CR-LDP) or the extended resource reservation protocol (extended RSVP), from a given node. This can be automated through a path management system with a point-and-click user graphical user interface. Such an LSP can override the internal gateway protocol (IGP) routing table in an LSR and thus enable traffic to be directed based on operator defined traffic engineering policies.

B.Constraint routed LSP (CR-LSP) – a network defined path, calculated by constraint routing protocols, enabled by IGP-extensions and signaled by means of extended RSVP or CR-LDP. The IGP protocol extensions provide an LSR with additional routing information, such as bandwidth availability of a downstream node for different classes of traffic, to enable traffic engineering applications.

The use of path management mechanisms is dependent on the type of services being offered in the network as well as operational and traffic engineering requirements. Alcatel brings years of experience in path management in carrier scale switch networks to our MPLS implementation, providing service providers with an unmatched solution in the industry.
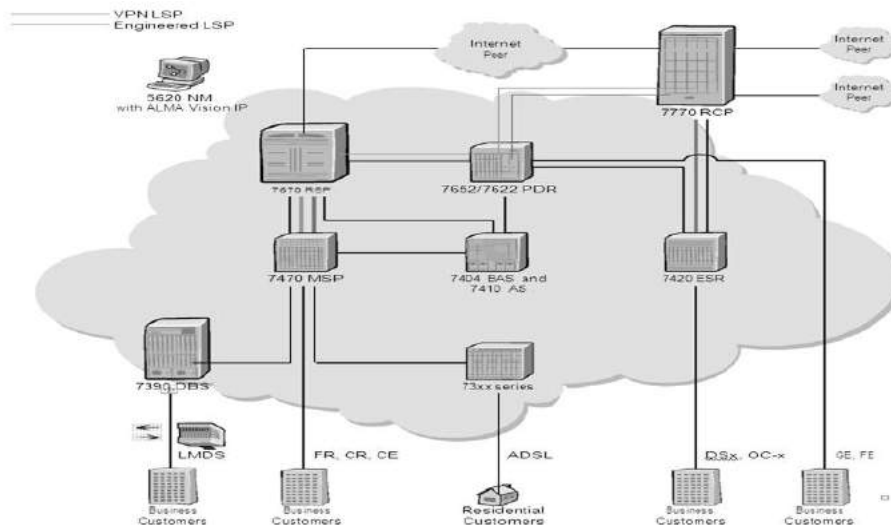
Figure 4: An example of an Alcatel next generation network

Whether it's network optimization with our MPLS Traffic Engineering tool, or LSP-based protection switching, Alcatel MPLS solutions excel.

VII. MPLS VS MULTICAST

Multicast was for the most part an after-thought in MPLS design. It was introduced by point-to-multipoint RSVP-TE. It was driven by Service Provider requirements to transport broadband video over MPLS. Since the inception of RFC 4875 there has been tremendous surge in interest and deployment of MPLS multicast and this has led to several new developments both in the IETF and in shipping products.

A. Comparison of MPLS versus Frame Relay

Frame relay aimed to make more efficient use of existing physical resources, which allow for the underprovisioning of data services by telecommunications companies (telcos) to their customers, as clients were unlikely to be utilizing a data service 100 percent of the time. In more recent years, frame relay has acquired a bad reputation in some markets because of excessive bandwidth overbooking by these telcos.

Telcos often sell frame relay to businesses looking for a cheaper alternative to dedicated lines; its use in different geographic areas depended greatly on governmental and telecommunication companies' policies.

AT&T is currently (as of June 2007) the largest frame relay service provider in the United States, with local networks in 22 states, plus national and international networks. This number is expected to change between 2007 and 2009 when most of these frame relay contracts expire. Many customers are likely to migrate from frame relay to MPLS over IP or Ethernet within the next two years, which in many cases will reduce costs and improve manageability and performance of their wide area networks.

B. Comparison of MPLS versus ATM

While the underlying protocols and technologies are different, both MPLS and ATM provide a connection-oriented service for transporting data across computer networks. In both technologies, connections are signaled between endpoints, connection state is maintained at each node in the path, and encapsulation techniques are used to carry data across the connection[7]. Excluding differences in the signaling protocols (RSVP/LDP for MPLS and PNNI:Private Network-to-Network Interface for ATM) there still remain significant differences in the behavior of the technologies.

Both ATM and MPLS support tunneling of connections inside connections. MPLS uses label stacking to accomplish this while ATM uses Virtual Paths. MPLS can stack multiple labels to form tunnels within tunnels. The ATM Virtual Path Indicator (VPI) and Virtual Circuit Indicator (VCI) are both carried together in the cell header, limiting ATM to a single level of tunnelling.

The biggest single advantage that MPLS has over ATM is that it was designed from the start to be complementary to IP. Modern routers are able to support both MPLS and IP natively across a common interface allowing network operators great flexibility in network design and operation. ATM's incompatibilities with IP require complex adaptation, making it comparatively less suitable for today's predominantly IP networks.

VIII.   THE FUTURE OF MPLS

With the adoption of optical transmission and switching technology, in particular wave division multiplexing (WDM), The number of usable wavelengths in a fiber optic strand has grown significantly. As the number of wavelengths or "lambdas" reach the density level practical for switching, a whole new practice of optical switching and routing appears on the horizon. The first generation device to make use of lambda switching is known as the optical cross connects (OXC), where an incoming lambda on a fiber strand is cross- connected with an outgoing lambda. But this is only the stepping stone as we envision further network convergence towards the ultimate intelligent optical IP network, in which an integrated cross-domain management platform can tie together the physical and logical network layers, enabling dynamic path allocation at physical or logical network layers, and protection and restoration schemes at the most convenient network layer.

The MPLS control plane could then become the integration point between multiprotocol lambda switching (MPLS) and labeled packet switching[8]. For example, MPLS provides a method for label stacking, which means a top level label could be used to map to a lambda between two LSRs, thus creating a method of label swapping for lambdas using basically the same MPLS control plane. Extensions to the MPLS suite of protocols would be needed to facilitate lambda label path setup, but the basic path control and management system for MPLS is indeed very extensible to this type of development.

The benefits of MPLS driven optical internetworking would enable network convergence to spread further into the physical transport core of the network, leading to simplified operations, integration with IP network and services, network optimization through automated topology discovery, and signaled optical paths (wavelength on demand), integrated traffic engineering and co-ordinate multilayer restoration. Just as we have been able to bring together the power of IP, MPLS, and ATM for the benefits of our customers, Alcatel will again leverage its technical leadership in optical networking and MPLS technology, to offer the best of both worlds to carriers.

IX CONCLUSION

We understand the real world problems service providers' face in order to deliver business-class IP services. We believe MPLS is a key technology that will enable IP networks to become more robust, reliable, and ready for the demands of next generation services that can support business applications, in addition to consumer-based Internet services. Moreover, we believe MPLS is a pivot for future internetworking, protecting investments in label switched routers (LSRs) independent of underlying link layer technologies. Thanks to our considerable experience with sophisticated traffic management regimes, Alcatel next generation network solutions can support value-added IP services in the most efficient and profitable manner possible. Alcatel's number one market position in the area of Internet broadband access and optical transport makes it uniquely positioned to help carriers become profitable in building next generation networks.

REFERENCES

[1] www.cisco.com (future of mpls in new world)By Robert Smith "Multi-Protocol Label Switching (MPLS) is becoming increasingly popular for enterprise WANs because it offers customers a number of advantages over traditional point-to-point technologies, including lower cost, greater scalability, quicker provisioning of new services and, in many cases, improved reliability.

[2] www.networkworld.com(the challenges facing next generation networks by (A.KARNIK)"Businesses are now using the

Internet and are demanding value-added services, as well as intranet and extranet services and applications from their service providers."

[3] www.cid.alcatel.com by R.A.Sorace (Traffic Management, Path Management)

[4] www.networkforus.com by C.Zhu, andS. Zang P.K.T. MOK Howmplswork?ApplyingMPLS"

[5] D. Sinicrope, A. Malis, MPLS PVC User to Network Interface, MPLS/FR Alliance2.0.1,May2003.

[6] A. Bhargava, T. Phelan, MPLS Proxy Admission Control Definition, MPLS/FrameRelayAlliance6.0.0,January2004.

[7] E. Rosen, A. Viswanathan, R. Callon, Multiprotocol Label Switching Architecture,RFC3031,January2001

[8] J. Boyle, V. Gill, A. Hanaan, D. Cooper, D. Awduche, B. Christian, W. S. Lai, "Applicability StatementFor Traffic Engineering with MPLS", RFC3346, August200

An Enhancement In Automatic Web Personalization Based On Web Usage Mining

Prof. Brinda Y Pandit*

Assistant Professor,Gandhinagar Institute of Technology,Gandhinagar ,382721,India

Abstract

Web mining is the application of the data mining which is useful to extract the knowledge/information. Web mining has been explored to different techniques that have been proposed for the variety of the application. Most research on Web mining has been from a 'data-centric' or information based point of view. Web usage mining, Web structure mining and Web content mining are the types of Web mining. Web usage mining is used to mine the data from the web server log files. Web Personalization is one of the areas of the Web usage mining that can be defined as delivery of content tailored to a particular user or can be defined as implicitly or explicitly collecting visitor information and leveraging that knowledge in content delivery framework to manipulate what information present to users and how you present it. The essence of personalization is the adaptability of information systems to the needs of their users. Here we propose a framework and algorithm with necessary implementation for enhancement of Automatic Web Personalization.

Keywords :Recommendations; Web personalization; web mining; web usage mining**.**

1. Introduction

Data mining is a relatively young and interdisciplinary field of computer science, is the process of discovering useful patterns or knowledge from data sources, e.g., databases, texts, images, the Web, etc. A data mining application usually starts with an understanding of the application domain by data analysts (data miners), who then identify suitable data sources and the target data; data mining can be performed on the data, which is usually carried out in three main steps:

- *Pre-Processing*
  The raw data is not suitable for mining. It may need to be cleaned so as to remove inconsistency and noises or abnormalities [17].
- *Data Mining*
  The processed data in then fed to mining algorithm which will produce interesting knowledge.
- *Post-Processing*
  Not all the discovered patterns and knowledge may be useful. This step will identify useful ones for the application with the help of various techniques to make the decision.

With the spectacularly speedy and unpredictable growth of information available over the Internet, World Wide Web has become a powerful platform to store and retrieve information as well as mine useful information; Web mining is becoming increasingly important and popular. The Web mining process is similar to the data mining process. The difference is usually in the data collection.

Due to the properties of the huge, diverse, dynamic and unstructured nature of Web data, Web data research has encountered a lot of challenges, such as scalability, multimedia and temporal issues etc [3]. Web data can be categorized into content, structure, usage, user profile [6].

Web mining is the application of data mining techniques to extract knowledge from Web data including web documents, hyperlinks between documents, usage logs of web sites, etc [11],[18].

Fig. 1 shows the three types of web mining namely web content mining, web structure mining and web usage mining. The web mining is decomposed into the sub tasks namely resource finding, information selection and pre-processing, generalization and analysis [14].

Each day, the Internet grows by roughly a million electronic pages, adding to the hundreds of millions pages already on-line. As a result, Web users are always drowning in an "ocean" of information and facing the problem of information

* Corresponding author. Tel.: +91-8347010841;
 *E-mail address:*brinda.pandit@git.org.in

overload when interacting with the web. Because of speedy growth of the information, the resulting arrangement of information lacks of organization and structure. Users often feel confused and get lost in that information overload that continues to expand [13]
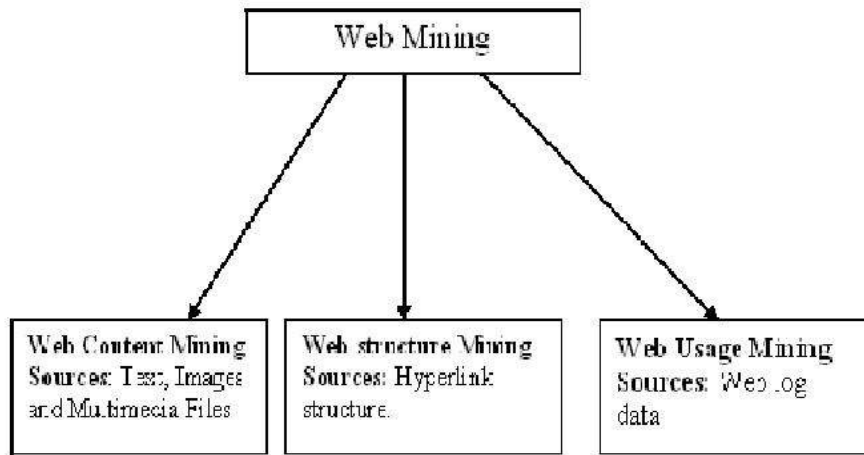
Fig. 1 Types of web mining

Web usage mining refers to the automatic discovery and analysis of patterns in click stream and associated data collected or generated as a result of user interactions with Web resources on one or more Web sites. Therefore, the crucial need nowadays is that of predicting the user needs in order to improve the usability and user retention of a web site. It is necessary for a Web developer or designer to know what the user really wants to do, predict which pages the user is potentially interested in, and present the customized Web pages to the user [3].

Web personalization is a strategy, a marketing tool, and an art [3]. The objective of a Web personalization system is to "provide users with the information they want or need, without expecting from them to ask for it explicitly" [18]. *In other words it* can be described, as any action that makes the Web experience of a user personalized to the user's taste [8]. The experience can be something as casual as browsing the Web or as (economically) significant as trading stocks or purchasing a car. The activities can range from simply making the presentation more pleasing to an individual to anticipating the needs of the user and providing the right information as well as performing a set of routine book-keeping functions automatically.

Principal elements of Web personalization include modelling of Web objects (pages, etc.) and subjects (users), categorization of objects and subjects, matching between and across objects and/or subjects, and determination of the set of actions to be recommended for personalization.
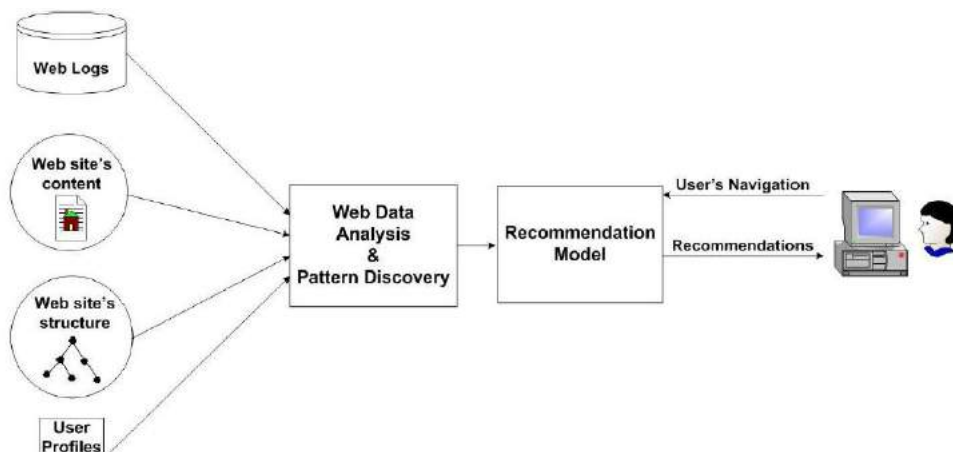
Fig. 2 Web personalization process [9]

The Web Personalization process divides into four distinct phases [9].

- *Collection of Web data*
  Implicit data includes past activities/click streams as recorded in Web server logs and/or via cookies or session tracking modules. Explicit data usually comes from registration forms and rating questionnaires.

- *Pre-Processing of Web data*
    Data is frequently pre-processed to put it into a format that is compatible with the analysis technique to be used in the next step.
- *Analysis of Web data*
    This step applies data mining techniques to discover interesting usage pattern and statistical correlation between web pages and user groups.
- *Decision making/Final recommendation*
    It makes use of the results of the previous analysis step to deliver recommendations to the user.

This paper presents novel method and technique that address the requirement of web personalization.

2. Motivation

Imagine a user that navigates through a web portal specializing in travel and hotel accommodation. The user tries to find information regarding various hotels and accommodation arrangement as per his destination preference .But he will be presented with the same order of information regardless of its destination preferences. Consider another example assume that any user wants to go for particular pages on the site as per his/her interest. Suppose we refer our web site name is *www.uvpatelcollege.com*. Now user checks every time events, syllabus, result and academic tabs. Based on this user's navigation, however, in combination with previous users' visits focusing on the same subject the system makes recommendations to the user. Assume, for example, that many users in the past have seen the page *www.uvpatelcollege.com/result.html,www.uvpatelcollege.com/syllabus.html* and other page link is *www.uvpatelcollege.com/ academic.html* during the same visit. If the current user visits the first two, the system can recommend the third one, based on the assumption that people with similar interests present similar navigational behaviour.

Finally, we also note that some pages of the "College" are more important than others in terms of previous users' navigation and their position in the web site's graph. Traditional general purpose web pages of today usually suffer from a "one-size-fits-all" problem.[15].A solution for the negative effects of the traditional "one-size-fits-all'' approach is to develop systems with an ability to adapt their behaviour to the goals, tasks, interests, and other features of individual users .This paper aimed to provide an approach for automatic personalization based on web usage mining. The knowledge obtained from the Web usage patterns could be directly applied to efficiently manage activities related to e-business, e-services, e-education and so on from the business and applications point of view.

Accurate Web usage information could help to attract new customers, retain current customers, improve cross marketing/sales, effectiveness of promotional campaigns, tracking leaving customers.

Proposed work to address the requirement of web personalization is motivated by the observation and study of current existing systems.

3. Related Work

In this Section, we provide a review of related research efforts, ranging from the earlier approaches that focus on web personalization. We then present requirements for the design of a Web Personalization System. We provide a summarized overview of existing systems. We then described related research gaps.

In [3], the author categorized various web personalization techniques. Some of them are as follows:

- *Memorization*

Simplest method. The system records and stores in its 'memory' information about the user, such as name and browsing history. When the user returns to the site, this information is used as a reminder of the user's past behaviour, without further processing.

- *Customization*

Takes as input a user's preferences from registration forms in order to customize the content and structure of a web page. Process tends to be static and manual or at best semi-Automatic.

- *Guidance or Recommender systems*

Tries to automatically recommend hyperlinks that are deemed to be relevant to the user's interests, in order to facilitate access to the needed information on a large website.

- *Task Performance Support*

A personal assistant executes actions on behalf of the user, in order to facilitate access to relevant information.

Other than these, many more techniques were used for web personalization. In [1], Web usage data mining personalization, the customer preference and the product association are automatically learned from click stream. In order to avoid the poor recommendations that will lead to disappoint customers, customers who are likely to buy recommended

products are selected using decision tree induction. In [5], Computational Intelligent combinations, provided the different information system which have been designed to provide Web users with the information they search, without expecting them to ask for it explicitly.

Novel online recommender system was described and implemented by the author in [7], which builds profiling models and offers suggestions without the user taking the lead. Automatic Personalization Based On Web Usage Mining as suggested in [8], in which the user preference is automatically learned from Web usage data, by using data mining techniques. Web caching is one of the effective technique which refers to the practice of saving content in memory in the hope that another user will request the same [16].

Requirements for the design of a Web Personalization System [4]:
- Domain Specification
- User Identification
- Efficient Acquisition of User Data
- Flexible Data Elaboration
- Efficient Construction of User Models
- Practical and Legal Considerations

Web personalization techniques are categorized into three generic approaches [12] as shown in Fig 3.

Approach	Description	Problems
Manual decision rule systems	➢ Web-based service is personalized via manual intervention of its designer and usually with the cooperation of the user ➢ Example Yahoo!'s personalization engine(Manber et al.,2000) and Websphere Personalization (IBM).	➢ Require considerable effort in construction and maintenance. ➢ Require the user's involvement.
Content-based filtering systems	➢ Applies machine learning methods to Web content, primarily text, in order to discover the personal preferences of a user. ➢ The focus is on *what* the user is interested in.	➢ Difficulty of analyzing the content of Web pages and arriving at semantic similarities.
Social or collaborative filtering systems	➢ To personalize a service, without requiring the analysis of Web content. ➢ Personalization is achieved by searching for common features in the preferences of different users, which are usually expressed explicitly by them, in the form of item ratings, and are recorded by the system. ➢ Focuses on *who* else is interested in the same things as the user.	➢ The quality of the recommendation depends on the number of ratings that a particular user has made, leading to low quality recommendations for users that have rated a small number of items. ➢ Do not scale well to large numbers of users. ➢ Do not provide any insight as to the usage patterns that existed in the data.

Fig.3 Generic approaches of web personalization

In [4], the author has summarized various existing systems as shown in Fig.4

Generic Categories	System	Personalization Functions			Technical Paramters for persoanlization policy of site			
		Memorization	Guidance/ Recommendation	Customization	Single/ Multi User	Static/ Dynamic	Context Sensitive/ Context Insensitive	Converging / Diverging
Multi Function Systems	SETA	✔	✔	✔	Single	Dynamic	Context Sensitive	Converging
	Tellim		✔	✔	Multi	Dynamic	Context Sensitive	Converging
	Schwarzkopf	✔	✔		Single	Dynamic	Context Sensitive	Diverging
	Oracle9iAS Personalization	✔	✔		Multi	Dynamic	Context Sensitive	Diverging
	Netmind		✔		Multi	Dynamic	Context Insensitive	Diverging
	Re:action		✔		Multi	Dynamic	Context Sensitive	Diverging
Single Function Systems	WebPersonalizer		✔		Multi	Static	Context Sensitive	Converging
	SiteHelper		✔		Multi	Static	Context Sensitive	Converging
	WUM		✔	✔	Multi	Static	Context Sensitive	Converging

Fig. 4 Summary of existing systems

From the literature review, we summarized the problems or the research gaps of web personalization based on the different techniques which we used.

According to the author as specified by in [2], researchers must perform more empirical studies that cover different types of online service providers (for example, game malls). Such work will help identify the generic architecture and common components (for example, profiling and matching) reusable in Web personalization. In [9], the author discussed about the problems in extracting useful patterns and rules from user navigational behaviour so that site reconstruction or modification can then be made by human. As well researchers can exploit and enable a more effective integration and mining of content, usage, and structure data from different sources promise to lead to the next generation of intelligent Web applications as mentioned in [3]. According to the authors, most current approaches to personalization by various Web-based companies rely heavily on human participation to collect profile information about users. This suffers from the problems of the profile data being subjective, as well getting out of date as the user preferences change over time.

A different but closely related problem is the incorporation of time in the discovered models. The behaviour of users varies over time and it should affect the construction of models. A Web personalization system should be able to adapt to the user's behaviour, when this changes. This issue was examined but yet it has not been given much attention.

Additionally, there are a number of open issues concerning the use of the extracted knowledge for personalization, e.g. how often a new customized Web page or recommendation should be generated, what amount of data is considered sufficient in order to customize a site or generate a recommendation, and how can the subsequent browsing of the user can be used as feedback to the personalization process. A related practical issue is the requirement for a common representation of the extracted knowledge, i.e., the user models generated by Web usage mining tools [4].

4. Proposed Solution

In this section we have briefly presented the proposed framework for Automatic Web Personalization (AWP) and we have developed an algorithm for the same.

A) Framework

The main objective of the AWP is to make the personalization process both automatic and dynamic, and hence up-to-date. This approach benefits from the combination and integration of technology advances in areas such as web mining, personalization. The framework represents the understanding, discovery and utilization of knowledge. The AWP system modules are classified into two stages: Offline stage and Online stage as illustrated in the Fig. 5.

The *Offline stage* is further having two modules: data preparation phase and usage mining phase. The main functionalities implemented in this stage are data filtering and cleaning as well as generating intermediate reports which can

be used to discover interesting knowledge.

- *Data preparation phase :*

Web data like website structure, web logs, user   profiles etc are collected. The   data collected   undergoes   the preprocessing step [10]. In   preprocessing,   data is   frequently pre-processed   to put it into a format that is compatible with the   analysis technique to be used in the next phase. Pre-   processing   may   include   cleaning   data   of inconsistencies, filtering out irrelevant information   according   to the goal of analysis [17].

- *Usage mining phase*:

In this phase various data mining techniques are   applied to discover interesting   usage pattern   (URL clusters, IP clusters) and statistical correlation   between web pages and user groups.

The *Online stage* makes use of the results of the previous analysis step to deliver recommendations to the user. As well as reports are generated which could be used by the website administrators so as to do website reconstruction or website optimization if necessary.

B) Pseudo code

The steps for pseudo code are:

1. Web data collected is pre-processed to put it into a format that is compatible with the analysis technique to be used in the next phase
   - Cleaning data to remove inconsistencies, filtering out irrelevant information according to the goal of analysis.
2. Specify minimum support threshold and confidence value so as to discover usage patterns.
3. The recommendation value of each candidate URL will be given if the discovered association rule satisfies minimum confidence criteria.
   - Rules in which the consequent contains the candidate URL.
4. If the rules satisfy specified minimum support and confidence criteria than candidate URL is added to Recommendation set.
5. Use this new generated recommendation set to provide customization to individual users and to measure various parameters like performance etc as well as for website reconstruction.
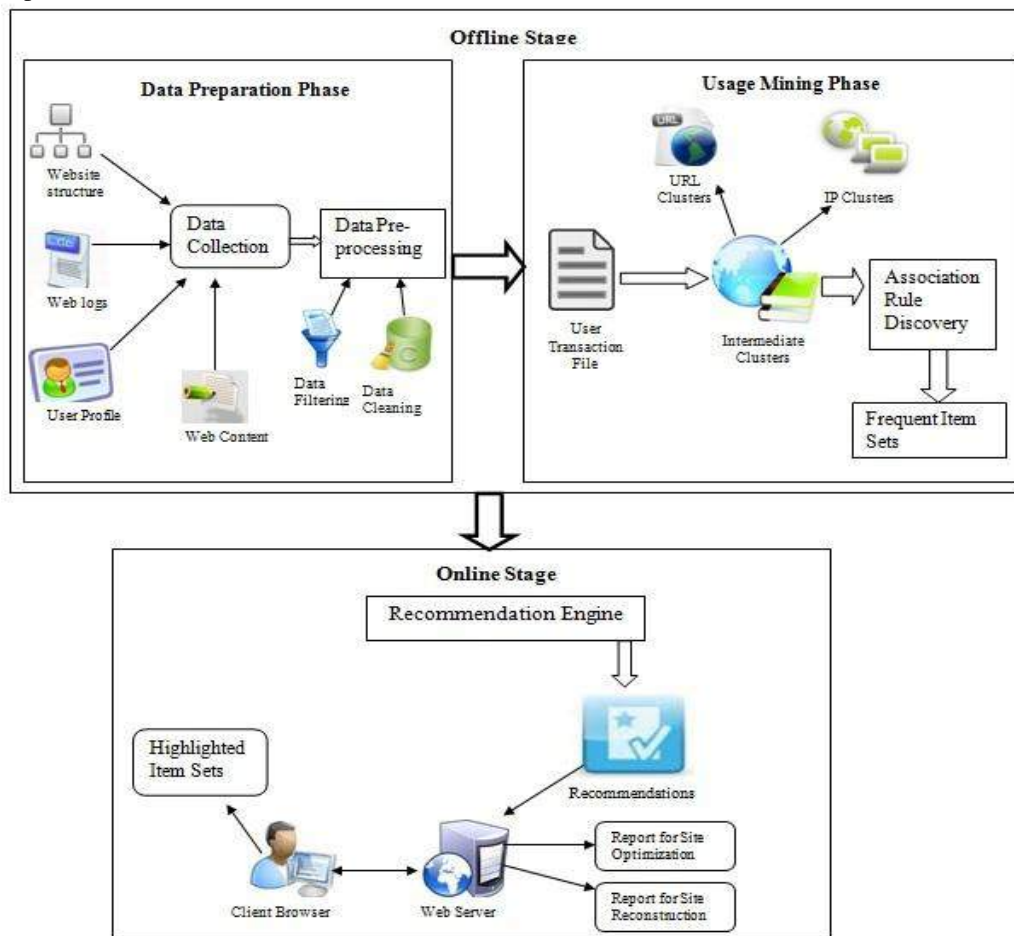
Fig. 5 Proposed framework for AWP

The basic outline of the algorithm is as shown in Fig. 6

Note that the input to the algorithm will be a formatted web log file. The input file is filtered and cleaned before it is used for the algorithm. The web site administrator will decide the minimum support and confidence value. The algorithm gives the result one web site at a time. Initially the recommendation set, *Recommend* and recommend score, *rec_score* are null.

For all the entries, *I*, in the input file, *f*, and its hit ratio is checked against each user. If it satisfies the minimum support and confidence value then that entry (link), *u*, is added to the recommend set, *Recommend*.

It should be noted that to find large enough item sets that could be used for providing recommendations depends upon the support threshold used in the above algorithm.

Input: a formatted web log file f

       Minimum support threshold σ

       Minimum confidence α

       Number of web pages n

$Recommend \leftarrow \varnothing$

$rec\_score \leftarrow \varnothing$

```
for each itemset I of f  do
    if support(I) ≥ σ then
        let c = confidence({u})
        if c ≥ α  then
            u.rec_score ← c *100/n
            Recommend ← Recommend ∪ {u}
        end if
    end if
end for
```

Fig. 6 Algorithm for AWP

5. Experimental Setup

The algorithms have been implemented using Asp.net 3.5 on a Window 7 with 3.0 GB of memory. The approach is tested on the Website of S K Pharmacy college (http://www.skpharmacycollege.org) as well as for IT corporate sector but the URL cannot be disclosed due to privacy issues.Two datasets have been used for the executions of the algorithms. First dataset is of S K Pharmacy college. This server log used is of 2 months for S K Pharmacy college. Second dataset is for IT corporate sector. This server log used is of 3 months for IT corporate sector. The log files are approximately of 50 MB size. The experiment which was implemented on the log file of http://www.skpharmacycollege.org have undergone the offline phase from the proposed framework, due to security reasons, permission was not granted to test the offline results for the online phase.

- *Results*

Here the results of the experiment implemented based on the proposed pseudo code is shown.

The unclean web log file which is used for the experiment. The data cleaned will be used for the next phase i.e. usage mining phase. Data cleaning was done by removing the web log entries with for eg. Status code having value equal to "404", as those entries will not deduce any useful information. The cleaned web log file generated is used to generate various intermediate analysis reports like view scores, urls-wise reports, user-wise reports. Reports for the overall system analysis which can deduce which link is used by users maximum time when they visited the website. As well as report is

generated which gives the URL-wise analysis i.e. how many times a particular url is hit from particular IP address and User-wise analysis i.e how many user hits a particular URL.

Fig. 7 Url-wise analysis

Fig. 8 User-wise analysis

Based on these analysed reports generated, we can provide the recommendation for personalization. Amongst the data in these reports only those information will be used which satisfies the minimum support value provided by website administrator so as to get personalization done on the data. The selected data will highlight. Various recommendation reports are generated based on specified criteria. These recommendation reports will be then used as input for next stage, online stage.

Fig. 9 User-wise Recommendation

Along with these reports, a performance report is generated for the website administrator which can be used for website reconstruction or optimization. The report gives the average time taken by url to complete the request. This kind of report is used so that the website administrator can improve the performance of the website so as to retain the customers/users.

Now these generated reports will be used as input to the online stage.

Fig. 10 Before analysis

Fig. 11 After analysis

6. Conclusion and Future Work

In this proposed work, for enhancement in automatic web personalization a proposed framework is suggested. Based on the framework, the algorithm have been developed which would generate the required knowledge for web personalization. Upon implementing the proposed algorithm, the results achieved are as follows:

- The pre-processed web log file are given as input to the algorithm and as an output various kinds of reports are generated namely User analysis, url analysis reports and performance analysis reports etc.
- These reports are then used for generating recommendations to the users automatically. Reports like User recommendation, Url recommendation, Performance reports etc are generated in offline mode, which then are used to provide the online recommendation automatically to the users.
- The offline results have been tested on the live IP for providing the enhancement in automatic web personalisation.

For implementing the proposed algorithm to apply automatic web personalization, the data used is web data. Web data can be of the form web structure, web content, web logs etc. The proposed algorithm has been tested using the data set as the web log files. These web log files are first converted to a specific format before it is used as an input to the algorithm suggested.

In future this particular limitation can be overcome that, the proposed algorithm requires a specific format web log file as input.

References

[1] S Cho, Y., Kim, J., and Kim, S. (2002): "A personalized recommender system based on web usage mining" 20th Computer Science Seminar SF2-T2-4 decision tree induction. Expert Systems with Applications. 23, Page 329-342**.**

[2] Sung Ho Ha(2002), *Kyungpook National University:* "Helping Online Customers Decide through Web Personalization". IEEE Intelligent systems, Page 32.

[3] A.Jebaraj Ratnakumar (2005): "An Implementation of Web Personalization Using Web Mining Techniques". Journal of Theoretical and Applied Information Technology. Page 1

[4] Dimitrios Pierrakos,Ge Orgios Paliouras,Christos Papatheodorou And Constantine D. Spyropoulos (2003): "Web Usage Mining as a Tool for Personalization: A Survey" User Modeling and User-Adapted Interaction Volume 13, Page 311.

[5] Dimitris Antoniou, Mersini Paschou, Efrosini Sourla, Athanasios Tsakalidis(2010): "A Semantic Web Personalizing Technique The case of bursts in web visits", IEEE Fourth International Conference on Semantic Computing, Pages 530 - 535.

[6] Jaideep Srivastava , Robert Cooley, Mukund Deshpande, Pang- Ning Tan(2000): "Web Usage Mining: Discovery and Applications of Usage Patterns from Web Data", SIGKDD Explorations, Volume1, Issue 2- Pages 12-23.

[7] Ranieri Baraglia, Fabrizio Silvestri (2007): **"**Dynamic Personalization of Web Sites Without User Intervention" - COMMUNICATIONS OF THE ACM February 2007/Vol. 50, No. 2 Page 63.

[8] Bamshad Mobasher, Robert Cooley, Jaideep Srivastava (2000): "Automatic Personalization Based on Web Usage Mining" Communications of the ACM ,Vol 43 Page142.

[9] Magdalini Eirinaki and Michalis Vazirgiannis(2003): "Web Mining for Web personalization." Athens University of Economics and Business. Journal ACM Transactions on Internet Technology (TOIT), Volume Issue 1, Page 1-27.

[10] K. R. Suneetha, Dr. R. Krishnamoorthi,(2009): "Identifying User Behavior by Analyzing Web Server Access Log File", IJCSNS International Journal of Computer Science and Network Security. , VOL.9 No.4, Page 327.

[11] J. Srivastava, P. Desikan, and V. Kumar(2002), "Web Mining: Accomplishments and Future Directions," Proc. US Nat'l Science Foundation Workshop on Next-Generation Data Mining (NGDM), Nat'l Science Foundation, Page 51.

[12] Mobasher, B.,Dai,H.,Luo,T.,Sung,Y. and Zhu,J.(2000): "Integrating web usage and content mining for more effective personalization", In : Proceedings of the International Conference on E-Commerce and Web Technologies (ECWeb2000), Greenwich, UK, Page 165,176.

[13] Chen L, Sycara K. (1998): "A Personal Agent for Browsing and Searching". In Proceedings of the 2nd International Conference on Autonomous Agents, Minneapolis/St. Paul, May, Page 132-139.

[14] Raymond Kosala, Hendrik Blockeel (2000): "Web Mining Research: A Survey", Newsletter, ACM SIGKDD Explorations Newsletter, Volume 2 Issue 1, Page 1.

[15] Bujar Raufi, Juliana Georgieva(2008): "Adaptive Web-Based Systems: Current Trends and Open Issues". International Scientific Conference Computer Science. Volume 3, *Page 1004.*

[16] Jia Wang (1999): A Survey of Web Caching scheme for the Internet. ACM SIGCOMM computer Communication, Volume 29, Issue5, Page 36.

[17] Brinda R. Parekh, Pooja Mehta, "Survey of Data Preprocessing for Web logs", GIT-Journal of Engineering and Technology (2012.ISSN 2249-6157), Gandhinagar, 2012.

[18] Brinda R. Parekh, Pooja Mehta, Prof. Kirit J. Modi, Prof. Paresh S. Solanki, "Web Personalization Using Web mining: Concept & Research Issues", International Journal of Information and Education Technology, Mumbai, 2012.

Gandhinagar Institute of Technology

| Home | Trustee | Editorial Board | Director Message | Papers | Contact Us |

Civil Engineering

Sr.No	Paper Title	Author Name	Institute Detail	Author E_Mail Id	Co-Authors Name
1	Comparison of Static and Dynamic Seismic Analysis for Tall Towers	Prof.Hemal J Shah	DR.S.&S.S.Ghandhy Government Engineering College,Surat	hemalbeena@yahoo.com	Prof.Urita A Mehta
2	Axial Response of Tapered Piles in Sand Using Plaxis 3d Foundation	Prof.Alka M Shah	Gandhinagar Institute of Technology, Gandhinagar	alka.shah@git.org.in	Dr.S P Dave
3	Traffic Volume Analysis	Mr.Dilawar Khan	Gandhinagar Institute of Technology, Gandhinagar	dilawarkhn1@gmail.com	Mr.Jatin Ahir
4	Liquefaction Potential Estimation of Soil Sites	Mr.Milan P Pandya	L. D. College of Engineering, Ahmedabad	milanpandya27@gmail.com	Prof.Madhu S Trivedi
5	Pressure filtration analysis in turbidity removal by graded sand and marble media	Ms.Priyanka S Mehta	Gandhinagar Institute of Technology, Gandhinagar	priyanka.mehta@git.org.in	
6	Linear Dynamic Analysis of Modhera Monument	Mr.Rudra Upadhyay	Gandhinagar Institute of Technology, Gandhinagar	upadhyay.rudra@gmail.com	Prof.Sandip Kapadiya
7	Shortest path algorithms using geotools	Prof.D R Vaghela	Gandhinagar Institute of Technology, Gandhinagar	dhiren.vaghela@git.org.in	

Comparison of Static and Dynamic Seismic Analysis for Tall Towers

Hemal J shah[a], Urita A Mehta[b]

[a]*Assistan Professor, Applied Mechanics Dept., Dr. S.&S.S.Ghandhy Govt. Engg. College, Surat.*
[b]*Assistant Professor, Civil Engg Department,SVBIT,Vasan, Gandhinagar*

Abstract

Tall television towers and other towers are constructed to transmit the television signals on the wider areas as well as for the mobile communication systems, This tall towers must be properly designed so that they will not fail during the natural disasters such as earthquakes. In the past various researchers had studied the effect of different earthquakes on 3 legged tall telecommunication towers. In the present study earthquake response of 4 legged television towers of various heights are studied considering different bracing system such as cross type M type and k type. The towers of different height are modeled in SAP 2000 software and static and dynamic analysis of the tower has been carried out. In addition to this acceleration time history of the Bhuj earthquake is applied on all tower and the response of the various towers are studied.

Keywords: Different Bracing systems; Television tower; seismic analysis;, aceeleration time history analysis; response of tower.

1. Introduction

The television and telecommunication industry plays a great role in human societies and thus much more attention is now being paid to telecommunication and mobile towers than it was in the past. During the natural disasters such as the earthquakes telecommunication and mobile towers have the crucial task of instant transmission of information from the affected areas to the rescue centers. So that relief works and evacuation of the people can be done as early as possible, In addition, performance of infrastructure such as dams, electric, gas, and fuel transmission stations, depends extensively on the information being transmitted via these towers. These tall towers are also used by Military and defense industries so it creates the necessity for further research on telecommunication towers. There are three types of steel telecommunication towers mainly known to engineers as guyed towers, self-supporting towers, and monopoles. Guyed towers normally provide an economical and efficient solution for tall towers of 150 m and above, compared to self-supporting towers. Self-supporting towers are categorized into two groups of 4-legged and 3-legged lattice towers.

Various researchers have studied static and dynamic response of the actual as well as 3 legged Television towers. Amiri G. G.,Boostan A[1] has studied the dynamic response of 3 legged towers while Chen W.H., LuZ. R., Lin W , Chen S.H., Ni Y.Q., Xia Y. , Liao W.Y [2] has tried to compare the experimental and theoretical results of seismic analysis of new gunzao television tower. Researcher Glanville M.J., Kwok K.C.S.[4] has studied the Dynamic Characteristics Of A Steel Frame Tower as well as he has applied wind load on the tower and its effects are studied. Gholamreza G. A [5] has done work on tall towers considering guyed ropes he has done seismic analysis of tall towers. While He M.J. Li X., Ma R.L. and Chen J.L.,[6] has modeled unsymmetrical tall tower having heavy mass situated at the central portin and done seismic Resistant Performance Analysis Of the Unsymmetrical Television Tower. In his research work Siddesha H.[8[, has studied effect of wind loads on television towers considering different bracing systems.

In my work the actual drawings of the towers are collected from the Indian government authorities. The various dimensions that is the width of the tower at base, height of the tower and different bracing system used are studied. The bracing system provided in the tower must be such that it has minimum weight so it gives less earthquake forces as well as higher stiffness so it can resist the earthquake forces more efficiently. For the analysis purpose the 3 bracing system as shown in the figure.1 are considered to study the earthquake response of the structure.

2. Modeling of towers

        To study the effect of different system on television towers different height of the tower such as 80 meter, 110 meter, 150 meter and 175 meter is considered. The towers of this 4 different height considering cross type, M

    (a)   Cross bracing   (b)   M bracing   (C) K bracing
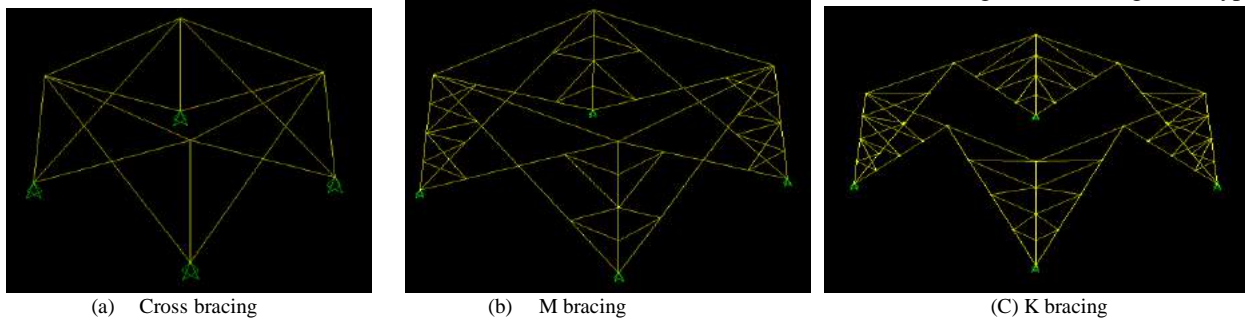
Fig. 1.Diffrent type of bracing systems

type and K type bracing are modelled in SAP 2000 software. Fig 2 shows the model of 80 meter and 110 meter high tower modelled in SAP 2000 software.

    (a)   Model of 80 meter tower   (b)   model of 175 meter tower
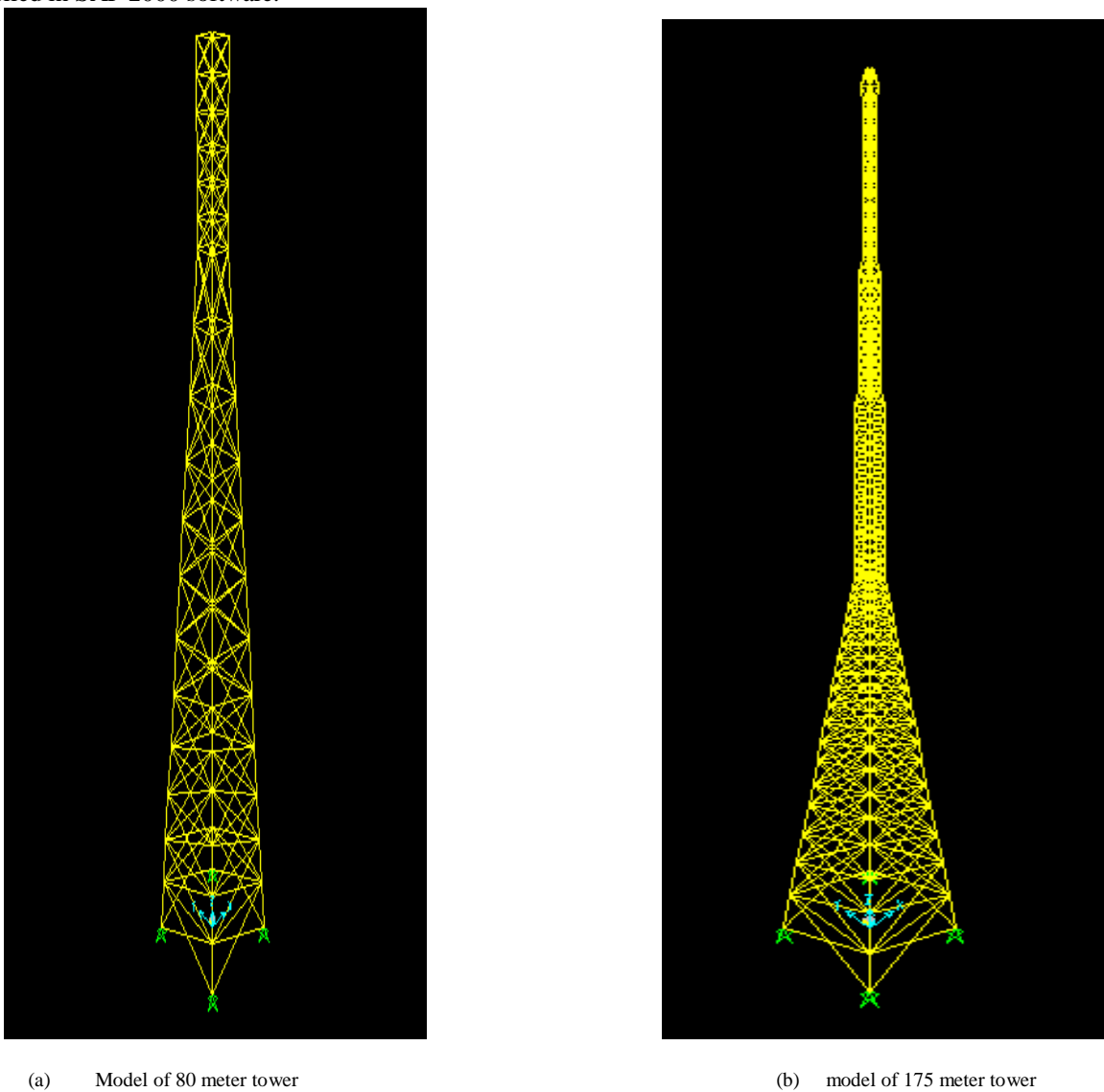
Fig. 2 Model of Tower

After modeling all 12 towers in the SAP 2000 software the towers were analyzed for the dead loads in the dead loads weight of antenna and weight of dish is also considered as shown in table 1 and result are obtained. The static and dynamic seismic analysis of all the 12 towers considering following data as per Indian standard I.S.- 1893-2002 has been carried out.

Table: 1 Details of antenna for TV tower

Type of aperture	Size of aperture 1. length 2. cross section	Net weight of antenna	Present/future requirement
Band –II (FM)	(a) 1800 mm (b) 2500 mm	3500 kg	Future requirement
Band –III	(a) 20000 mm (b) 1200 mm	4800 kg	Present requirement
UHF Band IV/V	(a) 20000 mm (b) 640 mm	4700 Kg	Future requirement
Dish of 2 m diameter	--	150 Kg	Future requirement
Communication antenna	-	20 kg	Future requirement

Data for static method
- Zone : Zone -II , Zone -III , Zone -IV and Zone - V
- Type of soil : Type –II medium soil
- Importance factor : 1.5
- Response Reduction factor : 5

In addition to static analysis of the towers the dynamic analysis of the tower considering acceleration time history method is also carried out. For acceleration time history method, the data of BHUJ earthquake occurred in Gujarat, India on 26 January 2001 is used and it is applied on the tower. The linear acceleration time history analysis of the tower has been carried out. The details of bhuj earthquake are as under. Fig. 3 shows the acceleration time history of bhuj earthquake.

- Name of acceleration time history : Bhuj
- Magnitude : 7.7
- Duration of earthquake: 133.53 second
- Peak ground acceleration : 1.0382 m/sec2
- Acceleration time for PGA : 46.940 second
- Duration: long
- Total no of acceleration records : 26706
- Acceleration time step :0.005 second
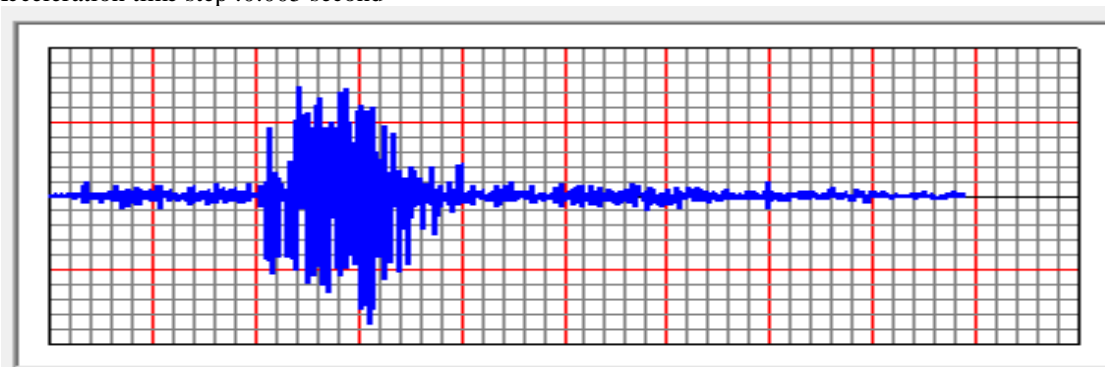
Fig. 3 Bhuj Acceleration time History

The static and dynamic analysis of all 12 towers has been carried out in SAP 2000 software. The no of mode shapes considered in dynamics analysis are such that dynamic participation factor is more than 90 percentage as per

the recommendation of the I.S. -1893-2002. To study the seismic response of all 12 towers the deflection of top joint of all the tower for different seismic cases has been calculated and compared. The base shear due to static load case for all the earthquake zones and aceeleration time history method has been compared.
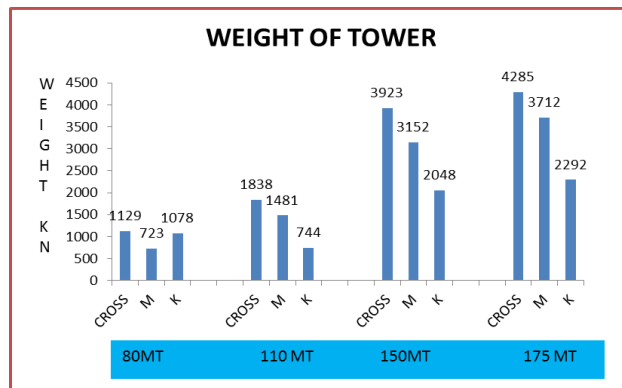
Fig. 4 Weight of Tower
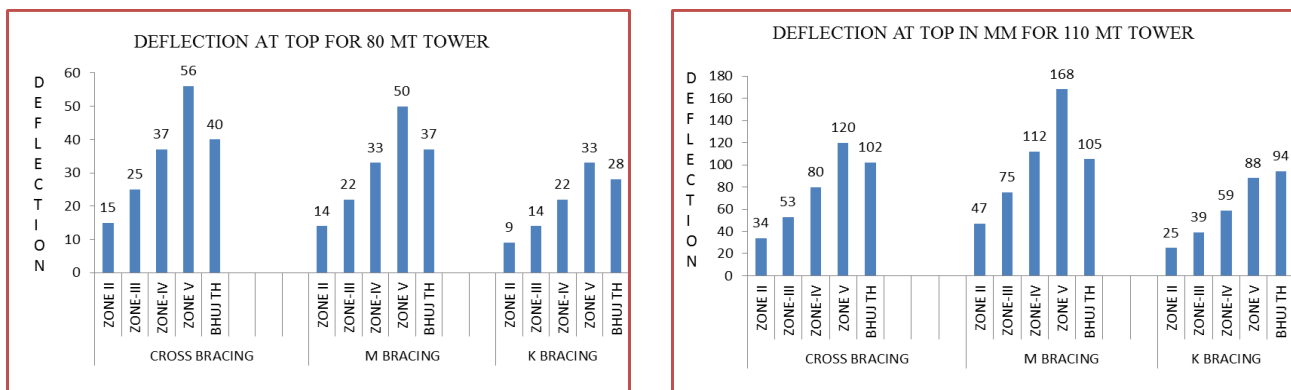
Fig. 5 Deflection at top for tower
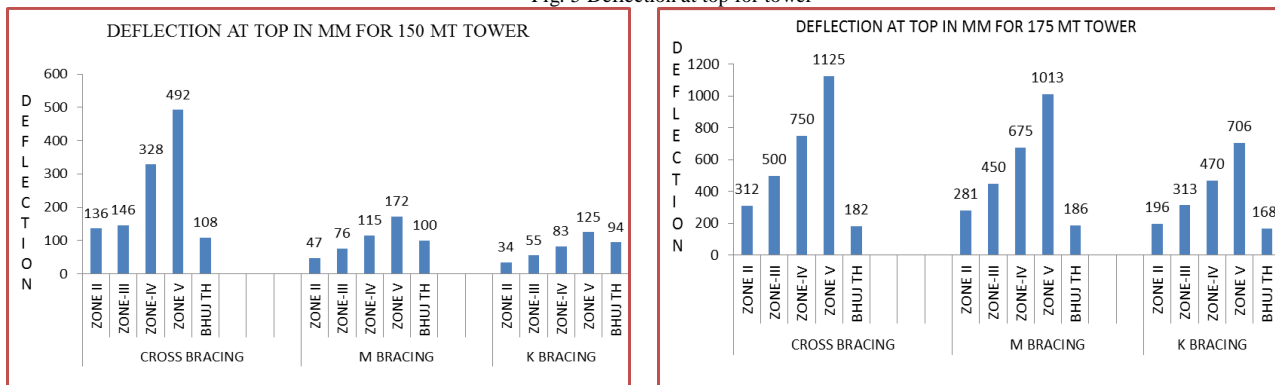
Fig. 6 Deflection at top for tower
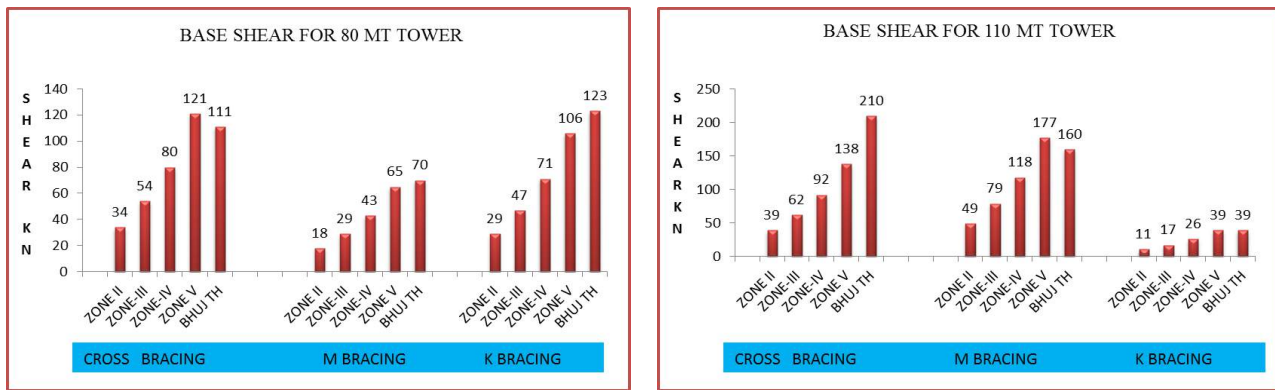
Fig. 7 Base shear for tower
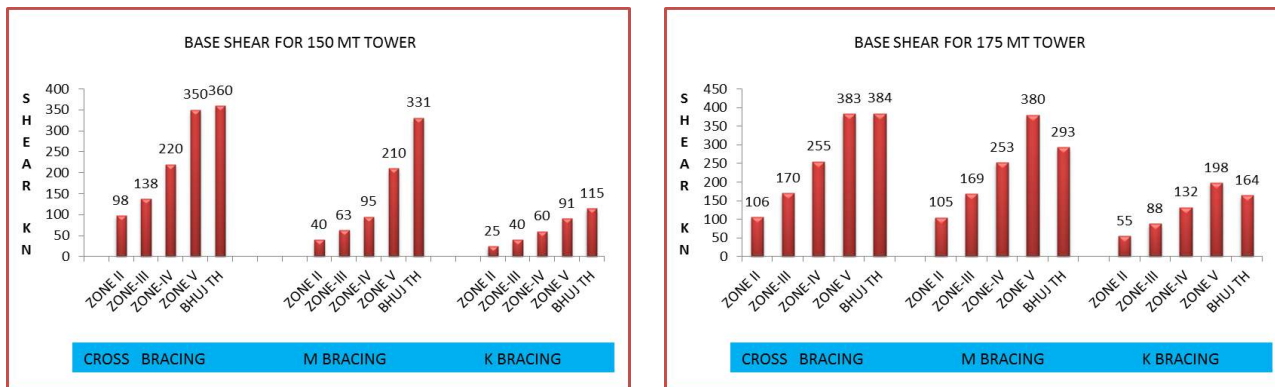
Fig. 8 Base shear for tower

3. Result and discussion.

Figure 4 shows the total weight of the entire tower for different type of bracing system, Fig. 5 and Fig. 6 shows the deflection at the top of tower and fig 7 and fig.8 shows the base shear due to seismic forces by static and dynamic analysis method.

The following points were observed from the study.

1) As the height of tower increase the weight of the tower increase, and hence the earthquake forces at the base i.e. base shear increases. We are getting maximum base shear for cross type bracing system in all 4 towers, hence the cross bracing is most uneconomical system for tall towers.
2) For the 80 meter high tower we are getting more deflection by static method than dynamic method and the difference of deflection by static/dynamic method is more in cross bracing because the stiffness of cross bracing is less
3) For the 110 meter high tower we are getting more deflection by static method than dynamic method and the difference of deflection by static/dynamic method is more in k type bracing so for tall tower we must use the dynamic methods of analysis.
4) For the 175 meter high tower we are getting 400 percentage more deflection by static method in comparison to dynamic method so for tall structures and the structures whose geometry is changing we must use the dynamic method of analysis to get accurate results.
5) For 80 metre high tower we are getting higher base shear by dynamic method so acceleration time history method gives more realistic value of base shear
6) For 110 metre tower we are getting very high value of base shear by static method in cross bracing because cross bracing has less stiffness.
7) For 150 metre high tower base shear by static method for m bracing is 56 percentages higher by static method.
8) For 175 metre high tower we are getting 30 percentage higher shear in M type bracing by static method.

4. Conclusion

From the above analysis we can conclude that the static method of earthquake analysis is based only on mass of the structures and it will not consider the dynamic properties of the structures. So for the structures whose mass and stiffness is changing such as tall towers we must use dynamic method of analysis to get more accurate results. The acceleration time history method is also one of the dynamic methods which give exact value of the seismic forces developed in the structure when ground shakes during earthquake, so we must use acceleration time history method to get actual forces developed in structure during strong ground shaking.

References

[1] Amiri G. G., Boostan A. " Dynamic Response Of Antenna-Supporting Structures", 4th Structural Specialty Conference of the Canadian Society for Civil Engineering, 2002

[2] Amiri G. G., Barkhordari M.A., Massah S. R., "Seismic Behavior Of 4-Legged Self-Supporting Telecommunication Towers", 13th World Conference on Earthquake Engineering., Canada August 2004 Paper No. 215

[3] Chen W.H., LuZ. R., Lin W , Chen S.H., Ni Y.Q., Xia Y. , Liao W.Y., "Theoretical and Experimental modal analysis of the Guangzhou New TELEVISION Tower" Elsevier engineering structure. Aug-2011

[4] Glanville M.J., Kwok K.C.S. "Dynamic Characteristics And Wind Induced Response Of A Steel Frame Tower" Journal of wind Engineering And Industrial Aerodynamics 1995 Paper No: 54

[5] Gholamreza G. A. "Seismic Sensitivity Of Tall Guyed Telecommunication Towers" Ph.D.   Thesis, February 1997, Mcgill University, Canada.

[6] He M.J. Li X., Ma R.L. and Chen J.L., "Seismic Resistant Performance Analysis On An Unsymmetrical Super-High Steel Television Tower" Tongji University, Shanghai 200092, China.

[7] IS: 1893(Part 1):2002,"Criteria for Earthquake Resistant Design of Structures (General Provisions & Buildings)", Bureau of Indian Standards

[8] Siddesha H., "Wind Analysis of Microwave Antenna Towers" , International Journal Of Applied Engineering Research, Dindigul Volume 1, No 3, 2010

Axial Response of Tapered Piles in Sand Using Plaxis 3d Foundation

Alka M. Shah[a], Dr S.P. Dave[b]*

[a]*Assistant Professor, Civil Engineering Department, Gandhinagar Institute of Technology, Gandhinagar -382721, India*
[b]*Professor & Head, Applied Mechanics Department, L.D.College of Engineering, Ahmadabad-380015, India*

Abstract

The axial behavior of tapered piles in sand using different materials, R.C.C., Steel and Timber are studied using Finite Element Method based program PLAXIS 3D FOUNDATION. Five single piles of each material including one Straight pile and four tapered piles with taper angles 0.5°, 1°, 1.5° & 2° are examined under same vertical loading. Five pile groups, two piles in each group, are also analyzed to study the response of single piles and pile groups. All piles have same head diameter and length. The tapered section of the pile has been analyzed by assuming stepped cylindrical segment (SSM-Segment by Segment Method). Linear elastic behavior is assumed for pile and the Mohr-coulomb criterion is considered for soil. Load carrying capacity, settlement and influence of stresses are discussed with respect to different material and change in taper angles. The result shows that the safe load carried by concrete pile is more than the steel and timber pile but settlement of steel pile is more compared to concrete and timber pile. The load carrying capacity of tapered pile group is more than the straight pile group.

Keywords: Tapered pile and pile group, Finite element method, Axial capacity, Settlement, Sand

Nomenclature	
c	cohesion
E	young's modulus
v	Poisson's ratio
Greek symbols	
γ	unit weight
Latin	
Φ	friction angle
Ψ	dilatancy angle

1. Introduction

Pile foundation is necessary for many structures and the capacity under vertical loading is important and also a controlling factor. There are many research exist on axial capacity of straight pile and pile group, but there are only few researches existing on tapered pile and pile group. That's why the bearing capacity of tapered piles is of significant concern to design engineers in recent years. This is because it has been shown that the bearing capacity of a tapered pile (TP) is greater than a straight pile [Kyuho Paik et al, 2012, Nabil F. Ismael,2010, Ghazavi et al, 2001; Ghazavi, 2000; Wei et al, 1998, Ghazavi et al, 1997,Jayantha et al, 1993]. Different types of piles with different material and section are used in practice. The extensive experience with tapered concrete, timber and steel piles at John F. Kennedy international airport offered a unique opportunity for the research into tapered piles. It has been proved that capacity of tapered concrete pile is more than the tapered timber and steel piles [John et. al, 2004, John et. al, 2004, Yasser et al, 2004].The capacity of steel taper pile is more with respect to straight pile because the shaft resistance is more in taper pile compared to steel pile [Kyuho Paik et al, 2012].

In most of the research work, for simplicity, a fully tapered pile has been idealized by a number of stepped prismatic segments connected rigidly to each other as shown in Fig.1. [Ahmad et al, 2012, Sudhendu Saha et al, 1986] using SSM-Segment by segment method. It was also proved that the difference between the bearing capacity of stepped and fully tapered piles is less than 10%. This demonstrates that simplifying a tapered pile to some prismatic segments is justified [Ghazavi et al, 1997]. In this study, the same method is used for analysis. This analysis presents the comparative behavior of tapered piles and pile groups with respect to single straight piles under vertical loading in sand.
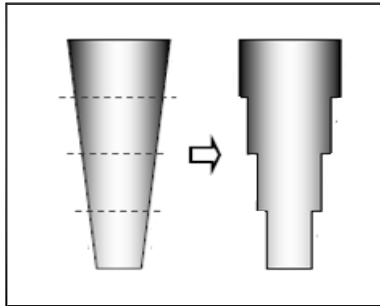
Fig.1 Actual taper pile and idealized taper pile
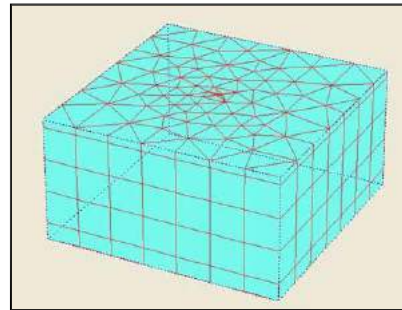
Fig.2 3D meshing of cylindrical pile

1.1 Materials and Methods

The analysis consists of modeling of single pile with different materials concrete, steel and timber in sand and also pile group with two piles. Overall 15 piles and 5 pile groups are investigated with different taper angle i.e.   0°, 0.5°, 1°, 1.5° & 2° (0° means Cylindrical straight pile). The head diameter is fixed for all piles, 0.5 m and toe diameter is different as per taper angle.   The length of all pile is 8 m. The soil and pile properties used for this analysis are illustrated in Table-1. The vertical load for all single pile is 300 kN.

The Finite element analysis is performed using Software PLAXIS 3D FOUNDATION. In this method, during the generation of the mesh, the continuum is divided into 15-node wedge elements and these elements divided in to numbers of nodes. Adjacent elements are connected through their common nodes. During finite element calculations, displacements are calculated at the nodes. Nodes may be pre-selected for the generation of load-displacement curves. The 3D meshing of cylindrical straight pile is shown in Fig.2. The model of straight pile is shown in Fig.3.The model of tapered pile in form of some step cylindrical segment is shown in Fig.4. The modeled pile group with two piles is shown in Fig.5.
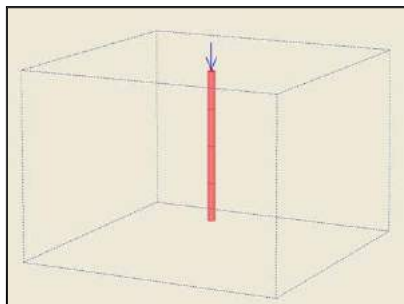
Fig.3 Modelled cylindrical pile
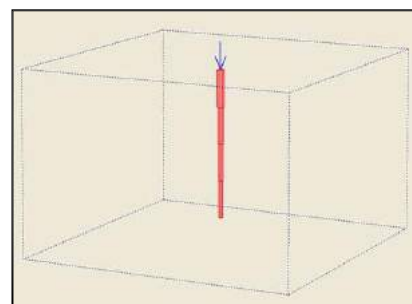
Fig.4 Modelled taper pile

Fig.5 Modelled pile group

1.2 Soil Model

The surrounding soil is modeled as a well-known Mohr-Coulomb model. The elastic-plastic behavior of model is based on parameters that are E, v, c, φ, and ψ, which are also useful in analysis of stress – strain behavior.

1.3 Structural member model

The linear elastic model is used to model massive structure in soli or bedrock layer like pile. This model represents Hook's law of isotropic linear elasticity. The model involves two elastic stiffness parameters, namely effective Young's modulus, E and effective Poisson's ratio, v. It is primarily used to model stiff structure in soil.

2. Result and Discussions

This analysis presents the axial behavior of tapered pile with different material and R.C.C. pile groups. For pile group analysis R.C.C. pile is taken because after the analysis of single pile, results show that the safe load of R.C.C. piles is more than the other two. Total 15 piles with different materials and 5 pile groups are tested with different taper angles. The results of study are shown in Table-2 and Table-3. One of the important factors affecting the axial behavior of pile is its settlement. It can be seen that steel pile settle more than the concrete pile and the settlement in timber pile is less compare to other two, but the safe load of concrete pile is more compare to steel and timber pile. There is not much effect of taper angle 0.5° on vertical settlement. For all type of piles the settlement decreases and safe load increases as taper angle increases compared to straight cylindrical pile. This is because the shaft resistance of tapered pile is composed of both frictional and compressive resistances, due to inclined pile, whereas the shaft resistance of the cylindrical pile is composed of only friction resistance. This phenomenon is shown in Fig.6. The stresses in soil mass decreases as taper angle increases. In case of pile groups the settlement is less than the single pile and safe load is more but there is significant effect of taper angle 1°.
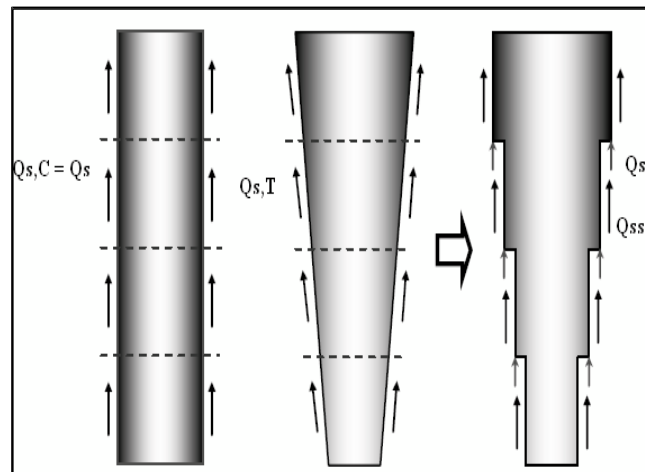
Fig.6

Where,

Qs = Shaft resistance   Qss = Frictional resistance

Qs, C = Shaft resistance of cylindrical pile   Qsc = Compressive resistance

Qs, T = Shaft resistance of tapered pile

2.1 *Table*

Table-1 Soil and pile parameters

Name	Sand	Pile			Unit
		Concrete	**Steel**	**Timber**	
γ_{unsat}	12	24	78.6	5.25	kN/m^3
γ_{sat}	18	-	-	-	kN/m^3
E_{ref}	22900	$3.27*10^7$	$2.00*10^7$	$1.05*10^7$	kN/m^2
v	0.3	0.150	0.26	0.0	-
C_{ref}	1	-	-	-	kN/m^2
Φ	31	-	-	-	°

Table-2 Safe load and % reduction in settlement under vertical load for single piles

Pile with diff. taper angle	R.C.C.			Steel			Timber		
	Settlement (mm)	% Reduction In settlement	Safe load (kN)	Settlement (mm)	% Reduction In settlement	Safe load (kN)	Settlement (mm)	% Reduction In settlement	Safe load (kN)
0°	10.20	-	120	11.90	-	100	5.94	-	90
0.5°	10.14	0.6	125	11.21	5.6	105	5.04	15	100
1°	8.19	19.7	138	9.05	24	110	4.13	30.5	105
1.5°	7.37	27.7	142	7.07	40.6	120	3.76	36.7	115
2°	6.68	34.5	145	6.80	43	140	3.47	41.5	125

Table-3 Safe load and % reduction in settlement under vertical load for pile groups

Pile with diff. taper angle	Single Pile (R.C.C.)			Pile Group (R.C.C.)		
	Settlement (mm)	% Reduction In settlement	Safe load (kN)	Settlement (mm)	% Reduction In settlement	Safe load (kN)
0°	10.20	-	120	9.60	-	150
0.5°	10.14	0.6	125	9.01	6.14	160
1°	8.19	19.7	138	7.80	18.8	165
1.5°	7.37	27.7	142	7.25	24.5	175
2°	6.68	34.5	145	6.50	32.3	190

2.2 *Conclusions*

- The settlement decreases as taper angle increases under the same vertical loading for all type of single piles.
- The steel piles settle more than the concrete and timber piles.
- The Load carrying capacity of concrete pile is more than steel and timber pile.
- There is no significant effect of taper angle of 0.5° on settlement as well as on load carrying capacity.
- The percentage reduction in settlement with respect to straight single pile is effective in case of 1° concrete and steel taper pile. From this it can be say that pile with taper angle 1° is effective, but for timber pile the effective angle is both 1° and 1.5°.
- The safe load carried by pile groups is more than the single piles, but it is more effective in case of 1°.
- The settlement is less in pile groups compare to single pile.
- The stresses decrease in soil mass as taper angle increases for both single pile and pile group.
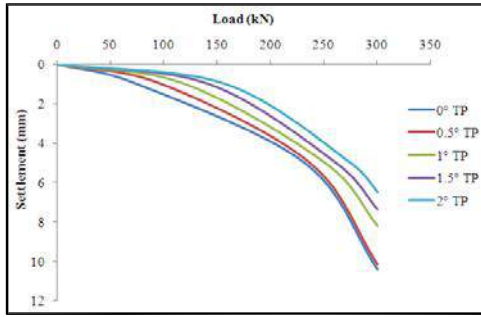
Fig.7 Load-Settlement curve for different
degree of taper angle (R.C.C. pile)
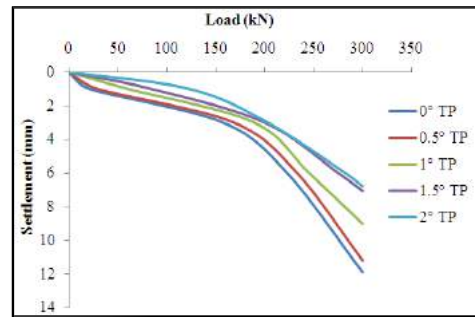
Fig.8 Load-Settlement curve for different
degree of taper angle (steel pile)
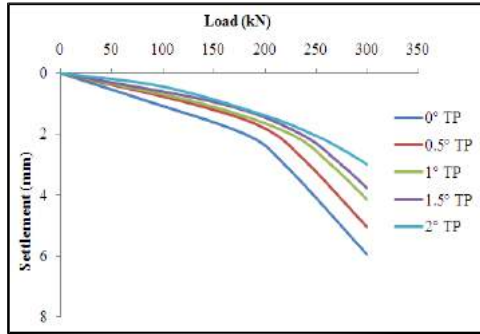
Fig.9 Load-Settlement curve for different
degree of taper angle (timber pile)
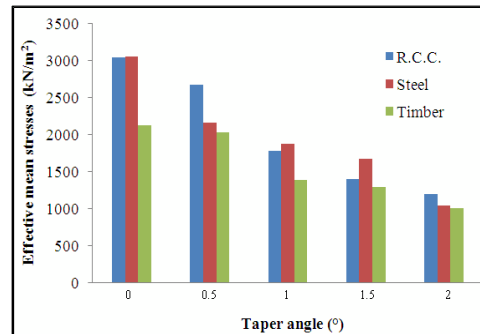
Fig.10 Effective mean stresses v/s taper
Angle for single piles
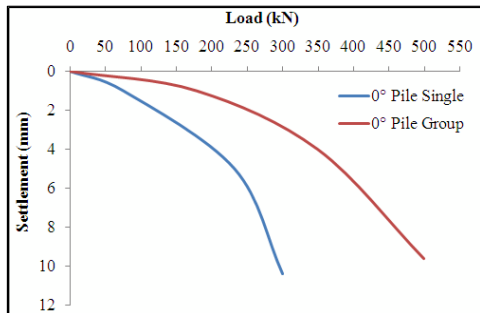
Fig.11 Load-Settlement curve straight
single pile and pile group
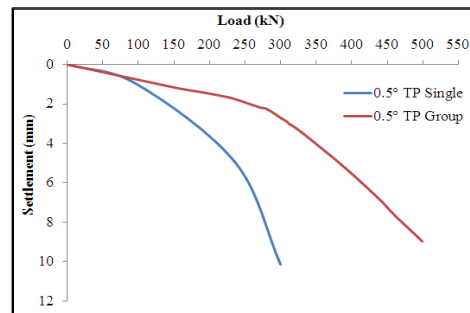
Fig.12 Load-Settlement curve 0.5°single
pile and pile group
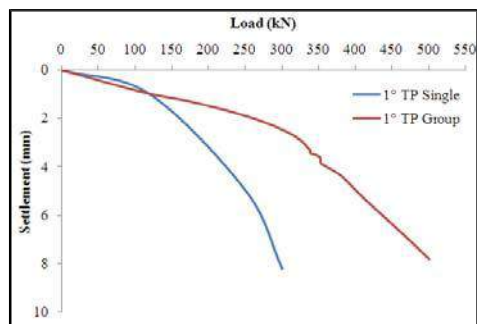
Fig.13 Load-Settlement curve 1°single
pile and pile group
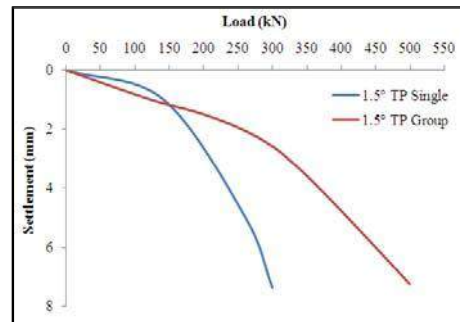
Fig.14 Load-Settlement curve 1.5°single
pile and pile group
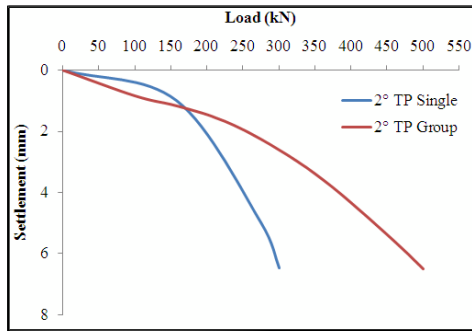
Fig.15 Load-Settlement curve 2°single
pile and pile group
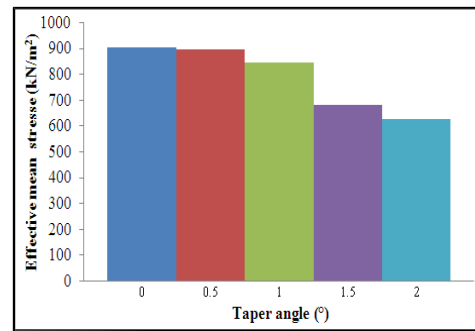
Fig.16 Effective mean stresses v/s taper
angle for pile groups

References

1) Ahmad Dehghanpoor and Mahmoud Ghazavi, (June 2012), "*Response Of Tapered Pile Under Lateral Harmonic Vibrations*", International journal of GEOMATE, vol 2,pp 261-265

2) Daniel J. Borello, Bassem Andrawes, Jerome F. Hajjar, Scott M. Olson and James Hansen (April 2010), " *Experimental and Analytical Investigation of Bridge Timber Piles Under Eccentric loads",* ELSEVIER, Journal of Engineering structure 32 (2237-2246)

3) John S. Horvath and Thomas Trochalidas (April 13-17,2004), *"A Half Century of Tapered-Pile usage at the john F. Kennedy International Airport"*, proceedings: Fifth international Conference on case Histories in Geotechnical Engineering, paper no.11.05

4) John S. Horvath, Thomas Trochalidas, Andrew Burns and Stanley Merjan (April 13-17,2004), *"Axial-Compressive Capacities of a new Type of Tapered Steel Pipe Pile at the John F.Kennedy International Airport"*, proceedings: Fifth international Conference on case Histories in Geotechnical Engineering, paper no.11.02

5) Jin Qi Wi, August (1998), "*Experimental Investigation of tapered pile*'', Thesis, The university of western Ontario, London, Ontario

6) Kyuho Paik, Junhwan Lee and Daehong Kim, (June 2012), "*Calculation of the axial bearing capacity of tapered bored piles*", ICE Geotechnical Engineering.

7) Mahmoud Ghazavi and Arash Alimardani Lavasan, (1997), "*Bearing Capacity of Tapered and Step-tapered Piles Subjected to Axial Compressive Loading*", thesis, Civil Engineering Department, K.N. Toosi University of Technology, Tehran, Iran.

8) Nabil F. Ismael, (May 2010), "*Behavior of Step Tapered Bored Piles in Sand under Static Lateral Loading*", journal of geotechnical and geoenvironmental engineering © ASCE, vol 136, pp 669-676

9) Nabil F. Ismael, (2001), "*Axial Load Tests on Bored Piles and Pile Groups in Cemented Sand* ", journal of geotechnical and geoenvironmental engineering © ASCE, pp 766-737

10) Ran Zhao, Zhi-liang Dong, You-yuan Wang, and Lin-wang Su (2012), *"Research on Pressed Pile Test and Finite Element Analysis of Large-diameter Steel Pipe Pile of Zhanjiang Port"*, World Academy of Science, Engineering and Technology 71, PP 1876-1880

11) Sudhendu Saha and D.P.Ghosh,(1986), "*Vertical Vibration Of Tapered Pile*", Journal of Geotechnical engineering at ASCE, vol 112, pp 290-302

12) Sri Dewi and Gouw Tjie-Liong, *"Analysis on Laterally Loaded Groups Pile by Plaxis 3D Foundation"*, Civil engineering department, Bina Nusantara University.

13) Text book of Braja Das, *"Principal of Foundation Engineering"* , 7th Edition,Publisher Global engineering, 2011

14) Text book of Joseph E. Bowles, , " *Foundation Analysis and Design"*, 5th Edition, Tata McGraw-Hill Companies, 1996

15) Yasser A. Hegazy, Andrew G.Cushing and Christopher J.Lewis (April 13-17,2004), *"Driven Pile Capacity In Clay And Drilled Shaft Capacity In Rock From Pile Load Tests"*, proceedings: Fifth international Conference on case Histories in Geotechnical Engineering, paper no.1.95

Traffic Volume Analysis

Jatin Ahir[a] , Dilawar Khan[b], Hemang Dalwadi*

[a]*Student of Civil Department, Gandhinagar Institute of Technology, Ahmedabad, 38007*
[b]*Student of Civil Department, Gandhinagar Institute of Technology, Ahmedabad, 38007*
Assistant Professor in Civil Department,Gandhinagar Institute of Technology, Ahmedabad, 38007

Abstract

There has been a significant increase in traffic during recent years due to vehicular traffic increase which lead to congestion on the street. Due to this noteworthy increase of vehicles, many problems like pollution, parking problems etc occurred. Therefore a parametric study has been carried out with the perspective of analysis the traffic volume. In this parametric study, level of service of different segment has been practically studied between destination points of Shyamal Cross Road toShivranjani cross Roadfacing heaviest traffic problems. Based on the result we can analyseproblems creating such heavy traffic and propose probable solution.

Keyword:Traffic Volume Analyisis,Level Of Service,shyamal/shivranjani

1. Introduction

In the recent scenario traffic is the major concern for any developing nation. There is a significant increase in trafficduring recent years caused by vehicular traffic increase which lead to congestion on the street. Traffic Engineering is the application of technology and scientific principles to the planning, functional design, operation and management of facilities for any mode of transportation in order to provide for the safe, efficient, rapid, comfortable, convenient, economical, and environmentally compatible movement of people and goods.The planning aspects of transport engineering relate to urban planning and involve technical forecasting decisions and political factors .Technical forecasting of passenger travel usually involves an urban transportation planning model, requiring the estimation of Trip Distribution,Trip Generation, Mode Choice,RouteAssignment .

We have analyzed thestretch of about 1.1 km which lies betweenShyamal cross road to Shivranjani cross road located in Ahmedabad,Gujarat,India.Reason for selecting this stretch is being one of the highest growing junctions. The parametric factors here are Level OfService,Peak Hours Factor,Passenger Car Unit,Volume/Capacity ratio.

2. Methodology

Mixture of manual and automatic traffic volume analysis method has been applied to do the parametric study of traffic capacity. In manual method ,which consist of assigning a person to record traffic as it passes , and were as in automatic method detection of vehicular presence and road occupancies has historically been performed primarily on or near the surface of the road .Level OfService (LOS):A qualitative measure used to relate the quality of traffic service. LOS is used to analyze highways by categorizing traffic flow and assigning quality levels of traffic based on performance measure like speed, density,etc.Peak Hours Factor(PHF): As the ratio of the volume occurring during the peak hour to the maximum rate flow during a given time period within the peak hour (15min) , it is average volume during the peak 60 minute period divided by four time the average volume during the peak 15 minute .

$$phf = \frac{Avg.volume \ during \ peak \ 60 \min period}{4*(Avg.volume \ during \ peak \ 15 \min period \ )} \ ,$$

Passenger Car Unit(PCU): As is the standard practice in urban transportation studies ,volume of different vehicles types are converted into single unit using the equivalent PCU factor, Volume/Capacity: Defined as the maximum number of vehicles, passengers, or the like, per unit time, which can be accommodated under given conditions with a reasonable expectation of occurrence.
$$\frac{v}{c} ratio = \frac{total \ traffic \ volume}{arterial \ capacity}$$

The effect of various parameter ratio were study on the stretch of 1.1km of Shyamal cross road to Shivranjaini cross road.

3. Scopeof Work

The mixed traffic comprising of number of modes having different physical characteristics and speed flow behaviour reflecting heterogeneity is main feature of Indian traffic plying on metropolitan road network. Obviously there is need of converting such heterogeneous traffic in to homogeneous one through passenger car equivalents introduce by Highway Capacity Manual (HCM) in 1965, with thrust on trucks and buses in the traffic stream. The PCE definition in HCM 2000 is 'the number of passenger car that are displaced by a single heavy vehicle of particular type under prevailing roadway, traffic and control conditions. The mixed traffic is converted to homogeneous equivalent passenger car units by applying respective PCU values. These values have been taken as mentioned in IRC 1990-106. It has been shown in Table 1. Lots of research work is carried and still going on to interrelate the wide variations in static and dynamic characteristic of mixed traffic with the passenger car equivalent using the different methodology and equivalency criteria. Most of the traffic engineers are adopting the static PCU specified by HCM or Indian Road Congress (IRC) in analysis of different traffic situations and deciding the road capacities and establishing LOS. However dynamic characteristics of mixed flow cannot be ignored in traffic system designing or operation. Therefore it may not be precisely correct to adopt a constant set of PCU values under different roadway and traffic conditions.

The purpose of the proposed traffic analysis is to determine the significant increase in the traffic capacity in the recent year.The process consist of different vehicle of various categories and has been listed in the table .The analysis is done during peak hours at morning and evening and classified under 15 min each interval the total vehicle of different category is being multiple by PCU so as to define all the vehicle as passenger car unit .After the multiplication the total no vehicle can be calculated and hence on the basis of the this outcome we able to determine theLevel Of Service ,Peak Hour Factors and Volume/Capacity ratio .

Table1.PCU units used as per IRC 1990-106

Vehicle types	Equivalent PCU factors	
Two wheeler, Motor Cycle, Scooter etc	0.5	0.75
Passenger car, Pick up van	1.0	1.0
Auto rickshaw	1.2	2.0
Light commercial Vehicle	1.4	2.0
Truck or Bus	2.2	3.7
Agriculture Tractor Trailer	4.0	5.0
Cycle	0.4	0.5
Cycle rickshaw	1.5	2.0
Tonga (horse drawn vehicle)	1.5	2.0
Hand cart	2.0	3.0

4. Result and Discussion

In this parametric study level of service of different segment has been practically studied of traffic volume between destination points Shyamal Cross RoadstoShivranjani cross roads facing heaviest traffic problems. During the recent study various outcome have been obtained and on which traffic capacity of the stretch was obtained.Table 2 represent the results for Shyamal cross road to Shivranjani cross road as obtain from the manually calculation.

Table 2 Results for Shyamal cross road to Shivranjani cross road.

	Volume/capacity ratio	LOS	Peak Hour Factor	LOS
Up(morning)	1.21	F	0.96	F
Down(morning)	1.14	F	0.98	F
Up(evening)	1.12	F	0.97	F
Down(evening)	1.20	F	0.92	F

Figure 1 show the percentage share by different vehicles all the stretch.
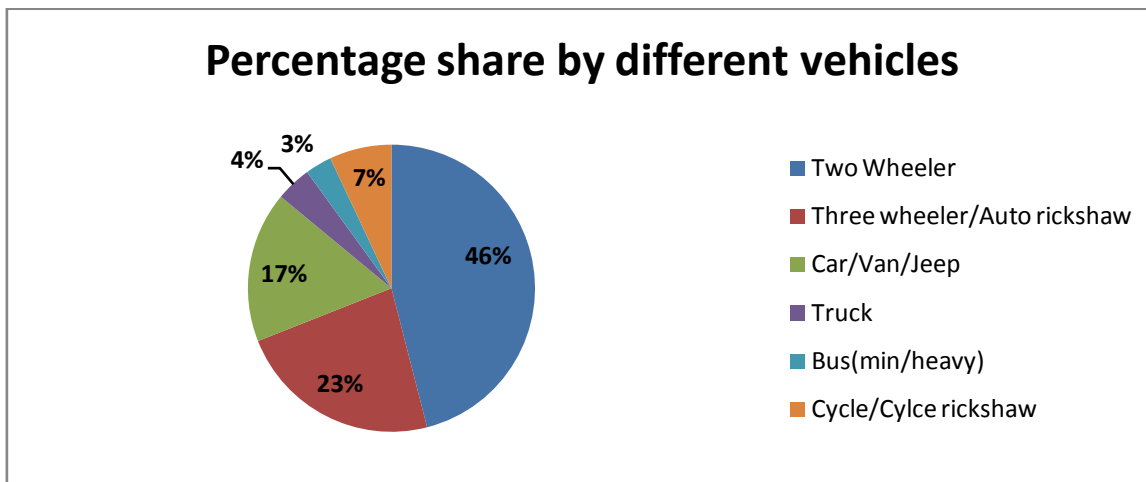
Figure1. Percentage share of Different Category Vehicles

Increases in the frequency of the vehicle on the stretch significantly descried in the above result in pie chart shows that on the basis of the manually acquired data various percentage of different categorized vehicles is obtained .On the basis of this we overcome on the result that this situation lies in the level of service of F and the traffic flow is mixed traffic flow which carry more amount of traffic capacity above its exiting carrying capacity during peak hours,as this area comes under the highly commercial and residential area where movement traffic is continues.

5. Conclusion

From the overheadstudy and result outcome we can determine that LOS of the stretch from Shyamal to Shivranjani is F. The reason behind this capacity is increase in trips by personal mode of transportation by using two wheelers and cars. Some of the other reasons are decrease in width of road by BRTS, improper management of traffic along the intersection, haphazard parking along the carriage way, merging of traffic from different directions etc.

6.Future scope

This type of the parametric study can be carried out on the various segments for which Individual traffic carrying capacity of the present period can be obtained and hence heavy intersection facing various types of problem can be effectively resolved.

7. References

[1]   Aggarwal Praveen (2008), "Passenger Car Unit Concept, Significance and affecting Factors", Indian Highways, Vol.36, pp. 23-31.
[2]   Dr. L.R.kadiyali ,"Traffic engineering and Transportation Engineering" .
[3]   Tom V. Mathew and K V Krishna Rao,'Introduction to Transportation Engineering '.
[4]   Sharma, S. C. 1994. Seasonal Traffic Counts for a Precise Estimation of AADT.ITE Journal, Vol.
       64, No. 9, pp. 34–41.
[5]   "Highway Capacity Manual" (2000) Special Rep. 209, Transportation Research Board, Washington, D.C.
       Indian Road Congress (1990) Guidelines for capacity of urban roads in plain areas, IRC: 106, New
       Delhi.
[6]   Marwah, B.R. and Singh, B. (2000) "Level of service classification for urban heterogeneous traffic: A
       case study of Kanpur Metropolis", Paper presented at the fourth international symposium on Highway
       Capacity, Hawaii, June-July 2000.
[7]   SantoshA.Jalihal and Dr. T. S. Reddy, "The Changing Traffic Composition; Its Impact And
       Implications", presented at National Seminar on "Road Transportation in India: Emerging
       Trends and Techniques (RORTRAN 2002)", IIT, Kharagpur (West Bengal), India.

Liquefaction Potential Estimation of Soil Sites

Milan P. Pandya[a] *, Prof. Madhu S. Trivedi[b]

[a]M. E Student, L. D. College of Engineering, Ahmedabad, Gujarat, India
[b] Assistant Professor, Civil Engineering Department, Gandhinagar Institute of Technology, Gandhinagar, Gujarat, India

Abstract

The study deals with the Liquefaction Potential Estimation of soils. Various parameters of liquefaction were studied and using the field methods particularly, SPT based (concepts of cyclic shear stress, cyclic stress ratio). Semi-empirical procedure for evaluation of liquefaction potential during earthquakes was carried out for the river banks of Sabarmati River front Area at Ahmedabad. Laboratory testing of bore log data, Standard Penetration test was studied at Institute of Seismological Research (ISR), Gandhinagar. SPT based assessment using Seed & Idriss (1971)[19] and Idriss & Boulanger (2008)[10] methods were used on Standard Penetration test data to estimate the factor of safety against liquefaction for the present case study. The paper gives the insight to understand liquefaction Potential of Soil and determination of the same at various depths at a particular place in the study area.

Keywords: Liquefaction Potential Estimation, Standard Penetration test, cyclic shear stress, cyclic stress ratio

Nomenclature

$(N_1)_{60cs}$	Clean-sand Corrected Blow Counts
C	Cohesion
CPT	Cone Penetration Test
α	Constant For Reduction Factor
β	Constant For Reduction Factor
$(N_1)_{60}$	Corrected Penetration Blow counts
$\Delta(N_1)_{60}$	Correction for Finer Content
C_S	Correction for Split Spoon Sampler
CRR	Cyclic Resistance Ratio
CSR	Cyclic Stress Ratio
Φ	Degree of Internal Friction
z	Depth Below Ground Level
DSU	Direct Shear Stress
DS	Disturb sample
$V_0^{'}$	Effective Vertical Stress
C_E	Energy Delivery Correction
GL	Ground Level
IS	Indian Standard
W_L	Liquid Limit
M	Magnitude of Earthquake
MSF	Magnitude Scaling Factor
N_m	Measured SPT Blow Counts
NRC	National Research Council
C_N	Overburden Correction
K	Overburden Correction Factor
τ_{max}	Peak Cyclic Shear Stress
a_{max}	Peak Ground Surface Acceleration
W_P	Plastic Limit

* Corresponding author. Tel.:+91-79-27434306 ;
E-mail address: milanpandya27@gmail.com

IP	Plasticity Index
C_R	Rod length Correction
V_s	Shear Wave Velocity
C_B	Standard Borehole Correction
SPT	Standard Penetration Test
r_d	Stress Reduction Factor
V_0	Total Vertical Stress
TCU	Triaxial Shear Test
USG	Undrained Compressive Strength

1. Introduction

Earthquakes accompanied with liquefaction have been observed for many years. In fact, written records dating back hundreds and even thousands of years have descriptions of earthquake effects that are now known to be associated with liquefaction. However, liquefaction has been so common in a number of recent earthquakes that it is often considered to be associated with them. Some of those earthquakes are

1. Alaska, USA (1964)
2. Niigata, Japan (1964)
3. Loma Prieta, USA (1989)
4. Kobe, Japan (1995)

There are many terms that introduce the phenomena of liquefaction in various aspects of losing strength or loading condition or it's behave and many more but we see the most common and technical based definition of liquefaction.

Liquefaction is the phenomena when there is loss of strength in saturated and cohesion-less soils because of increased pore water pressures and hence reduced effective stresses due to dynamic loading. It is a phenomenon in which the strength and stiffness of a soil is reduced by earthquake shaking or other rapid loading. Seismic waves, primarily shear waves, passing through saturated granular layers, distort the granular structure, and cause loosely packed groups of particles to collapse.
These collapses increase the pore-water pressure between the grains if drainage cannot occur. If the pore-water pressure rises to a level approaching the weight of the overlying soil, the granular layer temporarily behaves as a viscous liquid rather than a solid. This phenomenon is called Liquefaction. The term was first used by **Arthur Casagrande (1935)[1]** and later by **Mogami** and **Kubo (1953)[3],** Became popular during **Alaska and Niigata earthquake in 1964.**

1.1 Technical Physics of liquefaction

It is required to recognize the conditions that exist in a soil deposit before an earthquake in order to identify liquefaction. Soil is basically an assemblage of many soil particles which stay in contact with many neighboring soil. The contact forces produced by the weight of the overlying particles holds individual soil particle in its place and provide strength.

Fig.1. (a) Soil grains in a soil deposit. The height of the blue column to the right represents the level of pore water pressure
(Reference: www.ce.washington.edu/~liquefaction)

Fig.1. (b) The length of the arrows represents the size of the contact forces between individual soil grains. The contact forces are large when the pore water pressure is low.

Fig.1. (c) The contact forces are small at high water pressure. In an extreme case, the pore water pressure may become so high that many of the soil particles lose contact with each other.
(Reference: www.ce.washington.edu/~liquefaction)

1.2 Soil Site for Assessment of Liquefaction Potential

Fig.2. our soil site is Sabarmati River Front West bank of river Sabarmati.

2. Assessment of Liquefaction Potential

The stress-based approach for evaluating the potential for liquefaction triggering, initiated by Seed and Idriss (1967)[18], has been used widely for the last 45 years (e.g., Seed and Idriss 1971, Shibata 1981,Tokimatsu and Yoshimi 1983, NRC 1985[14], Seed et al. 1985, Youd et al. 2001, Cetin et al. 2004, Idriss and Boulanger 2004). The basic framework, as adopted by numerous researchers, compares the earthquake induced cyclic stress ratios (CSR) with the cyclic resistance ratios (CRR) of the soil. The components of this framework, as briefly summarized below, were developed to provide a rational treatment of the various factors that affect penetration resistance and cyclic resistance.Various methods suggested by different investigators. Most comprehensive liquefaction potential analysis is based on SPT blow counts (N spt). Evaluation of the liquefaction potential of saturated cohesion less soils during earthquakes were re-examined and revised using semi-empirical procedures for use in practice by I. M. Idriss, R. W. Boulanger[6-10]. The stress reduction factor (r_d), earthquake magnitude scaling factor for cyclic stress ratios (MSF), overburden correction factor for cyclic stress ratios (K), and the overburden normalization factor for penetration resistances (C_N) were discussed and recently modified relations were presented.

2.1. Estimating Cyclic Shear Stress Ratios (CSR) Induced by Earthquake Ground Motions

The Seed-Idriss (1971)[19] simplified procedure is used to estimate the CSR induced by earthquake ground motions, at a depth *z* below the ground surface, using the following equation

$$CSR = (\tau_{av}/\sigma'_{vo}) = 0.65(a_{max}/g)(\sigma_{vo}/\sigma'_{vo})r_d \quad \text{--Eq (1)}$$

Where,
a_{max} -maximum horizontal acceleration at the ground surface(PHA)
σ_{y0} - total vertical stress
σ'_{v0}-effective vertical stress at depth
z- Depth
r_d -stress reduction coefficient that accounts for the flexibility of the soil column

The peak horizontal acceleration (PHA) is the most commonly used type of ground acceleration in engineering applications, and is used to set design hazard risks. In an earthquake, damage to soil strength is related more closely to ground motion, rather than the magnitude of the earthquake. For moderate earthquakes, PGA is the best determinate of damage. Peak ground acceleration can be expressed in g (the acceleration due to Earth's gravity, equivalent to g-force) as either a decimal or percentage, in m/s^2 (1 *g* = 9.81 m/s^2). In India, areas with expected PHA values higher than 0.36*g* are classed as "Zone 5", or "Very High Damage Risk Zone". As we take 0.45g a_{max} (PHA) for study of liquefaction analysis of our study area.

The stress reduction coefficient r_d was introduced by Seed and Idriss (1971)[19] as a parameter describing the ratio of cyclic stresses for a flexible soil column to the cyclic stresses for a rigid soil column. They obtained values of r_d for a range of earthquake ground motions and soil profiles having sand in the upper 15± m (50 ft) and suggested an average curve for use as a function of depth. The average curve, which was extended only to a depth of about 12 m (40 ft), was intended for all earthquake magnitudes and for all profiles. Idriss (1999)[6] extended the work of Golesorkhi (1989)[4] And performed several hundred parametric site response analyses and concluded that for the conditions of most practical interest, the parameter r_d could be adequately expressed as a function of depth and earthquake magnitude (M). The following relation was derived using those results:

$$\text{Ln}(r_d)=\alpha(z)+\beta(z)M \quad \text{--Eq (2)}$$

$$\alpha(z)= -1.012-1.126 \sin\left(\frac{z}{11.73} + 5.133\right) \text{--Eq (3)}$$

$$\beta(z)=0.106+0.118 \sin\left(\frac{z}{11.28} + 5.142\right) \text{--Eq (4)}$$

These equations given above were considered for z<=34 m. for z >34 m the equation to
Be used is:

$$r_d = 0.12\exp(0.22M) \quad \text{--Eq (5)}$$

Where,
 z- Depth
M- Magnitude of the earthquake
r_d -stress reduction coefficient

2.2. Magnitude scaling factor, MSF

The magnitude scaling factor, MSF, has been used to adjust the induced CSR during earthquake magnitude M to an equivalent *CSR* for an earthquake magnitude, M = 7½. The MSF is thus defined as:

$$\textbf{MSF= CSR}_\textbf{M}\textbf{/CSR}_\textbf{M=7.5} \quad \textbf{--Eq (6)}$$

The values of MSF are calculated by combining correlations of the number of equivalent uniform cycles versus earthquake magnitude and the laboratory based relations between the cyclic stress ratio required to cause liquefaction and the number of uniform stress cycles. Idriss (1999)[6] re-evaluated the MSF derivation using results of cyclic tests on high quality samples obtained by frozen sampling techniques. The re-evaluated relation was slightly different from the simplified procedure (Seed & Idriss 1971)[19]. The MSF relation produced by this reevaluation is given by:

$$\textbf{MSF= 6.9 EXP(-M/4)-0.058} \quad \textbf{--Eq (7)}$$

Where,
 M- Magnitude of the earthquake

2.3. Cyclic resistance ratio (CRR)

The soil's CRR is usually correlated to an in-situ parameter such as SPT blow count (Number of blows per foot), CPT penetration resistance or shear wave velocity Vs. SPT blow counts are affected by a number of procedural details (rod lengths, hammer energy, sampler details, borehole size) and by effective overburden stress. Thus, the correlation to CRR is based on corrected penetration resistance,

$$\textbf{(N}_\textbf{1}\textbf{)}_\textbf{60}\textbf{= C}_\textbf{N}\textbf{.C}_\textbf{E}\textbf{.C}_\textbf{R}\textbf{.C}_\textbf{B}\textbf{.C}_\textbf{S}\textbf{.N}_\textbf{m} \quad \textbf{--Eq (8)}$$

The first correction factor (C_N) normalizes the measured blow count to an equivalent value under one atmosphere of effective overburden stress:

$$\textbf{C}_\textbf{N} = \sqrt{\frac{\textbf{\textit{Pa}}}{\boldsymbol{\sigma'vo}}} \leq \textbf{2.0} \quad \textbf{--Eq (9)}$$

Where:
σ'_{v0} is the vertical effective stress at the depth of NSPT and Pa is one atmosphere of pressure (101.325 kPa) in the same units as σ'_{v0}. The maximum value of 2.0 limits C_N at depths typically less than 1.5 m.

The factor C_E is used to correct the measured SPT blow count for the level of energy delivered by the SPT hammer. Using 60% of the theoretical maximum energy as a standard, this correction is given by:

$$\textbf{C}_\textbf{E}\textbf{=}\frac{\textit{Actual energy delivered to top of drill rod}}{\textbf{0.60}*\textit{theoretical maximum SPT hammer energy}} = \frac{\textbf{ER}}{\textbf{60}} \quad \textbf{--Eq (10)}$$

Where:
 ER is the energy ratio and the theoretical maximum SPT hammer energy is 4200 lb-in (from 140 weight dropping 30 inches in each blow). The energy ratio (ER) should be measured for the particular SPT equipment used. When such measurements are unavailable, the energy ratio and correction factor can be estimated from the average values given by Seed et al. (1985):

Country	Hammer Type:	Hammer Release	ER	C_E
United States	Rope and pulley	Safety	60	1
United States	Rope and pulley	Donut	45	0.75
Japan	Rope and pulley, special throw release	Donut	67	1.12
Japan	Free fall	Donut	78	1.30

The third correction factor in Equation (8), C_B is for borehole diameters outside the recommended range. The following values are recommended (Robertson and Fear 1998)[13]:

Diameter of Borehole	C_B
65 to 115 mm (2.5 to 4.5 inch)	1.00
150 mm (6 inch)	1.05
200 mm (8 inch)	1.15

The fourth correction factor in Equation (8), C_S, is for SPT samplers used without a sample liner. If the split spoon sampler is made to hold a liner but is used without one, the measured blow count should be corrected with $C_S=1.2$. Otherwise, $C_S=1.0$ for a standard sampler.

The last correction factor in Equation (8) is C_R, which is used to correct for the loss of energy through reflection in short lengths of drill rod. In the NCEER recommendations, values of the correction factor C_R are given for ranges of rod length. For the analysis of the EPOLLS case studies, these recommended values of C_R were approximated with a linear equation

- For $z \leq 3$ m: $C_R = 0.75$
- For $3 < z < 9$ m: $C_R = (15 + z) / 24$
- For $z \geq 9$ m: $C_R = 1.0$

The correlation for CRR is therefore developed for a reference M (Magnitude of earthquake) = 7.5 and $\sigma'_V = 1$ atm.

Equivalent clean-sand $(N_1)_{60cs}$
This is also known as finer content correction.

$$\Delta(N_1)_{60} = \exp\left(\frac{9.7}{FC} - \left(\frac{15.7}{FC}\right)^2\right) \qquad \text{--Eq (11)}$$

$$(N_1)_{60cs} = \Delta(N_1)_{60} + (N_1)_{60} \qquad \text{--Eq(12)}$$

$$CRR = \exp\left\{ \frac{(N1)60CS}{14.1} + \left(\frac{(N1)60CS}{126}\right)^2 - \left(\frac{(N1)60CS}{23.6}\right)3 + \left(\frac{(N1)60CS}{25.4}\right)^4 - 2.8 \right\} \qquad \text{--Eq (13)}$$

3. Result & Conclusion

- Ratio of two cyclic stresses is greater than one which concludes that soil at that depth is non-liquefied.
- This ratio known as factor of safety (FOS)
  FOS = CRR/CSR
- Total 22 boreholes of 20 m depth were taken into account for the liquefaction study on the two banks of the River Sabarmati as shown in the Figure 4

- After the completion of necessary analysis and calculation of the data acquired from the bore logs and SPT test results, conclusion is represented for the liquefaction status of the soil at various depths at various locations in below Table-I
  Illustration is given at appendix -A

Table – I Liquefaction Status of Soil at Various Depths

Bore Hole No	Depth (METER)	FOS values	Liquefied
2W	0-1.5	0.62	YES
	1.5-3	0.88	YES
3W	0-1.5	0.36	YES
4W	0-1.5	0.26	YES
	1.5-3	0.50	YES
5W	0-1.5	0.33	YES
	1.5-3	0.52	YES
6W	0-1.5	0.30	YES
7AW	-	-	NO
7BW	-	-	NO
7CW	-	-	NO
7DW	-	-	NO
7W	-	-	NO
8W	-	-	NO
9AW	-	-	NO
9BW	-	-	NO
9CW	-	-	NO
9W	0-1.5	0.27	YES
	1.5-3	0.91	YES
10AW	-	-	NO
10BW	-	-	NO
10W	0-1.5	0.41	YES
11W	-	-	NO
12W	-	-	NO
13W	0-1.5	0.46	YES
	1.5-3	0.63	YES
14W	0-1.5	0.52	YES
	1.5-3	0.71	YES
15W	0-3	0.69	YES
15WR	-	-	NO
16W	0-1.5	0.47	YES
	1.5-3	0.80	YES
17W	0-1.5	0.44	YES
18W	0-1.5	0.32	YES
	1.5-3	0.70	YES
19W	-	-	NO
20W	0-1.5	0.36	YES
21W	0-1.5	0.38	YES
22W	0-1.5	0.10	YES
	1.5-3	0.30	YES
	3-4.5	0.70	YES
23W	0-1.5	0.20	YES
	1.5-3	0.48	YES
P5W	0-1.5	0.43	YES
	1.5-3	0.62	YES

P5W1	-	-	NO
P6W	0-1.5	0.27	YES
P6W1	-	-	NO
P7W	0-1.5	0.47	YES
	1.5-3	0.92	YES
P7W1	-	-	NO

References

1. Braja M. Das, Ramana G.V. (2010) Principles of soil dynamics, C L Engineering.
2. Cetin, K. O., and Seed, R. B. (2004). "Nonlinear shear mass participation factor (r_d) for cyclic shear stress ratio evaluation." Soil Dynamics and Earthquake Engineering, Elsevier, 24.
3. Day, R.W. (2001) Geotechnical Earthquake Engineering Handbook, McGraw- Hill.
4. Golesorkhi, R. (1989). Factors Influencing the Computational Determination of Earthquake-Induced Shear Stresses in Sandy Soils, Ph.D. thesis, University of California at Berkeley.
5. https://www.ce.washington.edu/~liquefaction
6. Idriss, I. M. (1999). An update to the Seed-Idriss simplified procedure for evaluating liquefaction potential, in Proceedings, TRB Workshop on New Approaches to Liquefaction, Publication No. FHWARD- 99-165, Federal Highway Administration, January.
7. Idriss, I. M., and Boulanger, R. W. (2003). Relating K_α and K_σ to SPT blow count and to CPT tip resistance for use in evaluating liquefaction potential, in Proceedings of the 2003 Dam Safety Conference, ASDSO, September 7–10, Minneapolis, MN.
8. Idriss, I. M., and Boulanger, R. W. (2004). Semi-empirical procedures for evaluating liquefaction potential during earthquakes, in Proceedings, 11th International Conference on Soil Dynamics and Earthquake Engineering, and 3rd International Conference on Earthquake Geotechnical Engineering, D. Doolin et al., eds., Stallion Press, Vol. 1,
9. Idriss, I. M., and Boulanger, R. W. (2006). Semi-empirical procedures for evaluating liquefaction potential during earthquakes, J. Soil Dynamics and Earthquake Eng. 26.
10. Idriss, I. M., and Boulanger, R. W. (2008).Soil liquefaction during earthquakes. Monograph MNO-12, Earthquake Engineering Research Institute, Oakland, CA.
11. Ishihara, K., "Liquefaction and Flow Failure during earthquakes (Rankine Lecture)", Geotechnique, 43 (3), 1993.
12. Jefferies, M. Been, K. (2006) Soil Liquefaction: A critical state approach, Taylor & Francis.
13. Kramer, S.L. (1996) Geotechnical Earthquake Engineering, Prentice Hall.
14. National Research Council (NRC) (1985). Liquefaction of Soils During Earthquakes, National Academy Press, Washington, DC, 240.
15. Poulos, S.J., Castro, G., and France, W., 1985. Liquefaction evaluation procedure, J. Geotechnical Engineering Div., ASCE, Vol. 111.
16. Prakash, S. (1981) Soil Dynamics, McGraw-Hill.
17. Robert W. Day (2002) Geotechnical Earthquake Engineering Handbook McGraw-Hill.
18. Seed, H. B., and Idriss, I. M. (1967)."Analysis of liquefaction: Niigata earthquake", Proc., ASCE, 93(SM3).
19. Seed, H. B., and Idriss, I. M. (1971), "Simplified procedure for evaluating soil liquefaction potential." J. Soil Mechanics and Foundations Div., ASCE   97(SM9).
20. Seed, H. B., and Idriss, I. M. (1982). Ground Motions and Soil Liquefaction During Earthquakes, Earthquake Engineering Research Institute, Oakland, CA.
21. Youd, T. L., Noble, S. K. (1997). "Liquefaction Criteria Based on Statistical and Probabilistic Analyses", Proceedings of the NCEER Workshop on Evaluation of Liquefaction Resistance of Soils, December 31, 1997.

PROJECT : SABARMATI RIVER FRONT DEVELOPMENT PROJECT, AHMEDABAD

R.L. 47.958   Exploratory

Scale : 1:150   Bore Hole No.: 22 W

BORE HOLE LOG

METHOD OF DRILLING	CASINGS	BORE DIAMETER	DEPTH (METRE)	THICKNESS OF LAYER	SOIL CLASSI.	SOIL DESCRIPTION	STANDARD PENETRATION TEST OBSERVED 'N' - VALUES		U.D.S.	D.S.	REMARKS
			(m)				10 30 50 70				
ROTARY DRILLING		150 mm	1.5 — 3.0	3.50	SP	Brown loose medium sand	6 / 9			S / S	
			4.5 — 6.0	3.50	SP	Brown medium dense medium to coarse sand	12 / 15			S / S	GWL 6.0 m
	13.0 m	100 mm	7.5 — 9.0 — 10.5	3.70	SP	Light brown medium dense medium to coarse sand	17 / 20			S / S	
			12.0	2.30	GP	Dense gravel with coarse sand	27 / 33			S / S	
	BENTONITE CIRCULATION		13.5	1.70	CL	Light brown hard sandy clayey silt			U		
			15.0 — 16.5	2.30	SM	Light brown very dense silty sand with traces of clay	78 / >100			S / S	
			18.0 — 19.5	3.00		Lime cemented matrix of silty sand and coarse sand			CORE / CORE		Termination at 20.0 m Depth
			21.0								

Appendix A.

Soil Profile		Project: Sabarmati River Front Development Project, Ahmedabad				Termination Depth: 20 m				Table No.: 22W-2		
						Depth of Water Table: 6.0 m				Bore Hole No.: 22W		

Depth (m) From GL	Type of Sample	Grain Size Analysis				Atterberg's Limits			I.S. Classi-fication	Field Dry Density G/cm^3	Natural Water Cont. %	Shear Parameters			Silt Factor	UCS kg/cm^2	Sp. Gr. G	Consolidation Parameters		
		Gravel %	Sand %	Silt %	Clay %	w_L	w_P	I_p				Type	c kg/cm^2	▢ Deg.				C_C	e_0	p_C kg/cm^2
1.50	SPT	4	95	- 1 -		18	NP	-	SP	-	-	-	-	-	2.46	-	-	-	-	-
3.00	SPT	5	94	- 1 -		18	NP	-	SP	-	-	-	-	-	2.45	-	-	-	-	-
4.50	DS	2	97	- 1 -		18	NP	-	SP	2.00 (max)	1.57 (min)	DCU	0.00	37	2.41	-	2.63	-	-	-
6.00	SPT	6	93	- 1 -		18	NP	-	SP	-	-	-	-	-	2.83	-	-	-	-	-
7.50	DS	14	86	- 0 -		18	NP	-	SP	2.04 (max)	1.60 (min)	DCU	0.00	39	3.23	-	2.63	-	-	-
9.00	SPT	3	97	- 0 -		18	NP	-	SP	-	-	-	-	-	2.83	-	-	-	-	-
10.50	SPT	2	98	- 0 -		18	NP	-	SP	-	-	-	-	-	-	-	-	-	-	-
12.00	SPT	91	7	- 0 -		18	NP	-	SP	-	-	-	-	-	-	-	-	-	-	-
13.50	UDS	1	38	49	12	33	20	13	CL	1.69	7.82	TCU	0.10	30	-	-	-	-	-	-
15.00	SPT	-	83	- 17 -		20	NP	-	SM	-	-	-	-	-	-	-	-	-	-	-
16.50	SPT	2	80	- 18 -		23	20	3	SM	-	-	-	-	-	-	-	2.64	-	-	-
18.00	CORE	-	-	-		-	-	-	-	2.18	6.57	-	-	-	-	41.3	-	-	-	-
20.00	CORE	-	-	-		-	-	-	-	1.92	6.80	-	-	-	-	32.4	-	-	-	-

A.1. Analysis of Bore log No. 22w by empirical formulas

Bore Hole No.: 22w										
Depth (Meter)	**Finer Content In Percentage**	**N Measured (N)**	**N Value Corrected (N1)60**	**Correction For Fine Content**	**Clean-Sand Equivalent (N1)60**	**CRR**	**Rd**	**CSR (Cyclic Stress Ration Induced By Earthquake) 0.45g**	**Fos At 0.45g**	**Non-Liquefied At 0.45g**
1.500	1.000	6.000	4.331	0.000	4.331	0.093	0.995	0.973	**0.095**	**False**
3.000	1.000	9.000	7.088	0.000	7.088	0.135	0.982	0.450	**0.300**	**False**
4.500	1.000	12.000	10.238	0.000	10.238	0.230	0.966	0.332	**0.694**	**False**
6.000	1.000	15.000	13.781	0.000	13.781	0.478	0.949	0.278	**1.721**	**True**
7.500	0.000	17.000	15.938	0.000	15.938	0.800	0.930	0.246	**3.253**	**True**
9.000	0.000	20.000	20.000	0.000	20.000	2.494	0.910	0.224	**11.120**	**True**
10.500	0.000	27.000	28.688	0.000	28.688	70.061	0.889	0.208	**337.067**	**True**

Pressure filtration analysis in turbidity removal by graded sand and marble media

Priyanka S. Mehta[a]

[a]*Gandhinagar Institute of Technology Khatraj - Kalol Road, Vil. Moti Bhoyan, Tal. Kalol, Dist. Gandhinagar-38272,India*

Abstract

There is a need to find cheaper and simpler techniques for water filtration system for public supply & industries. Using a graded multi-media the flow rate of pressure sand filter can be increased & by increasing flow rate, area required can be reduce by two fold. In order to carry out the studies a pilot scale model was used with all provisions for experimentation & monitoring. Test runs were carried for the filtration, the filter backwashing and the filtration process monitoring. Filtration was carried at a rate of 490 Lt/hr. raw water modified through dosing bentonite clay for the desired turbidity was used as feed water. In this paper filter run results for turbidity & pressure variation are carried out & by using sand media the efficiency is between 80-97% & using crushed marble as media the efficiency is 60-80% .Even after operating the PSF for 25hrs the difference of inlet and outlet pressure is less than $0.8 Kg /cm^{2}$.

Keywords:Pressure Sand Filter ,Efficiency,Flow rate,Backwashing

1. Introduction

Water is one of the most essential requirements for human survival. To achieve high quality potable water, the water has to be given series of treatments. Surface water is the main source for water supply. The main problem in using surface water as source of water supply is high concentration of clay and suspended solids. Filtration is the most common method to remove clay and suspended solids. In filtration process, water is purified by passing through a bed of porous media which cause the retention of suspended matters within it. As the water flows through the filter media particles are deposited on the surfaces of the granules by interception, diffusion, inertial impaction, gravitational settling, electrical migration or a combination of two or more of these effects. In surface water filtration, slow sand filters and rapid sand filters are widely used for removal of suspended solids present in water Pressure sand filter are also rapid sand filter with only difference that they occupy less space and the driving force for filtration is achieved by pumping Liquid to be filtered.

The media grain size, which affects the efficiency of filtration, is considered to be an indicator of the size of the particles that could be removed by the media. The finer the media, the smaller the particle size removed, and the better the quality of the filtration process, although a smaller size requires more frequent cleaning. Media effective diameter (de) and its uniformity coefficient (UCs) are two indicators of the media filter grain size. The media effective diameter is defined as the size of the screen opening which will allow 10% of the total sand sample mass to pass The UCs is the ratio between the screen pores that let pass 60 and 10% of the sand. A uniform sand media has a low UCs value while a good graded media is characterized by a high UCs value. For pressure sand filters, a UCs of 2 is recommended although other researchers suggested working with lower UCs Suspended materials trapped by the filter decrease the water flow rate across the filter. The present study focuses on investigating the effect of different Medias, combinations of media on flow rate & efficiency of filtration.

Priyanka Jadhav. Tel.:09016478336.

E-mail address: priyanka.mehta@git.org.in

2. Materials and Methods

The entire study was divided into following parts

- *Characterization of the filter media*

- *Pilot scale filtration system set up*

- *Pilot scale experimentation on the sand media*

2.1. Characterization of the filter media

Under this element of work all the sand & crushed marble media procured were subjected to sieve analysis in order to find out the effective size uniformity coefficient. For sieve analysis following procedure was followed:

Known amount (2kg) filter media was dried & sieved through a series of nine screens ranging from 0.075 to 20 mm pores (pore size decreasing from top to bottom) by manual shaking. Then the material retained on each screen was weighed to determine the weight of retained sand. Sieve analysis results for sand & crushed marble shown in Table 1 & Table 2 respectively. Using the data given in the tables a graph of a particle size distribution was plotted on log probability graph paper. The graphs are shown at Fig 1. (a),(b) for sand and crushed marble respectively
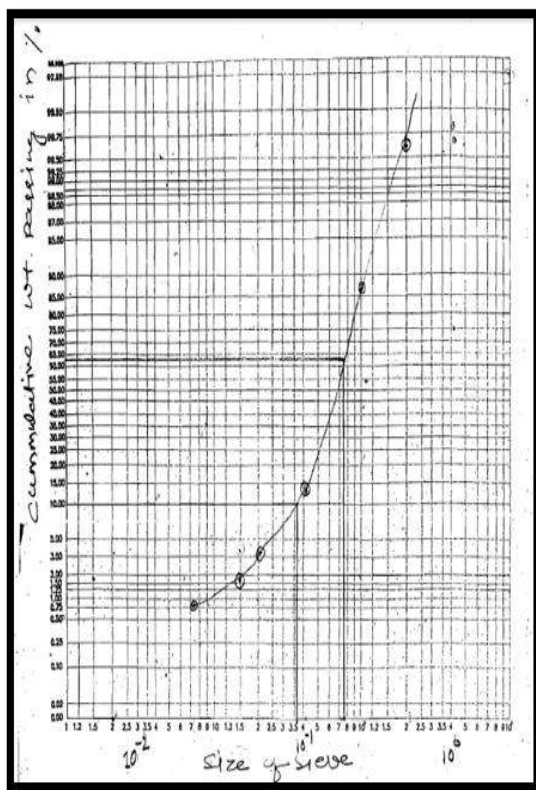
Table 1. Sand sieve analysis

Sieve Size (mm)	Mass retain (kg)	Cumulative wt. retained (kg)	Cumulative wt. retain (%)	Cumulative wt. Passing (%)
20	Nil	Nil	Nil	Nil
10	Nil	Nil	Nil	Nil
4.75	Nil	Nil	Nil	Nil
2	0.0075	0.0075	0.367	49.6
1	0.2595	0.267	13.39	86.61
.425	1.4515	1.7185	86.20	13.8
.212	0.212	1.9305	96.86	3.14
.150	0.0285	1.959	98.29	1.71
.075	0.0205	1.979	99.2	0.8
Nil	0.0135	1.993	100	0

Table 2. Crushed marble sieve analysis

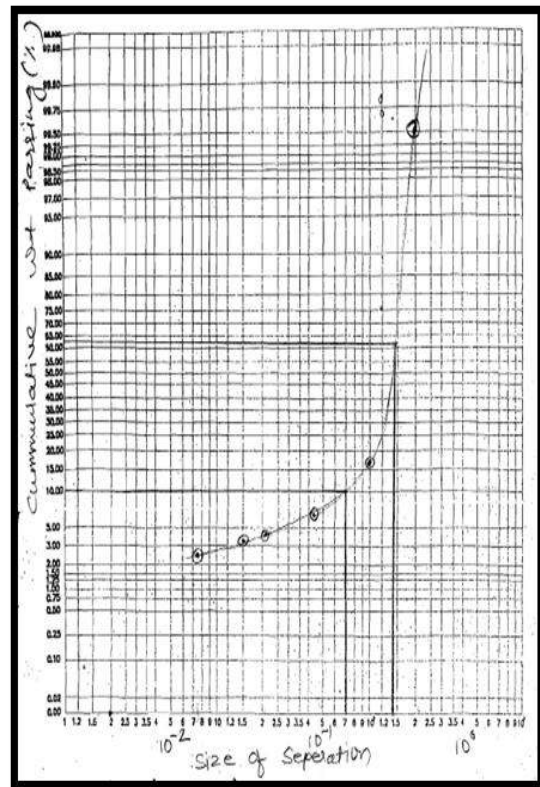| Sieve Size (mm)	Mass retained(kg)	Cumulative wt. retained (kg)	Cumulative wt. retained (%)	Cumulative wt. Passing (%)
20	Nil	Nil	Nil	Nil
10	Nil	Nil	Nil	Nil
4.75	Nil	Nil	Nil	Nil
2	0.010	0.010	0.50	99.5
1	1.631	1.641	82.41	17.59
.425	0.224	1.865	93.46	6.54
.212	0.0435	1.908	95.47	4.53
.150	0.015	1.923	96.48	3.52
.075	0.021	1.944	97.48	2.52
Nil	0.046	1.990	100	0

a)

b)

Fig.1. Graph of sieve analysis (a) Sand and (b)Crushed Marble.

2.2. Lab scale filtration system set up

The Lab scale study required following facilities. The specifications of lab scale model are given at Table 3. & its photograph is given at Fig 3.

- A pressure filtration system
- A pump with necessary flow control
- Raw water tank for preparing, storing, and dosing water of desired turbidity.
- Multi port valve
- Water tank for supply of water for backwashing.
- Pump with necessary piping and controls for pumping backwash water through the filter.
- Pressure and differential pressure monitoring system.

Design Calculation

Given-   Dia. =0.25 m, Straight shell ht. =1.3, Assume Rate of filtration 10m/hr (m3/m2 .hr)

$$Q = V/A$$

As the dia. is given ,Area $A = \pi/4(d^2) = 0.049m2$

Flow calculation

Q=V.A =10m/hr ✕0.049m2 = 0.490 m3/hr =490 lt/hr

Media thickness

A minimum of 50% freeboard is required for a total straight shell height Straight shell height = media ht. ✕(1+

0.5)1.37m=media ht. ✕(1+0.5) = 0.91m

Quantity of media

Media Quantity =Layer thickness ✕ A = .90m✕0.049m2

Backwash flow rate

Assume backwash for 10 mins,Rate of backwash =5(Rate of filtration) =5(10m/hr) = 50m/hr
Quantity of water requirement during Backwash =Rate of filtration✕ area ✕Backwasing time

=2.45 m3 /hr ✕10 mins = 0.408m3

Table 3.Specification of lab scale model

Sr No.	Item Description	Design Specification
1	Type	Vertical pressure vessel with Manual Butterfly /MPV Valve
2	M.O.C	FRP
3	Size of Vessel	250 mm Dia. X 1370 mm Dia.
6	Flow Rate	0.490m3 /hr
7	Operating Pressure	2-2.5 kg/cm2

8	Filtration Velocity	10 m/hr(8 -16 m/hr)
9	Filtration Area	0.0490sq.m
10	Total bed Depth	900mm
11	Type of Filter Media	River sand with pebbles & gravels as supporting media
12	Depth of Fine Sand	700mm
13	Effective size of Fine Sand	0.36 mm
14	Bulk Density of Sand	1250-1550kg/m3
16	Quantity of Sand	49 Kg
18	Service Cycle	Whenever press. Drop across unit exceeds 0.8Kg/cm2
19	Backwash Duration	15-20mins
20	Back Wash Mode	Manual
21	Back Wash Velocity	50m/hr
22	Design Flow	10m3 /hr

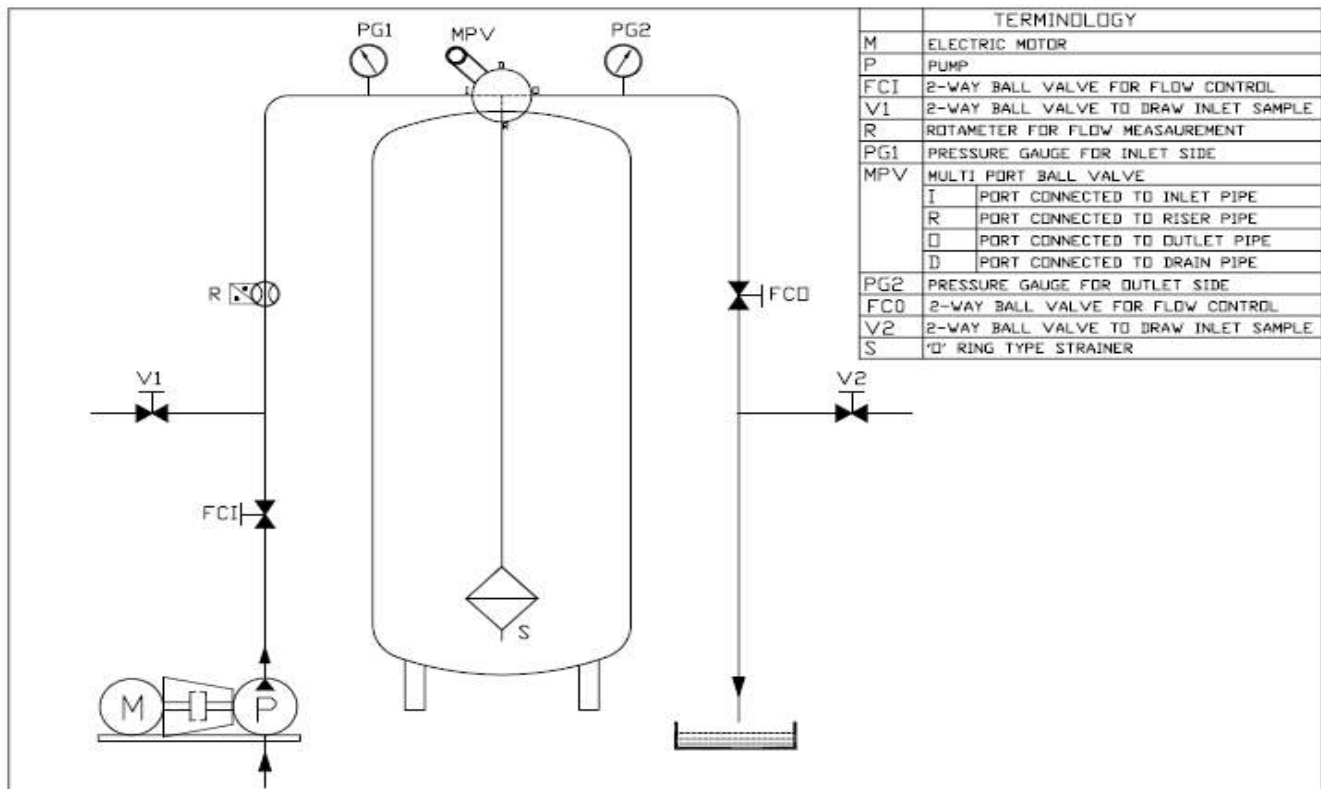|	TERMINOLOGY
M	ELECTRIC MOTOR
P	PUMP
FCI	2-WAY BALL VALVE FOR FLOW CONTROL
V1	2-WAY BALL VALVE TO DRAW INLET SAMPLE
R	ROTAMETER FOR FLOW MEASAUREMENT
PG1	PRESSURE GAUGE FOR INLET SIDE
MPV	MULTI PORT BALL VALVE
I	PORT CONNECTED TO INLET PIPE
R	PORT CONNECTED TO RISER PIPE
O	PORT CONNECTED TO OUTLET PIPE
D	PORT CONNECTED TO DRAIN PIPE
PG2	PRESSURE GAUGE FOR OUTLET SIDE
FCO	2-WAY BALL VALVE FOR FLOW CONTROL
V2	2-WAY BALL VALVE TO DRAW INLET SAMPLE
S	'O' RING TYPE STRAINER

Fig 3. Lab scale model of PSF

2.3. Pilot scale experimentation

To carry out experimentation firstly raw water was prepared.

- **Preparation of raw water:** A suspension was prepared by mixing bentonite clay with water a bucket. It was then added to the raw water tank and was allowed to be mix continuously for whole filter run using blowers, So as to maintain turbidity of 20-40 NTU.

- **Filtration run:** Set the MPV at filtration mode before starting pump, while keeping the tank contents completely mixed. The flow rate was set 490Lt/hr rate .To maintain the flow rate, by adjusting valves, the water was allowed to filter..Inlet and outlet samples were collected at regular intervals for filter monitoring. Also differential pressure at different points and overall pressure build up was also noted at regular intervals.

Backwashing of filter: When the pressure difference in inlet & outlet pressure gauges reached 0.8 Kg/cm^{2}filter was backwashed. Backwashing was done at the rate five times rate of filtration.MPV was set at backwash mode. Backwashing done for 15minutes.

3. Results and Discussions

3.1. Characteristics of the filter medium used

Characteristics filter medium used in pilot scale study obtained from sieve analysis is shown in Table 4.

Table 4.Showing D_{10}, D_{60} & value of uniformity coefficient for different media analysed

Media	D10(mm)	D60(mm)	D60/ D10
Sand	0.36	0.76	2.1
Crushed marble	0.70	1.4	2

3.2. Laboratory scale experimentation Analysis

Pressure filter with sand as media was run at 490Lt/hr rate on water with turbidity created through addition of bentonite clay, inlet turbidity was maintained at range 20-40 NTU. Filter run results obtained from such monitoring are given in Table 5. Results show that filter needs to be backwashed as the pressure difference in inlet &outlet pressure gauge is 0.8 Kg/cm2 backwashing was done at the rate of 50m/hr. Total time required for backwashing was found to 15to 20mins.Total amount of water required for backwashing was about 0.408m^3

Table 5.Filter run results for sand media

Sr. No.	Start time	Stop time	Duration (mins)	Pressure (Kg/cm²)		Turbidity (NTU)		
				Inlet	Outlet	Inlet	Outlet	Removal (%)
1	3 pm	3:30 pm	0	0.8	0.70	22.2	3.14	85.85
			15	0.80	0.75	21.5	0.61	97.16
			30	0.75	0.75	22.5	0.51	97.73
2	4:15 pm	4.45 pm	0	0.80	0.70	23.3	0.67	97.12
			15	0.85	0.80	22.5	0.66	97.06
			30	0.80	0.75	17.5	0.57	94.17

Table 6.Filter run results for crushed marble

Sr. No.	Start time	Stop time	Duration (mins)	Pressure (Kg/cm²)		Turbidity (NTU)		
				Inlet	Outlet	Inlet	Outlet	Removal (%)
1	3 pm	3:30 pm	0	0.5	0.45	23.2	3.35	85.5
			15	0.50	0.45	29.3	6.68	77.26
			30	0.50	0.45	24.5	6.67	72.7
2	4:15 pm	4.45 pm	0	0.5	0.45	2 5.2	6.6	75.5
			15	0.50	0.45	24.7	7.6	69.1
			30	0.50	0.45	28	8.81	68.5

Fig..4. Turbidity removal results

4. Conclusions

From the studies carried out following conclusions can be drawn

[A]Conclusions drawn from sieve analysis of media

1) Based on sieve analysis the effective size & Uniformity coefficient of sand and crushed marble were found to be 0.3 mm, 2mm &0.7 mm, 2.1mm.

2) Based on gradation analysis, the P_{usable} of crushed marble was found to be 50%.The sizes corresponding to $P_{toofine}$ & $P_{toocoarse}$ were 5% &55%.Hence by mechanical staining all the media particles less than 0.4 mm and greater then 1.1mm were removed.

3) A Total of 50 Kg crushed marble media was used in PSF & results were obtained.

[B]Conclusions drawn from lab runs on PSF

1) A lab scale study on PSF system was carried out for increasing flow rate without affecting efficiency based on the results given in Table 5& 6 it can be concluded that using sand media the efficiency is 80-97% & using crushed marble as media the efficiency is 60-80%.

2) Even after operating the PSF for 25 hrs the difference of inlet and outlet pressure is less than 0.8 Kg/cm^2.Hence it is concluded that the head loss development is less.

Acknowledgment

References

- Papers

1. R.sundarakumar ,2009. "Pilot scale study on floating media filtration for surface water treatment " Asian Institute of Technology School of environmental and Resources Development Bangkok, Thailand

2. Nidhi Tyagi ,2011. "Pilot scale study on pressure filtration system for evaluation of filtralite filter media" Thapar University

3. Derek Humenny,Dimtra panagiotoglou, 2010."Water filtration for developing Nations"

4. Chao-an chiu,Paul westerhoff and Amlan Ghosh, July 2012. "GAC removal of organic nitrogen and other DBP precursors", Journal of AWWA,volume 104,

5. Jonathana A. Brant,ismail koyuch,Helen lecoanet,srinivas veerapaneni,& mark wiesner , Dec 2011 ."Occurrence and composition of particulates in filter process streams",Journal AWWA,volume 103,pp34-37

- Websites

6. www.slideshare.net/imranlayyah/factors-affecting-of-filtration http://www.filtermedia.co.uk/installation.htm

7. en.wikipedia.org/wiki/Sand_filter

8. www.shubhamindia.com/pressure_sand_filter.html

9. www.watertreatmentequipments.net/pressure-filters.html

10. http://www.google.co.in/#hl=en&gs_rn=7&gs_ri=psy-ab&pq=pressure%20sand%20%20filter%20media%20typical%20properties

- Books

11. "Design of water treatment plant", by Dr. A.G. Bhole, Indian Water Works Association

12. "Wastewater Engineering Treatment and Reuse " by Metcalf & Eddy

13. "Water treatment manuals filtration" Published by the Environmental Protection Agency, Ireland.

Linear Dynamic Analysis of Modhera Monument

Rudra Upadhyay [a], Sandip Kapadiya [b]

[a]*Student of Civil Department, Gandhinagar Institute of Technology, Ahmedabad, 382721*
[b]*Assistant Professor in Civil Department,Gandhinagar Institute of Technology, Ahmedabad, 382721*

Abstract

Monuments are important part of our life. They represent our history and Culture. They have been standing over thousand years and faced many earthquakes yet very less damage has been occurred. The paper describes seismic assessment of Modhera sun temple. The 3D modelling and analysis is done by using F.E.M. based Sap2000V15 software to study seismic behaviour of ancient structures. Purpose of this project is to analyze the static and dynamic properties of ancient Indian monuments. The model was used to do linear static and linear dynamic analysis. For static analysis base of the temple is most in danger part while according to dynamic analysis dome of temple is susceptible.

Keywords: Modhera Suntemple, Time History, Linear Static Analysis, El Centro, Monument, Seismic Analysis

1. Introduction

Monuments have been standing over thousand years representing our history and culture. India is one of the oldest country and many monuments are present in its soil. Majority of the monuments are located on seismically active region of intensity 2 and 3 for example north and west region of Indian Continent. Amongst them Gujarat has many important monuments which played important part in Indian history. The monument here chosen for study is Modhera sun temple which was constructed in 1026 A.D. It is situated in Mahesana district under seismic zone IV. It is oldest monument in Gujarat state. There are three parts of this sun temple Ramakunda, Nritya Mandapa and Sun temple. It has faced many historical earthquake events. 52% of the structure was damaged in the various foreign invasions but it was restored by Gujarat government in 1972 but the new restored part was damaged during the 2001 Bhuj Earthquake where as old construction remained safe. Aim of this work is to do comparative study of seismic behavior for normal structure and monument and hence for that, here sun temple has been taken as the monument. Linear Static analysis has been performed on the model of monument and base shear at the bottom of the temple has been studied as well as Characteristics of El Centro time history are applied to the Sun Temple and its effect on monument is evaluated by time history method.

2. Modeling

The model of Modhera sun temple is been prepared in the F.E.M. base software Sap2000V15. Model is prepared as fix base model. To reduce the complexity in the analysis elements are assumed perfectly bonded. For creating 3D model of Modhera sun temple solid block components have been taken and properties of sandstone material are assigned to them. Solid Cubes creates hinge joint by being connected through edge points of one another. Model is been prepared using structural data provided by governmental department. Due to carving columns are in hexagonal shape but to avoid complexity in modeling, columns are taken as square element. Various carving is ignored to avoid the complexity. Table 1 shows the important dimensions of Temple. A near-real numerical model has been built to accurately reproduce the geometry of the structure complex, focusing on the variations in the dimensions at various openings, wall thickness and structural irregularities.

Table1. Model Dimensions

Element	Dimension
Plinth	1.020 m
Length	22.4 m
Width	12.7 m
No. of Columns	32
Height	8.8 m
Height of dome	1.5 m
Seal level	2.78 m
Dimension of Column	0.82 m X 0.82 m

2.2 Material Modelling

A crucial task in masonry building modeling is the evaluation of the mechanical properties. In the absence of the actual experimental material properties, based on the material elastic properties used by researchers available in literature material properties are assigned. Material used in Modhera sun temple is sandstone found near Kadi, Mahesana district and various properties of the sandstone is enlisted as below

Table2. Material Characteristics of Indian Sandstone [10]

Term	Value
Modulus of Elasticity	9700Mpa
Poisson's Ratio	0.3
Self Weight	21.57 kN/m^3
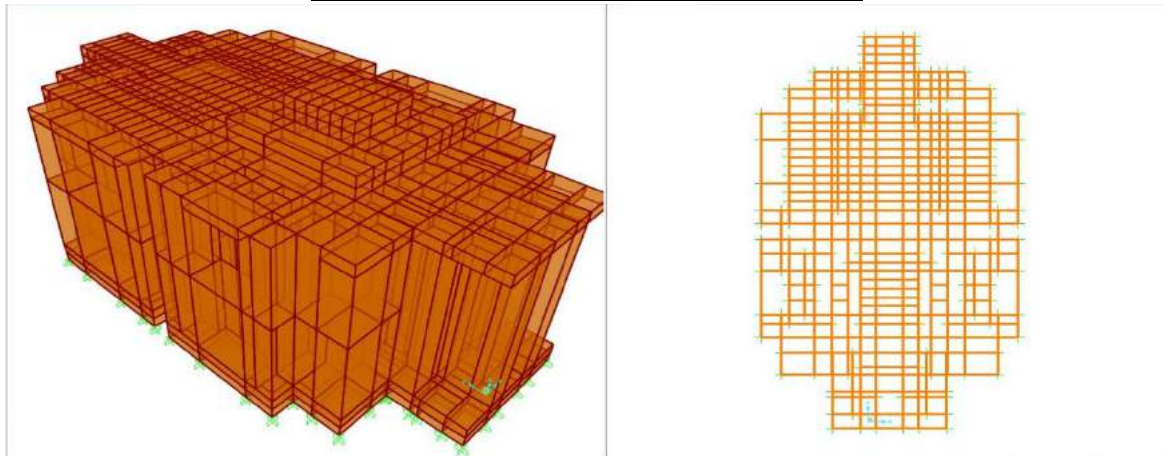
Fig3. 3D model of Modhera Sun Temple in Sap2000V15

3. Dynamic Analysis

To determine effect of earthquake on monument seismic study has been carried out. The main parameter here considered is the effect of El-Centro time-history on the dome and openings in Modhera sun temple. Three types of analysis Linear Static, Modal Analysis and Time-History are carried out and based on output, variance in time period and frequency with the change in different modes are studied as well as graphs are prepared of deflection v/s time-period and pseudo-acceleration v/s time-period.

4. Results and Discussion

4.1 Linear Static Analysis

The static structural behaviour of the masonry monumental structure has been analysed under constant vertical loads deriving from the own weight. Linear elastic material behaviour is used in the analyses. The overall structure has been analysed in the linear elastic range. To study the inertia force generated on the foundation of Modhera Sun Temple considering all the factors as mentioned in IS 1893:2002 base shear was calculated. Table 3 shows the Base shear values of Temple. The base shear value is considerably very high in compare to normal residential structure of same dimension. The reason of high base shear is due less time period, high Importance factor, high zone factor as well as high self weight.

Table 3. Base Shear Values of Sun Temple

Force in X Direction	Force in Y Direction	Force in Z Direction	Moment in X Direction	Moment in Y direction	Moment in Z direction
5139.753 kN	4086.583 kN	2359.744 kN	18781.6071 kN-m	28952.20 kN-m	58331.72 kN-m

4.2 Time-History Analysis

To study the behavior of monument under the earthquake, el-Centro time-history is applied to the monument and final deflection, development of stresses and behavior of structure is studied. These parameters are studied on dome and on openings as they are most vulnerable in shear loading. After the application of the time-history, based on the output, stress distribution diagram was plotted in which it can be seen that stress distribution on whole model is almost equal except dome portion so further parametric study was carried out on dome. It can be seen that maximum pseudo acceleration on the dome was almost equal to 0.3g where as maximum deflection was almost 0.6mm. Reason of such earthquake resistant behavior of monument is due to well defined joint of columns with the slab, high number of columns to transfer load to the ground as well as the lower stiffness of structure which makes structure flexible and leads to less deflection but high frequency. In monument no adhesive or mortar is provided to join two sandstones, instead of mortar, similar to curved shape butt joint is provided and wooden stick of sag tree is used as joint as shown in fig 7. In addition Connections between main columns are shown in Fig 8.
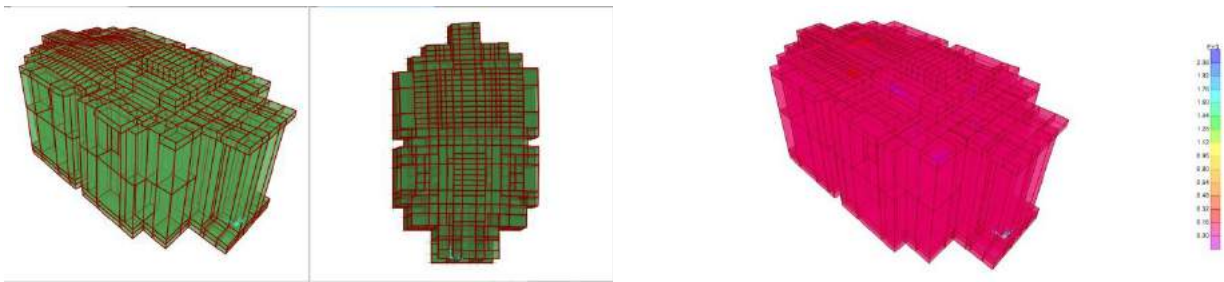
Fig4. Deformed Shape and Stress Distribution Diagram of Modhera Sun Temple under El Centro Earthquake
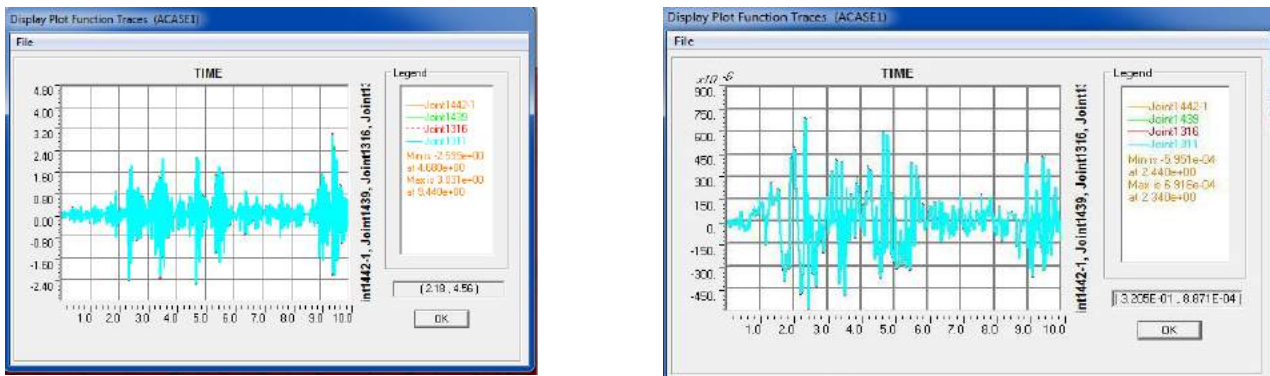
Fig5. Time History curve for Absolute Deflection and Pseudo Acceleration in respect to time for dome of Modhera Sun Temple
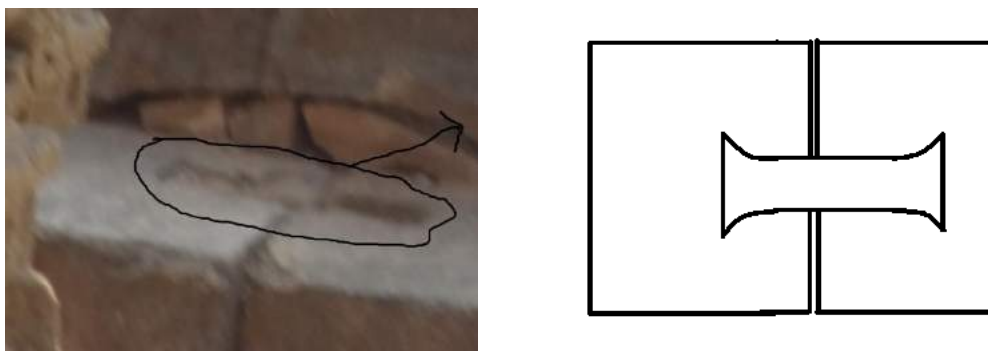
Fig 6. Uses of wooden sticks as butt joints in sandstone material

5. Conclusion

The paper approaches the assessment of the static and dynamic behaviour of a monumental structure 'Modhera Sun Temple' through a finite element methodology. A numerical model has been used to evaluate the static behaviour of the masonry complex under gravity and live loads. For that purpose different mode shapes are derived and time history analysis has been carried out. Time History of El Centro earthquake was applied to the monument. The static analysis shows that, in general, the structural configuration of the monument is adequate to withstand vertical loads. The result shows high Pseudo acceleration around 0.3g due to monument's flexible behaviour but deflection is almost 0.6mm. This earthquake resistant behaviour is caused by well defined butt joints between main structural components, less spacing between columns to convert seismic loadings into vertical loading.

References

[1]. R.N.Dubey, Shashi Thakkar, Akash Gupta, Seismic Analysis Of The   Safety evaluation of the Taj Mahal,11th world conference of Earthquake Engineering

[2]. Jag MohanHumar, Dynamic Analysis of Buildings for Earthquake   Resistant Design

[3]. Anil K Chopra, Dynamics of the Structure, ISBN 978-81-317-1329

[4]. Mario Paz, Structural Dynamics, ISBN 81-239-09-78-0

[5]. Report on 1985 Mexico City Earthquake from "EQ Facts & Lists: Large Historical Earthquakes", USGS.

[6]. Newark, N. M., and Hall, W. J. 1982. "Earthquake Spectra and Design," Engineering Monographs on Earthquake Criteria, Structural Design, and Strong Motion Records, Vol 3, Earthquake Engineering Research Institute, Oakland, CA.

[7]. Lin, Rong-Gong; Allen, Sam (26 February 2011). "New Zealand quake raises questions about L.A.buildings". *Los Angeles Times* (Tribune). Retrieved 27 February 2011.

[8]. Structural Details from Archeological Survey of India

[9]. Dr. K.R. Arora, Soil Mechanics and Foundation Engineering, ISBN 81- 8014-112-8

[10]. R.G.Flesch, Earthquake Resistant Design Of High Rise Building

[11]. Vladimir Smirnov, Seismic Isolation of the Buildings and Historical Monuments

[12]. N.Torunblanci, Evolution Of Earthquake Resistant building for low rise isolated base

Gandhinagar Institute of Technology

| Home | Trustee | Editorial Board | Director Message | Papers | Contact Us |

Others

Sr.No	Paper Title	Author Name	Institute Detail	Author E-Mail Id	Co-Authors Name
1	Design and Comparison of Quaternary Logic Blocks	Prof.Ashish B Pandya	Gandhinagar Institute of Technology, Gandhinagar	ashish.pandya@git.org.in	Prof.Jatin Chakravarti Prof.Pratik J Gohel
2	A Phase determination for ICRH Transmission Line on Aditya/SST-1 using Least Square Technique	Mrs.Ila Rahul Vaghela	Gandhinagar Institute of Technology, Gandhinagar	ila.vaghela@git.org.in	Prof.Rahul Vaghela
3	A Comparison of MAC Strategies for Cognitive Radio Networks	Mr.Smit B Tripathi	G H Patel College of Engg. And Technology; VV Nagar	smittripathi007@gmail.com	Prof.Mehul B Shah Prof.Hardik H Bhatt
4	Effect of Solar Outbursts on X-ray Astronomical Objects	Prof.Nirav Pandya	Gandhinagar Institute of Technology, Gandhinagar	nirav.pandya@git.org.in	
5	Growing Demand of English Communication Competence for Engineering Students to Keep up with Employability	Prof.Nirupama Patel	Gandhinagar Institute of Technology, Gandhinagar	nirupama.patel@git.org.in	
6	Snap log based Monitoring and Controlling System for 3-Phase Induction Motor Drive	Prof.Sanjay K Patel	Gandhinagar Institute of Technology, Gandhinagar	sanjay.patel@git.org.in	Dr.Vinod John
7	Cross sections for Electron Scattering with C6H6 and C6F6 – A Theoretical investigation	Prof.Umang Patel	Gandhinagar Institute of Technology, Gandhinagar	umangpatel193@yahoo.ca	Dr.K N Joshipura

Effect of Solar Outbursts on X-ray Astronomical Objects

Prof. Nirav Y Pandya

Gandhinagar Institute of Technology, Moti Bhoyan, Khatraj-Kalol road, Gandhinagar-382721, India

Abstract

The sun is a massive object comprised of intensely hot, ionized gases. We know usually that various phenomena take place in Sun's atmosphere due to its activity. Solar activity follows the 11 year magnetic activity cycle in which number of sunspots (dark region on sun's surface) changes on the basis of activity cycle. During this solar activity, solar outbursts mean Solar flares, CME (Coronal Mass Ejection), Solar wind and highly accelerated particles coming out from the Sun's atmosphere. During the Solar flare, high speed electrons hurled out into planetary space where they affect satellites, earth's atmosphere and various astronomical objects. Solar flares are always located near sunspot and occur more often when sunspots are most numerous. The aim of my work is mainly to understand that among these outbursts, "How Solar flares affect the X-ray astronomical objects?" It is necessary to study such effects observe in the universe because if there exists very faint sources compared to the background surrounding X-ray sources, X-ray astronomical satellite cannot detect this type of faint sources and it can be go for false prediction about that sources. By studying about other solar outbursts: CME and Solar wind; we can predict about their effect on satellite and other astronomical objects and also protect them from the damage.

1. Introduction

We know that various phenomena take place in the sun's atmosphere due to its activity. Solar flare is one such violent phenomenon. During the solar flare, high speed electrons hurled out into planetary space where they affect satellites, earth's atmosphere and various astronomical objects. [1] The aim of my research work is to understand how the solar outbursts affect the X-ray astronomical objects?

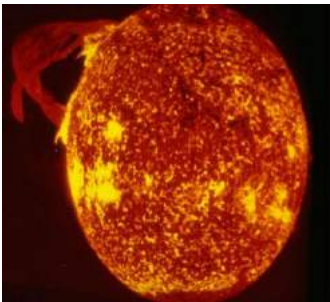## 2. Solar flare: A brief explosion in the Sun

Fig. 1.Sun with a solar flare [2]

Fig. 2. After a solar flare [9]

2.1. What is a solar flare?

A solar flare is defined as a sudden and brief explosion from the active region on the sun's surface with the energy equivalent to 2.5million terrestrial nuclear bombs, each with a destructive force of 100 megatons (10^{11} kg) of TNT (trinitrotoluene). A solar flare occurs when the magnetic energy that has built up in the solar atmosphere is suddenly released. Radiation is emitted across virtually the entire electromagnetic spectrum from radio waves at higher wavelength end to the x-ray and the gamma rays at the shorter wavelength. [1]

2.2. X- ray solar flare

Since solar flares are very hot, they emit the bulk of their energy at x-ray wavelengths. For a short while large flare can outshine the entire sun in x-rays. Here an image of Sun in soft x-rays is shown in Fig.2. The white (brightest) region on the right hand side shows post-flare. loops, hot loops that remain after a solar flare. Image is taken from the Yohkoh Soft X-ray Telescope, from NASA's Observatories.

Solar flare can be characterized by their brightness in X-rays as observed by monitoring satellites near the earth. The biggest flares are X-class flare which has the flux of 10^{-4} and above. M-class flares have one tenth the X-ray flux of an x-class one and the c-class has one hundredth of the x-class flux. [1]

2.3 Effect of solar flares in the space

During the sudden and brief outbursts protons and electrons can be accelerated to nearly the speed of light. The high speed electrons and protons are also hurled out into interplanetary space where they can threaten astronauts and satellites. During the solar flare, the phenomenon of coronal mass ejection takes place which also affect the interplanetary space and earth's atmosphere. The intense radiation from a solar flare travels to earth in eight minutes. As a result:

● The earth's upper atmosphere becomes more ionized and expands.
● Long distance radio signals can be disrupted by the resulting change in the ionosphere.
● A satellite orbit around the earth can be disturbed by the enhanced drag on the satellite from the expanded atmosphere.
● Satellite's electronic component can be damaged.

3. Preface of X-ray Astronomy

Normal x-rays are part of the electromagnetic spectrum whereas astronomical x-ray is usually imaged in a different way from normal x-rays. In astronomy we image the source of x-ray itself. The X-ray astronomical object has million degree K temperature and X-rays are emit from the hot object. So study of the astronomy at x-ray wavelength can give us more information about astronomical object. So X-ray astronomy was started. Today the study of x-ray astronomy to be carried out using data from a host of satellites past and present, the HEAO series, EXOSAT, Ginga, CGRO,RXTE, ROSAT, ASCA. On 20th July 1999, the CHANDRA observatory launched by NASA and on December 10, 1999 the European x-ray satellite XMM (x-ray multi mirror mission) NEWTON was launched for x-ray observation. [3]

The Sun, Stars, Comets, X-ray Binaries, Supernova Remnants, Quasars and Active Galactic Nuclei are most interesting X-ray sources. Roentgen used photographic plates to detect x-rays for his experiment. Now astronomers use more modern methods of detection. Today CCD (CHARGE COUPLED DEVICE) is used as x-ray detector. A CCD is an image sensor, consisting of an integrated circuit containing an array of linked or coupled, light sensitive capacitors. [3]

We know that x-rays are absorbed by earth's atmosphere and due to this reason the satellites are better option for the detection of x-ray sources which can lift the payload above the earth's upper atmosphere. So that for the purpose of X-ray astronomy, the Chandra x-ray observatory in honour of Subramanian Chandrasekhar; XMM (X-ray Multi Mirror) Newton Observatory and also few new mission (ASTRO E2 "SUZAKU") were launched. [3]

4. X-ray flux solar flare data from GOES

The Space Environmental Centre of the National oceanic and atmospheric administration, or NOAA provides the peak soft x-ray flux for solar flares seen from their Geostationary operational environmental satellites or GOES for short. The satellite hovers above the points in the earth's western hemisphere, orbiting at the same rate that that earth spins. I have taken the soft x-ray flux data for solar flare from GOES Space Environmental monitor. There are various GOES satellite provides the data of the x-ray flux for the solar flare. [4]

GOES-5 (Jan 1, 1986-Mar 31, 1987)
GOES -6(Jan 1, 1986-nov 30, 1984)
GOES-7 (Mar 1, 1995-June 30, 2003)
GOES-8 (Mar 1, 1995-June 30, 2003)
GOES-9 (Apr 1, 1996-Aug 31, 1998)

GOES-10(Jul 1, 1998-Apr30, 2007)
GOES-11 (Aug 1, 2000-Apr 30, 2007)
GOES-12 (Jan 1, 2003-Apr 30, 2007)

Here I have taken the data of the solar x-ray flux from 2000 to 2006 using the GOES-10 satellite. Here I want to find out the date and time on which the highest X-ray flux solar flare had occurred. For it, I have taken the curve of the solar x-ray flux in w/m^2 versus UT (universal time) for the duration of the every five days and collect the data for the time and flux for the different x-ray flares. In this data I have found large number of M-class solar flare and few numbers of the highest x-ray solar flare i.e. X-class solar flare. Here I got approximately hundred X-class solar flares in which the highest solar flare occurred on 28 October, 2003 at 11:00 UT with the highest X-ray flux of 0.0025 W/m^2. This solar flare had great effect on the solar system. The image of highest X-ray flux solar flare occurs on 28th October 2003 is shown in Fig.4. [5]
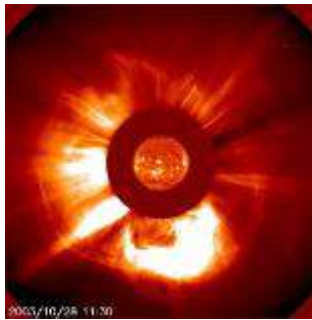
Fig.3 Image of highest X-ray Solar flare [5]
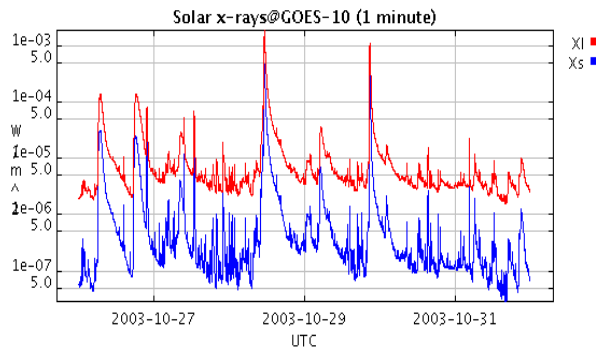
Fig. 4. XL 1-8 Ang X-ray flux (watt/m^2)
XS 0.5-3 Ang X-ray flux (watt/ m^2)

The curve of X-ray flux versus UTC for this highest X-ray solar flare is shown in above fig.4. Here we can see that the first and third highest flux solar flare occur within a week. The first highest and third highest solar flare occurs on 28 October, 2003 a11:00 UT and 29th October, 2003 at 22:00 UT. Due to these two highest X-ray flux solar flares, tremendous effect is observed on the earth's atmosphere, which we will see later in result.

5. XMM Newton data preparation

The basic reduction of XMM-Newton data is provided by the SAS software package produced by the XMM- Newton Survey Science Centre (SSC). The SAS provides tasks to produced calibrated photon event files from the observation data format (ODF) files supplied to the user as well as some basic analysis tools. These include data filtering and extraction, production of rmfs and arfs for spectral analysis, and source detection routines. The SAS was not designed for high level scientific analysis such as spectral fitting and temporal analysis. However, the SAS product files are designed to OGIP standards, so theoretically any higher energy is capable of processing XMM-Newton data. [6] For example,

o HEASoft from the High Energy Astrophysics Science Archive Research Centre (HEASARC)
o CIAO from the Chandra X-ray observatory centre (CXC)

These both can be used for XMM-Newton data analysis. The high energy astrophysics science archive research centre (HEASARC) is the primary archive for high-energy astronomy missions, in the extreme ultraviolet, X-ray and gamma-ray wavelengths. The HEASARC provides archival data, multi mission software and analysis tools, and information about current and past observatory missions. We can download XMM-Newton data on a CD-ROM or from the public archive at VILSPA or also from HEASARC. HEASARC provides the data for all the observatories, data analysis tools etc. [7]

I have downloaded XMM-Newton data for randomly selection of 15 highest X-class solar flare. For ex: Highest solar flare occurs on 28 October, 2003 so I have downloaded XMM-Newton data for the duration of one day before to six days after means from 27 october,2003 to 03 November,2003. There are various types of data available in HEASARC browse archive for the XMM-Newton data. Among them I have taken it from XMM master (XMM master log and public archive).

Once if we got our XMM observation data, we can choose it between the observation data file (ODF) and the already processed product files created by an automatic pipeline. The advantage of the pipeline products is that you do not have to create the event files etc. yourself on your machine, which sometimes takes several hours and you can start immediately working with the scientifically data. The ODF data contains all of the observation specific data necessary for reprocessing

the observation. The pipeline data contain among other things calibrated photon event files, source lists and images. Here I have used only pipeline product data. [8]

6. XMM Newton data analysis

6.1 Examine and filter an Epic data

The EPIC event lists in the EEVLIS group of the Pipeline Processing will have names of the form:

`PiiiiiijjkkaaSlllcIEVLI0000.FTZ`, where

`iiiiiijjkk` - observation number
`aa` - detector (`M1` - MOS1, `M2` - MOS2, `PN` - PN)
`lll` - exposure number within the observation
`c` - detector (`M` - MOS1 or MOS2, `P` - PN, `T` - Timing Mode)

The following sections describe the use of SAS tasks using the both the command-line and GUI interfaces, except in cases where one of the methods is particularly easy. The SAS GUI provides a very simple method for producing and displaying images, spectra, and light curves, and is the recommended method for extracting data unless large numbers of sources are being analyzed. [8]

6.2 Initialize SAS and prepare the data

(1) Gunzip the PP event list to be examined (not really necessary) and for practical purposes shorten the file name as well, e.g.:
`mv P0123700101M1S001MIEVLI0000.FTZ mos1.fits.gz`
`gunzip mos1.fits.gz`
(2) For initializing SAS GUI sasinit
(3) Invoke the sas GUI (in below fig.)
(4) Invoke the xmmselect GUI from the SAS GUI; double click on the task name.

When xmmselect is invoked, a dialog box will first appear which request for a file name. Then select "event files" and extension for it. The directory GUI will then disappear and then click "RUN" on the selection GUI. After the filename has been submitted, the xmmselect GUI will appear along with a dialog box offering to display the selection expression which includes the filtering done to the specific point on the event file. [8]
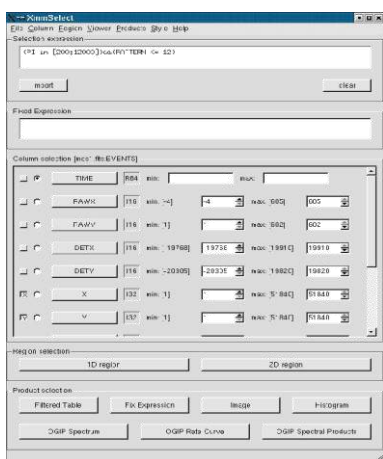
6.3 Create and Display an image
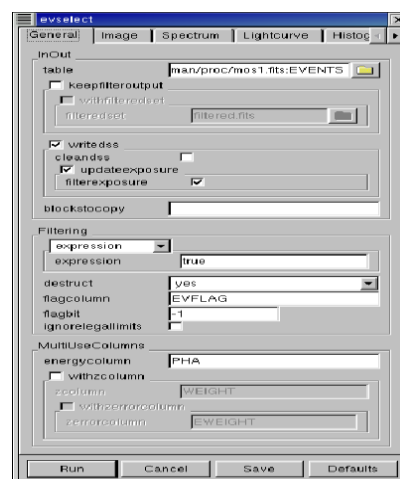

Fig.5.(a) Create and Display an image   Fig. 5. (b) Create and Display an image

- To create an image of the data in sky coordinates, check the square boxes to the left of the ``X'' and ``Y'' entries.
- Click on the ``Image'' button near the bottom of the page. This brings up the evselect GUI.
- The default settings are reasonable for a basic image so click on the ``Run'' button at the lower left corner of the evselect GUI. Different bindings and other selections can be invoked by accessing the ``Image'' tab at the top of the GUI.
- The resultant image is written to the file `image.ds`, and the image is automatically displayed using ds9.
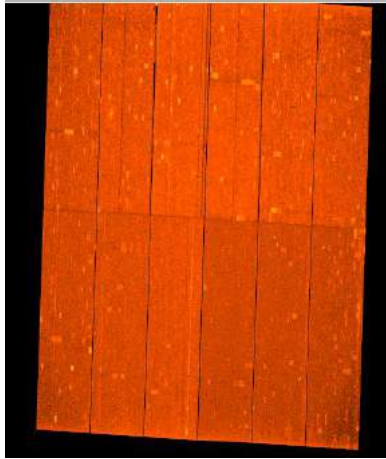
Fig. 6. (a) Image of a X-ray astronomical object
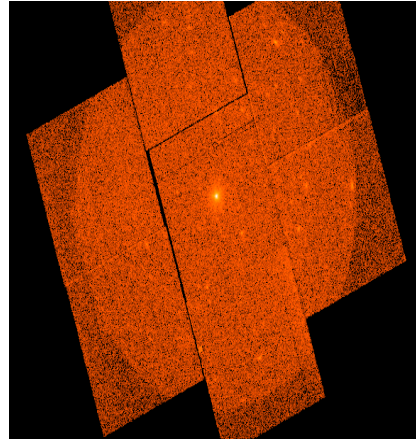
Fig. 6. (b) Image of a X-ray astronomical object

Two different images for EPIC MOS1 and in EPIC PN are shown in above fig. the right side fig. is for EPIC MOS with seven CCD and left side is for EPIC PN with 12 CCD.

6.4 Create and Display a light curve

- To create a light curve check the round box to the left of the ``Time'' entry.
- Click on the ``OGIP Rate Curve'' button near the bottom of the page. This brings up the evselect GUI.
- The default setting is for a one-second bin which is a bit fine, so access the ``Light curve'' tab and change the ``timebinsize'' to, e.g., 100 (100 s). Click on the ``Run'' button at the lower left corner of the evselect GUI.
- The resultant light curve is written to the file rates.ds, and is displayed automatically using Grace.
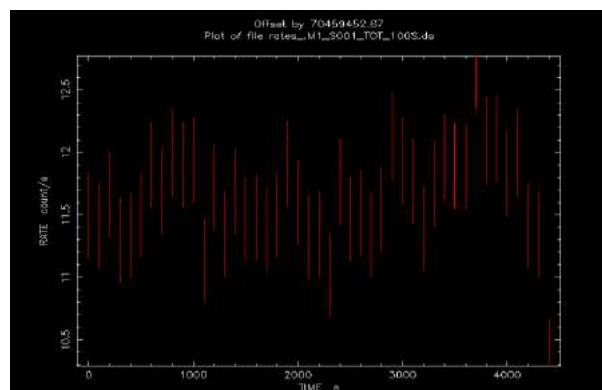

Fig. 7.Total light curve with X-ray source

Above fig. shows the total light curve with the X-ray source for MOS1 which indicates that count rate for peak flare is 12.8 c/s on time 3700s for 100s background light curve.

6.5 Filter the Data and Create a New Event File

Filter the data using the xmmselect GUI. Here purpose of filtering is to get the background image of the MOS1 data and light curve for this background images. For it, in the image source and we want to extract the sources and we want to keep only the background area of the image.

For it, we select the each region belong to the xmmselect and then click 2D region. Doing in this way we can get the selection expression for the selected source region and then to extract it, we put "!" sign before it. So we can get only background region in the images. Then click on IMAGE and giving particular name for the background image. Thus we obtain background image. Two different background images for EPIC MOS and EPIC PN are shown as below.
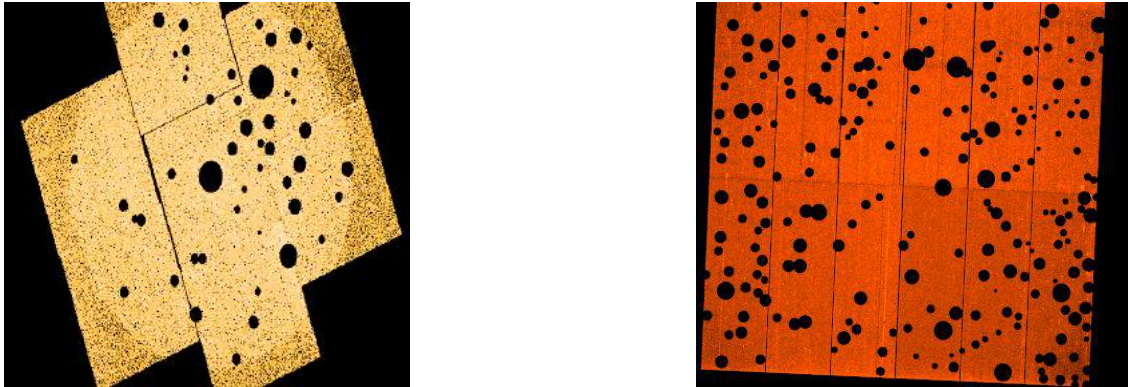
Fig. 8. Images of background of X-ray Astronomical Objects

6.6 Create and display a Background light curve

Here we got the selection expression for the background region of the images. Now select OGIP rate curve in xmmselect and then give particular name to it and get the background light curve for the particular time. The background light curve for this type of selection expression in which the x-ray source region is extracted is shown in above fig. 8.
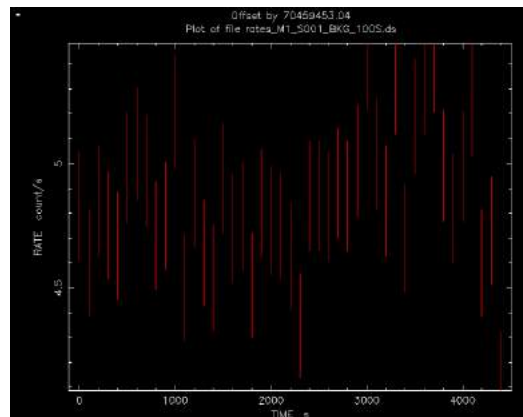

Fig. 9. Average background count rate for 100s light curve

Here I have used the command 'fplot', 'mo.' (model), 'co.'(constant) and then fit it for finding out the average background count rate for base level of each 100s light curve. Then I have plotted the graph of avg. background count rate versus the range of the X-ray flux for selected flare. From it I have got important result which is shown below.

7. Results

● There are two important plots, which are shown below, describe the important result of my work. The second plot is main result of my research work which is for the combined observation of both MOS1 and MOS2. It is the graph for background count rate versus flux of the selected X-ray flare. Here we can clearly see that as the flux increases the background also increases. It is not very clear result but we can see that background increases with the flux of X-ray solar flare.

● Now in the below fig 10, the background light curve for the duration of the highest X-ray solar flare which clearly indicates that the background clearly increases after the highest X-ray flux solar flare. Thus we can see that the emission of the outbursts during the solar flare, increase the background of any X-ray astronomical objects (Stars, Comets, X-ray Binaries etc.).
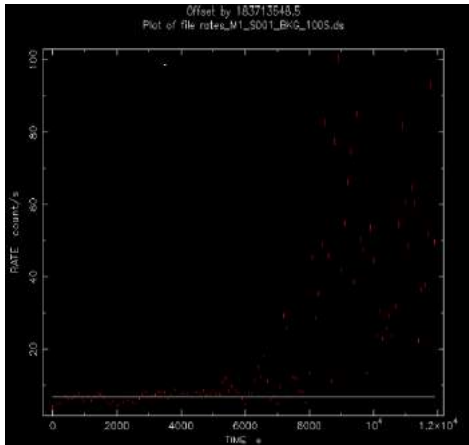

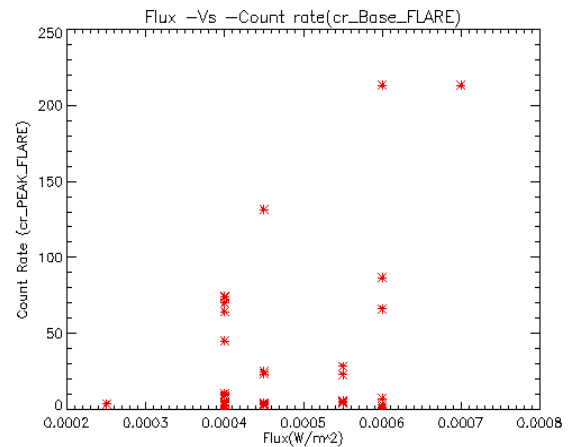Fig.10   Light Curve for highest X-ray Solar flare   Fig.11. Plot of background count rate versus x-ray flux

● I have observed one interesting effect of solar flares on the XMM-Newton satellite. Before the highest X-ray flux solar flare took place on 28th October 2003, the XMM-Newton was working properly and providing the data of X-ray solar flares. But after it, I was not able to get my X-ray solar flares data because it has stopped to work and again it has started to work on 9th November, 2003. Thus I observed the tremendous effect of solar outbursts on XMM Newton satellite.

8. Conclusion

   From this work on the topic of "Effect of solar Outbursts on x-ray astronomical objects," finally I conclude that due to the outbursts coming out during the solar flares, the background of x-ray astronomical objects increase and it also major affect the satellites.

   It is necessary to study such increase in the background of x-ray astronomical objects because if there exists very faint sources compared to the background surrounding them, the x-ray astronomy satellite can't detect this type of sources and it can be go for false prediction about those sources. By studying about other solar outbursts: CME and Solar wind; we can predict about their effect on satellite and other astronomical objects and also protect them from the damage.

   Here I have taken the XMM-Newton data for sparsely selected highest X-class solar flare. If we take XMM-Newton data for all the X-class Solar flares, we can study the effect of solar flare on the background of the X-ray astronomical object more completely. I have studied the background light curve only for the 100s duration in this work. If we study the background light curve for 1s duration, then we can understand the effect of the solar flare on the temporal studies of the X-ray astronomical objects more precisely. Similarly if we include the spectral analysis method, we can get more important information about the effect of solar flare on the X-ray Spectral studies of the X-ray astronomical objects.

References

[1] K. R. Lang: The Cambridge encyclopaedia of the sun

[2] http://carliniinstitute.com

[3] E. M. Schlegel, The restless universe: understanding X-ray astronomy in the age of Chandra and Newton, Oxford University

[4] GOES data archive: http://goes.ngdc.noaa.gov

[5] http://web.mit.edu

[6] XMM –Newton data cookbook: http://wave.xray.mpe.mpg.de/xmm/cookbook

[7] HEASARC browses archive: http://heasarc.nasa.gov/W3Browse

[8] XMM-Newton ABC Guide: http://heasarc.gsfc.nasa.gov/docs/xmm/abc/abc.html

[9] http://qrg.nothwestern.edu

Growing Demand of English Communication Competence for Engineering Students to Keep up with Employability

Prof. Nirupama Patel

Gandhinagar Institute of Technology, Khatraj-Kalol Road. Moti Bhoyan,Gandhinagar-382721,India

Abstract

As globalization and competitiveness become the benchmark of any MNC, it becomes obviously important for employees to be equipped with good communication and soft skills. Therefore engineering graduates require an ever increasing range of skills to maintain relevance with the global environment of the era. Increasing pressures and challenges arising from the broadening roles of engineers has enhanced the need for the Indian engineers to acquire good English communication skills. Good English Communication Skills is a vital element of an engineer's profession and the lack of such skills only undermines the image of an engineer. There is a great need to frame course material and develop methods and strategies to enhance various skills of communication of engineering graduates. This paper reviews the importance of these skills for engineers with an emphasis on how such communication courses can be designed and incorporated into the engineering curriculum. The different methods of teaching communication skills and its assessment are discussed in the paper for enhancing communication of technical students.

Keywords: Globlization; Competitiveness; Curriculum.

1. Need of English Communication Skills

There is a clear necessity for effective English communication skills for engineers in the current globalised environment. A course in English for Specific Purposes (ESP) will enhance English language training and an engineering student's communication skills. It will also aid in the globalisation of education and the internationalization of practicing engineers. The English language has become a major medium for communication across borders globally; a deficiency in this area may result in barriers for graduates' professional development. ESP focuses the learner's attention on the language and communication requirements in a particular professional field. The concept of ESP achieves more in the education of engineering students by focusing the learner's attention on the particular terminology and communication skills required in the professional field.. Teaching English to engineers is a delicate and demanding matter in terms of content, methods and techniques, and deciding which are appropriate for this particular area of engineering and English. That is, the aim in such an interdisciplinary course is to develop and master relevant communication and professional skills, using English as a means and a kind of mediator in shaping future engineers. To achieve this goal, ESP teachers have to plan the course they teach and provide the materials for it.

Engineering communication skills basically constitute several core elements such as the fluency in English language and the fundamentals of visual communication. Evidence indicates that communication skills have helped humankind develop into the advanced societies. However, these skills have become stifled in the very discipline that has brought so many advancements, and that is engineering. There is ample evidence that graduate engineers lack the required standard of communication skills, particularly when compared to the needs of industry internationally. To be successful in any field one need to know and understand how to communicate effectively. Communication is the most important function a human being performs in his/her life .Communication like birth, death growth and decay is a part of individual life as well as organizational existence. Its importance is self-explanatory and is an experience of all as well. Communication skill is essential for an Engineer who aspire to carry out his professional practice in the global arena.

Engineering is the biggest field of study in the world. First of all English is a tool that significantly affect engineering students in academic life. While most of the theories in engineering are taught in English, it requires to have good English communication competence. In academic life ,engineering students have to deal with the countless English lectures, tutorials, labs, project reports and papers. most engineering professors in various universities are also conducting lectures in English. The most convenient source of information i.e. Internet provides most of the information in English.

During the job seeking process in interviews, GD's, it is but of crucial importance to achieve mastery in English proficiency. After securing the job they are required to work in groups since their task seldom be solved by an individual. So, being an engineer requires to co-operate and communicate with different people from different part of the world.

English is used as the working language on large extent. In order to co-ordinate with the colleagues, engineers have to speak fluent English. So, English communication competence plays an important role in the academic life and career of engineering students

The lack of communication skills only serves to undermine the whole profile of the professional engineer. Globalization directly influences industry's needs; a global engineer must be able to easily cross national and cultural boundaries. This in turn directly affects engineering education. A common code for communication is required. Those education institutions, which meet the language requirements for the new global engineer, will be ready to face the new millennium. Sakran and Awad emphasizes the need for engineers to be able to integrate technical expertise with behavioral and societal issues, to work on solving complex problems in teams composed of professionals from many disciplines and exhibit high level communication skills[1].

H.P. Jensen states that employers want: *a number of new competencies, with an emphasis on an increased ability to communicate…and good foreign language skills* [2]. This is also reinforced in N. Grunewald's study of competencies required by the *engineer of tomorrow*, which includes hard skills like good foreign language skills. He goes further to claim that cross-disciplinary language skills are not sufficiently taught [3]. This indicates a lack of a direct fit between graduate skills and those required by industry. Engineers can relate the same theories of mathematics, of mechanics and technology, but the modern engineer must also be able to communicate effectively in a shared tongue.

Neglecting the learning opportunities in communication skills at the university level can lead to a shallow level of understanding in the engineer, if he or she does not see the relevance and application of these skills in engineering profession. These skills should be acquired within the four years of an engineering education at the university. As discussed on how best to teach these skills or conversely how students can most effectively learn these skills, a *situative approach* of teaching has proven to be successful in enticing the engineering students to participate and contribute in lectures. The *situative approach* emphasizes that the educational process be linked directly to real life situations in context. Bringing real world practices into the engineering curriculum through such English communication programmes will expose the engineering students to have a broader vision.

The incorporation of communication skills courses in English for engineers at the universities is becoming an essential element of continuous learning.. The aim has been to develop good English communication skills abilities in its engineers. The goal of developing communicatively competent users of English, , can be realized effectively if elementary schools, junior high and senior high schools and universities take the initiative in improving the educational system in respect of English education from their respective positions. The incorporation of language and communication improvement courses is an important element of continuous learning, and will ultimately contribute to the process of life-long learning. This should in turn facilitate advancements in engineering and, indeed, engineering education through streamlining fundamental communication skills.

2. Remedies

Knowing the importance and growing demand of English communication competence for engineering students, there is a need for the teachers as well the students to make integrated efforts.

2.1. Provide more Exposure to English Language

Faculty is expected to fulfil their assigned responsibilities. But apart from that they should think it as their moral responsibility to take more efforts to provide more exposure to English language for students as to achieve communication competence. The students when forced to learn communication on their own, they find it as a herculean task. So, they expect assistance and warmth understanding from teachers. Now days a comprehensive course which focus on both writing and speaking skills is introduced in most of the universities in Maharashtra. So, during the interactive sessions the students should be encouraged and helped to talk .So, that the students can built an ability to participate in various activities such as paper presentations, GD's, mock interviews, role plays etc. to develop English communication competence. It is necessary that Students Talk Time (STT) should be higher than Teacher Talk Time (TTT).

2.2. Use of Technical Dictionary

Students from the secondary and higher secondary level should be given dictionary of technical words with their meanings in regional language for use. The technical teachers should help students in understanding the technical words in English and their equivalents in regional languages. Again they should help the students to understand the meanings of long and complicated sentences in technical subjects.

2.3. Learn Grammar of English as Second Language

Grammar should be taught in the form of application of it in day to day life. When we learnt first language ,it requires a lot of time .We get a lot of exposure to it as all our communication deals takes place in the regional language. So, it is but natural that it does not require to learn the grammar of regional language. Unfortunately it does not happen with English which is a second language. From the experience ,it is essential to learn grammar of English as second language for getting confidence of speaking and performing the best in all walks of life.

2.4. New Trends and Methods of Teaching

In this modern era, new trends and methods of teaching are emerging in the learning of the English language competence which involves the use of Computer assisted language learning(CALL) in the Language Labs. Most of the students are tired of the traditional way of teaching and are more interested in doing exercises on a computer than by hand. This system works more effectively when the ratio of computer and student is 1:1
CALL mostly includes:

- Use of Audio /video clips.
- Interlingua method-Listen and see clippings in regional language and English.
- Language Learning-vocabulary-synonyms and antonyms.
- Etymology reading.
- Grammar.
- Role plays-Speaking task.
- Translation.
- Fluency Task.

By these methods of learning students are provided a lot of practice and exposure to the English language. This method leads to individualization of learning, where teachers acts as mentor, trainer and aspirant to facilitate learning. The teachers should be aware of the latest technologies ,explore new ideas and have certain amount of specialization in the subject. Refresher courses for these teachers at national level can help in achieving proficiency in use of CALL.

2.5.Efforts by Students

Students on their own should make use of English journals, television programs, newspapers, magazines, English language Resource centers to acquire the English communication skills.

2.6.Utilization of Current Technology

Current technology should be utilized, or at least demonstrated to the students, so that they are aware of what is in use beyond the university walls. The Irish study cited earlier found that instructors in communications need to review and update methods due to the rapid advances in communication technology [4]. It is expected from the practicing engineering graduates that they have the knowledge of basic MS Office applications , as well as other technical elements including Web page design, e-mail and graphic design, Word, Excel and PowerPoint, and these were the prime tools utilized in oral presentations.

According to the survey, carried out by a number of agencies, more than 70 percent of our engineering graduates are not employable. Dr Kalam has rightly said that India does not have problem of unemployment but unemployability. The graduates lack other skills beside the academic or technical skills. The top three most important general skills identified were integrity, reliability and teamwork, while the top three most important specific skills are entrepreneurship, communication in English and use of modern tools and technologies.

If colleges want to improve the employability of their graduates, they have to focus on reducing these important skill gaps through improvements in curriculum and teaching methods. The Universities are required to play a significant role for the same so that graduates have to be able to formulate, analyze, and solve a real life problem using standard engineering techniques.

Each institution should define the set of skills that a graduate is supposed to have after each semester. Further, colleges need to change pedagogical style from teacher-centric to student-centric, and include more assignments for students to independently analyze and apply tools on real life problems. Only through such changes in the teaching-learning process will the future engineers become more employable.

Conclusion

To be successful in any field one need to know and understand how to communicate effectively. Communication is the most important function a human being performs in his/her life .Communication like birth, death growth and decay is a part of individual life as well as organizational existence. Its importance is self-explanatory and is an experience of all as well. Communication skill is essential for an Engineer who aspire to carry out his professional practice in the global arena. The rapid globalization of the world's economy has placed a significant impact on the way Indian engineers work. The role of engineers in society is changing and places new pressures and demands on engineering faculties in the Universities around the world. Engineering education requires a more outward look with the ability to produce graduates who would be able to lead the engineering profession with its increasing pressures and challenges arising from the broadening roles of an engineer. Engineers are required to perform not only in technical capacities but also in the non technical capacities. English language is not the mother tongue of our country India and hence do not degrade yourself in case you are poor in English communication skills. In our considered opinion, one can tremendously improve his communication skills in English with more practice and regular use of spoken English. For speaking good English, one should have burning zeal to learn English and has to put enough efforts.

References

1. EL Sakran, T.M. and A. Awad, 2012.Voices from the United Arab Emirates: Engineering graduates' labour market requisite competencies, International Journal of Engineering Education, p.105

2. Jensen, H.P., 2000. Strategic planning for the education process in the next century. *Global J. of Engng Educ.*, p. 35.

3. Grünwald, N., 1999. Quo vadis German engineering education. *Proc. 2nd Asia-Pacific Forum on Engineering Technology Education*, Sydney, Australia, pp.371.

4. Keane, A. and Gibson, I.S., 1999. Communication trends in engineering firms: implications for undergraduate   engineering courses. *International J. of Engng. Educ.*, p.115.

.

Shortest path algorithms using geotools

D.R.Vaghela

Assistant Professor, Gandhiagar Institute of Technology

Abstract

GIS or Geographic Information System has the ability to query and analyse geographic information in a variety of different contexts. .GIS is a technology which is ideally suited for analysis of the market values of properties, since such values are based upon spatial comparisons as well as individual property attributes. It is well known that computing shortest paths over a network is an important task in many network and transportation related analysis. Choosing an adequate algorithm from the numerous algorithms reported in the literature is a critical step in many applications involving real road networks. The work over here is concentrated on applying a shortest path algorithm on a graph generated from a shape-file's feature of road network with the distance as the weight-age of a graph node and displaying shortest path with its node information in this tool.

Keywords: shortest path algorithms, Geographical information system (GIS), Dijkstra algorithm, shape-file, geotools, graph, maven eclipse.

1. Introduction

With the development of geographic information systems (GIS) technology, its analysis power is applied in many fields of real world problems. A mathematical model of any network or 3D representation of objects is possible with the consideration of different forces. We can apply GIS to calculate the shortest path algorithms on .SHP file. The Esri shape-file, or simply a shape file, is a popular geospatial vector data format for geographic information system software . It is developed and regulated by Esri as an open specification for data interoperability among Esri and other GIS software products. Shape-files spatially describe vector features: points, line and polygons, representing, for example, water body, well, rivers, and lakes etc. Each item usually has attributes that describe it, such as name or temperature [1]. One can apply shortest path algorithms like Dijkstra on Shape-file file with the help of GEOTOOLS (osgeo) library available in Java .GEOTOOLS can be used with the help of MAVEN. Apache Maven is a software project management and comprehension tool. Based on the concept of a project object model (POM), Maven can manage a project's build, reporting and documentation from a central piece of information. Maven uses an XML file to describe the software project being built, its dependencies on other external modules and components, the build order, directories, and required plug-ins. It comes with pre-defined targets for performing certain well-defined tasks such as compilation of code and its packaging [2]. With the help of this kind of model, we can select direct source point to destination point with its node and attributes information in a real time scenario.

2 SHORTEST PATH USING DIJKSTRA

Dijkstra's algorithm was developed by Dutch computer scientist Edsger Dijkstra in 1956 and published in 1959. It is based on graph search, the edge and vertex, gives the shortest path between two vertex .For a given source vertex (node) in the graph, the algorithm finds the path with lowest cost (i.e. the shortest path) between that vertex and every other vertex. It can also be used for finding costs of shortest paths from a single vertex to a single destination vertex by stopping the algorithm once the shortest path to the destination vertex has been determined [3]. The algorithm is represented in brief as below [4].

G = (V,E) where   **V** is a set of vertices and
                    E is a set of edges.
Dijkstra's algorithm keeps two sets of vertices:
            S the set of vertices whose shortest paths from the source have already been determined
            V-S *the remaining vertices.*

The other data structures needed are:

        D array of best estimates of shortest path to each vertex

        Pi an array of predecessors for each vertex

2.1 The basic mode of operation is:

1. Initialise **d** and **pi**,
2. Set **S** to empty,
3. While there are still vertices in **V-S**,

      3.1. Sort the vertices in **V-S** according to the current best estimate of their distance from the source,

      3.2. Add **u**, the closest vertex in **V-S**, to **S**,

      3.3. relax all the vertices still in **V-S** connected to **u.**

3 USING OPEN SOURCE GeoTools

GeoTools is a free software GIS toolkit for developing standards compliant solutions. It provides an implementation of Open Geospatial Consortium (OGC) specifications as they are developed. GeoTools is a contributor to the GeoAPI project - a vendor-neutral set of Java interfaces derived from OGC specifications - and implements a subset of those libraries.

A Shapefile is a common file format which contains numerous features of the same type. Each shapefile has a single feature type [5].

The classic three files:

1. filename.shp: shapes
2. filename.shx: shapes to attributes index
3. filename.dbf: attributes

Basic metadata: * filename.prj: projection

Open source extensions:

1. filename.qix: quadtree spatial index
2. filename.fix: feature id index
3. filename.sld: style-layer-descriptor style xml object

ESRI extensions:

1. filename.sbn: attribute index
2. filename.sbx: spatial index
3. filename.lyr: arcmap-only style object
4. filename.avl: arcview style object
5. filename.shp.xml: fgdc metadata

The gt-graph package defines the concept of a graph (or network) made up of .shp file Features. The graph provides flexible way to make computation in directed and undirected networks. For a given road network we have to create a graph of that road network with the distance as their weightage. The shape-file is a vector data file containing the feature and its attributes where graph is having edges and nodes. So we have to take a Hash Map to map the feature with its respective edge in the graph. To select a point on a shape-file we are creating a filter of 5x5 pixel square .selected feature's node are passed to the algorithms to calculate the shortest path. The path is calculated on the basic of the distance. It also represents the node visited during the graph traverse.

3.1 METHODOLOGY

The methods of the class used to convert shape-file into graph are shown as below. A Graph-Builder is used to build and retrieve information from shape-file [6]. The graph module makes the use of Feature, FeatureType, FeatureID. At low level, graph generation is done by GraphBuilder.
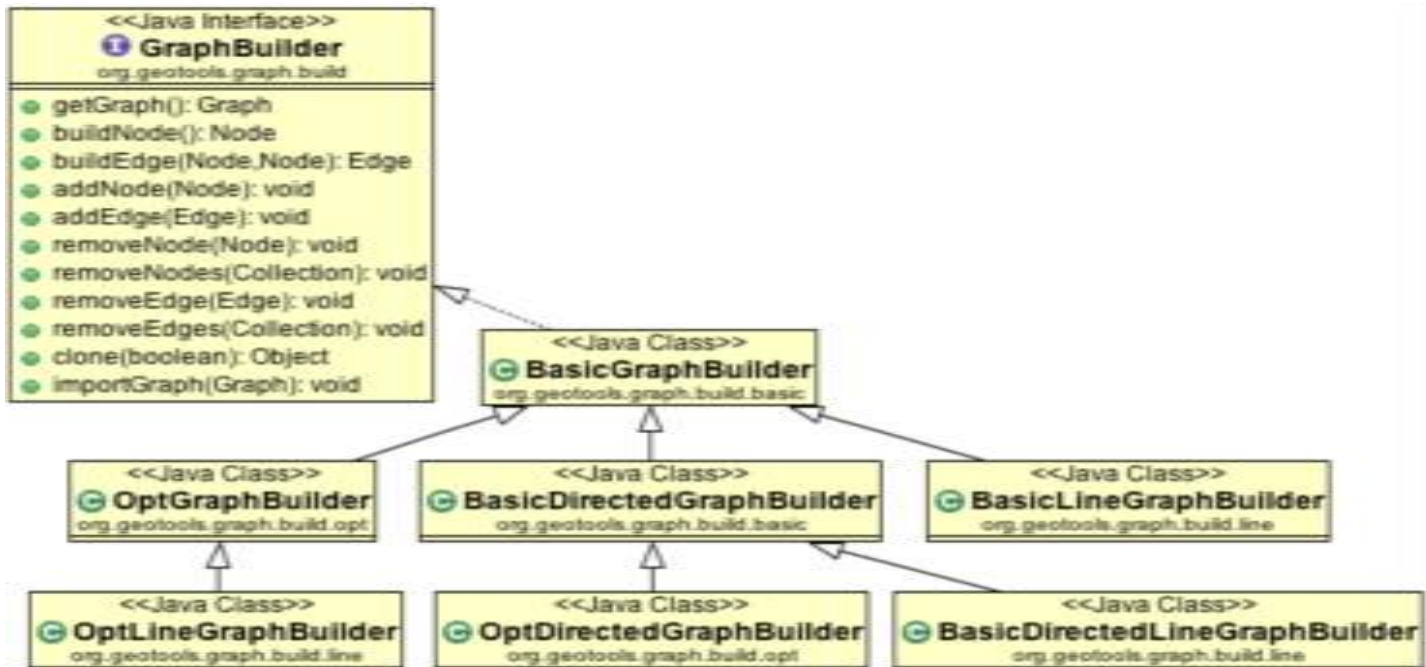

Fig-1 The Class Diagram to generate graph

getGraph() method is used to retrieve the generated graph. BasicLineGraphGenerator() is used to build a line network. With the help of different types of GraphGenerator, one can create directed or undirected graph as per the need.

4 CODE SNIPPET FOR DIJKSTRA

We have a number of ways to calculate the shortest path between two nodes .The class DijkstraShortestPathFindercan be used to calculate a path using Dijkstra's Shortest Path algorithm [7].

```
DijkstraIterator.EdgeWeigter weighter = new DijkstraIterator.EdgeWeighter() {
  public double getWeight(Edge e) {
    SimpleFeature feature = (SimpleFeature) e.getObject();
    Geometry geometry = (Geometry) feature.getDefaultGeometry();
    return gometry.getLength();
  }
}

// Create GraphWalker - in this case DijkstraShortestPathFinder
DijkstraShortestPathFinder pf = new DijkstraShortestPathFinder( graph, start, weighter );
pf.calculate();

//find some destinations to calculate paths to
List/*<Node>*/ destinations = destination_node;

//calculate the paths
for ( Iterator d = destinations.iterator(); d.hasNext(); ) {
```

```
Node destination = (Node) d.next();
Path path = pf.getPath( destination );

//do something with the path
}
```

5 EXPERIMENTS AND RESULT

Shortest path algorithm has been applied on GIS dataset with the help of geo-tools open source libraries. USA road network shape-file is referred. Its attributes and projection information is populated in a tabular format. A graph which represents shape-file features with distance as its weightage is generated. A hash map is constructed to store feature id and the graph edges. A 5x5 pixel filter is used to select a source point and a destination point to calculate a path in real time.
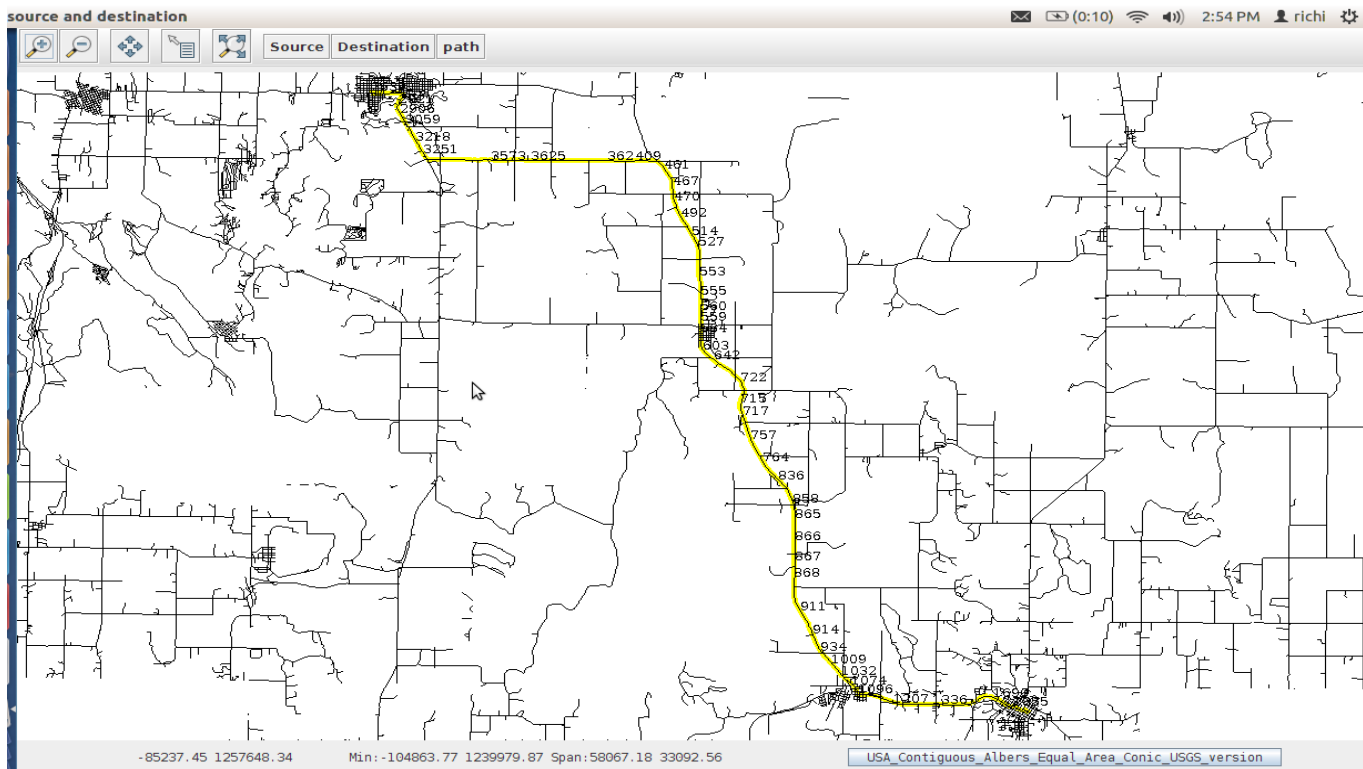
Fig-2 way of traverse between two selected nodes

The model highlights the shortest path in a yellow colour between selected two nodes in a sequential way of traverse.

6 EXTENSION OF WORK

The model requires longer period of time to calculate the shortest distance for a lager GIS road network dataset. To eliminate this issue, GIS network should be preprocessed. Preprocessed output of the graph generation can be used in this model. BOINC can be used to generate the graph on the server with the help of distributed computing [5]. The Berkeley Open Infrastructure for Network Computing (BOINC) is an open source middleware system for volunteer and grid computing. BOINC is designed to be a free structure for anyone wishing to start a volunteer computing project. Most BOINC projects are non profit and rely heavily, if not completely, on volunteers. Graph generation process can be done on the server with the help of BOINC.

7 CONCLUSION

The demand for GIS network analysis is increasing day by day. To the work done in this paper it can be concluded that for finding the shortest path, if automation is applied to certain extent, then, the use of Geo tools for map making purposes or finding routes would be a swift job. Further, use of open source tools such as linux would make the reliability as well as the cost and performance parameters compatible with the ongoing research in GIS environment. Open source geotools libraries and BOINC for preprocessing of GIS dataset can be used in distributed computation environment to improve efficiency.

8 REFERENCES

1. "Esri Shape-file for GIS software as vector data format" ,Internet : http://en.wikipedia.org/wiki/Shapefile .[11 aug 2013]
2. "Apache Maven Introduction", Internet: http://maven.apache.org/ [10 aug 2013]
3. "Dijkstra algorithm " ,Internet : http://en.wikipedia.org/wiki/Dijkstra%27s_algorithm [10 aug 2013]
4. "Dijkstra algorithm flow and pseudo-code for shortest path calculation" ,Internet : http://www.cs.auckland.ac.nz/software/AlgAnim/dijkstra.html.[11 aug 2013]
5. "Shape-file", Internet: http://docs.geotools.org/latest/userguide/library/data/shape.html [10 aug 2013]
6. "geotools ", Internet : http://docs.geotools.org/latest/userguide/extension/graph/index.html, [5 aug 2013]
7. "geotools graph ", Internet : http://docs.geotools.org/latest/userguide/extension/graph/index.html. [15 aug 2013]
8. Kang-Tsung-Chang "Introduction to GIS", Tata McGraw Hill, 4th ed., 2008.
9. Heywood Ian ,Sarah Cornelius ,Steve Carver" An Introduction To Geographical Information Systems ", Pearson ,3rd ed,2010.

Design and Comparison of Quaternary Logic Blocks

Ashish B Pandya[a], Jatin M Chakravarti[b], Pratik J Gohel[c] *

[a, b, c] *Gandhinagar Institute of Technology, Moti Bhoyan, Gandhinagar-382721, India*

Abstract

In this paper design of quaternary logic blocks and comparison between basic binary logic blocks and the quaternary logic blocks using VHDL is given. In multi value logic (MVL) quaternary logic system is used. In quaternary system four bits represent as ('0', '1', '2', '3'). We have shown the comparison between binary logic gates and quaternary logic gates using VHDL compilation. We have also shown the simulation and compilation result between binary and quaternary logic gates, with simulation and designing of the basic Quaternary gates with the CMOS transistors.

Keywords: VHDL compilation, quaternary gates, timing analysis, simulation

1. Introduction

Increased data density, reduced dynamic power dissipation, and increased computational ability are among some of the key benefits of Multiple Valued Logic (MVL). Several implementation methods have been proposed in the recent papers to realize the MVL circuits [1, 2]. Quaternary states (0, 1, 2, 3) can be imagined as 2-bit binary equivalents 00, 01, 10, 11 shown in [3]. If the bits of the binary equivalent interchange their positions and still the quaternary state remains unchanged, then it is said to have binary symmetry; otherwise it is asymmetrical. Thus 0, 3 are symmetrical and 1, 2 are asymmetrical. When expressed as a number, a single quaternary digit is called a qudit and the basic gates like NOT, NAND, and NOR are represented in quaternary logic.

The binary logic is limited to only two states '1' and '0', where as Multi-Valued Logic (MVL) is a set of finite or infinite number of values. The MVL is implemented in two modes i.e. current mode and voltage mode. In current mode, MVL states are defined in terms of output current, which is an integral multiple of reference current and in voltage mode, MVL states are in terms of distinct voltage levels.

Today's VLSI technology offers ways to realize MVL circuits in order to bring their full potential into many operational circuits. Many authors have directed their efforts to the implementation of Multi-Valued logic looking for benefit from all advantages it possess over the binary logic. It is possible for ternary logic to achieve simplicity and energy efficiency in digital design since the logic reduces the complexity of interconnects and chip area, in turn, reducing the chip delay. It also offers better utilization of transmission channels because of the higher information content carried by each line [4]. It gives more efficient error detection and correction codes and possesses potentially higher density of information storage. One of the main advantages of ternary logic is that it reduces the number of required computation steps.

Multiple-valued logic circuits have received an increased attention in recent years, due to possibility of reduction in number of interconnections and the potential for increased information content per unit chip area [4]. With an increasing density of the chips, the number of inter chip connections is greatly increased as more and more functions are put on the same chip, thus the size and performance of the chip is mostly dominated by wiring rather than devices. One of the approaches to solve these interconnection problems is the use of multi-valued logic (MVL) inside the VLSI chip. Multiple-Valued Logic system is one of the most promising approaches to realize future beyond-binary electronics and systems.

In a typical binary VLSI circuit, interconnect accounts for 70% of the chip's area while the processing transistors occupy only 10% of the chip. The remaining 20% is devoted to insulation. Thus the design of the binary logic circuits is limited by the requirement of the interconnections. A more cost effective way of providing interconnections could thus be of great benefit.

---

* *Corresponding Author*: Ashish B Pandya. M: +91 9924827216
E-mail address: ashish.pandya@git.org.in

In this paper, Section 2 includes the basic quaternary logic gates and their truth table representation in quaternary system. After quaternary logic gate representation there is some basic designs of the logic gates with simulation results. In Section 3 we talk about quaternary T-Gate. Section 4 includes comparison between binary and quaternary gates in VHDL compilation using VHDL. Section 5 includes the result and the analysis of the quaternary gates and their comparison. We also show the output combinations of different logic gates.

2. Quaternary Basic Gates

2.1 Basic Inverter

Quaternary inverter circuit is an elementary form of various logic circuits. Function of inverter is to just complement the input signal.

Figure 2.1: Inverter Symbol

The output signal expression or the complement function is calculated as

$$X_o = r - 1 - X_i$$

Where r is radix of the system.

Table 2.1 shows the Truth Table of a quaternary inverter. Here the output is just a complement of the input signal.

X_i	X_o
0	3
1	2
2	1
3	0

Table 2.1: Truth Table of a quaternary inverter

2.1.1. Gate Level Representation

Circuit complexity has been reduced by using three values of enhancement mode threshold voltage and by utilizing a priority rule in establishing the output voltage i.e. the priority is given to lowest level at all times when several transistors are in the ON state. This principle of operation leads to the marked decrease in the in the transistor number and exact transient response.

Inverter consists of five enhancement mode n-MOS and p-MOS each. Threshold voltages of the transistors T1, T2, T3 to which input is applied are 0.5, 1.5, and 2.5 and act as switches. There is a correspondence between magnitude of logic level and of voltage value i.e. logic threshold of 0.5 means, threshold voltage between logic level 0 and 1. Similar is the case with 1.5 and 2.5 logic thresholds. Transistors T4 and T5 form a voltage divider network. Threshold voltages of T4 and T5 are to be adjusted to obtain the results nearer to ideal case.
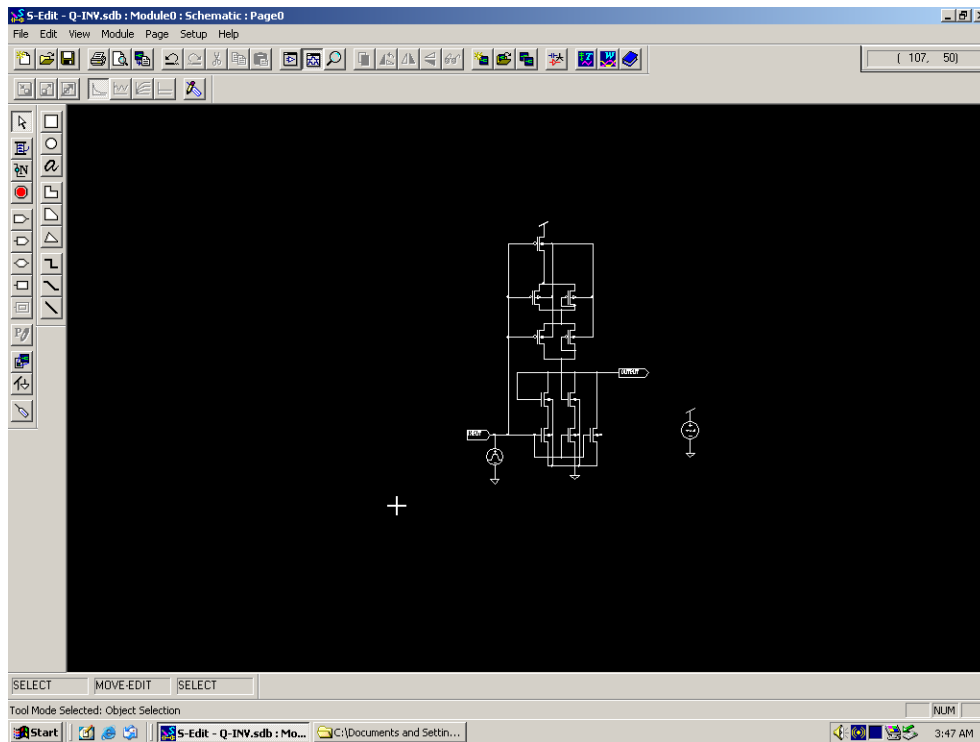
Figure 2.2: Gate Level Representation of Quaternary Inverter

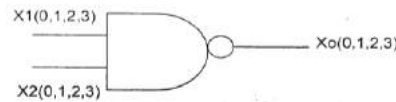## 2.2. Quaternary NAND Gate

Figure 2.3: Quaternary NAND Gate

The output signal expression is calculated as

$$X_o = X1.X2$$

The output of Basic NAND gate is multiplication of two input signal, and in quaternary there are 4 bits represented as '0','1','2','3'. The output is shown in figure below.

	0	1	2	3
0	3	3	3	3
1	3	2	2	2
2	3	2	1	1
3	3	2	1	0

Table 3.2: Quaternary NAND truth table

2.2.2. Gate level Representation of Quaternary NAND gate.

The principle of operation of quaternary NAND gate is based on the standard INVERTER. Three more transistors are added in parallel with transistors T1, T2, T3 each. Thus second input is applied to the added three transistors. Fundamental of threshold voltage is similar to the standard inverter.
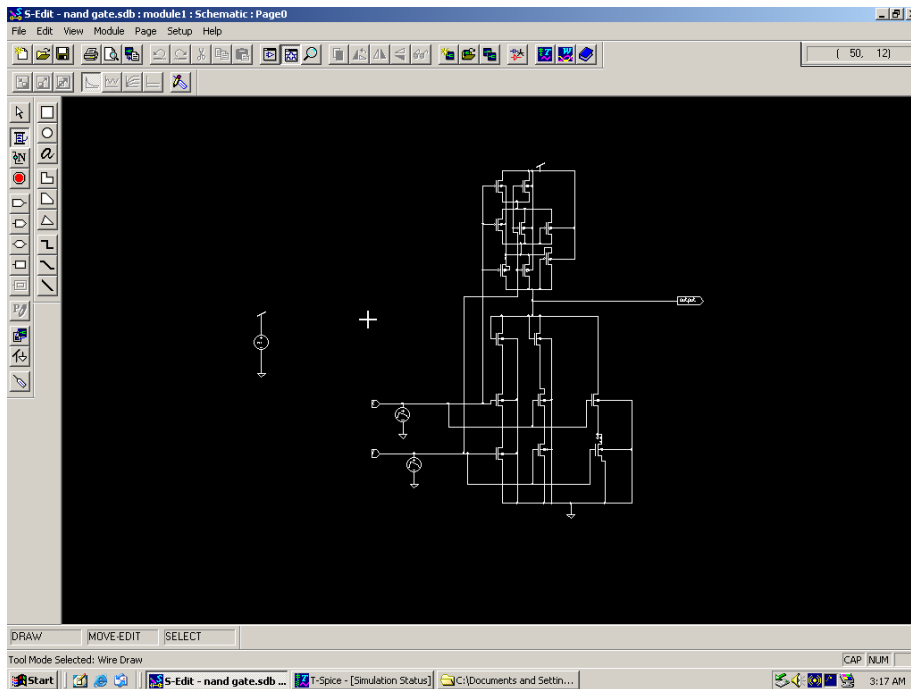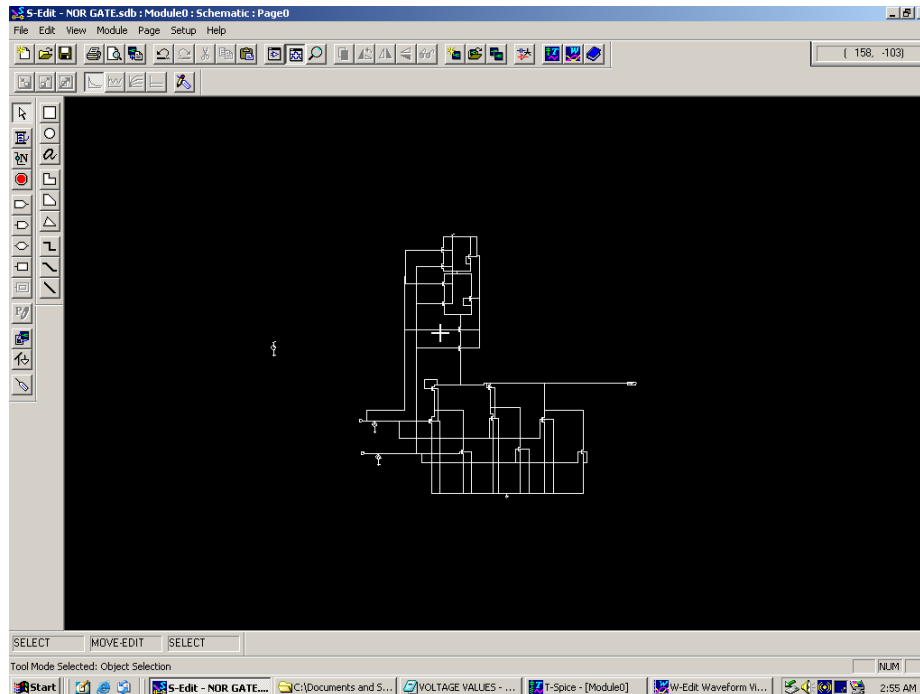

Figure 2.4: Gate Level Representation of Quaternary NAND Gate

2.3 *Quaternary NOR Gate*

Figure2.5: Quaternary NOR gate

	0	1	2	3
0	3	2	1	0
1	2	2	1	0
2	1	1	1	0
3	0	0	0	0

Table 2.3: Quaternary NOR Gate Truth Table

2.3.1 Gate level Representation of Quaternary NOR gate.

       The principle of operation of quaternary NOR gate is based on the standard INVERTER. Three more transistors are added in parallel with transistors T1, T2, T3 each. Thus second input is applied to the added three transistors. Fundamental of threshold voltage is similar to the standard inverter.

Figure 2.6: Gate Level Representation of Quaternary NOR Gate

3. Quaternary T-gate: A Universal Building Block

Conceptually transmission gate (T-gate) is simply a multiplexer adapted for multi-valued logic operations. For an r valued system, T gate has (r+1) inputs. One of them is an r valued control input. The value of this variable decides which of the remaining r-valued inputs will be produced at the output. Quaternary system T-gate has five inputs. Out of which one will be the controlling or select input. Depending upon the value of control input, corresponding input will be selected at the output.

Transmission gate is qualified as a universal element in several different senses. T-gate is logically complete: that is, all multiple-valued functions of one or more variables can be created with T-gates. Its operation is intuitive: that is, one can relatively easily understand what it does, both as single basic element and also in a combination of several gates. It is easy to implement: Its fabrication in most of the available technologies is straight forward. It highlights two essential aspects of any logic gate i.e. logic value thresholding and logic signal connection or switching. Thus, for multiple-valued logic, T-gate is a useful general purpose tool. T-gate may not always give the optimized circuit.

3.1 Gate Level Representation of Quaternary T-Gates

Complete gate level schematic of T-gate is as shown below. Simple transmission gate is required to transmit the external input to the output, depending upon the content control input. Simple inverter is required to get desired bias condition for PMOS of Transmission gate.
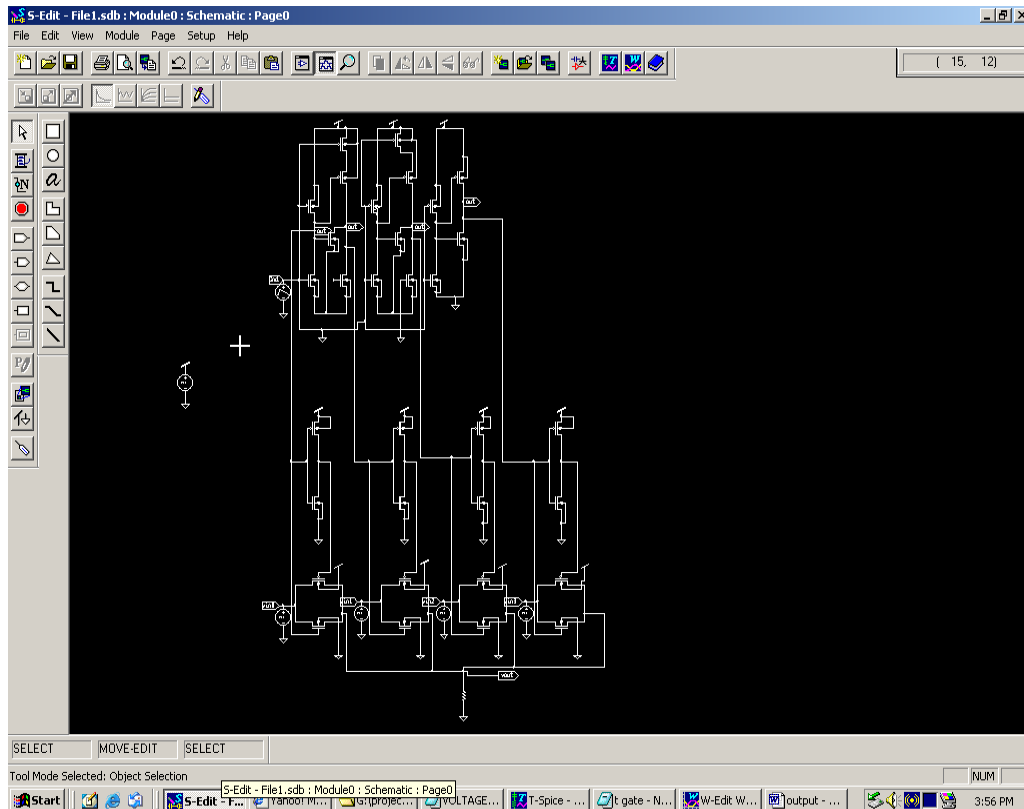

Figure 3.1: Gate Level Representations of Quaternary T-Gates

3.2. T -gate Applications

Single variable function implementation T-gate, being a multiplexer under the control of r-valued selecting input, can be used directly to implement any function of single r-valued variable. The selected input corresponding to each selecting-input value is connected to a reference value appropriate to the output required by the desired the single variable function.

4. Result Analysis

Using quartus EDA tool the simulation result of basic gates as shown below in figure.
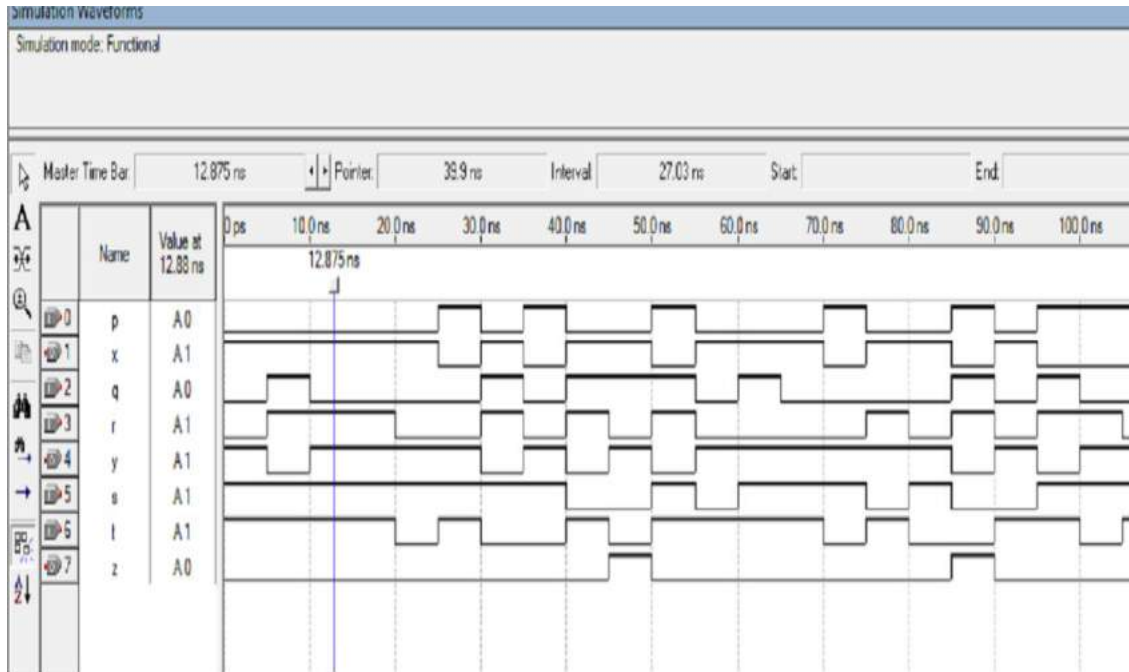
Figure 4.1 Waveform analysis of binary gates

Binary Inverter	Binary NAND	Binary NOR
P (i/p)	Q (i/p)	S (i/p)
X (o/p)	R (i/p)	T (i/p)
	Y (o/p)	Z (o/p)

Table 4.1

It is the analysis of the binary gates and the result as shown above. Now for the quaternary gates result analysis is shown in Figure 4.2. Here the result shows the whole package of all basic gates like NOT, NAND, NOR gate. And the result is given in one waveform. And we can see that the basic gate analysis is given. In that we get output of the basic analysis of the gates, and the result is shown.
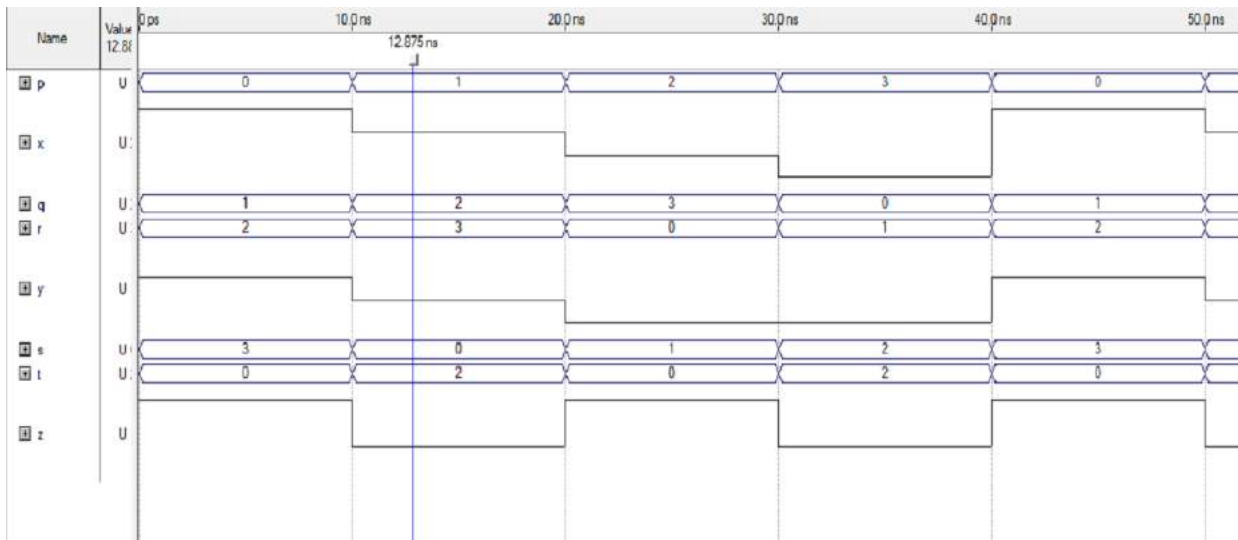
Figure 4.2: waveform analysis of quaternary logic gates.

Quaternary Inverter	Quaternary NAND	Quaternary NOR
P (i/p)	Q (i/p)	S (i/p)
X (o/p)	R (i/p)	T (i/p)
	Y (o/p)	Z (o/p)

Table 4.2

In the analysis of quaternary basic gates we get the output waveform. By using quaternary gate truth table we get the output waveform. And the simulation and compilation analysis is given as shown in Figure 4.2. In this quaternary logic there are 4 bits is used as input sequence.

4.1 Comparison between Binary and Quaternary Gates

After using VHDL code for the basic gates and the quaternary gates the compilation result is given as shown below. After comparing both the systems the result shows that in binary logic the total number of pins required is very less compare to the quaternary logic. In quaternary logic the total time required is less compare to the binary logic. So here it says that quaternary logic system take less time. So it can be useful for that.

It is used in Quartus EDA tool and the compilation analysis and simulation analysis will be taken and the result and comparison is given.

	Basic Gate	Quaternary Gate
Total pins	8/158 (5%)	16/158 (10%)
Total Logic Elements	2/4608	4/4608
Actual Time	9.410ns	9.159ns

Table4.3

5. Conclusion

In this paper design and comparison between binary and quaternary logic gates are shown. We have shown the analysis of basic inverter, NAND, NOR, XOR and their gate level analysis. The coding is done by using the truth tables of the mentioned logic gates. Using the codes we have shown the comparison between binary and quaternary logic. The above work can be further implemented for flip-flops and latches. Implementation on FPGA and analysis of power and delay is also possible.

References

[1] Mrs. Yashika, A. Gaidhani, Mrs. Monica, N. Kalbande, "Design of Some Useful Logic Blocks Using Quaternary Algebra", UACEE International Journal of Advances in Computer Networks and its Security.

[2] Shahid Latif, Junaid Qayyum, Muhammad Lal, Faheem Khan, "Novel Approach to the Learning of Various Number Systems", *International Journal of Computer Applications*, Volume 26– No.7, July 2011.

[3] Ifat Jahangir 1, Dihan Md. Nuruddin Hasan, Md. Shamim Reza, " Design of Some Quaternary Combinational Logic Blocks Using a New Logic System", TENCON 2009, IEEE.

[4] A.P.Dhande, R.C.Jaiswal and S.S.Dudam, "Ternary Logic Simulator Using VHDL" 4th International Conference: Sciences of Electronic, Technologies of Information and Telecommunications, March 25-29, 2007 – TUNISIA

[5] Snehal B. Sahastrabudhey, K. M. Bogawar, "Arithmetical Operations in Quaternary System Using VHDL", IJCSET, Vol. 2, Issue 4, April 2012.

[6] Vasundara Patel K S, K S Gurumurthy," Design of High Performance Quaternary Adders", International Journal of Computer Theory and Engineering, Vol.2, No.6, December, 2010,1793-8201.

[7] Volnei A. Pedroni, 2004. Circuit Design with VHDL, The MIT Press.

A Phase determination for ICRH Transmission Line on Aditya/SST-1 using Least Square Technique

Ila vaghela, Rahul Vaghela

Gandhinagar Institute of Technology, Moti-bhoyan, Gndhinagar, 382721, India

Abstract

ICRH is one of the better heating technique for increasing the plasma temperature. The key problems in ICRH are RF power coupling to plasma. Plasma has very low resistive impedance due to its ionized matter. The impedance matching of RF source with the plasma is essential for ICRH heating. The following paper discusses the traditional method of impedance determination and also discusses the method used with fixed probe technique for measuring Plasma impedance. It reviews least square method used to minimize the error between the impedance match. Here in this paper we present best curve fitting method to minimizing the error and the number of voltage probes to find the phase of the reflection coefficient.

Keywords: Ion Cyclotron Resonance Heating (ICRH), SST-1

1. Introduction

Ion Cyclotron Resonance Heating (ICRH) has been established as one of the better heating technique for increasing the plasma temperature. But one of the major problems in ICRH is RF power coupling to plasma. Plasma being an ionized matter has very low resistive impedance. So matching the RF source impedance with the plasma impedance is necessary for ICRF heating. In order to match the plasma impedance, it should be known first. In conventional methods plasma impedance is determined using VSWR curve method. In Aditya and SST-1 tokamak machines; RF power fed to the plasma is of the order of few hundreds of KW. With such high power levels, VSWR curve cannot be determined using conventional technique of sliding probe. Hence fixed probe technique is used to determine plasma impedance. The probe voltage picked up from the transmission line is processed to find magnitude and phase of the reflection coefficient and hence plasma impedance. Voltage probe data is carried over a distance of about 50 meter for Aditya and 150 meter for SST-1. In all this process error is introduced into the probe data. In order to get better estimate of plasma impedance, this error in the probe data should be minimized. To minimise this error least square method has been used over the voltage probe data. A program has been developed in LabVIEW ® using least square technique. LabVIEW has been used in order to make the experimentation easy because it involves data input/output and processing. Program has also been used in order to optimize the number of probes and the distance over which probes are laid. Here in this paper we present best curve fitting method to minimizing the error and the number of voltage probes to find the phase of the reflection coefficient. The magnitude of the reflection coefficient has been found out using directional coupler.

2. VSWR Curve Formulation

The single frequency time harmonic voltage distribution on a uniform two-wire transmission line is given by

$$V(z) = V_1 e^{-\gamma z} + V_2 e^{+\gamma z} \tag{1}$$

where V_1 and V_2 are the arbitrary phasor voltages and $\gamma = \alpha + j\beta$ is the propagation constant. The transmission circuit is shown below
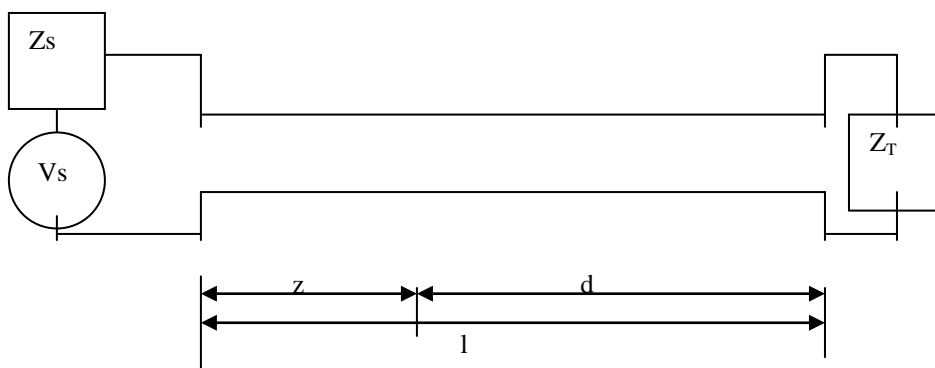
Fig. 1. RF Power Flow

The reflection coefficient at the terminal load end is given by

$$\rho_T = \frac{V_2 e^{+\gamma l}}{V_1 e^{-\gamma l}} = \frac{\dfrac{Z_T}{Z_0} - 1}{\dfrac{Z_T}{Z_0} + 1}$$

(1.2)

The equation (1.1) can be rewritten using $z = l - d$ and equation (1.2) as

$$V(d) = V_1 e^{-\gamma(l-d)} + V_2 e^{+\gamma(l-d)}$$

$$V(d) = V_1 e^{-\gamma l + \gamma d} + V_2 e^{\gamma l - \gamma d}$$

$$V(d) = V_1 e^{-\gamma l} (e^{\gamma d} + \frac{V_2 e^{\gamma l}}{V_1 e^{-\gamma l}} e^{-\gamma d})$$

$$V(d) = V_1 e^{-\gamma l} (e^{\gamma d} + \rho_T e^{-\gamma d})$$

(1.3)

For perfect reflection $|\rho_T| = 1$ and for lossless transmission line $\alpha = 0$ and hence $\gamma = j\beta$, so for perfect reflection and for lossless transmission line, magnitude of RF voltage on the transmission line can be written as

$$|V(d)| = 2A|\cos \beta d|$$

where A is scaling factor.

To obtain the graphical expression for general case of reflection; ρ_T must be expressed as an exponential number. Let

$$\rho_T = |\rho_T| e^{j\phi_T} = e^{-2(p+jq)}$$

.

$$|\rho_T| = e^{-2p}, \qquad e^{2p} = \frac{1}{|\rho_T|}$$

where

$$e^p = \frac{1}{\sqrt{|\rho_T|}}, \qquad p = \ln \frac{1}{\sqrt{|\rho_T|}} \qquad \text{and} \qquad \phi_T = -2q \quad \text{or} \quad q = -\frac{\phi_T}{2}.$$

Putting this value of ρ_T into (1.3) and for lossless transmission line ($\gamma = j\beta$)

$$V(d) = 2V_1 e^{-j\beta.l} \sqrt{\rho_T} \cosh\{p + j(\beta d + q)\}$$

$$V(d) = 2V_1 e^{-j\beta.l} \sqrt{\rho_T} [\cosh p \cosh(j(\beta d + q)) + \sinh p \sinh(j(\beta d + q))]$$

$$V(d) = 2V_1 e^{-j\beta.l} \sqrt{\rho_T} [\cosh p \cos(\beta d + q) + j \sinh p \sin(\beta d + q)]$$

From above equation, the magnitude of the standing wave can be written as:

$$|V(d)| = \left|2V_1 e^{-j\beta.l} \sqrt{\rho_T}\right| \{\cosh^2 p \cos^2(\beta d + q) + \sinh^2 p \sin^2(\beta d + q)\}^{1/2}$$

$$= \left|2V_1 e^{-j\beta.l} \sqrt{\rho_T}\right| \{(1 + \sinh^2 p)\cos^2(\beta d + q) + \sinh^2 p \sin^2(\beta d + q)\}^{1/2}$$

$$= \left|2V_1 e^{-j\beta.l} \sqrt{\rho_T}\right| \{(\cos^2(\beta d + q) + \sinh^2 p\}^{1/2}$$

The scaling factor $\left|2V_1 e^{-\gamma l} \sqrt{\rho_T}\right|$ in the magnitude term has no significance since it will just shift the curve up or down. But

for finding magnitude of ρ the ratio of the maxima and minima will be needed and hence the multiplication factor will cancel out there and hence its magnitude will not matter. Also for finding position of the minima, the scaling factor will not matter as it will not affect the position of minima. So making $\left|2V_1 e^{-\gamma d}\sqrt{\rho_T}\right|$ as unity, we get

$$|V(d)| = \left\{\sinh^2(\alpha d + p) + \cos^2(\beta d + q)\right\}^{1/2}$$

(1.4)

No assumption has been made at arriving this equation (except the scaling factor) so this equation gives the values of the VSWR curve for different values of distance (d) from the terminal load.

$\sinh^2 p$ depends on Z_0 and Z_T and for fixed value of load it is constant and does not vary with distance from load. So the VSWR curve is just an offset curve of $\cos^2(\beta d + q)$.

The voltage maxima will occur when $\cos^2(\beta d + q)=1$ and minima will occur when $\cos^2(\beta d + q)=0$.

For position of voltage minima $d_{v(\min)}$, $\cos^2(\beta d_{v(\min)} + q)=0$.

Using the identity

$$\cos^2\theta = \frac{\cos 2\theta + 1}{2}, \qquad \cos^2(\beta d_{v(\min)} + q)= \frac{\cos 2(\beta d_{v(\min)} + q) + 1}{2} = 0$$

Or

$$\cos 2(\beta d_{v(\min)} + q) = -1, \text{ or } \quad 2(\beta d_{v(\min)} + q) = \{2(\pm n) + 1\}\pi$$

$$\because \cos\theta = -1 \text{ for } \theta = \{2(\pm n) + 1\}\pi \text{ where n=0,1,2,3......)}$$

$$\beta d_{v(\min)} = \{2(\pm n) + 1\}\frac{\pi}{2} - q, \quad d_{v(\min)} = \{2(\pm n) + 1\}\frac{\pi}{2\beta} - \frac{q}{\beta}, \quad d_{v(\min)} = \{2(\pm n) + 1\}\frac{\pi\lambda}{4\pi} - \frac{q\lambda}{2\pi}$$

$$d_{v(\min)} = \{2(\pm n) + 1\}\frac{\lambda}{4} + \frac{\phi_T \lambda}{4\pi}, \left(q = -\frac{\phi_T}{2}\right), \quad d_{v(\min)} = [\pm\frac{n}{2} + \frac{1}{4} + \frac{\phi_T}{4\pi}]\lambda, \quad d_{v(\min)} = [\pm\frac{n}{2} + \frac{1}{4}(1 + \frac{\phi_T}{\pi})]\lambda$$

If position of nth minima is known, then the phase of the reflection coefficient can be found out from the above equation as

$$\frac{1}{4}(1 + \frac{\phi_T}{\pi}) = \frac{d_{v(\min)}}{\lambda} \pm \frac{n}{2}, \quad \phi_T = 4\pi(\frac{d_{v(\min)}}{\lambda} \pm \frac{n}{2}) - \pi$$

So the VSWR curve will be determined from voltage probe data and position of nth minima will be found out. From this information, phase of reflection coefficient will be found out.

3. Least Square Technique

In our case a series of voltage probes have been installed on the transmission line. These probes pick up the voltage signal. There could be some errors in the signal levels picked up by these probes. So the best curve fitting technique is used to minimise these errors. For no loss line the voltage signal is given by the Eq. (1.4) as

$$|V(d)| = \left\{\sinh^2 p + \cos^2(\beta d + q)\right\}^{1/2}$$

Squaring it on both sides

$$V^2(d) = \sinh^2 p + \cos^2(\beta d + q)$$

where the value of the $\sinh^2 p$ depends upon the magnitude of the reflection coefficient. Using trigonometric identity

$$V^2(d) = \sinh^2 p + \frac{\cos 2(\beta d + q) + 1}{2}$$

$$2V^2(d) - 1 = 2\sinh^2 p + \cos 2\beta d \cos 2q - \sin 2\beta d \sin 2q$$

or

$$y = a_1 + a_2 \cos 2\beta d - a_3 \sin 2\beta d$$

where

$$y = 2V^2(d) - 1, \quad a_1 = 2\sinh^2 p, \quad a_2 = \cos 2q, \quad a_3 = \sin 2q$$

Using least squares approximation technique, the sum of squares of errors S is found out as

$$S = \sum_i (y_i - y)^2$$

(1.7)

where y_i gives the observed value and y gives the calculated value or function value at a particular distance. Putting the value of y in this equation, we get

$$S = \sum_i (y_i - a_1 - a_2 \cos 2\beta d_i + a_3 \sin 2\beta d_i)^2$$

(1.8)

Differentiating Eq. (1.8) with respect to a_2 and a_3 and equating with zero for minimum error; we get

$$\frac{dS}{da_2} = 2\sum_i (y_i - a_1 - a_2 \cos 2\beta d_i + a_3 \sin 2\beta d_i)(-\cos 2\beta d_i) = 0$$

$$\frac{dS}{da_3} = 2\sum_i (y_i - a_1 - a_2 \cos 2\beta d_i + a_3 \sin 2\beta d_i)(-\sin 2\beta d_i) = 0$$

Simplifying further

$$\sum_i y_i \cos 2\beta d_i = a_1 \sum_i \cos 2\beta d_i + a_2 \sum_i \cos^2 2\beta d_i - a_3 \sum_i \cos 2\beta d_i \sin 2\beta d_i$$

$$\sum_i y_i \sin 2\beta d_i = a_1 \sum_i \sin 2\beta d_i + a_2 \sum_i \cos 2\beta d_i \sin 2\beta d_i - a_3 \sum_i \sin^2 2\beta d_i$$

These equations can be written in matrix form as

$$\begin{bmatrix} \sum_i \cos^2 2\beta d_i & -\sum_i \cos 2\beta d_i \sin 2\beta d_i \\ \sum_i \cos 2\beta d_i \sin 2\beta d_i & -\sum_i \sin^2 2\beta d_i \end{bmatrix} \begin{bmatrix} a_2 \\ a_3 \end{bmatrix} = \begin{bmatrix} \sum_i y_i \cos 2\beta d_i \\ \sum_i y_i \sin 2\beta d_i \end{bmatrix}$$

Solving these simultaneous linear equations where:

$$\Delta = \begin{vmatrix} \sum_i \cos^2 2\beta d_i & -\sum_i \cos 2\beta d_i \sin 2\beta d_i \\ \sum_i \cos 2\beta d_i \sin 2\beta d_i & -\sum_i \sin^2 2\beta d_i \end{vmatrix}$$

$$= \left(\sum_i \cos 2\beta d_i \sin 2\beta d_i\right)^2 - \sum_i \cos^2 2\beta d_i \sum_i \sin^2 2\beta d_i$$

$$\Delta a_2 = \begin{vmatrix} \sum_i y_i \cos 2\beta d_i - a_1 \sum_i \cos 2\beta d_i & -\sum_i \cos 2\beta d_i \sin 2\beta d_i \\ \sum_i y_i \sin 2\beta d_i - a_1 \sum_i \sin 2\beta d_i & -\sum_i \sin^2 2\beta d_i \end{vmatrix}$$

$$= \sum_i \cos 2\beta d_i \sin 2\beta d_i (\sum_i y_i \sin 2\beta d_i - a_1 \sum_i \sin 2\beta d_i) - \sum_i \sin^2 2\beta d_i (\sum_i y_i \cos 2\beta d_i - a_1 \sum_i \cos 2\beta d_i)$$

$$\Delta a_3 = \begin{vmatrix} \sum_i \cos^2 2\beta d_i & \sum_i y_i \cos 2\beta d_i - a_1 \sum_i \cos 2\beta d_i \\ \sum_i \cos 2\beta d_i \sin 2\beta d_i & \sum_i y_i \sin 2\beta d_i - a_1 \sum_i \sin 2\beta d_i \end{vmatrix}$$

$$= \sum_i \cos^2 2\beta d_i (\sum_i y_i \sin 2\beta d_i - a_1 \sum_i \sin 2\beta d_i) - \sum_i \cos 2\beta d_i \sin 2\beta d_i (\sum_i y_i \cos 2\beta d_i - a_1 \sum_i \cos 2\beta d_i)$$

Using Cramer's rule

$$a_2 = \frac{\Delta a_2}{\Delta} , \qquad a_3 = \frac{\Delta a_3}{\Delta}$$

The phase of the reflection coefficient is found out from the values of a_2 and a_3 as:

$$a_2 = \cos 2q \text{ and } a_3 = \sin 2q$$

So

$$\tan 2q = \frac{a_3}{a_2}$$

But

$$q = -\frac{\phi_T}{2}$$

So

$$\tan 2q = \tan(-\phi_T) = -\tan \phi_T = \frac{a_3}{a_2}$$

Hence

$$\phi_T = \tan^{-1}(-\frac{a_3}{a_2}) , \text{ or } \phi_T = -\tan^{-1}(\frac{a_3}{a_2}) .$$

So the phase of the reflection coefficient may be found out by knowing the voltage probe values Vi and the probe position di on the transmission line. A program in LabVIEW has been developed to verify this technique. This program takes the voltage probe values at desired probe positions as input and then calculates the phase of the reflection coefficient at the terminal load using the least square technique explained above.

4. Testing and Results

The method has been tested using LabVIEW™ and ADC (analog to digital converter) from National Instruments. A setup has been prepared to create VSWR in a section of 3.0 m length of 3 1/8" coaxial transmission line. A stub has been attached along with a 50 Ohm load to create a variable load. At the source end another stub is attached to "match" this deliberately created "mismatch". This is necessary to protect the RF source. We are not using variable phase shifter and hence this set up can work for a certain bands of frequencies. One such band is found to be from 74 to 79 MHz. Below in Table 1.1 we have shown the theoretical as well as practical values of frequencies on which the system can be matched. There are minor variations in the stub tuner length due to many practical parameters involved.

Table 1.1 Range of frequencies

Theoretical			Practical				
Frequency (MHz)	Stub position at load end (cm)	Stub position at source end (cm)	Frequency (MHz)	Stub position at load end (cm)	Stub position at source end (cm)	Impedance at source end	Return loss (dB)
74	68.00	67.83	74	68	69	50.3+0.22i	-47.48
74	67.00	66.90	74.15	67	68	50.1+0.28i	-50.63
74	66.00	66.00	74.31	66	67	49.9+0.28i	-51.61
74	65.00	65.10	74.31	65	66	50.1+0.07i	-59.00
75	60.00	59.70	74.94	59	60	49.7-0.15i	-50.72
75	59.00	58.90	74.94	58	59	50.3-0.24i	-50.52
75	58.00	58.10	75.1	57	58	50.0-0.17i	-54.63
75	57.00	57.30	75.25	56	57	49.8-0.19i	-53.15
76	51.00	51.10	76.04	50	51	49.7-0.28i	-46.49
77	45.00	45.00	76.83	44	45	49.8-0.22i	-48.9
78	40.00	39.70	77.77	38	39	49.8-0.21i	-50.55
79	34.00	34.20	78.7	33	34	49.4-0.5i	-42.5

The practical setup has been shown in the diagram below.
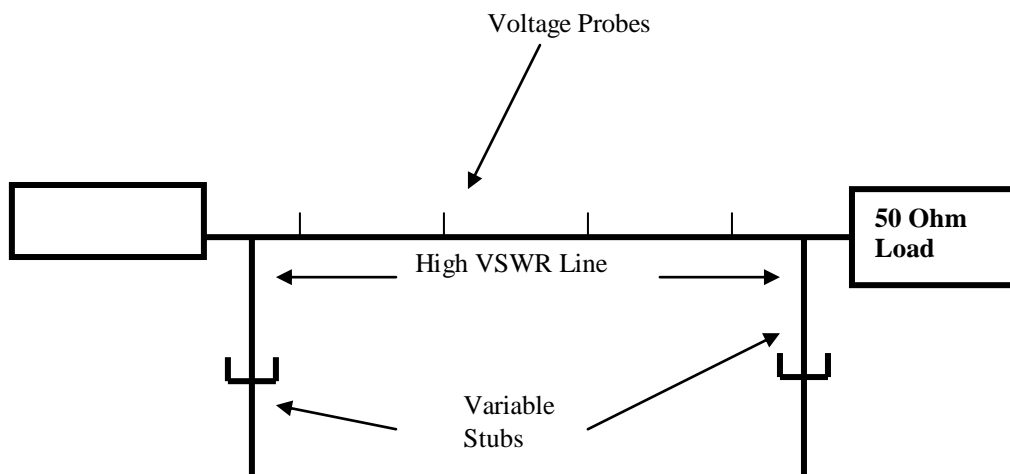
Fig. 2. Schematic of Experimental Setup.

Snapshots from the LabVIEW of the above observations have been shown in Appendix I. The phase value of reflection coefficient has been calculated from a_2 and a_3 while the magnitude has been taken from theoretical value which will otherwise be taken from directional coupler. The best curve fit is quite close to the theoretical values and has a good improvement to the actual practical curve (drawn using unprocessed voltage values). It shows that the curve fitting technique has minimised the error.

5. Conclusion

The least square technique has given a good improvement over the raw data technique. This can be seen into the snapshot at Appendix – I where both the VSWR curves are shown – one curve is of the raw data of the probes while the other curve is after applying least square technique to the raw data. The second set of curves shows a very good improvement and is very close to actual value. The load impedance has been found quite accurately with the VSWR curve which has been achieved by using least square fitting technique.

The advantage of this technique is that it minimise the error of voltage probes. A different voltage value on each and every probes of transmission line that is raw data and it will give the accurate value of the VSWR curve. It will reduce the error from the actual value.

References

[1] Kirk T. McDonald, 2005, Impedance matching of transmission lines, Joseph henry laboratories, Princeton university, Princeton, NJ 08544

[2] S.Zheng and J.M.Brennan, computer aided design of stub tuners for impedance matching.

[3] David K.Cheng, computer solution of double stub impedance matching problems, IEEE transactions on educations.

[4] Pan Yaping, Wang Lei, Zhao Yanping, Qin Chengmin, Xue Diye, Deng Xu,Mao Yuzhou, Ding Jiayi, T.Watari, R.Kumazawa, T.Seki, 2004.Design and realization of liquid stub tuner control system.

[5] Raj Singh, Sunil Dani, S.V.Kulkarni & ICRH-RF Group, 2008, Liquid phase shifter for ICRH for long pule operation at SST-1, IOP Science

[6] Jae Sung Yoon, Young Dug Bae, Jong Gu Kwak and Bong Guen Hong, Jae Sung Yoon,_ Young Dug Bae, Jong Gu Kwak and Bong Guen Hong, " Development of an Insulator and Liquid Phase Shifter for the KSTAR Tokamak", Journal of the Korean Physical Society, Vol. 44, No. 5, May 2004, pp. 1203_1206

[7] Raj Singh, Sunil Dani, S.V. Kulkarni & ICRH-RF Group, "Liquid Phase Shifter for ICRH for Long Pulse Operation at SST-1", 23rd National Symposium on Plasma Science & Technology (PLASMA-2008) IOP Publishing, Journal of Physics: Conference Series 208 (2010) 012018

Appendix – I

Snapshot from LABView – curve on the right is of raw data while on left is after processing the data with least square technique
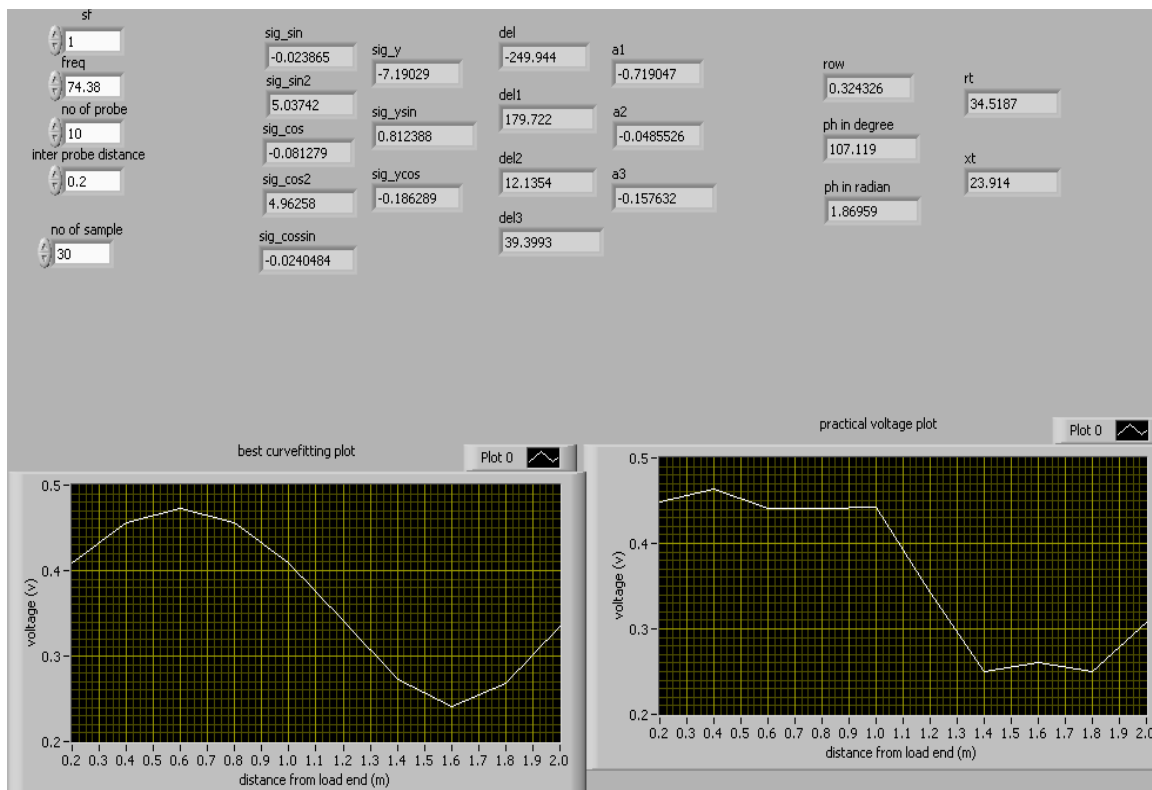
Snapshot –1

A Comparison of MAC Strategies for Cognitive Radio Networks

Smit B Tripathi[a], Mehul B Shah[b] ,Hardik H Bhatt[c]*

[a] Student, G.H.Patel College of Engineering and Technology, Vallabh vidyanagar-388120, India
[b]Assistant Prof., G.H.Patel College of Engineering and Technology, Vallabh vidyanagar-388120, India
[c]Assistant Prof., Gandhinagar Institue of Technology,Gandhinagar-382721, India.

Abstract

Medium Access Control (MAC) protocols plays very important role in Cognitive Radio (CR) networks. The two main functions of the CR MAC are interference control and avoidance for Primary User (PU) and collision avoidance among Secondary User (SU). MAC Protocols allow the SUs to exploit the underutilized/unutilized spectrum resulting into more efficiency of the available resources, improving coexistence between PUs and SUs until the Quality of Service (QoS) is acceptable, spectral mobility. The contribution of this paper is threefold. First, we identify the significance of MAC layer in CR networks. Second, we carry out the classification of the existing MAC protocols. Third, drawbacks along with the advantages of cognitive MAC protocols are carried out.

Keywords: **Cognitive Radio, Medium Access Control protocols, Spectrum Sensing, Spectrum Access, Multi-Channel MAC protocols, Common Control Channel.**

1. Introduction

With the increasing demand of the wireless services, the frequency spectrum which is in mostly 3 kHz to 300 GHz is largely occupied. Many surveys conducted thus far reveal that most of the frequency bands are occupied but this allocation schemes causes temporal and geographical holes [1] of the spectrum usage in licensed bands. In recent times, the development of the technologies such as Bluetooth, Wi-Fi, etc. has resulted into the problem of interference between these heterogeneous systems. The most suitable solution to overcome the difficulty is cognitive radio. Cognitive Radio is an upcoming technology which emerges as a means to improve the spectrum utilization in both the licensed and the unlicensed bands. It allows the SUs to opportunistically sense and access the spectrum when vacant and carry out their own transmission until the existence of PUs or even along with the PUs but with Quality of Service (QoS) in acceptable level.

Cognitive radio will lead to a revolution in wireless communication with significant impacts on technology as well as regulation of spectrum usage to overcome existing barriers. Cognitive radio, including SDR (Software Defined Radio) as enabling technology, is suggested to realize a flexible and efficient usage of spectrum. Cognitive radio is an enhancement of SR (Software Radio) which again emerged from SDR. Thus, Cognitive radio is the consequent step from a flexible physical layer to a flexible system as a whole similar to reconfigurable radio.

The Federal Communications Commission (FCC) has identified in [2] the following features that cognitive radios can incorporate to enable a more efficient and flexible usage of spectrum: (i) Frequency Agility: The radio is able to change its operating frequency to optimize its use in adapting to the environment (ii) Dynamic Frequency Selection (DFS): The radio sense signals from nearby transmitters to choose an optimal operation environment (iii) Adaptive Modulation: The transmission characteristics and waveforms can be reconfigured to exploit all opportunities for the usage of spectrum (iv) Transmit Power Control (TPC): The transmission power is adapted to full power limits when necessary on the one hand and to lower level on the other hand to allow greater sharing of spectrum (v) Location Awareness: The radio is able to determine its location and the location of other devices operating in the same spectrum to optimize transmission parameters for increasing spectrum re-use (vi) Negotiated Use: The cognitive radio may have algorithms enabling the sharing of spectrum in terms of prearranged agreements between a licensee and a third party or on an ad-hoc/real-time basis.

The CR MAC protocols are differentiated from their classical MAC schemes based on the close coupling with the physical layer and the hardware support on the device. As an example, the carrier sense mechanism at the MAC layer may not reveal complete information regarding the channel owing to its inability to distinguish between the energy radiated by

other CR users and the active PUs in the spectrum. A general framework of the spectrum functions and the inter-layer coupling is shown in Fig. 1. [3].
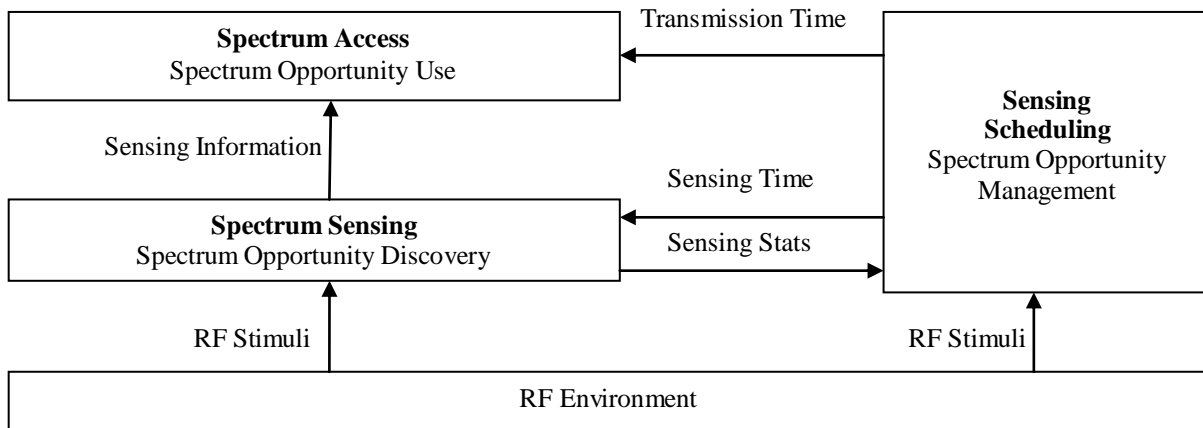

Fig. 1 Spectrum functions at the CR MAC [3]

Based on the radio frequency (RF) stimuli from the physical layer RF environment, the sensing scheduler at the MAC layer can determine the sensing and transmission times. The availability of the spectrum is coordinated by the spectrum access function. The spectrum sensing block plays a crucial role, both in terms of long term channel characterization and ensuring that the channel is available at the time of actual data transmission.

2. Classification Of MAC Protocols In Cognitive Radio

A general overview of cognitive MAC protocols can be obtained from [6], where they are classified as follows: Architecture, Spectrum Sharing Behavior, Spectrum Sharing Mode and Access Mode.
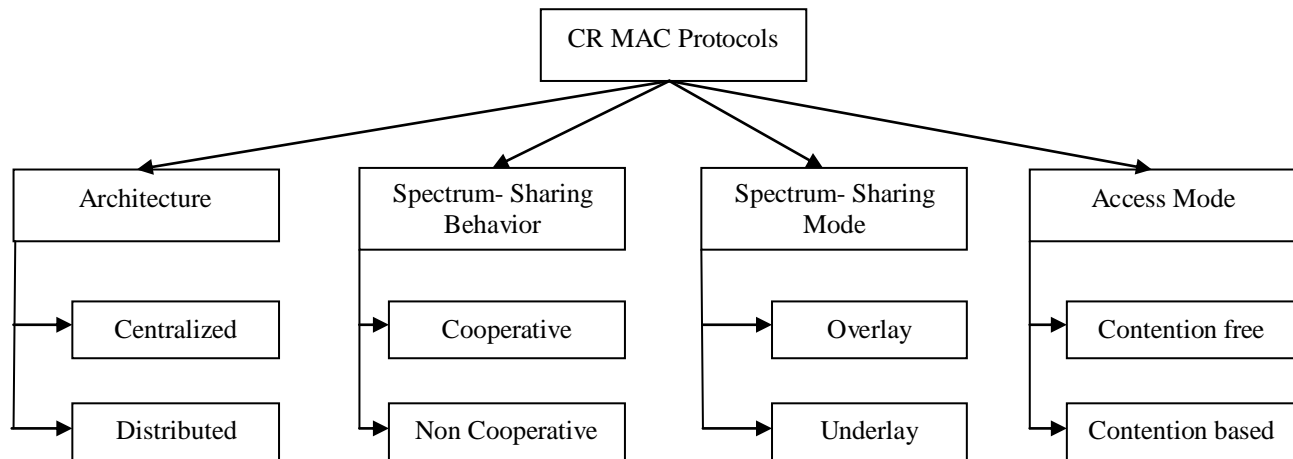
Fig. 2 Classification of CR MAC protocols [6]

Figure 2 show that according to architectures, MAC protocols are classified into two categories: centralized and distributed. In centralized MAC, there is a central controller i.e. base station [BS] to coordinate the channel sensing and access of SUs, for example, in the IEEE 802.22 draft standard [5] and the Dynamic Spectrum Access Protocol (DSAP) [8]. In case of distributed MAC, there is no central entity or base station. Based upon the sensing information, the nodes in the network carry out the hand shaking phenomenon for channel negotiations. In spectrum-sharing behaviors, MAC protocols can be classified into another two categories: cooperative MAC and non cooperative MAC. In a cooperative MAC, the SUs work cooperatively to maximize a predefined network utility, such as throughput. In a non cooperative MAC, each SU works independently and tries to maximize its own utility.

TABLE 1 MAC Protocols with Issues

Name	Architecture	Spectrum Sharing Behaviour	Spectrum Sharing Mode	Access Mode	Multiple Transceiver	Signalling
IEEE 802.22	Centralized	Cooperative	Overlay	Time Slotted	Yes	In-band
CSMA-MAC	Centralized	Cooperative	Underlay	Random Access	No	
DSA-MAC	Cluster		Overlay	Hybrid	No	
OS-MAC	Distributed		Overlay	Hybrid	No	Out-of-band
HC-MAC	Distributed	Non Cooperative	Overlay	Random Access	No	Out-of-band
DOSS-MAC	Distributed	Non Cooperative		Random Access	Yes	Out-of-band
DCA-MAC	Distributed	Non Cooperative		Random Access	Yes	
SRAC-MAC	Distributed	Non Cooperative		Random Access	No	In-band
C-MAC	Distributed	Non Cooperative	Overlay	Time Slotted	Yes	Out-of-band
SYN-MAC	Distributed	Non Cooperative	Overlay	Hybrid	No	In-band

For different spectrum-sharing modes, there are two kinds of modes: (i) the overlay mode in which SUs can only use the spectrum that is not occupied by PUs [6]. (ii) The underlay mode in which SUs and PUs can coexist and share the same spectrum with each other provided the interferences from SUs to PUs are under the predefined thresholds. According to the spectrum access mode, the CR MAC protocols are classified into two categories: contention-free (time slotted) and contention-based (random access) MAC protocols. In contention-free CR MAC, SUs access the spectrum as per the time slots in a frame structure while in contention-based CR MAC, SUs contend a channel for transmission opportunities like the Carrier Sense Multiple Access with Collision Avoidance (CSMA/CA). Note that there are several other factors which influence the classification of CR MAC protocols such as control information exchange i.e. in-band or out-of-band control channels as well as the number of transceivers. Moreover a given MAC protocol may belong to more than one category as the earlier mentioned categories are dependent on each other. For example, IEEE 802.22 MAC is not only a centralized MAC but also an overlay, contention-free MAC. For simplicity, we have broadly arranged the CR MAC protocols in distributed and centralized classes.

3. MAC Protocols For Cognitive Radio Centralized Networks

The protocols for centralization based networks needs a central entity or the base station which will govern the network wide tasks. It manages the synchronization and coordination among the network nodes. Furthermore, this architecture helps in channel sensing as well as the channel access activities among the CR users in the given network and eventually resulting in higher efficient of the available channels. However, the centralized networks can be further classified as random access, time slotted and a hybrid approach that partially combines the both of the previously mentioned access modes.

3.1 Random Access Protocols

In [7] a CSMA based random access scheme has been proposed which uses a single transceiver. This protocol ensures coexistence between the PUs and the SUs. It does so by varying the transmission power and the data rate. However, in this, there are separate base stations of Cognitive User and the Primary User though having overlapping areas of coverage. The major advantage of this scheme is that CR users carry out simultaneous transmissions even in the presence of the PUs but when the interference caused to PUs is well below the predetermined threshold level. Note that the interval of carrier sensing carried out by the CR user is more than that of the PUs. The CR user is allowed to send just one packet during first round in order to minimize the risk of interference to the existing PUs.
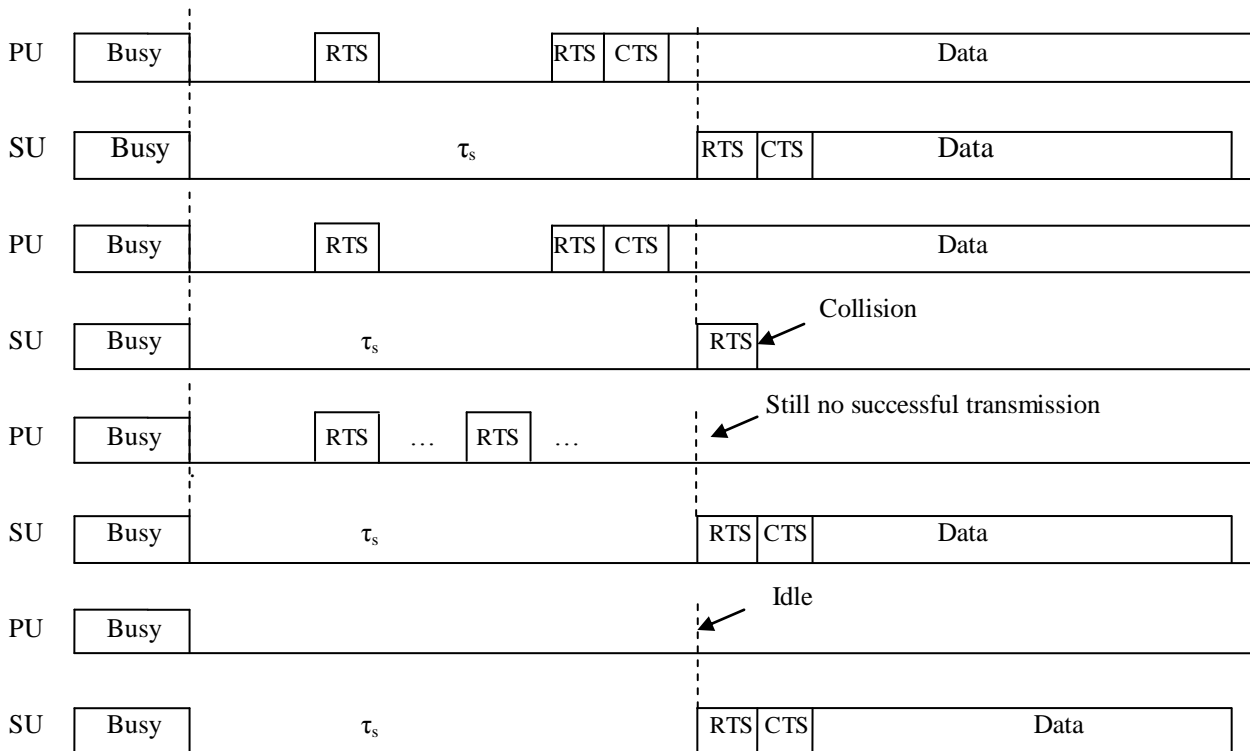
Fig. 3 CSMA based protocols with four-way handshaking procedure coexists with the PS. [3]

Fig. 3 shows the working of the protocol in [3] detailed manner with the horizontal axis showing the time scale with four different cases (1- 4).
Case (1): The PU gets access to the channel after carrier sensing and backoff and sends its data. The CR user senses the channel for a period τ_s, and on finding the channel vacant (i.e. assuming the transmitting PU and the CR user are separated by a large distance), the CR user contends to gain the access to the channel through the RTS–CTS handshake. It then starts transmitting data with the power and rate suggested by the base station so that the concurrently occurring PU transmission is unaffected. Case (2): The RTS packet sent by the CR user experiences collision. The user must now wait for the next transmission opportunity after repeating the previous sensing process. Case (3): The PU sends repeated RTS packets but incurs collision each time. Here, the CR user can start transmission independently of the primary network, i.e. without adjusting its power and rate. Case (4): PU has no packet to send, thus the channel stays idle during the CR user's sensing period. Similar to the previous case, the CR user can start transmission without considering the primary network.

3.2 Time Slotted Protocols

The IEEE 802.22 MAC [18] is not only a centralized MAC but also an overlay, contention-free MAC protocol.
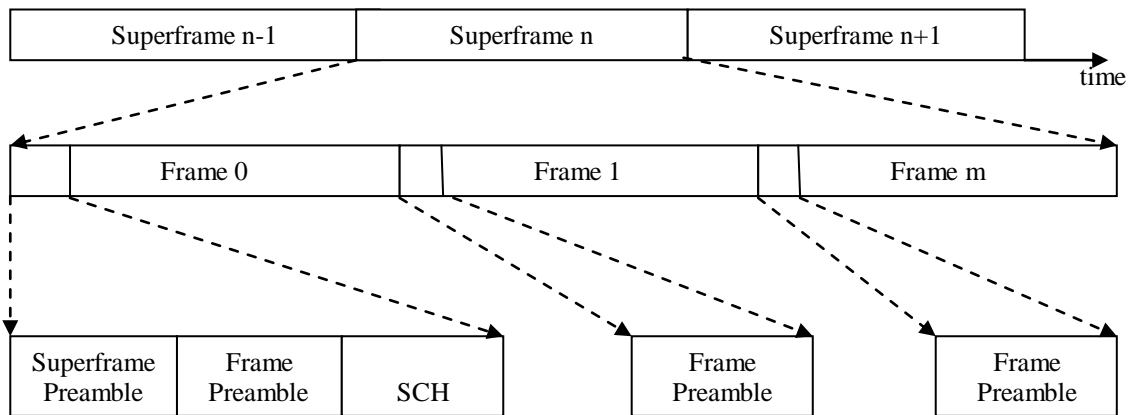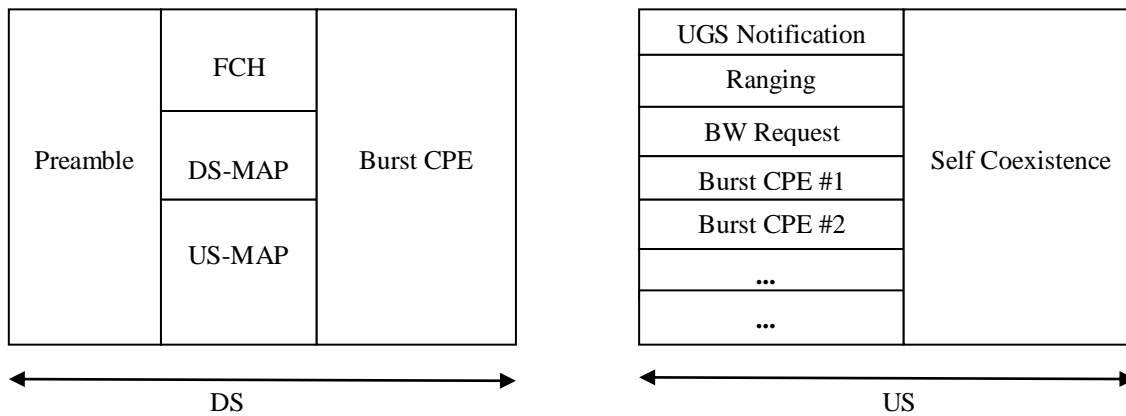

Fig. 4 Superframe Structure in IEEE 802.22. [5]

Fig. 5 Frame Structure in IEEE 802.22 [5]

It uses a central entity in order to carry out the activities of the channel access and sharing operations. The CR base station manages its own cell operations along with the CR users called the Customer Premise Equipment (CPE). In 802.22, for upstream (US) uses Time Division Multiplexing while for the Downstream (DS) it uses demand assigned Time Division Multiple Access.

The protocol operation consists of hierarchy of frames as shown in fig.4. Here, in [3] expresses that at the apex, a superframe is defined, each of which is composed of multiple MAC frames preceded by the frame preamble. At the start of each superframe, there is also a superframe control header (SCH) that is used to inform the CR users of the current available channels, different bandwidths supported, future spectrum access time, among others. The MAC frame is formed by two parts in the frame structure, as shown in fig. 5 – DS subframe and US subframe. The DS subframe contains a single packet burst from a given CPE, while the US subframe has multiple packet bursts, each transmitted from different CPEs. The different fields in these two subframes are as follows: In the DS subframe, the preamble deals with synchronization and channel estimation, the frame control header (FCH) contains the size of the DS- and US-MAP fields together with channel descriptors, and the DS/US-MAPs give the scheduling information for user bursts. In the US subframe, the urgent coexistence situation (UCS) notification informs of the incumbent licensees that have just been detected, while the other fields are used to derive the distance from the base station (ranging), and the individual bandwidth (BW) requests.

The major drawback of this scheme is the time synchronization and the significant amount of the control header exchanges. It may result in decreased throughput or lesser utilization of the channel.

3.3 Hybrid Protocols

In [8], a game theoretic dynamic spectrum access (DSA) scheme is proposed. The control signaling uses random access scheme while the data transfer occurs in time slotted manner, making it a hybrid protocol. Furthermore, this scheme is cluster based one and the policy in such that each cluster is managed by a central entity within the cluster. The proposed MAC protocol has several advantages. They are as follows: collision free spectrum access with QoS and more efficient spectrum utilization. This protocol consists of four major schemes: (a) *DSA Algorithm* (b) *Negotiation Mechanism* (c) *Collision Avoidance Mechanism* (d) *Clustering Algorithm.*

4. MAC Protocols For Cognitive Radio Distributed Networks

These protocols are, as the name suggests, distributed in nature i.e. they do not have a base station for network operation. The architecture is scalable, depending on the number of nodes, and is flexible to deploy resulting in the best solution for emergency networks. Though maintaining the time synchronization is a critical factor when designing the network.

4.1 Random Access Protocol

In [9] the protocol provides and innovative solution to address the hidden node and exposed node problems. Three radios are assigned distinctly to the control, data and busy tone band, respectively. The spectrum bands used for data

transfer are mapped to the frequencies in the busy tone band. Thus, whenever a node transmits or receives data on a given channel, it also emits a busy signal in the corresponding busy tone band [3]. The DOSS protocol consists of five steps: (1) *detection of primary users' presence*, (2) *set-up of three operational frequency bands/channels: a busy tone band, a control channel, and a data band,* (3) *spectrum mapping,* (4) *spectrum negotiation,* and (5) *data transmission.*

The pros of the DOSS protocol: (1) it yields real-time and efficient spectrum allocation, (2) it is scalable, (3) it eliminates the hidden terminal problem and exposed terminal problem. The cons of DOSS protocol is the need for multiple radio transceivers.

In [10] a distributed channel assignment (DCA) protocol is proposed. It is just the extension of the IEEE 802.11 CSMA/CA protocol which uses a dedicated out-of-band common control channel for signaling. One important task is the spectrum pooling which when carried out helps to enhance spectral efficiency by reliable detection the activities of the primary network. The algorithm utilizes two systems: *spectrum pooling* [12] and *Distributed Channel Assignment* (DCA).The protocol operates in following manner: (a) *Spectrum Pooling*: Each mobile user maintains two data structures called the Current Usage List (CUL) and the Free Channel List (FCL). Each node's CUL maintains the information of its neighbors which includes their addresses, corresponding data channels along with the anticipated usage time. (b) *Data transfer*: This process is similar to the data transfer stage of [9], where the FCL is matched at both the sender and receiver ends using the RTS-CTS handshake. The drawback of the DCA MAC is the use of separate CCC. It results in the wastage of the spectrum. Moreover, there is no specific provision for spectrum sensing and PU related adaptation and it also uses multiple transceivers.

In paper [11] a single radio adaptive channel (SRAC) algorithm is proposed which enables dynamic spectrum access in multi-hop wireless ad hoc networks where each node has only one half-duplex radio (transceiver). It characterized three features: (a) *dynamic channelization in response to jamming, primary spectrum users and channel load*, (b) *cross channel communications*, (c) *as-needed use of spectrum*. The three features are described as follows:

- *Adaptive Channelization*: Initially, an atomic channel is defined. It has a minimum bandwidth b (Hz) of all permissible channels. These atomic channels are then combined together to form composite channel. The odd multiple of the actual bands i.e. $f_0 + (m + 1/2)b$ where f_0 is the carrier frequency and m is a multiplier. It results in the increase of the probable transmission bands even more than the actual existing bands. Thus, on the basis of demand of the spectrum, the transmission can be adapted. Furthermore, the bands vary as the activities of the PU and the variation in the load.
- *Cross-Channel Communications*: For overcoming the problems of frequency jamming and the unprecedented existence of PU on a given channel, a node may choose different frequency bands for transmission and reception. In order to achieve this, a channel reservation approach may be carried out. Moreover, the CR users maintain a list of the existing spectrum bands used by its neighbours. It results in efficient utilization of the channels.
- *As-Needed Use of Spectrum:* when the capacity load is more the number of channels are kept low resulting in better multicast support. The provision in which a node is not allowed to change its receive channel until necessary is proposed. If initialized to share a common receive channel, the node will keep on sharing the pre-assigned channel as much as it can. Note that a node is allowed to transmit via its own receive channel.

The drawbacks of this protocol are that, it does not completely address the means to detect the presence of a jammer along with distinguishing malicious activity from legitimate network conditions. There will be significant deaf periods as the control messages sent on receive spectrum bands will not be monitored. The third drawback is the signaling overhead which will be created when maintaining the updated frequency band information of the neighboring nodes.

In paper [13] the hardware constrained MAC protocol is proposed which aims at efficient spectrum sensing as well as spectrum access tasks by taking into account the hardware constrained, which are, the operational constraint of single radio, partial spectrum sensing along with the spectrum aggregation constraints. It has common control channel and a single radio. The hardware constraints have been classified into two categories which are as follows: (a) sensing constraints and (b) transmission constraints.

The general structure of the protocol is given. The time frame in HC-MAC is depicted in Figure 6. The whole time frame can be separated to 3 parts: contention, sensing, transmission. Three types of packets are introduced which are sent on the common channel. They are as follows: a) C-RTS/C-CTS: contention and spectrum reservation in contention part. b) S-

RTS/S-CTS: exchange channel availability information between sender and receiver in each sensing slot. c) T-RTS/T-CTS: notify the neighboring nodes the completion of the transmission.
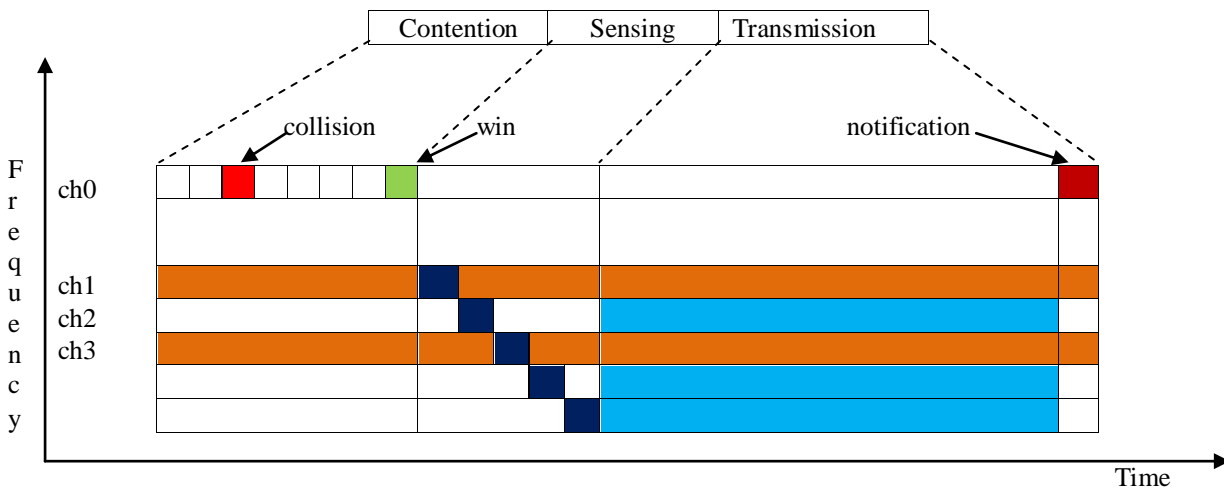

Fig. 6 MAC operation phases

The drawback of this scheme is that if the nodes are engaged in carrying out their own transmission than the control messages, used for channel negotiations, might not get heard. The control overhead is also significant.

4.2 Time Slotted Protocols

In paper [14] the synchronized and time slotted cognitive MAC (C-MAC) protocol is proposed. The goal of the protocol is to achieve higher throughput along with robustness to frequency band modifications. It uses multiple transceivers. This protocol introduces two essential concepts: the Rendezvous Channel (RC) and the Backup Channel (BC). The RC is selected when there is need of uninterrupted traffic throughout the network. It is generally selected for carrying our higher throughput among all channels. Moreover, it is also used for the operations such as PU detection, mutual cooperation of existing users and for multiple channel reservations. The BC does relatively small task similar to RC. It provides immediate choice of alternate channels available upon the appearance of PU.
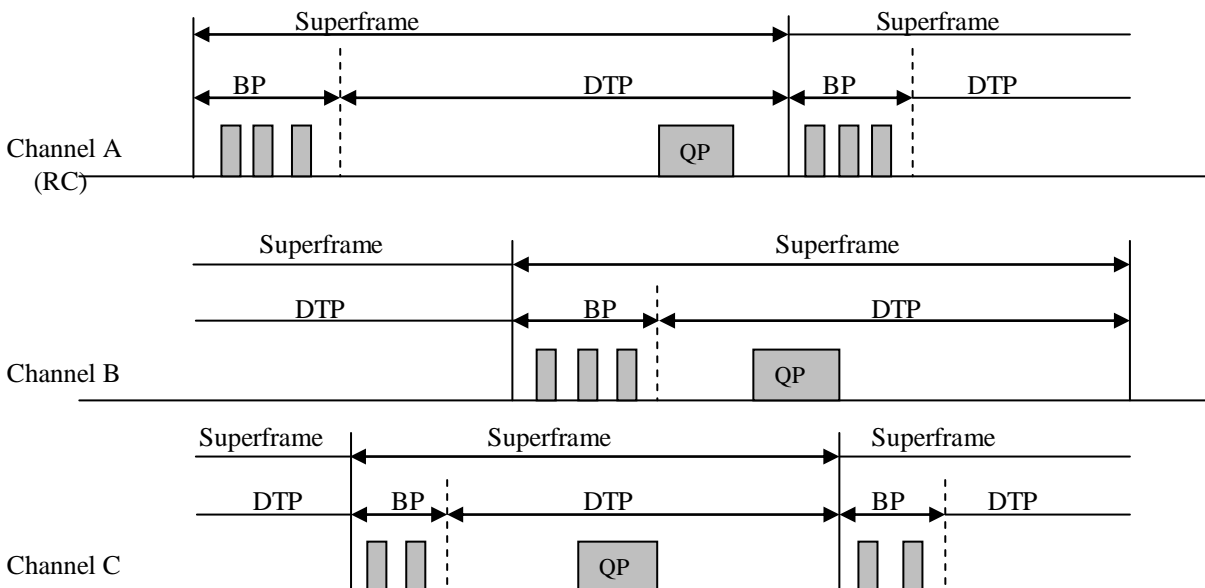

Fig. 7 Multi-channel superframe structure in C-MAC (each channel is structured in the form of superframes whose beacon periods (BPs) are non-overlapping across channels) [14].

The operation of the protocol is introduced as follows:

(a) Distributed Beaconing: The BP is further divided into time slots which cause the CR users to have their own beacons avoiding any obstruction. Re-broadcasting is carried out by the CR users for informing the network nodes.

(b) Inter-channel coordination: Within a certain time period, the CR user periodically connects to RC transmitting their beacons. When there is need to set up new channels, the CR users should announce during their beacons over RC. The periodic tuning to RC helps in re-synchronization. The superframe structure is shown in fig. 7.

(c) Coexistence: There are non-overlapping QPs for a given channels as a result of time slot operations of this protocol. It helps in separation of the PUs and SUs. The transmission of the beacons is carried out using most robust modulation and coding. During this, one of the channels from the BC is chosen.

(d) Load Balancing: Due to time slotted scheme, there are fixed periods. By observing the load sharing stats from the beacon intervals, which does the reservation of the nodes for the current superframe helps to maintain load balancing mechanism.

The major drawbacks of this scheme are: Convergence of RC to unaltered frequency bands over a period of time, unspecified mechanism of how the execution of BPs and QPs without a base station or central entity, lower scalability.

4.3 Hybrid Protocols

An Opportunistic Spectrum MAC (OS-MAC) protocol is proposed. This protocol uses pre-determined window periods for coordinating the choice of spectrum among the CR users and exchanging control information to separate the latter into groups [15]. Moreover, the spectrum access within each window is random, which makes it a hybrid scheme. The communication of control message is assumed to be on common channel while for data transmission non-overlapping bands are used. It uses single transceiver. The protocol operation is discussed as follows:

- *Network initialization phase*: In this phase, the CR users form cluster. In each cluster, all the members of the same cluster wish to communicate with each other. The node entering the cluster has the option of either forming its own cluster or combining with the existing cluster. During the formation of cluster, the CR user keeps its radio connected to CCC. Here, only one CR user, called delegate, remains active in a cluster.

- *Session initialization phase*: In this phase, the active delegate i.e. a CR user, chooses the channel for in order to carry out communication and communicates to all the members of the cluster.

- *Data communication phase*: In this phase, the CR users in a cluster employ IEEE 802.11 DCF for spectrum access. Meanwhile, the active delegate or CR user keeps a check on the CCC for environment statistics. It passes the collected information to all the cluster members to change the bands as per the requirements.

- *Update phase*: In this phase, active delegate in each cluster passes the load statistics to its own cluster to the other delegates over the CCC and after transferring information it returns to the currently used bands.

- *Select phase*: In this phase, upon learning the traffic information of the neighboring clusters, the cluster delegate may decide whether to change the spectrum used in the cluster.

- *Delegate phase*: In this phase, the role of the delegate is forwarded to another CR user within the same cluster for the next round of operation.

In paper [16] SYN-MAC protocol is proposed. It has a dedicated radio for listening messages on the control channel while it does not require CCC. However, a second radio is used for data transmission. The main protocol activities are as following: the time interval is divided into the time slots wherein each slot resembles specific control channel. The control signaling is carried out during the slot time while the data transmission is done on any of the channels found unutilized. Thus, control signaling resembles slow frequency hopping. Initially during each of the slot time, the CR users set up their transceiver to the channel specified by it. The CR users which intend to carry out the transmission send out a beacon at this time. The neighbors who seek to connect with that user respond with their own list of available channels, and then the communication is carried out based on the channel selected during the channel selection exchanges.

5. Conclusion And Future Directions

In this paper, we have presented the comparison of the various existing MAC protocol schemes in the form of overview of that protocol, for cognitive radio. The currently existing MAC protocols works in two major functions of MAC protocol: spectrum sensing and spectrum access. Regarding spectrum sensing, we propose that there is need to devise efficient MAC protocols which will decrease the false alarm and missed detection problems. The simple traffic models such as ON/OFF for

the primary users are not sufficient and more work needs to be done to have significant outcomes. Regarding the spectrum access scheme, there are several open challenges. One major factor is the absence of fully functional spectrum sensing. That is, most of the protocols proposed till date partially take into account the sensing function resulting in decreased sensing accuracy. Moreover, there is also essential scope for developing models which will modify their own transmission depending upon the type of interference. The cognitive technology is regarded as futurist technology which will provide the solution of the spectrum holes and scarcity of spectrum bands. Finally, we believe that overall there is a great scope of research which will help to devise efficient MAC protocols in both the fields such as industry as well as academics.

References

[1] I.F. Akyildiz, W.-Y. Lee, K.R. Chowdhury, Cognitive radio ad hoc networks: research challenges, to appear in Ad Hoc Networks Journal, Elsevier, 2009.

[2] "FCC report of the spectrum efficiency working group," FCC Spectrum Policy Task Force, Tech. Rep., Nov. 2002 [accessed 19 May 2012]. Available: http://www.fcc.gov/sptf/files/SEWGFinalReport_1.pdf

[3] Claudia Cormio, Kaushik R. Chowdhury, "A survey on MAC protocols for cognitive radio networks", Elsevier Journal, Ad Hoc Networks 7 (2009) pp. 1315-1329

[4] C. Cordeiro, K. Challapali, C-MAC: A cognitive MAC protocol for multichannel wireless networks, in: Proceedings of IEEE DySPAN, April 2007, pp. 147–157.

[5] C. Cordeiro, K. Challapali, D. Birru, S. Shankar, IEEE 802.22: The first world-wide wireless standard based on cognitive radios, in: Proceedings of IEEE DySPAN, November 2005, pp. 328–337.

[6] Yan Zhang, Jun Zheng, Hsaio-Hwa chen, "Cognitive Radio Networks", CRC PRESS, CRC PRESS, © 2010 by Taylor & Francis Group, LLC.

[7] S S.-Y. Lien, C.-C. Tseng, K.-C. Chen, Carrier sensing based multiple access protocols for cognitive radio networks, in: Proceedings of IEEE International Conference on Communications (ICC), May 2008, pp.3208–3214.

[8] C. Zhou, C. Chigan, A game theoretic DSA-driven MAC framework for cognitive radio networks, in: Proceedings of IEEE International Conference on Communications (ICC), May 2008, pp. 4165–4169.

[9] L. Ma, X. Han, C.-C. Shen, Dynamic open spectrum sharing for wireless ad hoc networks, in: Proceedings of IEEE DySPAN, November 2005, pp. 203–213.

[10] P. Pawelczak, R. Venkatesha Prasad, Liang Xia, Ignas G.M.M. Niemegeers, Cognitive radio emergency networks – requirements and design, in: Proceedings of IEEE DySPAN, November 2005, pp.601–606.

[11] L. Ma, C.-C. Shen, B. Ryu, Single-radio adaptive channel algorithm for spectrum agile wireless ad hoc networks, in: Proceedings of IEEE DySPAN, April 2007, pp. 547–558.

[12] H. Kim, K.G. Shin, Efficient discovery of spectrum opportunities with MAC-layer sensing in cognitive radio networks, IEEE Trans. Mobile Comp. 7 (2008) 533–545 May.

[13] J. Jia, Q. Zhang, X. Shen, HC-MAC: a hardware-constrained cognitive MAC for efficient spectrum management, IEEE J. Selected Areas Commun. 26 (1) (2008) 106–117.

[14] C. Cordeiro, K. Challapali, C-MAC: A cognitive MAC protocol for multichannel wireless networks, in: Proceedings of IEEE DySPAN, April 2007, pp. 147–157.

[15] H. Su, X. Zhang, Opportunistic MAC protocols for cognitive radio based wireless networks, in: Proceedings of Annual Conference on Information Sciences and Systems, March 2007, pp. 363–368.

[16] Y.R. Kondareddy, P. Agrawal, Synchronized MAC protocol for multihop cognitive radio networks, in: Proceedings of IEEE International Conference on Communications (ICC), May 2008, pp. 3198–3202.

[17] B. Hamdaoui, K.G. Shin, OS-MAC: an efficient MAC protocol for spectrum-agile wireless networks, IEEE Trans. Mobile Comp. 7 (8) (2008) 915–930.

[18] IEEE 802.22 Working Group on Wireless Regional Area Networks.

[19] C. Cordeiro, K. Challapali, M. Ghosh, Cognitive PHY and MAC layers for dynamic spectrum access and sharing of TV bands, in: Proceedings of IEEE International Workshop on Technology and Policy for Accessing Spectrum, August 2006, p. 222.

Snap log based Monitoring and Controlling System
for 3-Phase Induction Motor Drive

Sanjay Patel, Dr. Vinod John

Assistant Professor, Electrical Engineering Department, GIT, Gandhinagar, India

Associate Professor, Electrical Engineering Department, IISc, Bangalore, India

Abstract

The aim of this paper is to develop a real time monitoring system for 3-phase Squirrel Cage Induction Motor operating with V/F control. It acquires current and voltage signals from the IMD set-up and Calculates different important electrical quantities like RMS value of voltage and currents signal, active/reactive power, power factor etc. in a fast, low cost, Low power and high performance capability Digital Signal Processor, TMS320LF2407from Texas Instruments. It sends those data to Personal Computer (PC) via RS-232 serial link and displays the data in to a GUI, built in Visual Basic platform.

Keywords: Front End Converter (FEC), Digital Signal Processor (DSP), Graphical User Interface (GUI), Analog to Digital Converter (ADC), Digital to Analog Converter (DAC).

1. Introduction

THIS Induction Motor Drive (IMD) set up consists of a large number of complex subsystems and Monitoring system for that is added to aggregate information from various parts. Hence, user can continuously visualize the status of the over all electrical system based on the monitoring system. This drive consists of two mechanically coupled induction motors one is Squirrel Cage Induction Motor (SCIM) and other is Slip Ring Induction Motor (SRIM). The SCIM is supplied by Converter-2 which acts as a inverter. The stator of SRIM is connected to converter-3A and rotor to converter-3B (both operate in inverter mode). They are fed from two separated DC bus which are maintained by converter-1,4 which both acts as a active front end converter (FEC). These two converters are capable of handling bidirectional power flow and can regulate dc link voltage. All converters are rated for 415 Volts and 10KVA.Three independent DSP controllers, as shown in Fig.1, control the five converters.[1]

The main purpose of the system is to display the important variables of the set up in PC screen in real time. Here controlling algorithms for the electrical system are implemented in DSP's which has 30 MIPS operating speed at maximum with 33ns cycle time and It is a 16 bit Fixed -point processor of modified Harvard Architecture. Because of controlling operation, Memory and time required for storing power quality monitoring quantities is very less and the additional computing time and memory available is used for implementing the algorithm to control the system.

1.1. Main Objective of the paper

This paper presents the development of power quality monitoring system which needs the following test to be qualified for 10 KVA Inverters as a part of the project.

- Testing of PD card (Protection and Delay)
- Testing of Annunciation card.
- Testing of GD cards (Gate Drive).
- Testing of Voltage sensor cards.
- Testing of Current sensing cards.
- Chopper test for Semiconductor switches.

To controlling the drives and to implement monitoring algorithm, Knowledge of DSP is necessary .which includes the start-up level programming like generating the sine/cosine wave and displaying the same through DACs, ADC interfacing as well as V/Hz programme for speed control of three phase induction motor drive.

2. Testing of 10kVA Inverter

2.1. Protection and Delay Card

PD card is used to perform the following function.
1. Protection
   a. Over current (OC) for a maximum of 4 currents.
   b. Over voltage (OV) for a maximum of 2 voltages.
   c. Under voltage (OC) for a maximum of 2 voltages.
   d. Short circuit protection based on a maximum of 4 V_{CE} sensing status signals.
   e. Protection based on extra signal.
2. Lock-out between top and bottom devices of the same leg to avoid short circuit between buses.
3. Provides different protection status signals as outputs for indication
4. Generate 6-PWM base drive signals by complementing 3-PWM base drive input signal.

2.2. Annunciation Card / Indicator Card

This card has following features.
1. Provides visual indication of power supply and gate drive ON / OFF with de-bouncing circuit.
2. Provides visual indication of various faults till a fault is removed and inverter reset.

2.3. Gate Drive Card

Functionality available with Gate drive card is to:
1. Provides the optical isolation between power ground and DSP ground using HP3101
2. Increase the driving capability by using MIC4425 driver ICs which improve the current sourcing and sinking ability.
3. In built isolated (Fly back converter) power supply for driver circuits.
4. Provide the negative voltage to turn off the device to avoid conduction due to charge accumulate in internal capacitance.
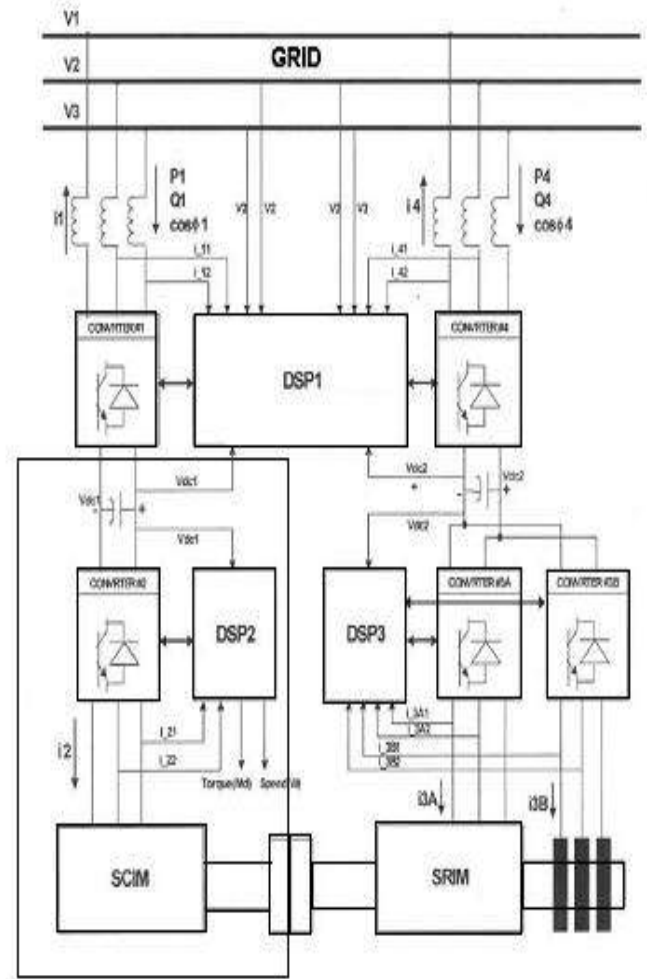

Fig. 1. Induction Motor Drive Set-up

Here result shown in fig. 2 shows the input output relationship of GD card for 50 % duty cycle, 5 kHz and 10 V (peak to peak) square wave input signal taken from function generator. It gives 30 V (peak to peak) square wave signal across G' and E' terminal of GD card with considerable amount of propagation delay (780 ns) as shown in fig. 3. This is due to CD4011 logic gate (i.e. NAND gate).
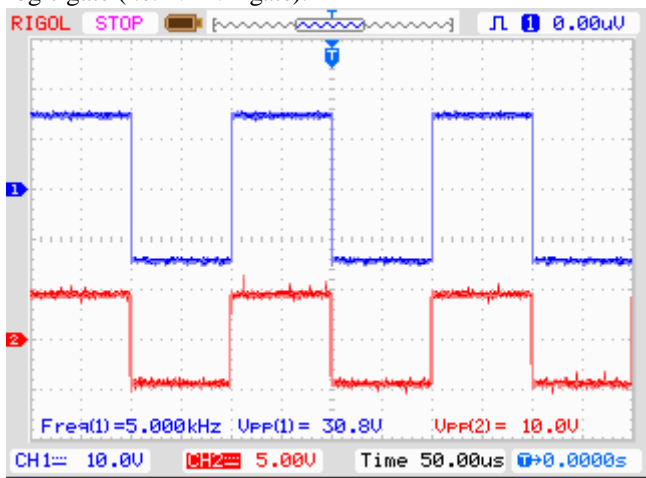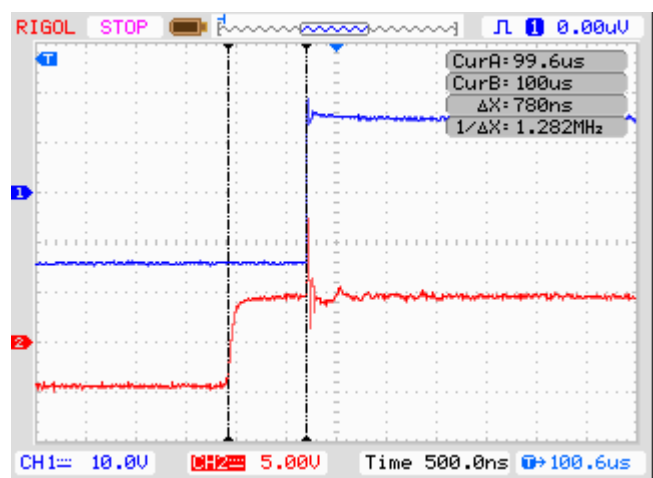

Fig. 2. Input and Output of GD card

Fig. 3. Delay introduce due to GD card

2.4. Voltage Sensing Card

In Voltage sensing card, HP7800 a high CMR (15kVμs at V_{CM} = 1000 V) isolation amplifier has been used. Typical gain of the device is 8 with a tolerance of ±5 %. So for around ±200mV differential input voltage range, its output varies between ± 1.6 V approximately.

Table 1. Linearity Test Result

Sr. No.	Input Voltage (Volt)	Output Voltages	
		V+ (Volt)	V- (Volt)
1	± 30	0.321	- 0.353
2	± 60	0.653	- 0.681
3	± 90	0.982	- 1.007
4	± 120	1.315	- 1.341
5	± 150	1.644	- 1.669
6	± 200	2.200	- 2.223
7	± 240	2.643	- 2.666
8	± 270	2.973	- 2.996
9	± 300	3.311	- 3.333

Linearity Gain = slope of curve = 0.011 V/V.
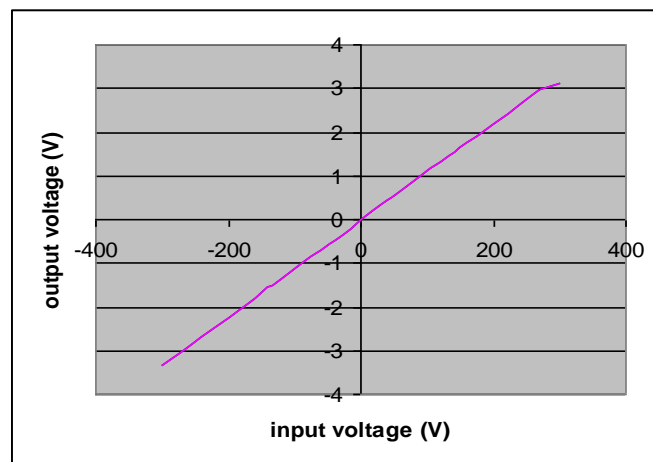
Fig. 4. Transfer Characteristics of Voltage sensing Card

2.5. Current Sensing Card

In Current sensing Card, TELCON HTP50,a Hall Effect current transformer (CT) has been used to measure the current from − 5A to + 5A.

2.6. Chopper Test

Chopper test is used to qualify the IGBT module to be working perfectly or not. Each Module consist two IGBT and formed a one leg of the inverter. Fig. 5 shown below is the circuit arrangement for the Chopper test. Here load can be either resistive or inductive or combination of both. For sake of simplicity this test can be done with resistive load but it should be limit the current passing through the device to avoid damage to IGBT module or overheating.

For DC Bus testing Voltage V_{DC} = 300 V and R_{LOAD} = 60 Ω
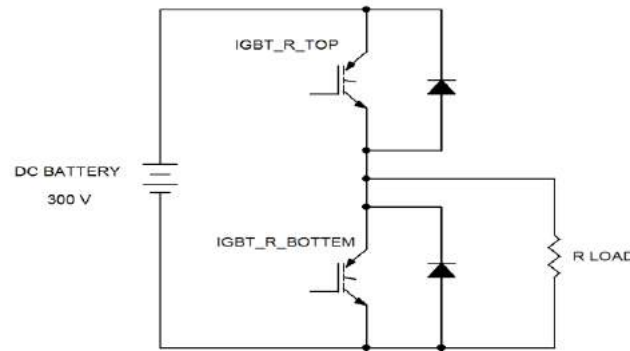Maximum allowable passing current through Device I_{DC} = V_{DC} / R_{LOAD} = 5A

Fig. 5. Circuit diagram for Chopper test

2.7. Study of DSP Board

1. Event manager modules (EVA and EVB)

The event-manager modules include general-purpose (GP) timers, full-compare / PWM units, capture units, and quadrature encoder pulse (QEP) circuits. EVA's and EVB's timers, compare units, and capture units function identically. However, timer / unit names differ for EVA and EVB. [3], [4]

2. Serial Communications Interface (SCI) module

The 240x devices include a serial communications interface (SCI) module. The SCI module supports digital communications between the CPU and other asynchronous peripherals.[2]

3. Analog to Digital Converter (ADC) module

The ADC module consists of a 10-bit ADC with a built-in sample-and-hold (S/H) circuit. It has 16 channel with total conversion time of 500 ns. The digital value of the input analog voltage is derived by:

$$\text{Digital Value} \ = \ 1023 \ \times \ \frac{\text{Input Analog Voltage} - V_{REFLO}}{V_{REFHI} - V_{REFLO}}$$

4. Digital to Analog Converter (DAC)

The 'C24x evaluation board has an on-board, quad, 12-bit, double-buffered digital -to- analog converter (DAC). The four on board DAC channels and the DAC update register are mapped into the I/O space of the 'F240 device. [3], [4]
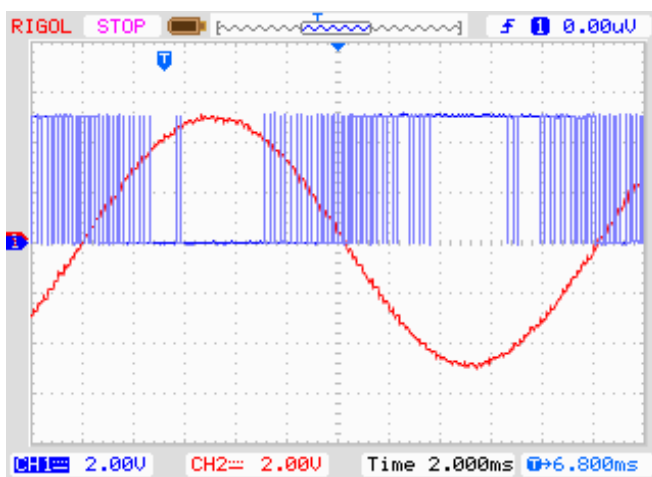

Fig. 6. 50 Hz reference sine wave and its corresponding PWM signal, generated using sine-triangle comparison technique at DSP board pin (40 - pin Berg-stick connector of DSP board)
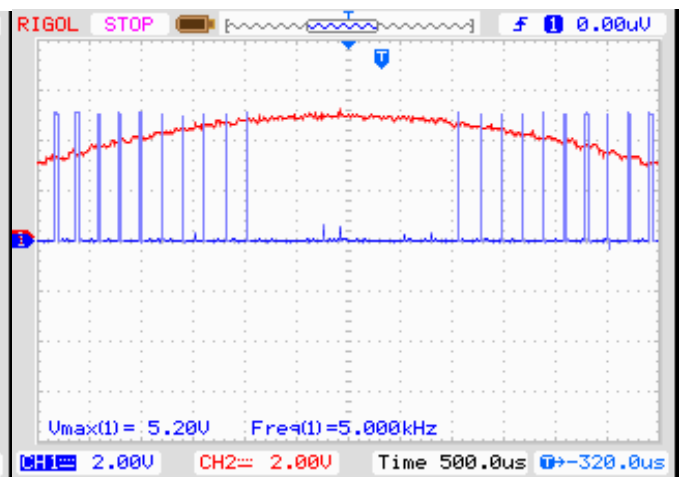
Fig. 7. Sine Triangle Comparison based PWM signal of 5 kHz with its reference sine wave

3. Conclusion

The DSP is having a 30 MHz clock as the system clock and so the instruction execution time is the lowest of 33ns for a single cycle instruction. The time to calculate the display quantities is taking very much less compared to the sampling time of 100 µs. The fast calculation algorithm is required and the display data is transmitted to PC and displayed in the GUI built in VB environment.

Acknowledgements

References

[1] Rabindra Nath Bhuniya and Vinod John, "Monitoring system for High Power Induction Motor Drive," National Power Electronic Conference (NPEC) - 2007,Bangalore.

[2] V Sravan and Vinod John, A project report on "Grid Power Quality Analysis of 3-Phase and 1-Phase Systems".

[3] "TMS320LF240 DSP Controllers Reference Guide" CPU and Instruction set, Literature number SPRU160C, Texas Instruments.

[4] "TMS320F/C24x DSP Controllers Evaluation Module Technical Reference" Literature number SPRU248B, Texas Instruments.

[5] "Automated Event Retrieval Reduces Operating Costs," Todd osenberger, Oncor Electric Delivery and David Prestwich, Matthew Watkins, and Mark Weber, Schweitzer Engineering Laboratories, Inc.

Cross sections for Electron Scattering with C_6H_6 and C_6F_6 – A Theoretical investigation

Umang R Patel[a,b,*], K N Joshipura[b]

[a]*Gandhinagar Institute of Technology, Moti Bhoyan, Gandhinagar-382721, Gujarat, India*

[b]*Sardar Patel University, Vallabh Vidyanagar-388120, Gujarat, India*

Abstract

In this paper we report theoretical electron scattering cross sections for C_6H_6 and C_6F_6 from threshold to 2000 eV. Theoretical formalism employed presently, viz., *Complex Scattering Potential- ionization contribution* method has been used successfully for a variety of polyatomic molecules. The present calculations are very important since results available for the studied targets are either scarce or none.

Comparisons of the present ionization cross sections for C_6H_6 and C_6F_6 are made wherever possible, and new data are also presented.

1. Introduction

Collisions of electrons with molecular targets, leading to various processes, are found to occur in many natural and laboratory environments. Such collision processes lead to both chemical and physical changes of matter in environments associated with radiation chemistry; plasma enhanced chemical vapour deposition, lighting industry and plasma processing of materials for microelectronics. In most cases, collisional interactions of low to intermediate energy electrons are the precursors for the production of critical species in low temperature plasmas and plasma processing gas discharges [1, 2]. About one third of the processes needed to make a modern microchip involve plasma based processes. Both hydrocarbons and perfluorocarbons play an important role in plasma assisted fabrication processes. Therefore both classes of molecules have received research attention from theorists as well as experimentalists over the past few years. For optimal design of gaseous insulators, there must be full identification and understanding of basic processes preventing transition of a gas medium from an insulating to conducting state under an imposed electric field and this requires access to comprehensive and reliable sets of quantitative electron impact cross section data [3].

The scenario depicted above points to the need of the study taken up in this paper. We report here the electron impact ionization cross sections for C_6H_6 and C_6F_6. Very little work has been reported on these species to the best of our knowledge. The present study is also guided by small but important differences in the first ionization energies of the present targets, as reported in different sources [4]. We have employed here the Complex Scattering Potential ionization contribution (CSP-*ic*) method developed and applied successfully by us, over a wide range of molecular targets in the recent years [5-9]. The present calculations have been performed in the group additivity approach, as has been necessary for the large polyatomic molecules, each consisting of several functional chemical groups. Section 2 describes the theoretical methodology adopted here, followed by the results and discussions along with conclusions.

2. Theoretical methodology

At the incident energies (E_i) from ionization threshold to 2000 eV, it becomes meaningful to represent the electron - molecule system by a complex (Spherical) potential, which seeks to club together all admissible inelastic (including ionization) channels in the background of elastic scattering. For an electron interacting with a molecule (or a functional chemical group), the total complex potential $V(r, E_i) = V_R(r, E_i) + iV_I(r, E_i)$, consists of real potential V_R and imaginary potential V_I. The real part comprises of static, exchange and polarization potentials while the imaginary part is the inelastic 'absorption' potential V_{abs}. Further, r is the radial distance from the mass-centre of the target (group). The basic input in constructing all these model potentials is the target charge density. The molecular spherical charge density is constructed through a single-centre expansion of the atomic charge density at the molecular mass-centre [6]. The static potential is determined directly from the target charge density and the exchange potential is calculated using the models of [10].

The total complex potential $V(r, E_i)$ introduced in the Schrodinger equation, along with its solution obtained numerically, leads to the total (complete) cross section Q_T defined as follows.

Corresponding author: +91 8347010863

umangpatel193@yahoo.ca

$$Q_T(E_i) = Q_{el}(E_i) + Q_{inel}(E_i) \tag{1}$$

Where, Q_{el} is the total elastic cross section while its inelastic counterpart is denoted by Q_{inel}. The total (cumulative) inelastic cross section Q_{inel} includes all energetically allowed electronic excitation as well as ionization channels of scattering, so that

$$Q_{inel}(E_i) = \sum Q_{exc}(E_i) + \sum Q_{ion}(E_i) \tag{2}$$

On the right hand side of Eq. (2), the first term $\sum Q_{exc}$, to be called electronic sum, includes all accessible electronic excitation channels in the target, and the second term $\sum Q_{ion}$ stands for the total cross sections of all allowed (parent, dissociative, single, double etc.) ionization channels. Our focus is on finding total ionization cross section, and the second term will hence forth be denoted simply by Q_{ion}.

The absorption potential mentioned above is an energy dependant potential that accounts for all possible inelastic scattering channels cumulatively, and has the generic form, first developed by Staszewska *et al.* [11], in atomic units

$$V_{abs}(r, E_i) = -\tfrac{1}{2} \rho(r) V_{loc} \sigma_{ee}$$
$$= -\rho(r) \left(\tfrac{T_{loc}}{2}\right)^{\frac{1}{2}} \left(\tfrac{8\pi}{10 k_F^3 E_i}\right) \times \theta\left(p^2 - k_F^2 - 2\Delta\right)\left(A_1 + A_2 + A_3\right) \tag{3}$$

Here, V_{loc} is the local speed of the external electron, and σ_{ee} denotes the average cross section for binary collision of the external electron with one of the target electrons. In equation (3), $p^2 = 2E_i$, k_F is the Fermi wave-vector magnitude and Δ is an energy parameter. Blanco and Garcia [12] suggested a variable form of Δ in order to account for screening effects of the target charge cloud on V_{abs}. The modification introduced by us is to consider Δ as a function of E_i, as discussed in [9]. Accordingly,

$$\Delta(E_i) = 0.8I + \beta(E_i - I) \tag{4}$$

Let us denote by 'E_p' the value of E_i at which our Q_{inel} attains its maximum. In equation (4) β is then obtained by requiring that $\Delta = I + 1$ (eV) at $E_i = E_p$, beyond which Δ is held constant. The expression for $\Delta(E_i)$, in equation (4), is meaningful since Δ fixed at I would not allow even excitation at incident energy $E_i \leq I$. On the other hand, if the parameter Δ is much less than the ionization threshold, then V_{abs} becomes unduly high near the peak position. In short the present form of $\Delta(E_i)$, in equation (4), balances all these aspects and allows us to obtain the satisfactory values of Q_{ion} for a given target [9]. With the V_{abs} thus modified, we solve the Schrödinger equation numerically, to extract the complex partial wave phase-shifts δ_l, for different angular momenta l at desired energies.

The inelastic cross section Q_{inel} is not a directly measurable quantity in a single experiment, but in view of the equation (2), we have in general,

$$Q_{inel}(E_i) \geq Q_{ion}(E_i) \tag{5}$$

At incident energies above I, the ionization processes begin to play a dominant role due to the availability of infinitely many open channels of scattering. There is no rigorous way of projecting out Q_{ion} from the theoretical quantity Q_{inel}. Hence, we have introduced an approximation by defining a ratio function,

$$R(E_i) = \frac{Q_{ion}(E_i)}{Q_{inel}(E_i)} \tag{6}$$

Obviously $R = 0$ when $E_i \leq I$. For a number of stable atomic – molecular targets like Ne, Ar, O_2, N_2, CH_4, H_2O, etc., for which several experimental ionization cross section data-sets are known accurately [5-9], the ratio is seen to be rising steadily as the energy increases above the threshold, and approaching unity at high energies. Thus,

$$R(E_i) = 0, \ for \ E_i \leq I \tag{7a}$$
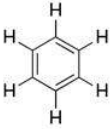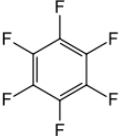
$$R(E_i) = R_p, \ for \ E_i = E_p \tag{7b}$$

$$R(E_i) \leq 1, \ for \ E_i \gg E_p \tag{7c}$$

Here $R_p = 0.7$ stands for the value of R at $E_i = E_p$. The choice of this value [5-9] is approximate but crucial. The peak position E_p of the cross section Q_{inel} occurs at incident energy where the discrete excitation-sum is decreasing while Q_{ion} is rising fast, suggesting the R_p value to be between 0.5 and 1. We follow the general observation [5-9] that at energies close to peak of Q_{inel} the ionization contribution Q_{ion} is about 70-80% in the total inelastic cross section Q_{inel} and it increases with energy. An indirect support in this regard is also obtained from the correlation between the maximum ionization cross section denoted by σ_{max}, and the molecular properties viz., polarizability and ionization threshold. It has been demonstrated in our publications [5-9] that total ionization cross sections can be reasonably determined from this approximation and the resulting Q_{ion} are within the experimental uncertainties of about 10-15%. Now, for the actual calculation of Q_{ion} from Q_{inel} we need R as a continuous function of energy E_i. Hence, we represent [6] the ratio $R(E_i)$ in the following manner.

$$R(E_i) = 1 - f(U_i) = 1 - C_1 \left[\frac{C_2}{(U_i + a)} + \frac{\ln U_i}{U_i} \right] \tag{8}$$

Where $U_i = E_i/I$, is a dimensionless and target-specific variable corresponding to energy E_i. The reason for adopting a particular functional form of $f(U_i)$ i.e. second term of the right hand side of equation (8) is as follows. As E_i increases above I, the ratio R increases from zero and approaches value 1, since the ionization contribution rises and the discrete excitation-sum in equation (2) decreases. The discrete excitation cross sections, dominated by dipole transitions, fall off as $ln(U_i)/U_i$ at high energies. Accordingly the decrease of the function $f(U_i)$ must also be proportional to $ln(U_i)/U_i$ in the high range of energy. However, the two-term representation of $f(U_i)$ given in equation (8) is more appropriate since the 1st term in the square bracket ensures a better energy dependence at low and intermediate E_i. Equation (8) involves dimensionless parameters C_1, C_2, and a, characteristic of the target in question. The three conditions stated in equation (7a-c) are used to determine these three parameters, in an iterative manner [6]. Thus we first assume $a=0$ and consider a two-parameter expression in equation (8). We employ therein the two conditions (7a) and (7b) to obtain C_1 and C_2. The two-parameter equation is then used to determine the value of R at a high energy $E_i = 10 E_p$, and the same value is employed in equation (7c) to obtain the new set of three parameters C_1, C_2 and a. Having thus obtained the parameters we calculate Q_{ion} from equation (6), and therefore generate R_p value from these Q_{ion}. The resulting R_p value is used next as an input to the equation (7b) iteratively to finally calculate Q_{ion}. Equations (5 - 8) describe our CSP- *ic* method. The above calculation is basically carried out for a functional group in the target molecule in question. As the studied molecules are complex, a single centre approach is not feasible for the entire molecule. Hence the calculation is made on a molecular functional group as a scattering centre, and the group additivity method is employed, where the geometrical structure of the molecule is taken into account. Table 2 shows the molecular properties of the title targets.

Table 1 Properties of the targets studied

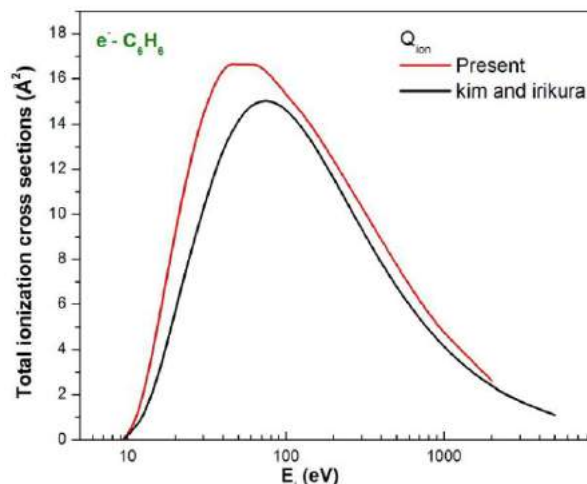| Target	Geometry	Ionization Potential (eV)	Bond length (Å)
C_6H_6		9.244	C-C 1.39 C-H 1.08
C_6F_6		9.8	C-C 1.40 C-F 1.32

3. Results and discussions

Fig. 1. Q_{ion} for e$^-$ - C$_6$H$_6$, Red solid line; Present Result and black solid line; BEB Q_{ion} by Kim and Irikura [2]

In fig. 1 we have compared Q_{ion} of C$_6$H$_6$ (Benzene) by electron impact with the other available results. Present results are in agreement with the BEB cross sections by Kim and Irikura [2]. Small shift in magnitude is observed due to differences in the ionization threshold used in presented results.

Fig. 2. Shows the comparison of Q_{ion} for e$^-$ - C$_6$H$_6$ and e$^-$ - C$_6$F$_6$ scattering. It's very interesting to compare both these results as it is observed that, though the fluorine is a reactive and heavy atom, their cross sections are found to be lower compared to hydrocarbons. The similar observation is found here which shows the effect on cross section by substituting F atom for H atom in C$_6$H$_6$. No other comparison was available for C$_6$F$_6$.
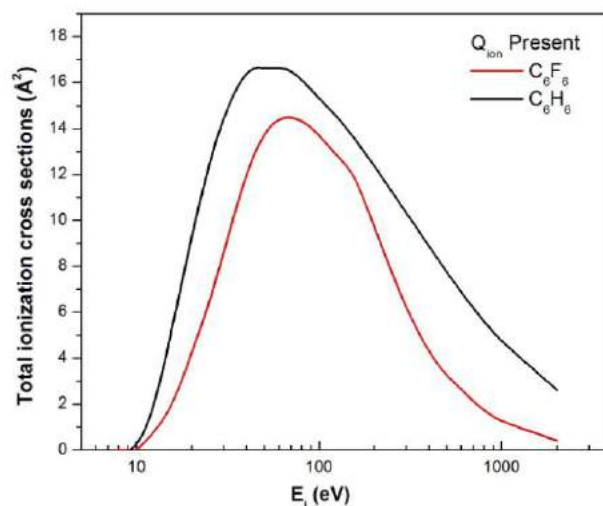

Fig. 2. Present Q_{ion} for e$^-$ - C$_6$H$_6$; black solid line and e$^-$ - C$_6$F$_6$; red solid line

4. Conclusions

We have successfully calculated the electron impact ionization cross sections for e$^-$ - C$_6$F$_6$ and e$^-$ - C$_6$H$_6$. Present results are compared with available data from published literature, which are in a good accord with each other. An important observation of magnitude difference in cross sections has been found by comparing Q_{ion} on e$^-$ - C$_6$H$_6$ with BEB cross sections by Kim and Irikura [2]. Another observation of substitution effect (i.e. substitution of H atom by F atom in e$^-$ - C$_6$H$_6$) is satisfied as like previous observations. Calculations for total cross sections are under study which are equally important but shows some strange behavior due to reactive nature of fluorine. So we have not discussed it in this paper.

4

References

[1] Brunger M., Cho H., Tanaka H and Buckman S., 2006, Measurements of electron collision cross sections of relevance to plasma and gas discharge physics, Jpn. J. of appl. Sci. 45, p. 8183.

[2] Kim Y. and Irikura K., 2000, Electron impact ionization cross sections for polyatomic molecules, radicals and ions, Proc. 2nd Int. Conf. on Atom. Molec. Data and Their Applications, AIP Conf. Proc. (AIP, New York, NY) 543, p. 220

[3] Kasperski G., Mozejko P. and Szmytkowski C., 1997, Electron scattering on C_6F_6 and SF_6 molecules, Z. Phys. D 42, p. 187-19

[4] www.cccbdb.nist.gov *Computational Chemistry Comparison and Benchmark Database*

[5] Patel U., Joshipura K., Kothari H. and Pandya S., 2014, Electron ionization of open/closed chain isocarbonic molecules relevant in plasma processing: theoretical cross sections, J. Chem. Phys. 140 p. 044302

[6] Joshipura K., Vinodkumar M., Limbachiya C. and Antony B., 2004, Calculated total cross sections of electron-impact ionization and excitations in tetrahedral (XY_4) and SF_6 molecules, Phys. Rev. A 69, p. 022705

[7] Pandya S., Shelat F., Joshipura K. and Vaishnav B., 2012, Electron ionization of exotic molecular targets CN, C_2N_2, HCN, HNC and BF—Theoretical cross sections, Int. J. Mass Spectrom. 28, p. 323-324

[8] Kothari H., Pandya S. and Joshipura K., Electron impact ionization of plasma important $SiCl_X$ (X = 1–4) molecules: theoretical cross sections, J Phys. B At. Mol. Opt. Phys. 44, 125202 (2011)

[9] Joshipura K., Kothari H., Shelat F., Bhowmik P., Mason N., 2010, Electron scattering with metastable $H_2^*(c^3\Pi_u)$ molecules; Ionization and other total cross-sections ,J Phys. B At. Mol. Opt. Phys. 43, p. 135207

[10] Hara S., 1967, Free gas exchange model, J. Phys. Soc. Japan, 22 p. 710

[11] Staszewska D., Schwenke D., Thirumalai D., Trulhar D., 1984, Investigation of the shape of the imaginary part of the optical-model potential for electron scattering by rare gases, Phys. Rev. A. 29, p. 3078

[12] Blanco F. and Garcia G., 2003, Screening corrections for calculations of electron scattering from polyatomic molecules, Phys. Lett. A. 317, p. 458

Gandhinagar Institute of Technology

ROUTE MAP OF GIT
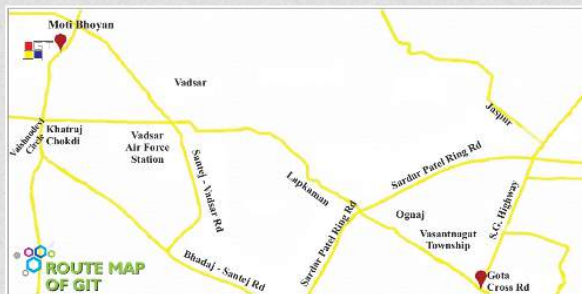
Institute Address

Gandhinagar Institute of Technology
Khatraj - Kalol Road,
Village Moti Bhoyan,
Tal. Kalol
Gandhinagar-382721
Mobile No: +919904405900
Ph No: +91-02764-281860/61
Fax No: +91-02764-281862
E-mail Address: director@git.org.in